1982 - 18

FINAL REPORT

SOUTHWEST FLORIDA SHELF CIRCULATION MODEL

Volume I

PREPARED FOR

MINERALS MANAGEMENT SERVICE

CONTRACT NO. AA851-CTO-72

OCTOBER 1982

NESS Inc., Bangor, Maine

DISCLAIMER

This report has been reviewed by the Minerals Management Service and approved for publication. Approval does not signify that the contents necessarily reflect the views and policies of the Bureau, nor does mention of trade names or commercial products constitute endorsement or recommendation for use.

ABSTRACT

Southwest Florida Shelf Circulation Model

This report summarizes an 18 month study funded by the Minerals Management Service. Motivation for the study arose from the Service's intention to grant leases for oil exploration, and the attendant need to estimate the probable destination of water-borne pollutants originating from drilling and production activities. The purpose of the study was to develop a capability for predicting seasonal water circulation on the southwest Florida continental shelf. Because of modeling considerations, the study area was expanded to include the contiguous West Florida Shelf (WFS) extending from the Florida Keys in the south to Apalachicola in the north, and the 200 m isobath to the west.

The study involved four phases: literature review and data search; model modifications and sensitivity studies; model verification and tuning; and prediction of seasonal circulation patterns. These phases produced the following results:

1. A thorough review of the literature and available data base indicated that there have been very few historical attempts to form a coherent picture of overall circulation on the WFS, and no attempts which have incorporated some of the more recent data bases. In situ data measurements on the shelf were sparse - high quality current data were limited to two studies yielding a total of 6 meter-months of data. Other current measurements exist but they were taken in deeper water near the shelf break. As a result of the limited data base, circulation on the WFS remains poorly understood. Important forcing mechanisms which were identified for inclusion into the model were: the Loop Current, winds, and density gradients.

2. The model used in the study was based on a numerical solution of the conservation of momentum and mass equations. The model could predict the temporal and 3-D spatial changes of the horizontal velocity field, and included forcing due to: the atmosphere, earth's rotation, inertia, and horizontal pressure gradients. Realistic bottom topography was included. Vertical and horizontal dissipation was modeled via eddy viscosity and bottom friction coefficients. Several improvements to the original model were implemented to better simulate processes of importance on the WFS. These modifications were verified by comparing the model results to analytic solutions of simple flow problems.

3. Following modification and initial sensitivity studies, the model was used to hindcast three data sets in real time. Two of these were about one month in duration taken during the winters of 1973 and 1978. The winter data included in situ current meter and coastal surface elevation data. The third data set was limited to two months of coastal surface elevation data taken during the summer of 1974. A reasonable simulation of the winter 1978 data and surface elevation data for the winter 1973 was obtained. Summer surface elevations and winter 1973 currents were difficult to simulate largely because available data were inadequate to specify external forcing. In the case of the 1973 data, eddies from the Loop Current strongly influenced current observations but could not be modeled because of insufficient hydrographic data and model limitations.

4. Seasonal descriptions of wind, horizontal density gradients, and the Loop Current were derived from available data.

   Winds were broken into three seasons: fall-winter, spring, and summer. Net resultant wind stresses for each of these seasons were calculated based on five years of data from Key West.

All available hydrographic data consisting of more than 35,000 measurements were processed and analyzed. The results indicated statistically significant horizontal density gradients only during the summer. It is suspected that the averaging process tended to obscure any gradients which may in fact exist. Averaging was necessary, however, because of the lack of synoptic shelf-wide hydrographic data. Currents resulting from this gradient were less than 1 cm s^{-1}. The hydrographic summary was also used to determine the vertical stratification during the summer which did prove to have a substantial effect on modeled currents.

Including Loop Current effects in the seasonal circulation pattern involved a number of serious uncertainties. As a best estimate, the Loop Current effect was modeled using a steady, alongshore velocity applied at the model western boundary. The northern limit of intrusion of the Loop Current into the Gulf of Mexico was varied according to season with maximum penetration occurring in the summer.

The model results indicated a composite fall-winter circulation with a dominant southerly flow at all levels. Surface currents were on the order of 10 cm s^{-1} on the shelf. The spring and summer currents were generally smaller in magnitude and had a more complicated pattern characterized by northerly surface currents in waters within 50 km of the coast and southerly currents elsewhere. These features were consistent with available drifter observations and in situ current data. The model did not include any effects of migrating Loop Current eddies as this was not justified by the existing data base and was beyond the present formulation of the model.

Further studies will be severely constrained by the existing data base, but four areas with some potential were suggested. It was recommended that further refinement of the model be performed as soon as additional data became available. The most likely source of future data was the Mineral

Management Service's Gulf-wide oceanographic data collection program which was to start in 1982. The proposed program was regarded as appropriate, but based on the data review, it was recommended that the program be augmented by a specific attempt to monitor migrating eddies on the shelf.

FINAL REPORT
SOUTHWEST FLORIDA SHELF
CIRCULATION MODEL
VOLUME I

Prepared for:

United States Minerals Management Service
Contract No. AA851-CTO-72
July 1982

Prepared by:

NECE, Inc
Penobscot Plaza
Bangor, ME 04401

Table of Contents

VOLUME II

LIST OF FIGURES

LIST OF TABLES

Chapter 1

Executive Summary

The southwest Florida Shelf is an area in the Gulf of Mexico bounded on the east by the Florida coast, on the west by the 100 meter depth contour (isobath), on the south by the Florida Keys, and on the north by latitude 28°N. Because of modeling considerations, the area was expanded northward to include the area from 28° to Apalachicola (30°N), and westward to the 200m isobath - essentially the contiguous West Florida Shelf (WFS). The motivation for the this study arises from the Minerals Management Service's (MMS) intention to grant leases for oil exploration on the southern shelf, and the Service's attendant need to estimate the probable destination of water-borne pollutants originating from drilling and production activities.

The purpose of the study described in this report was to develop a capability for predicting seasonal water circulation on the WFS. The study involved four separate phases:

1. Literature review and data search;
2. Model modifications and basic sensitivity studies;
3. Model verification and tuning; and
4. Prediction of seasonal circulation patterns.

Chapter 2 of this report discusses the results of Phase 1. Details are

included in Appendix A. Chapters 3 and 4 and Appendices E and F present the results of Phase 2. Chapter 5 and Appendices B and G describe Phase 3 efforts, and Chapter 6 summarizes Phase 4. Recommendations for future work are given in Chapter 7. Appendix C contains technical papers written and presented by NECE which involve work on the WFS circulation model and Appendix D contains a summary of the model input parameters for important model runs. Appendices H and I present a detailed User's Manual for the model and are available as a separate volume.

PHASE I: THE WEST FLORIDA SHELF ENVIRONMENT

Our review of the literature and available data base indicates that there have been very few historical attempts to form a coherent picture of circulation on the WFS, and no attempts which incorporate some of the more recent and substantial data bases such as the Shelf Dynamics Experiment (SDE) and satellite data.

In situ data measurements on the shelf are sparse. High quality current data are limited to two studies yielding a total of six meter-months of data, (i.e. one meter-month is equal to the data from one meter deployed for one month). No current meter data exists for summer conditions. Only three meter-months of these data were taken in the southern portion of the shelf. Existing current meter data allows ample room for speculation, but permit few firm conclusions to be drawn concerning overall WFS circulation.

Three drifter studies have been performed on the WFS. When viewed as a whole these studies indicate: (1) an overwhelming number of drifters found in the Florida Keys and Florida east coast during the fall and winter; (2) substantial numbers of drifters found in in this same area during the remainder of the year; and (3) virtually no drifters found on the west Florida coast at any time except from release sites within about 20 km of shore and obviously under the influence of land-sea breezes. When these results are compared with the seasonal resultant winds, they strongly imply

the existence of a year round southerly surface drift on the WFS.

The Loop Current (LC) dominates the circulation pattern in the eastern Gulf of Mexico. Its northern boundary varies between roughly 24 and 30^{o}N latitude during a quasi-annual period. Several investigators have suggested an annual cycle with the maximum northward intrusion occurring in early summer, but it is apparent that this is subject to considerable year-to-year variability. Given the proximity, magnitude and intensity of the LC it is not surprising that the LC interacts with the shelf in a number complex ways.

At the interface between the LC and shelf, eddies are often observed both in the satellite and SDE data. At the shelf break, these eddies appear as alternating anticyclonic and cyclonic eddies. The low frequency current spectra are dominated by the eddies. There is good evidence that eddies, meanders, and tongues from the LC migrate well onto the shelf. These eddies have time and length scales of 200 km and 15 days . It is likely that these eddies cause net advection but there are no known Lagrangian current measurements nor sufficient Eulerian measurements to quantify this advection. It is unknown what roles density and momentum play in driving the eddies.

Several investigators have suggested that the LC behaves as a jet which applies a southerly lateral shear along the shelf break. This mechanism would create predominately southerly circulation with a time scale tied to the seasonal migration of the LC. The drift card data tend to support this hypothesis.

The tidal regime on the shelf has a mean range of 0.3 m. Typical tidal current maxima are 10 cm s^{-1} which cause a maximum net advection during a half-tidal cycle of about 1 km. There is no evidence of residual currents due to tides. In other parts of the world, residual currents are typically small unless the tidal amplitude is very large such as in the Bay of Fundy. Even in such areas, tidal residual currents are typically and order of

magnitude less than the peak tidal currents. If this is taken as a rule of thumb, then residual tidal currents on the WFS would be expected to be about 1 cm s^{-1}, clearly a negligible quantity. Therefore, the considerable complication of including tidal forcing in the model was deemed unnecessary.

Over 35,000 hydrographic measurements were analyzed. The results indicated statistically significant horizontal density gradients only during the summer. It is suspected that the averaging process necessitated by the lack of synoptic shelf-wide data tended to obscure any gradients which may in fact exist. Currents resulting from this gradient were less than one cm s^{-1}. The hydrographic data were also used to determine vertical density stratification during the summer, which did prove to have a substantial effect on modeled currents.

In summary, the literature and data review indicate that circulation on the WFS is poorly understood, in large part because of a dramatic absence of high quality in situ data. Existing data indicate a complex flow regime which is strongly influenced by migrating eddies from the LC and by a larger scale lateral shear mechanism. Important forcing mechanisms which should be included in the model are: the LC, winds, and density gradients.

PHASE II: ADJUSTING THE MODEL

Phase II involved modifying the original model by Cooper and Pearce (1977) to suit the precise site conditions of the WFS. Major modifications included: (1) provision for model forcing due to horizontal density gradients and (2) improvement of lateral shear stress transfer capability. These modifications were checked with simple analytic solutions to verify model coding and theoretical representation. Phase II also involved fundamental studies to investigate model sensitivity to changes in input parameters such as: lateral boundary conditions, grid configuration, bottom friction, vertical and lateral eddy viscosity, and spatial variations of the Coriolis parameter. Various forcing mechanisms were investigated such as the LC, wind, and

horizontal density gradients. Vertical stratification was also considered.

PHASE III: TUNING AND VERIFICATION

Phase III involved tuning and verification using three data sets collected on the shelf. Comparisons were restricted to synoptic scales (i.e., time periods of two to thirty days). Shorter time scales were not requested in the scope of work and longer time scales are not possible because of insufficient data duration. Two of the data sets, collected during February-March 1973 and February-March 1978, contained both offshore current velocity and coastal surface elevation data, and each had a duration of approximately one month . The third data set from July-August of 1974 contained only coastal surface elevation data and had a duration of two months.

Winter 1978. Comparison of modeled and observed data for the winter of 1978 demonstrated the following:

1. the model predicted real time residual currents typically to within 5 cm s^{-1} over a range of 40 cm s^{-1};

2. sensitivity studies implied that the discrepancy between the modeled and observed currents was not due to an inadequate choice of the various model dissipation coefficients. The discrepancy may have been due to any number of other factors such as measurement error, inadequately modeled wind field, unmodeled effects of the LC or horizontal density gradients. There were insufficient hydrographic data to model the latter two possibilities; and

3. the model hindcasted the surface elevations at the coast quite well, peaks being predicted to about +/- 2 cm over a range of 40 cm. Phase discrepancies of about 5 hours were sometimes observed. The hindcast of Key West elevations was not as good, but there are several

characteristics of the site which make it a difficult one to model.

Winter 1973. Comparison of modeled and observed data for the winter of 1973 demonstrated the following:

1. The modeled coastal surface elevations compared well to observed values, typically being within 5 cm in amplitude and 5 hours in phase. The model underestimates the surge peaks by about 10 cm.

2. Inspection of the current data for the 1973 period indicates that all the current meters were substantially affected by LC effects. Interpretation of the exact nature of these effects varies, so two hypotheses were investigated using the model: (1) an eddy wave field proposed by Niiler (1976), and (2) a lateral shear mechanism suggested by our review of existing data.

3. The model was forced at the shelf break using a barotropic eddy wave suggested by Niiler (1976), and the results were compared to the current data at three stations. A reasonable hindcast of the current data was made using a somewhat slower phase speed for the wave field than that suggested by Niiler. This LC forcing overpredicted the surface elevations at the break by a factor of three and at the coast by a factor ten. There were a number of possible reasons for this failure, the most probable being the neglect of: (1) the baroclinic component of the eddies and (2) the nonlinear terms in the model.

4. An alternative lateral shear mechanism was used to model the LC. This was implemented by specifying a constant alongshore velocity along the shelf break. This forcing gave reasonable comparisons to the observed current data during the time period when the current meter sites were not affected by the passage of an invading frontal system originating from the LC. Note that the existence of a lateral shear mechanism does

not preclude the existence of eddies but regards them more as random events rather than organized into a consistent eddy wave field.

Summer 1974. Comparison of modeled and observed surface elevation data for the summer of 1974 demonstrated that the modeled surface elevations were of the same order of magnitude as the observations, but the phase was consistently in error. Data analysis showed the winds to be more spatially variable than during the winter. This implied that the poor model results were probably due to improper specification of the wind field, a problem which could not be easily circumvented because of the lack of spatial resolution in the available wind data.

PHASE IV: SEASONAL CIRCULATION PATTERNS

Phase IV of the study involved derivation of seasonally averaged wind fields, density gradients, and LC effects.

Winds were divided into three seasons: fall-winter with northeasterly winds of 4.5 m s^{-1}; spring with south-southeasterly winds of 5.5 m s^{-1}; and summer with southeasterly winds of 4 m s^{-1}. These results are based on wind measurements at Key West which were of reasonably long duration and were not substantially affected by land effects. Comparisons between Key West winds and NDBO buoy 42003 suggested that the seasonal wind curl was quite small, at least in the region of primary interest to the MMS on the southwestern Florida shelf. Analysis of other land stations indicated that they were not representative of offshore winds, being biased both in speed and direction.

All available hydrographic data, consisting of more than 35,000 measurements, were processed and analyzed. It is suspected that the averaging process tended to obscure any gradients which may in fact exist. Averaging was necessary, however, because of the lack of synoptic shelf-wide hydrographic data. The results did indicate statistically significant horizontal density gradients during the summer, when differential heating of shallow shelf

waters creates a thin zone of less dense water within about 50 km of the coast. Currents resulting from this gradient were less than 1 cm s^{-1}. The hydrographic summary was also used to determine the vertical stratification during the summer which did prove to have a substantial effect on modeled currents.

Including LC effects in the seasonal circulation pattern involved a number of uncertainties, particularly regarding the seasonal position of the LC and the mechanism by which the LC directly affects shelf waters. As a best estimate, the LC effects were modeled using a lateral shear mechanism consisting of a steady, alongshore velocity applied at the model western boundary with a magnitude varying linearly from 0 at the northern tangent to 100 cm s^{-1} at the southwestern corner. In the vertical, the current was applied on the upper 50 m of the water column. The northern tangent of the LC with the shelf was assumed to be 24, 26, and 28^{o}N latitude for the fall-winter, spring and summer seasons, respectively. This is consistent with the existing theory on the annual cycle of the LC.

The total fall-winter circulation indicates a dominant southerly flow at all levels. Surface currents are on the order of 10 cm s^{-1} on the shelf. The spring and summer currents are generally smaller in magnitude and have a more complicated circulation pattern characterized by a southerly surface current in waters seaward of the 50 m isobath and a northerly surface current along the coast extending north to Apalachicola. These features are consistent with drift bottle observations and the in situ current data. The model in its present form does not include any effects of migrating eddies as this is not justified by the existing data base and is beyond the present formulation of the model.

RECOMMENDATIONS

Model verification, tuning and production runs were severely limited by the lack of high quality in situ current and coincident hydrographic data.

Further work with the existing data sets should include: (1) real time hindcasts of the drifter data, (2) analysis of long term coastal surface elevations to determine possible LC effects, and (3) investigation of the eddies observed on the shelf during the Winter 1973 SDE experiment.

Present results of the model should be regarded as preliminary and should be upgraded as new data become available. Within the next two years a number of new data sets will exist including:

1. current meters deployed at four sites by Florida State University east of Cedar Key during the winter of 1981-82;

2. hydrographic data taken on the southwest Florida shelf for MMS by Woodward-Clyde; and

3. oceanographic data on the shelf taken as part of MMS's Gulf-wide long-term data collection program.

It is strongly recommended that the MMS study include a specific attempt to measure the surface elevations, currents and hydrography of migrating eddies on the shelf. This is probably best accomplished by using Lagrangian drifters or by frequent relocation of Eulerian devices.

Chapter 2

Introduction

2.1 Study Purpose

The southwest Florida Shelf is an area in the Gulf of Mexico bounded on the east by the Florida coast, on the west by the 100 meter depth contour, on the south by the Florida Keys, and on the north by latitude 28°N. Because of modeling considerations, the area was expanded northward to include the area from 28° to Apalachicola (30° N), and westward to the 200 m isobath - essentially the contiguous West Florida Shelf (WFS). Figure 2.1.1 denotes the study area.

The motivation for the this study arises from the Minerals Management Service's (MMS) intention to grant leases for oil exploration on the southern shelf, and the Service's attendant need to estimate the probable destination of water-borne pollutants originating from drilling and production activities. Having information on the seasonal circulation patterns of shelf waters is essential in determining the eventual fate of pollutants.

The purpose of the study described in this report was to develop a capability for predicting seasonal water circulation on the WFS. This predictive capability was developed by:

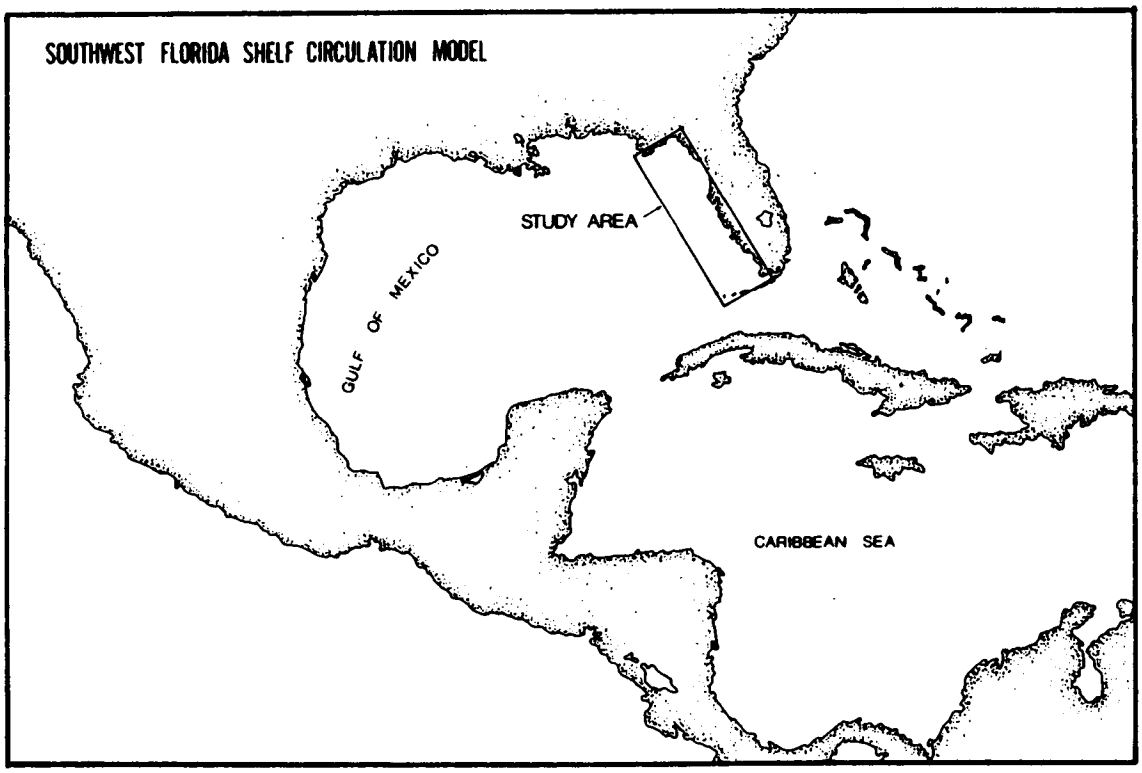

Figure 2.1.1: West Florida Shelf Study Area

1. adapting an existing numerical hydrodynamic model to the shelf;

2. testing the model with appropriate existing data from the shelf;

3. recommending additional data collection efforts needed to improve the model's effectiveness, and;

4. documenting the model for use by MMS personnel.

In addition, the model results are to provide quantitative values of residual surface circulation for use in the Department of the Interior's oil spill risk analysis model. The term residual is defined here to denote time scales on the order of several days to months. Shorter term wind phenomena are accounted for by Interior's risk analysis model.

Because information about currents at the surface, mid-depth and bottom of the water column was required, a fully three-dimensional model was necessary. The numerical model selected for use in this study is a Galerkin, three-dimensional model (Cooper and Pearce, 1977, 1982), referred to in this report as "GAL", and described in Chapter 3.

2.2 Methodology

The study involved four separate phases:

1. Literature review and data search;

2. Model modifications and basic sensitivity studies;

3. Model verification and tuning; and

4. Prediction of seasonal circulation patterns

During Phase 1, an exhaustive search of the oceanographic literature and data bases was undertaken to identify previous studies which concerned either the Gulf Loop Current (LC) or the WFS. The initial effort was subcontracted to Tetra Tech, Inc. and their results are available as a separate report. There were two purposes to the search: to review analytical and interpretive sources which discussed the WFS circulation, and to gather sources which might provide the raw data needed for model forcing inputs and for comparison to model results. The initial effort by Tetra Tech was updated by NECE throughout the study.

Phase 2 involved modifying the original model to suit the precise site conditions of the WFS. Major modifications included:

1. Provision for model forcing due to horizontal density gradients,

2. Improvement of lateral shear stress parameterization,

3. Horizontal discretization (grid system selection) to suit the WFS and its unique boundary conditions,

4. Provision for spatially variable Coriolis parameter, required by the large scale of the modeled area, and

5. Reorganization of the program coding into modular units.

Several of the changes in the model required analytical verification. That is, the model was run and compared to simple cases for which analytic results could be computed. These tests confirmed the validity of the model coding and implementation of the modification.

During Phase 3 of the study, hindcasts were made of historical events on the WFS. Three real-time periods were selected in which other investigators had collected either current velocity data or water surface elevation data, and for which information on winds over the WFS was also available. The wind data were used to drive the model and results were compared to low-frequency, real-time velocity and sea level data. Model parameters (e.g., bottom friction and eddy viscosity) were then adjusted (within bounds justified by physics) to achieve a best fit between model results and data. Upon completion of Phase 3, the model had been shown to be theoretically valid and to give a reasonable reproduction of observed hydrodynamics of the WFS.

For Phase 4, it was necessary to develop a long-term picture of the forces driving the WFS circulation. Review of the data on the WFS in conjunction with model sensitivity studies indicated that the residual circulation was primarily governed by three mechanisms: the LC, differential heating, and wind. The long-term values of these driving forces were used separately as model inputs, and the model exercised for each one until it reached steady-state. Superposition of the individual results produced an atlas of the composite residual circulation.

The model itself was fully documented and training of MMS personnel in its use was conducted.

Chapter 2 of this report discusses the results of Phase 1. A graphical summary is included in Appendix A. Chapters 3 and 4 and Appendices E and F include the results of Phase 2. Chapter 5 and Appendices B and G describe Phase 3 efforts, and Chapter 6 summarizes Phase 4. Recommendations for future work are given in Chapter 7. Appendix C contains technical papers written and presented by NECE which involve work on the WFS circulation model and Appendix D contains a summary of the model input parameters for important model runs. Appendices H and I present a detailed User's Manual for the model and are available as a separate volume.

2.3 Overview of the West Florida Shelf

BATHYMETRY

The WFS slopes gently (1:2000) from the coast to a shelf break at the 100 m isobath which lies approximately 200 km from the coast. The Florida escarpment is generally reached within 50 km of the 100 m isobath. Bottom contours in the study area are generally regular and parallel to the coast (Figure 2.3.1). To the north, the Florida panhandle forms a solid barrier and to the south, the Dry Tortugas and Florida Keys form a partial barrier to shelf circulation.

METEOROLOGY

WFS weather patterns may be classified into three seasons as implied by the monthly resultant wind vectors at Key West (Figure 2.3.2). Summers (May-September) are dominated in the southern portion of the shelf by the southeasterly trades and cumulous convection systems. Tropical storms occur infrequently during mid and late summer but can significantly bias short term wind records. Average winds during the summer are the weakest of any season. Figure 2.3.3 shows typical low-frequency (i.e. periods of greater than one day) offshore wind stress during the summer of 1974.

Fall-winter (October-February) meteorology is dominated by the passage of frontal systems every 7 to 10 days as illustrated in Figures 2.3.4-5. The first figure shows the low-frequency wind vectors at the NDBO data buoy during February 1978. The sinusoidal character of the winds is due to the passage of the frontal systems, an example of which is shown in Figure 2.3.5.

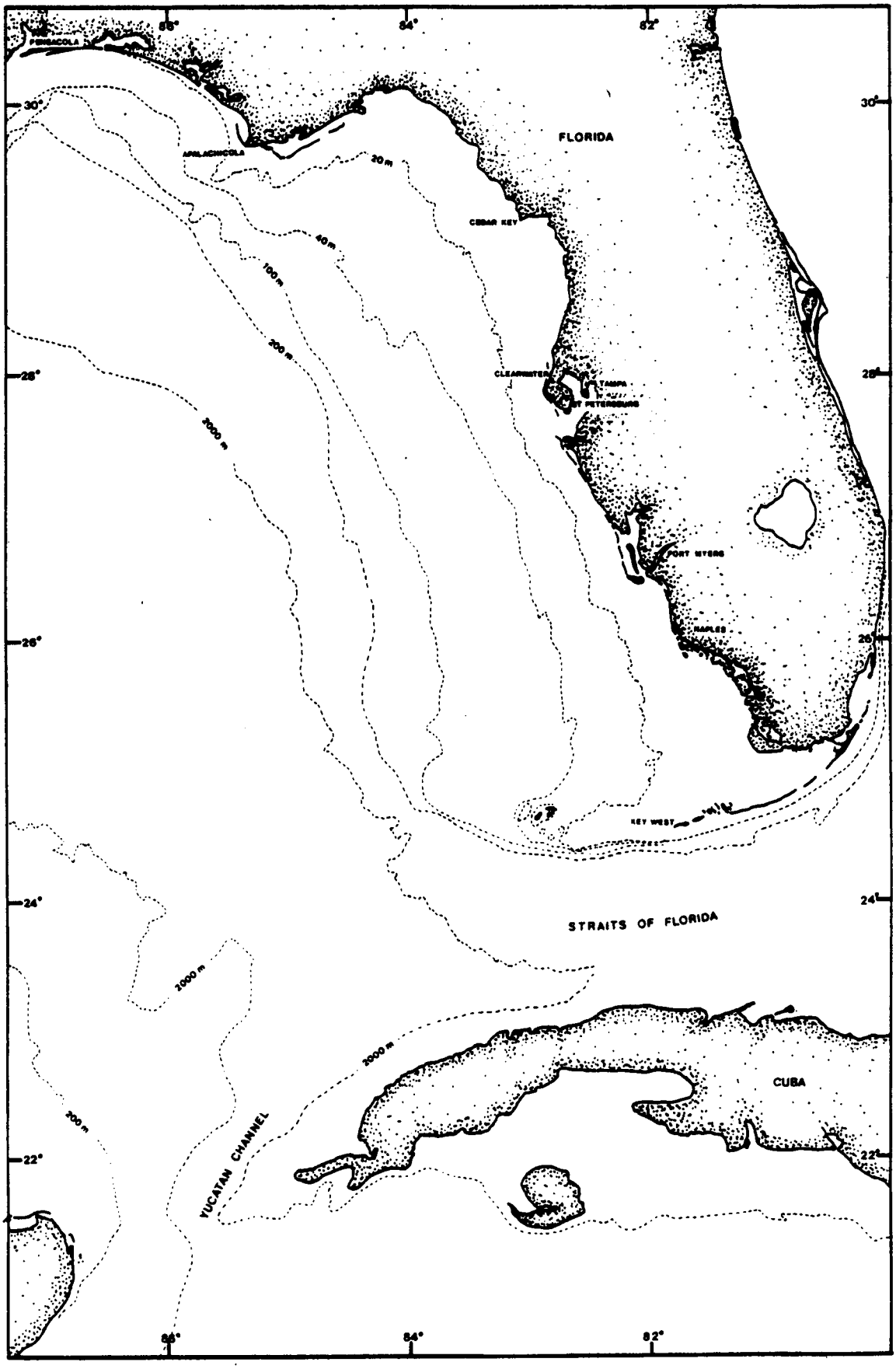

Figure 2.3.1: Bathymetric Chart of Study Area (from NOAA 411).

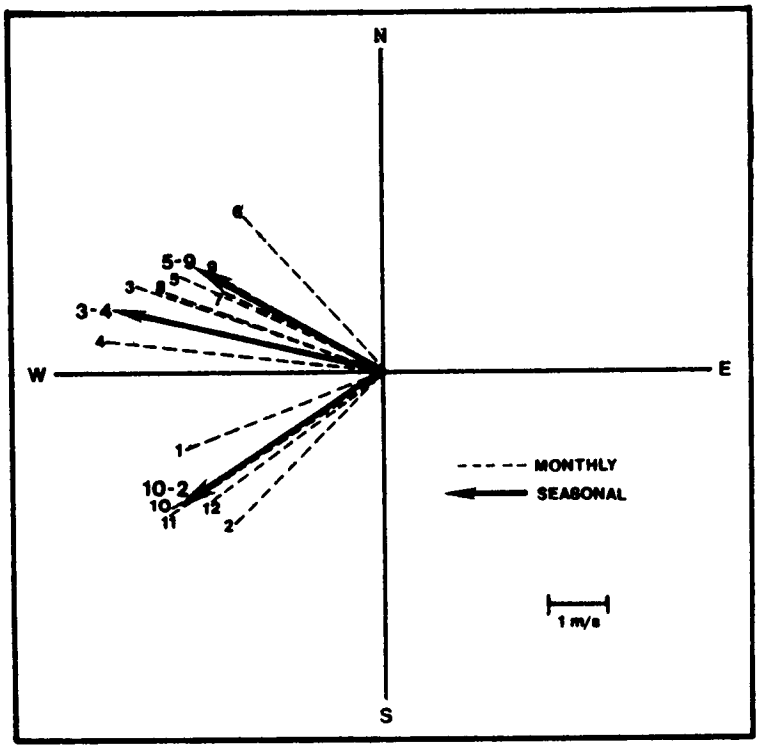

Figure 2.3.2: Mean monthly and seasonal winds at Key West, as derived from average monthly wind stress according to Wu (1980).

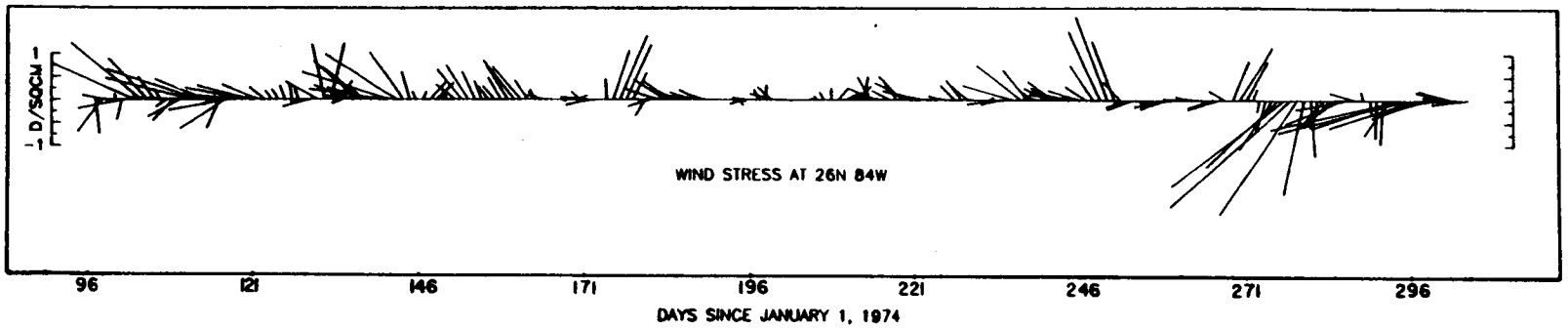

Figure 2.3.3: Vector plot of offshore wind stress for summer 1974 (Partagas, 1973a).

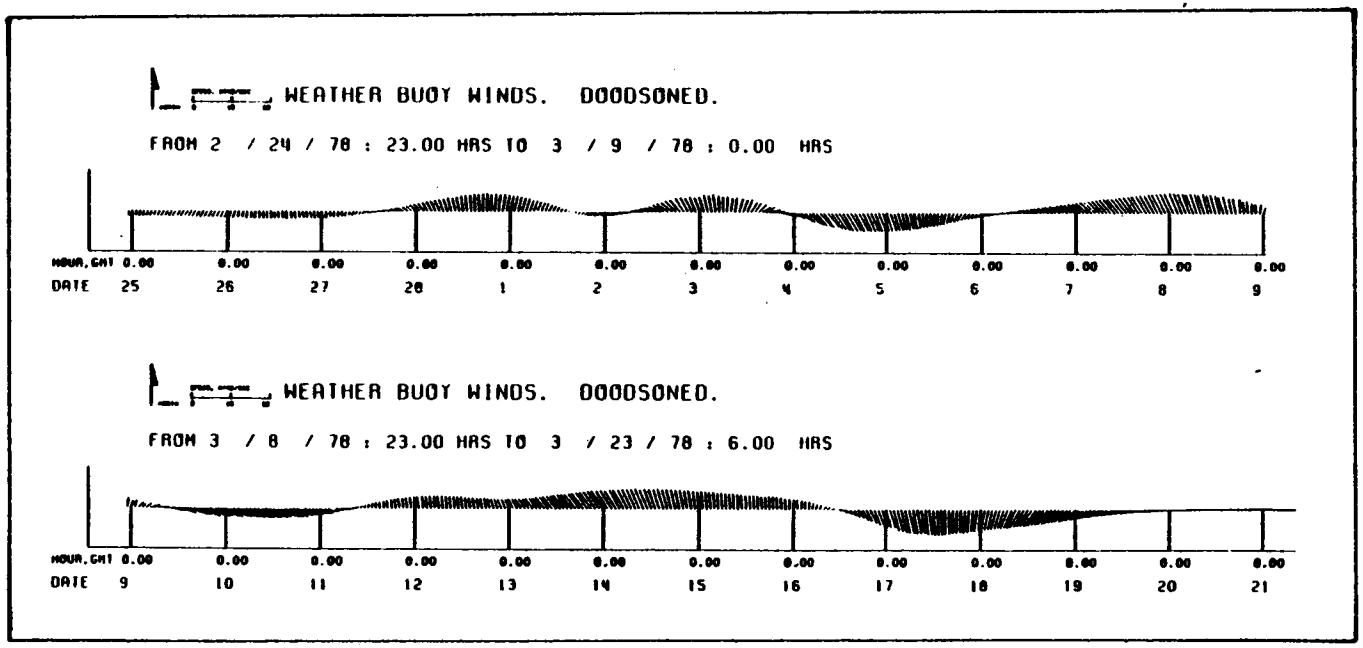

Figure 2.3.4: Vector plot of offshore winds for February, 1978.

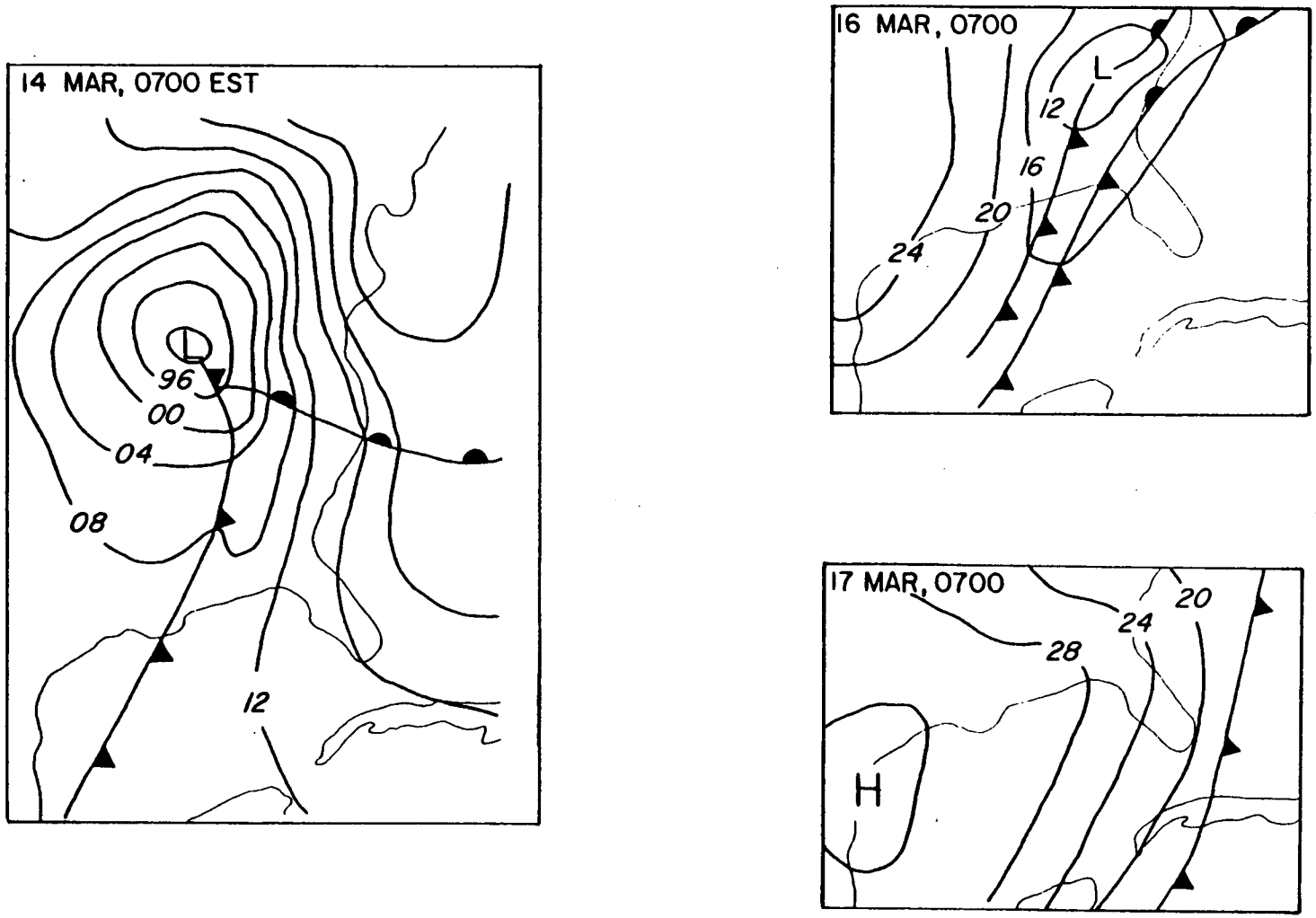

Figure 2.3.5: Typical movement of fronts which dominate winter meteorology on the WFS (Molinari, 1978).

The low on 14 March generated an extended period of southerly winds on the WFS as seen in the wind record at the data buoy. During the following three days a high pressure system moved into the area from the west and caused a shift to northerly winds.

Spring (March-April) is a transition period. While wind direction is very similar to the summer, the mean wind speeds for this period are substantially stronger than either the summer or winter winds.

TIDES

The mean range of the astronomical tide is 0.40 meters at Key West, and 0.30 meters near Apalachicola. The tide on the coast is diurnal and mixed semi-diurnal in the south; becoming primarily diurnal in the north at Pensacola. Figure 2.3.6 shows M2 tidal current ellipses for several stations in the southern portion of the shelf. The extreme current occurs at station V and is less than 10 cm s^{-1}. This would cause less than 1 km of advection during a half tidal cycle. There is no evidence of residual currents due to tides. However, in some regions, such as the North Sea and the Bay of Fundy, tides do contribute substantially to net advection. Typically these residual tidal currents are an order of magnitude less than the peak tidal currents. If this relationship is taken as a rule of thumb, then residual tidal currents on the WFS would be expected to be about 1 cm s^{-1}, clearly a negligible quantity. Therefore, tidal forcing was not included in the modeling effort.

LOOP CURRENT

The LC is the dominant flow regime in the eastern Gulf and clearly affects sites on the WFS. Entering the Gulf of Mexico in the Yucatan Channel with velocities on the order of 100 cm s^{-1} (Chew, 1974), the LC swings northerly and easterly in a wide loop, before exiting the Gulf via the Florida Straits, to become the Atlantic Ocean's Gulf Stream. Occasionally, large anticyclonic

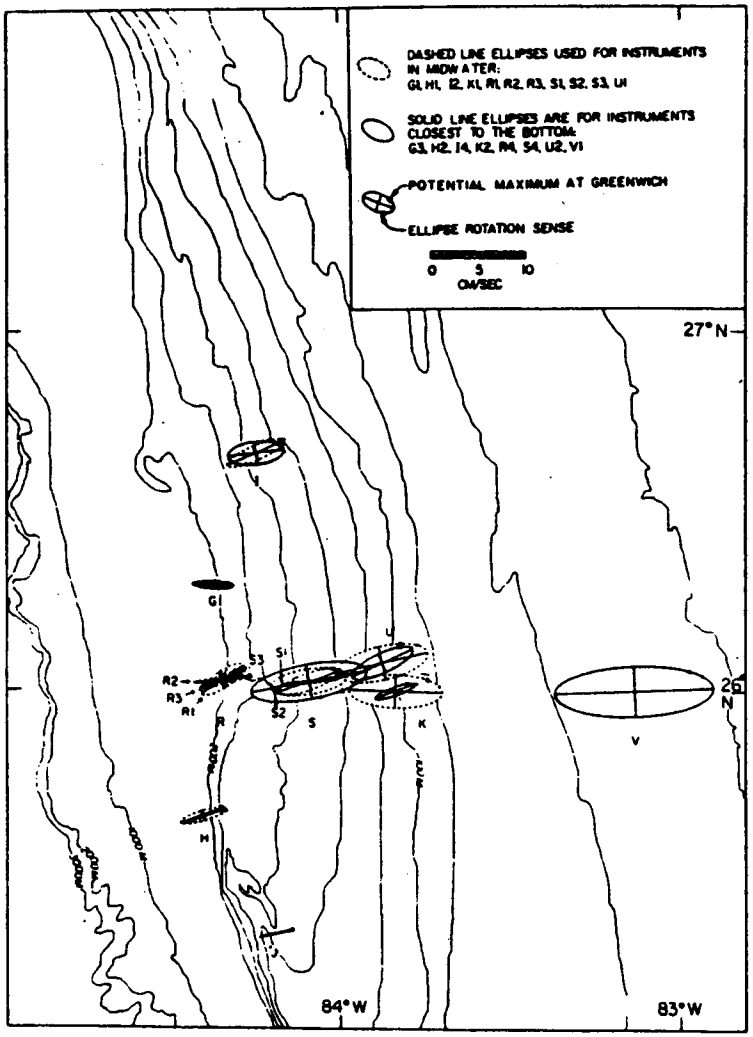

Figure 2.3.6: M2 tidal current ellipses (Koblinsky and Niiler, 1980)

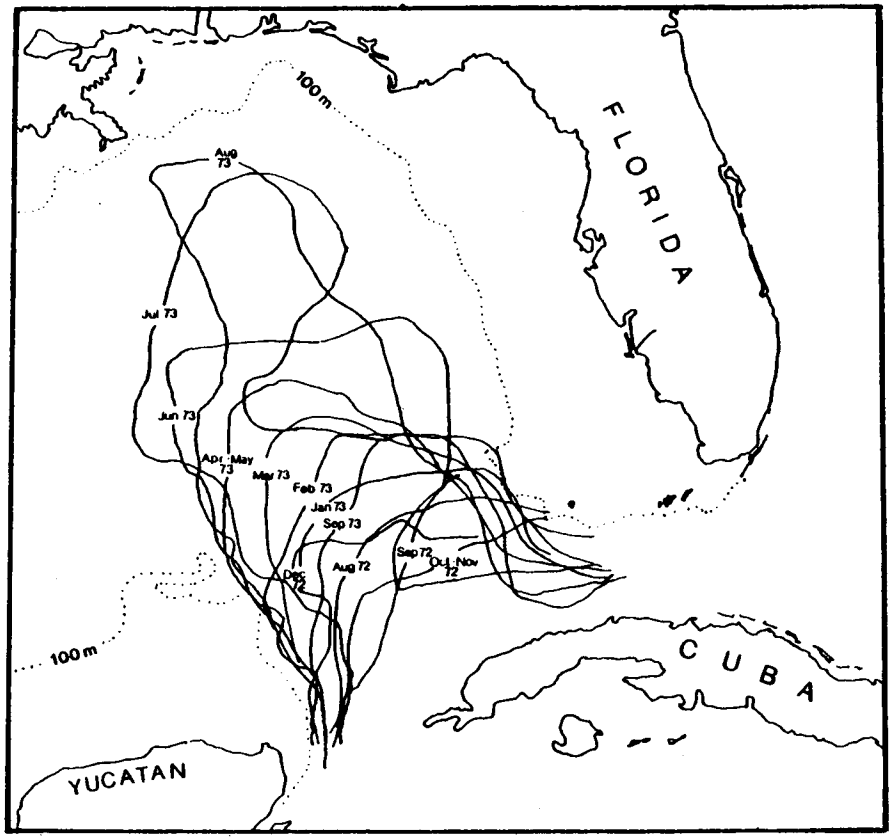

Figure 2.3.7: Monthly mean position of the northward extent of the Gulf Loop Current during 14 months of observations (Maul, 1974).

gyres break off from the LC. These eddies migrate to the western Gulf with a speed on the order of 1 cm s^{-1} and diameter on the order of 100 km.

Usually the LC is channeled on the east by the edge of the WFS, but frequently LC waters intrude onto the WFS itself. The LC is marked by high salinity (greater than 36.3 °/oo) and its intrusions on the WFS can be identified by the occurrence of high salinity water masses.

The northward extent of the LC varies substantially in time, covering approximately 500 km during quasi-annual periods. Figure 2.3.7 demonstrates the mobility of the LC, showing the mean monthly position of the northward extent of the LC for several years. Leipper (1970), Behringer et al. (1977), and others have argued that the LC displays a yearly cycle - intruding during the spring and retreating in the fall. However, the evidence is by no means overwhelming, and at the very least displays considerable scatter.

HYDROGRAPHY

The hydrographic regime on the WFS shows substantial variability, some of which is due to seasonal changes and some due to the LC. In the winter, the shallow shelf waters are well mixed and no vertical density gradient is normally apparent. Seaward of the 100 m isobath, a mixed layer does appear. The mean winter densities range from 24.5 to 26.4 as sigma-t (Table 6.1.2). Normally, no horizontal gradients may be expected in the winter, except during periods of LC intrusion when warm, saline LC waters may cause local horizontal density gradients. These anomalies from the LC can be traced to at least the 50 m isobath. Figure 2.3.8 shows a typical winter transect. A 100 m mixed layer is apparent as is a frontal zone (station 314) originating from the LC.

In summer the mixed layer depth is about 30 meters (Niiler, 1976). Mean densities in this upper mixed layer range from 22.3 to 23.6 as sigma-t (Table

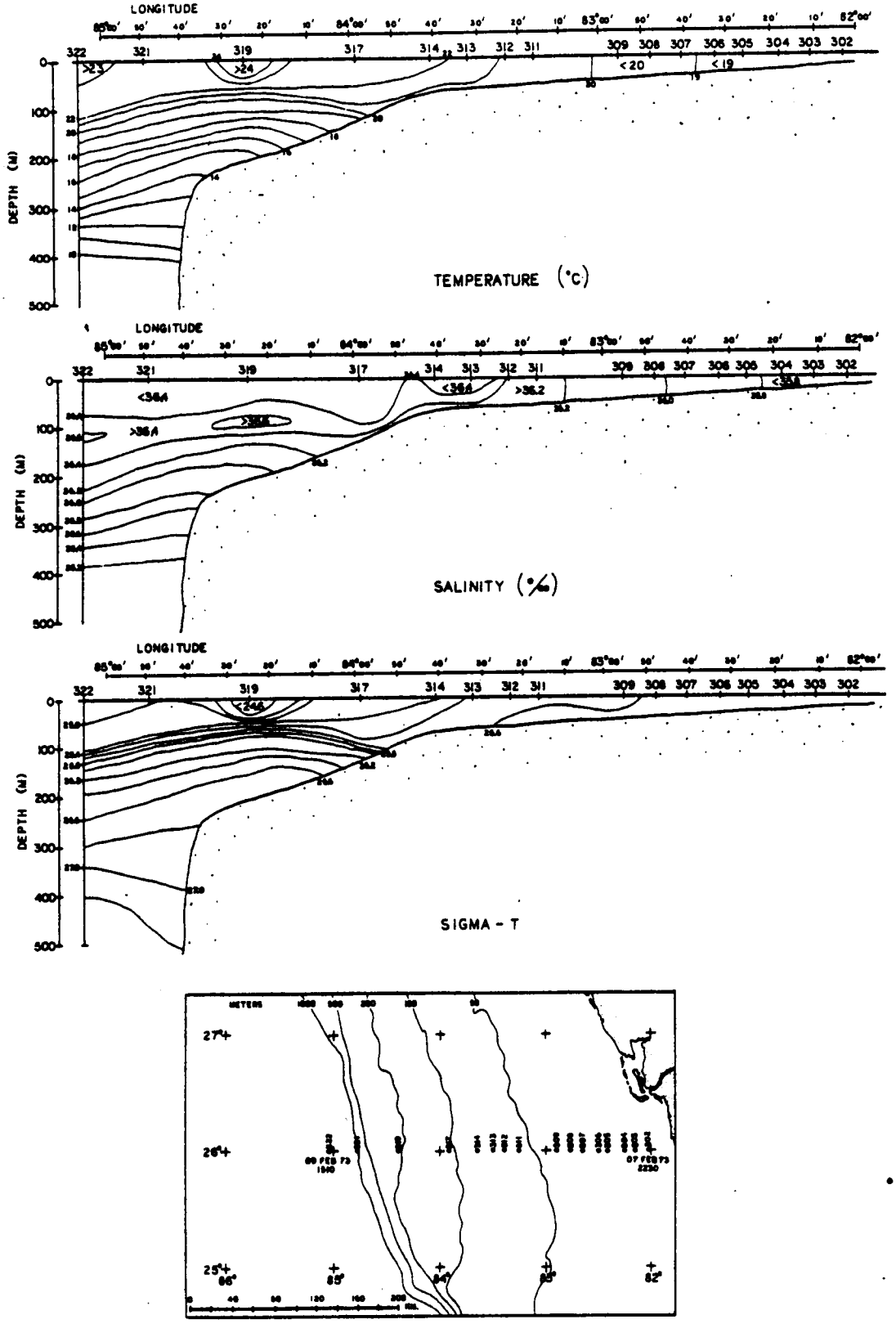

Figure 2.3.8: Winter Hydrographic Transect (Price and Mooers, 1974d)

6.1.1). The lower layer exhibits a range of 23.2 to 25.6. Mean horizontal gradients of up to 1.9 (sigma-t) per 100 km are observed in summer. Figure 2.3.9 shows a hydrographic transect taken in early fall. Stratification typical of summer conditions is still readily apparent.

Hydrographic data demonstrate that complex eddies and frontal systems densely populate the WFS and that these are due to the interaction of shelf water with the LC. The influence of these systems on circulation is poorly understood.

2.4 Overview of Existing Data

A number of circulation studies have been conducted on the WFS, and the locations of the major studies are shown in Figure 2.4.1. A more complete description of the available data base is given in Appendix A. Briefly, the studies include:

1. Shelf Dynamics Experiment (SDE) (e.g. Price and Mooers, 1974a,b,c,d) consisting of extensive current meter arrays, bottom mounted pressure gauges, and hydrographic transects covering approximately 2 years beginning in October 1973.

2. FSU (Mitchum and Sturges, 1981) study consisting of two current meter arrays deployed for 22 days in February-March 1978.

3. Hourglass (Williams, et al, 1977) study involving release of drift bottles from 16 sites for 28 months beginning in 1965.

4. Tolbert and Salsman (1964) study involving release of drift bottles for

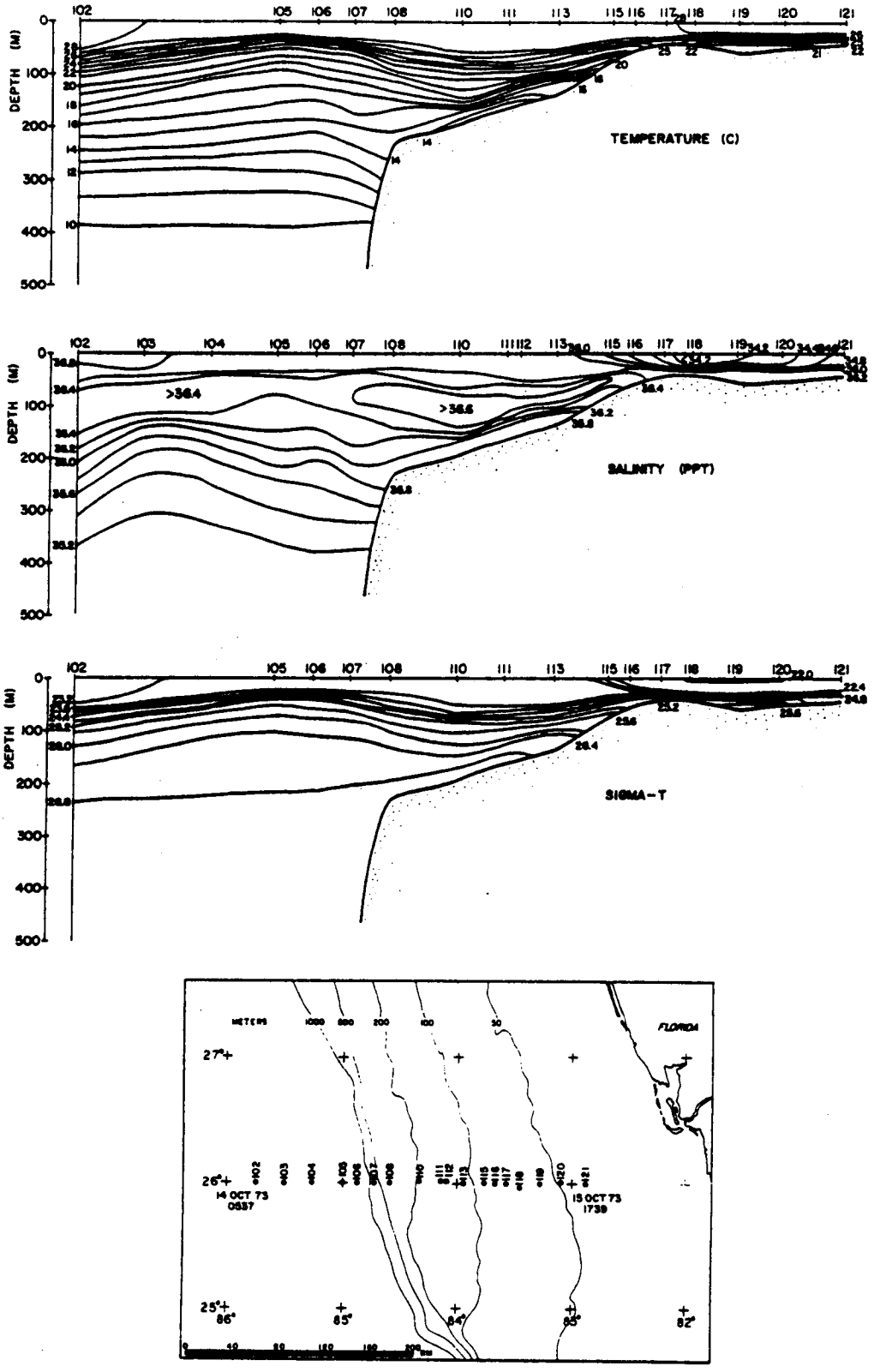

Figure 2.3.9: Fall Hydrographic Transect (Price and Mooers, 1974b).

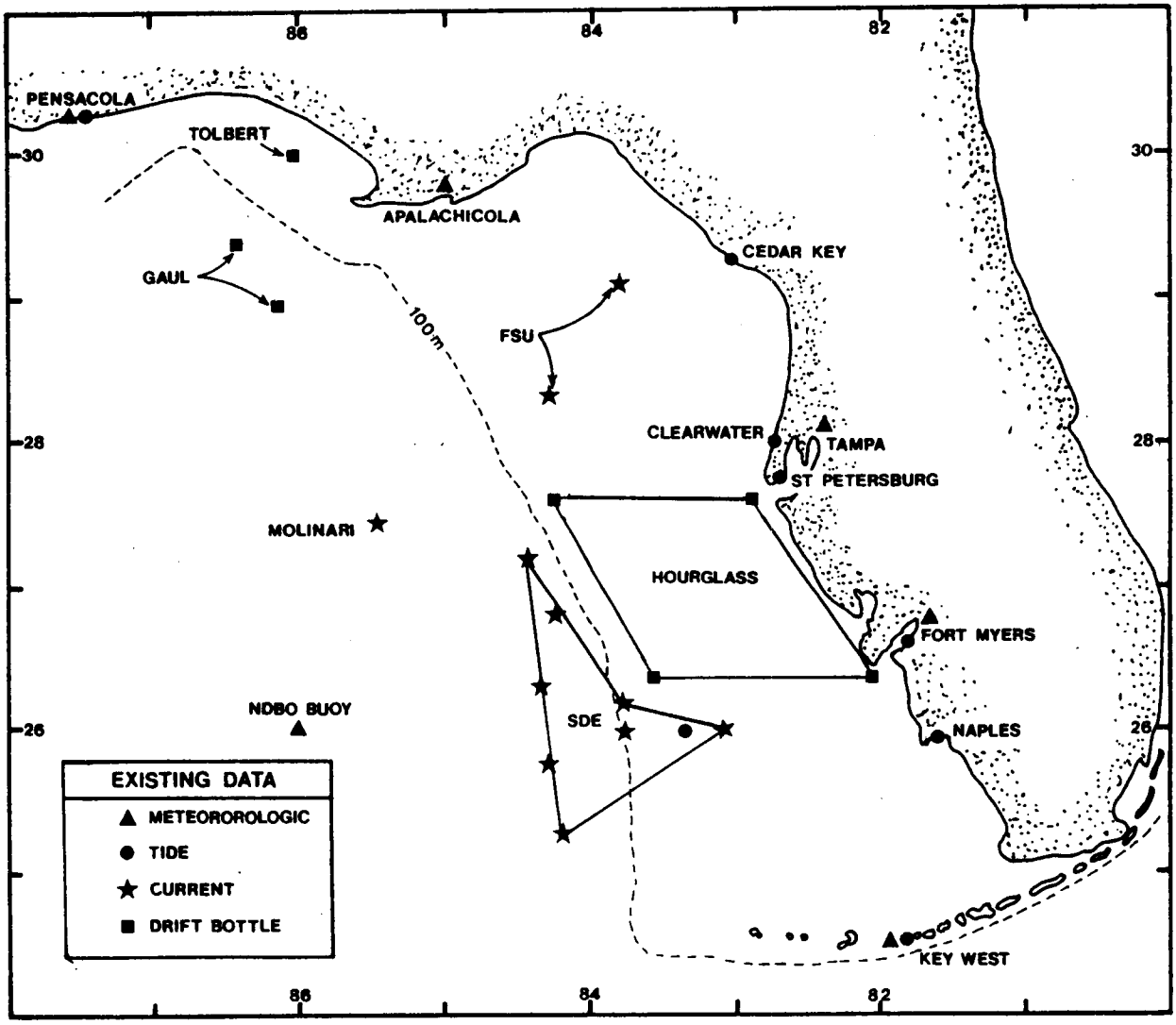

Figure 2.4.1: Source sites of major, existing oceanographic and meteorologic data.

28 months starting in September 1960.

5. Gaul (1967) study involving release of drift bottles for approximately 18 months in 1964-1965.

6. Molinari et al. (1979) study based on deployment of one current meter mooring for approximately 6 months.

The most extensive data set taken on the WFS is the SDE which covered the period January 1973 - May 1975. The study was a joint effort by Nova University, The University of Miami, and Florida State University. Figure 2.4.2 shows the location of the various stations where current meter and pressure data were recorded. All stations except W1 and L2 consisted of current meter arrays. Deployment schedules for specific instruments are given in Koblinsky and Niiler (1980). One of the most important aspects of the schedule from the standpoint of this study is the lack of long term current data on the shelf itself. Only two stations were located well onto the shelf (F and V on the 50 m isobath) and these stations yielded a total of about three meter months of data, all during the winter season.

In addition to institutional sources listed above, data are available from a number of government and private installations including:

1. National Weather Service (NWS) meteorology stations at Pensacola, Apalachicola, Tampa, Fort Myers, and Key West;

2. National Ocean Survey tide gauges at Pensacola, Cedar Key, Clearwater, St. Petersburg, Fort Myers, Naples, and Key West; and

3. National Data Buoy Office meteorology buoy #42003.

Appendix A gives a graphical summary of the locations and time of availability of the various types of data.

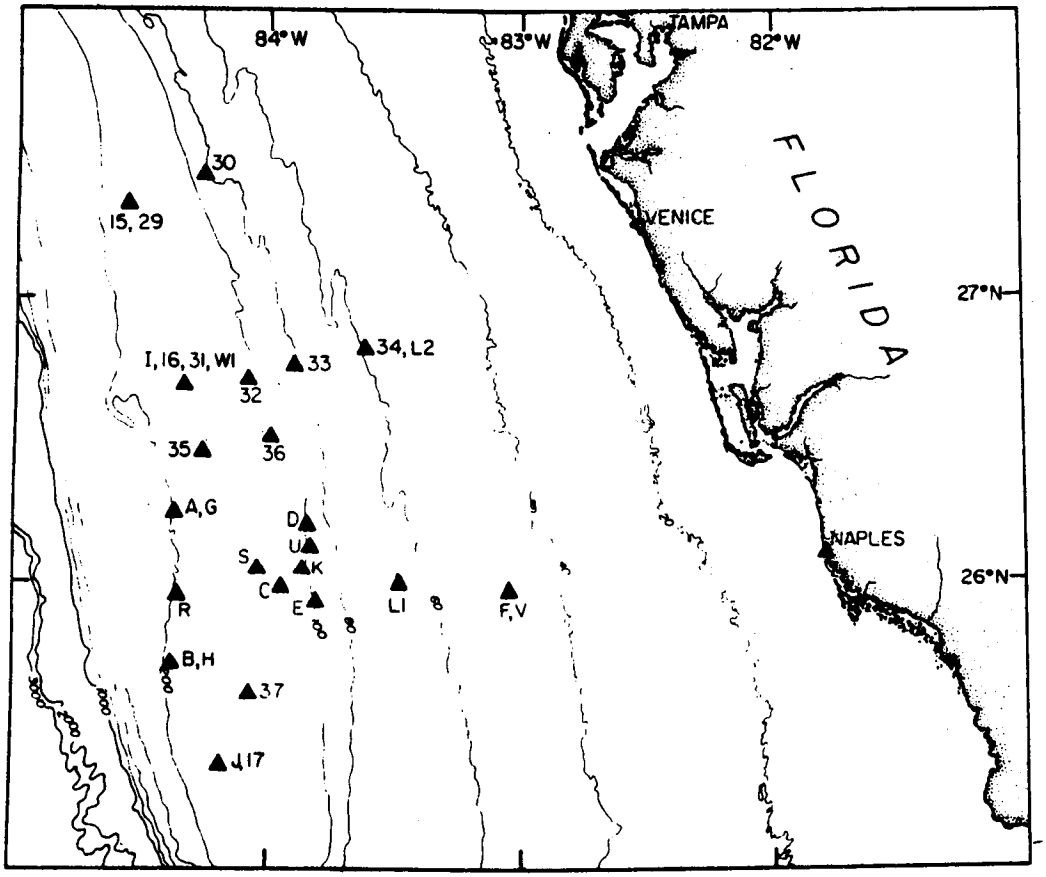

Figure 2.4.2: Shelf Dynamics Experiment array locations (Koblinsky & Niiler, 1980)

2.5 Literature Survey

Several investigators have contributed to knowledge of the circulation of WFS waters, using analytical, numerical, and interpretive methods.

A number of data reports were published from the SDE including Price and Mooers (1974a,b,c,d), Van Leer et al. (1974) and Plaisted et al (1975). These reports concentrated entirely on data presentation and reduction. Koblinsky and Niiler (1980) and Niiler (1976) seem to have been the only ones to offer published interpretation of the data. The analysis by Koblinsky and Niiler was restricted mainly to the M2 component of the astronomical tides. Neither publication attempted to relate the observed average currents to circulation patterns on the entire shelf, but this is understandable given the complexity of the currents at the SDE sites.

Niiler's (1976) discussion is the most relevant to this study. He focused on low frequency currents at sites near the shelf break in water of 100 m or deeper. He found:

1. no correlation between currents and wind except during the winter when weak coherence at the upper meters was apparent;

2. longshore currents were more energetic than cross-shelf currents. A broad peak in the spectrum existed between 0.04 cpd and 0.10 cpd;

3. Strong vertical coherence was found in this low frequency range for meters on the same mooring. There was significant horizontal coherence for these frequencies between stations on the same isobath; and

4. mean drift was dependent on depth, horizontal location, and season.

LOOP CURRENT EDDIES

Niiler suggested that the hydrodynamics in the study area were dominated by low frequency turbulence (i.e. eddies) derived from the LC. Maximum currents within the eddies are on the order of 60 cm s^{-1}. He conjectured the existence of an eddy field consisting of alternating cyclonic and anticyclonic, barotropic eddies which moved northward along the 150 m isobath as depicted in Figure 2.5.1. The eddies shown in the figure are part of a large sinusoid with a length of 600 km and 16 day period.

Kroll and Niiler (1976) studied the propagation of barotropic waves onto a shelf with characteristics similar to the WFS. They found the transmission of the waves to be dependent on wavelength with the most efficient transmission occurring for waves with a 12 day period and 600 km wavelength. The maximum penetration of the wave was the 40 m isobath.

Vukovich et al. (1978) studied the movement of meanders along the LC-WFS interface using satellite imagery. Figure 2.5.2 is a qualitative graphical sketch of the meanders. They reported that one to two meanders were observed each month with typical lengths of 200 km and periods of about 8 days. These characteristics are about one-half those suggested by Niiler, but it is not clear whether these processes are the same. For instance, Vukovich et al. (1978) observed the meanders to travel in a southerly direction as opposed to the northerly migration suggested by Niiler.

LOOP CURRENT INTRUSIONS

There is considerable evidence of intrusions of warm LC water onto the shelf. Vukovich et al. (1980) made the following comments regarding observed intrusions:

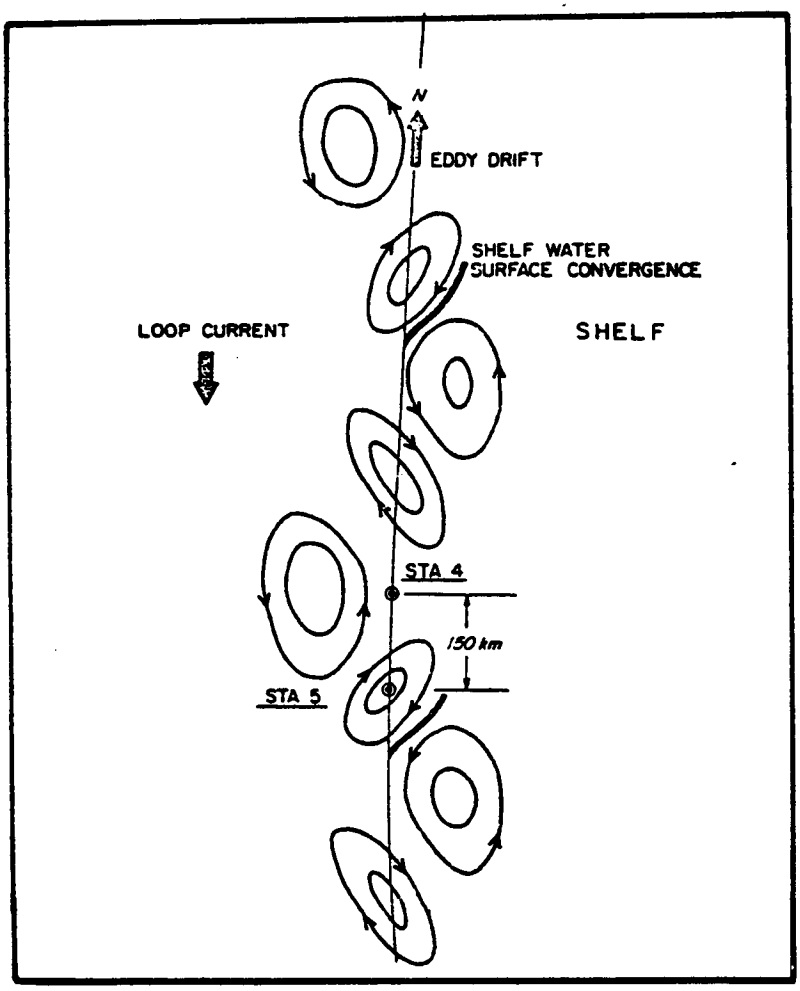

Figure 2.5.1: Eddy circulation conjectured by Niiler (1976).

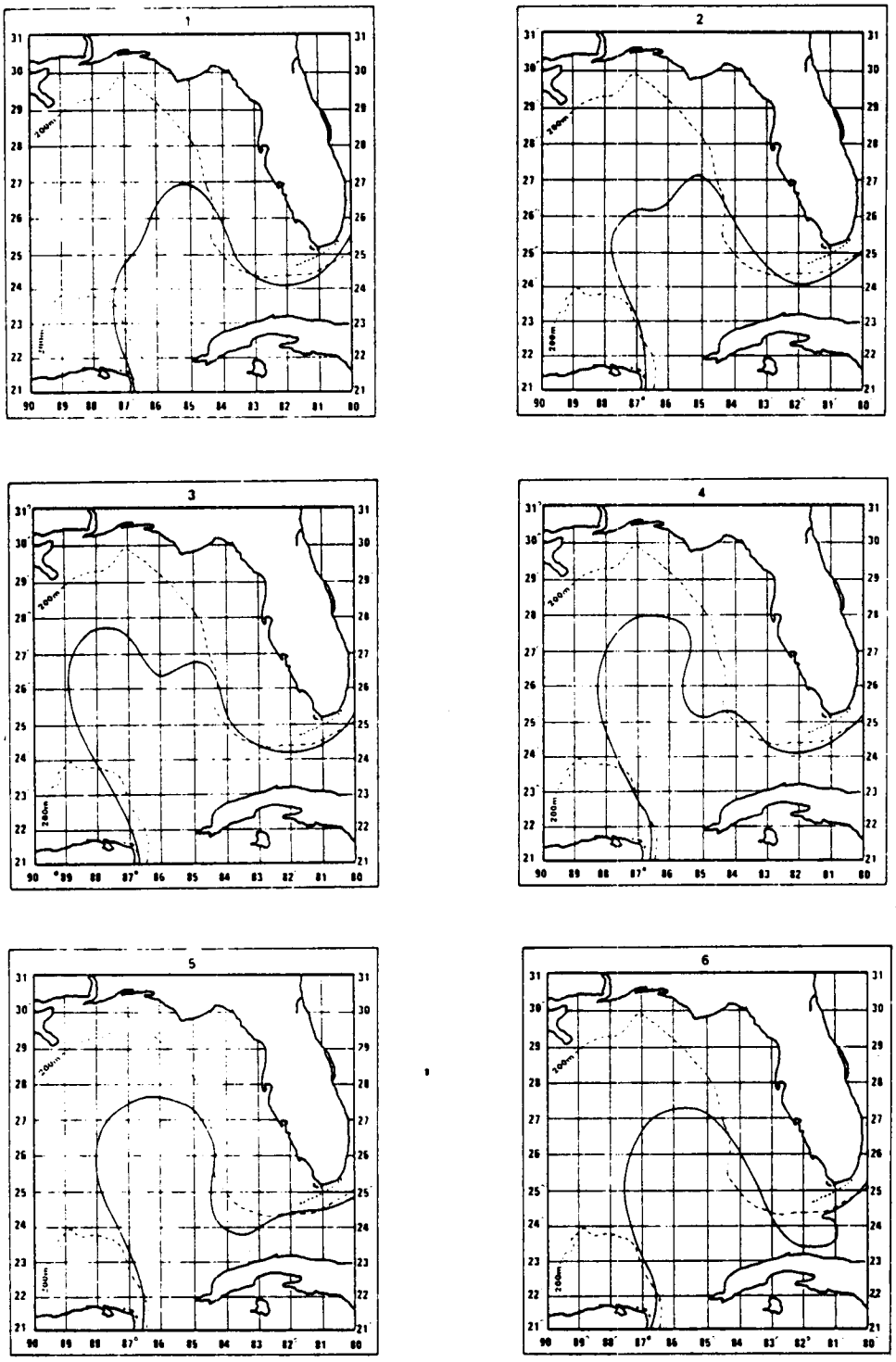

Figure 2.5.2: Movement of meanders on the boundary of the LC (Vukovich et al., 1978)

1. intrusions appear to be associated with the development of meanders;

2. intrusions typically lasted about 14 days suggesting that they were shallow in depth and extended on the order of 100 km from the main body of the LC; and

3. there were suggestions of cyclonic motion associated with the intrusions.

Huh et al. (1981) tracked an intrusion of LC water up DeSoto Canyon and onto the WFS to within 8 km of the Florida coast near Panama City during February 1977. Boat, aircraft, and satellite data were used to estimate the space and time scales of the intrusion. The duration of the event was 18 days and the speed of advance was 20 cm s^{-1}. They suggest that approximately half the intruded water receded off the shelf, and half dispersed and combined with indigenous shelf waters.

ANNUAL CYCLE OF LOOP CURRENT

As indicated previously, the northward extent of the LC varies by about 500 km during time periods on the order of one year. Cochrane (1965) proposed that the path for the LC might vary in response to an annual variation in the strength and cross-stream structure of the surface currents in the Yucatan Straits. Leipper (1970), Cochrane (1972), Maul (1977) and others have contributed limited observational evidence for a seasonal cycle in the LC, although each author identified considerable year-to-year variability in the data. Leipper and Maul hypothesized that the LC exhibited an annual cycle with an intrusion northward into the Gulf beginning in the spring, and subsequent spreading to the west in the fall.

Behringer et al. (1977) reviewed existing hydrographic data from 47 cruises and satellite data in the Gulf. They found that the penetration of the LC into the Gulf increased during the winter and spring, and reached a maximum in the early summer. They also found that there were substantial deviations

from the average sequence of events; the period between intrusions was as short as eight months and as long as seventeen months. Figure 2.5.3 is a plot of the compiled data as well as a temporal variation suggested by Behringer et al.

Recently, the annual cycle of the LC has been challenged by several including Molinari (1978) who pointed out that the data upon which the annual cycle was based were severely biased by the temporal sampling distribution. He cited maximum penetration during the winters (not summer) of 1966, 1969, 1973, and 1974 as evidence against the annual cycle.

Molinari's argument is supported by Vukovich et al. (1978, 1979). They presented satellite infrared and in situ data covering five years. The data indicated that major intrusions occurred during the winter as shown in Figure 2.5.4, and that there was significant variation in the LC position for any given month and year. These figures indicated little variation of the mean position of the LC from month to month due to the large variance associated with each month.

Hurlburt and Thompson (1980) have recently investigated the LC using a series of numerical models. They found that the LC penetrated into the Gulf, bent westward, and shed realistic anticyclonic eddies with 8-10 month periods. Periodic shedding of eddies was achieved without temporal variations in the inflow or outflow through the Yucatan and Florida Straits, and without considering baroclinic effects. Differential rotation (i.e. Beta effect) and the WFS topography were found to be essential for eddy shedding to occur in a realistic manner.

OFFSHORE CURRENTS

Current meter data off the WFS west of Tampa were taken by Molinari et al. (1979) at a site in 1000 m of water (Figure 2.4.1). Four current meters were installed at nominal depths of 150, 250, 550, and 950 meters. Data were

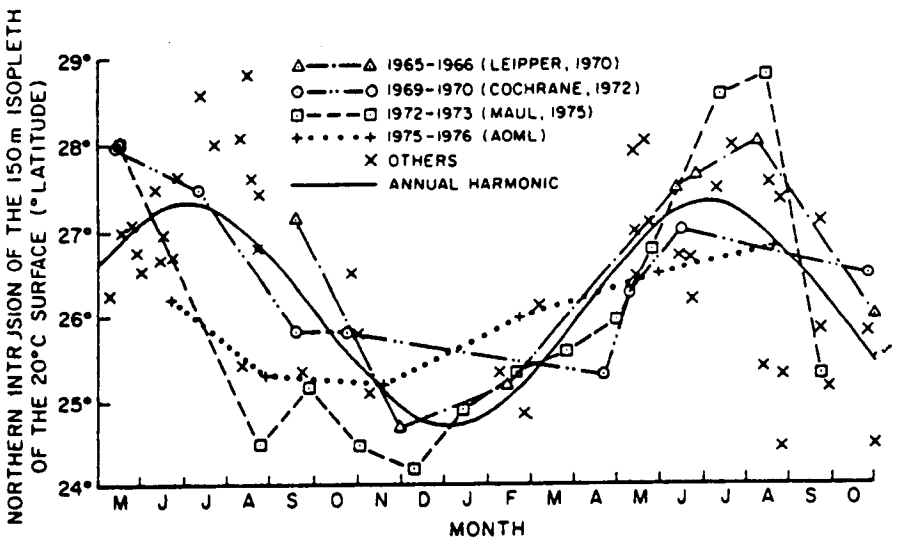

Figure 2.5.3: Annual cycle of the Loop Current (Behringer, et al., 1977)

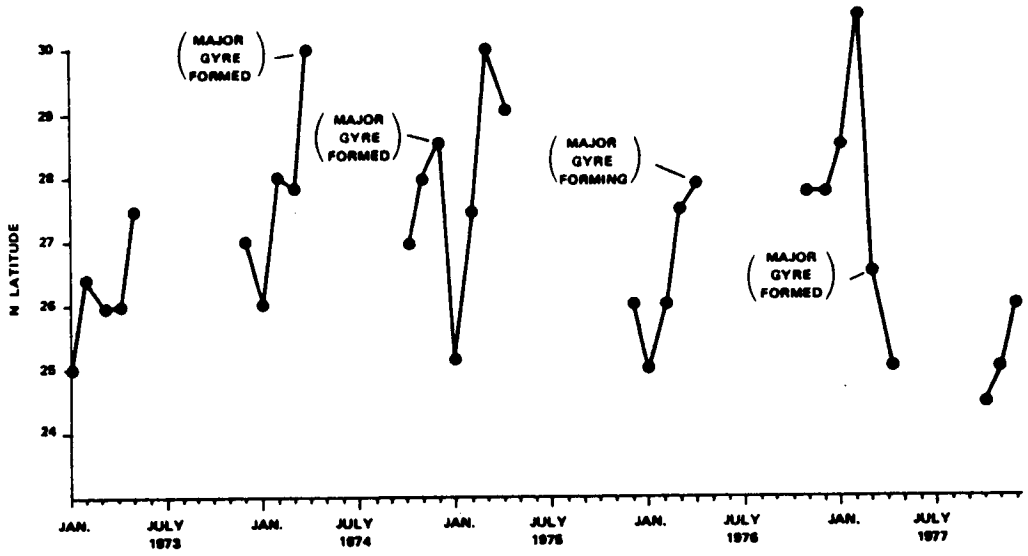

Figure 2.5.4: Northernmost position of the LC versus time based on satellite data (Vukovich, et al., 1978)

taken over a six month period beginning in June 1978. Although the site is some distance from the WFS, Molinari et al. (1979) offered some interesting and relevant conclusions:

1. roughly 10% of the average speeds exceeded 22-25 cm s^{-1} at all depths. Approximately 50% of the average speeds exceeded 10 cm s^{-1} at all depths;

2. a maximum speed of 70 cm s^{-1} was recorded at 150 m depth coincident with a cold front passage;

3. the mean flow was to the northwest at all depths;

4. effects of the LC were not generally detectable except for one occurrence when the LC reached to within 50 km of the site; and

5. mixed layer depths ranged from 60 m in winter to 5-10 m in summer.

RESIDUAL CURRENTS

There are a number of theories regarding residual currents on the shelf itself. Chew (1955a,b) interpreted summertime STD (salinity, temperature and depth) data and biological data to postulate the existence of two large cyclonic eddies; one off Tampa, extending to the 200 m isobath, the other east of the Mississippi Delta and extending eastward to Panama City. The first eddy he named the Florida West Coast Cyclonic Eddy. Chew hypothesized that the southbound LC acted as a Rossby jet, entraining WFS waters. The LC discharged some water onto the WFS to furnish power to drive the southern part of the cyclonic eddy.

Austin (1974) inferred currents on the northwest WFS from density fields, using data taken in early May, 1970. He suggested the existence of a cyclonic gyre in the bight between Tampa and Apalachicola. Other researchers have

utilized hydrographic data to infer current structure including Nowlin et al. (1968), Rinkel (1971), Rinkel and Jones (1973) and SUSIO (1975). These studies suggested a highly dynamic system which is significantly influenced at times by the LC.

Sturges and Shang (1978) have offered the sketch shown in Figure 2.5.5 as a means of stimulating discussion. The eddy shown in the drawing is similar to that proposed by Chew (1955a, b) and Austin (1974).

DRIFT BOTTLE STUDIES

In general, caution must be used when attempting to interpret drifter results, as they can be easily biased by a number of factors, including high frequency oceanographic processes, and coastal population distributions. After close scrutiny, it appears the drifter studies on the WFS have escaped these pitfalls and therefore can yield useful information.

Three major drift bottle studies have been conducted on the WFS. Project Hourglass, reported by Williams et al. (1977), lasted 28 months from 1965 to 1967. Surface drift bottles were released periodically from the area shown in Figure 2.4.1 at 16 sites shown in Figure 2.5.6. Williams et al. suggested that eddy complexes from the LC were an important feature which may have influenced circulation of surface waters from the release area. These eddies seem to be the most plausible explanation for the rapid divergence seen in some of the releases, e.g. Figure 2.5.6a. Note that there were several cases similar to the release at station E in which bottles released at the same point and time, end up hundreds of kilometers apart. Williams et al. also noticed a northerly longshore current in spring and summer (e.g. 2.5.6b) and attributed it to: "cyclonic eddies associated with the LC". Several of the release sites were situated within 30 km of the shore and were clearly dominated by the land-sea breeze. Over 60% of the bottles landed in the Keys or the East Coast. Only about 8% were found in the northern and western portion of the Gulf.

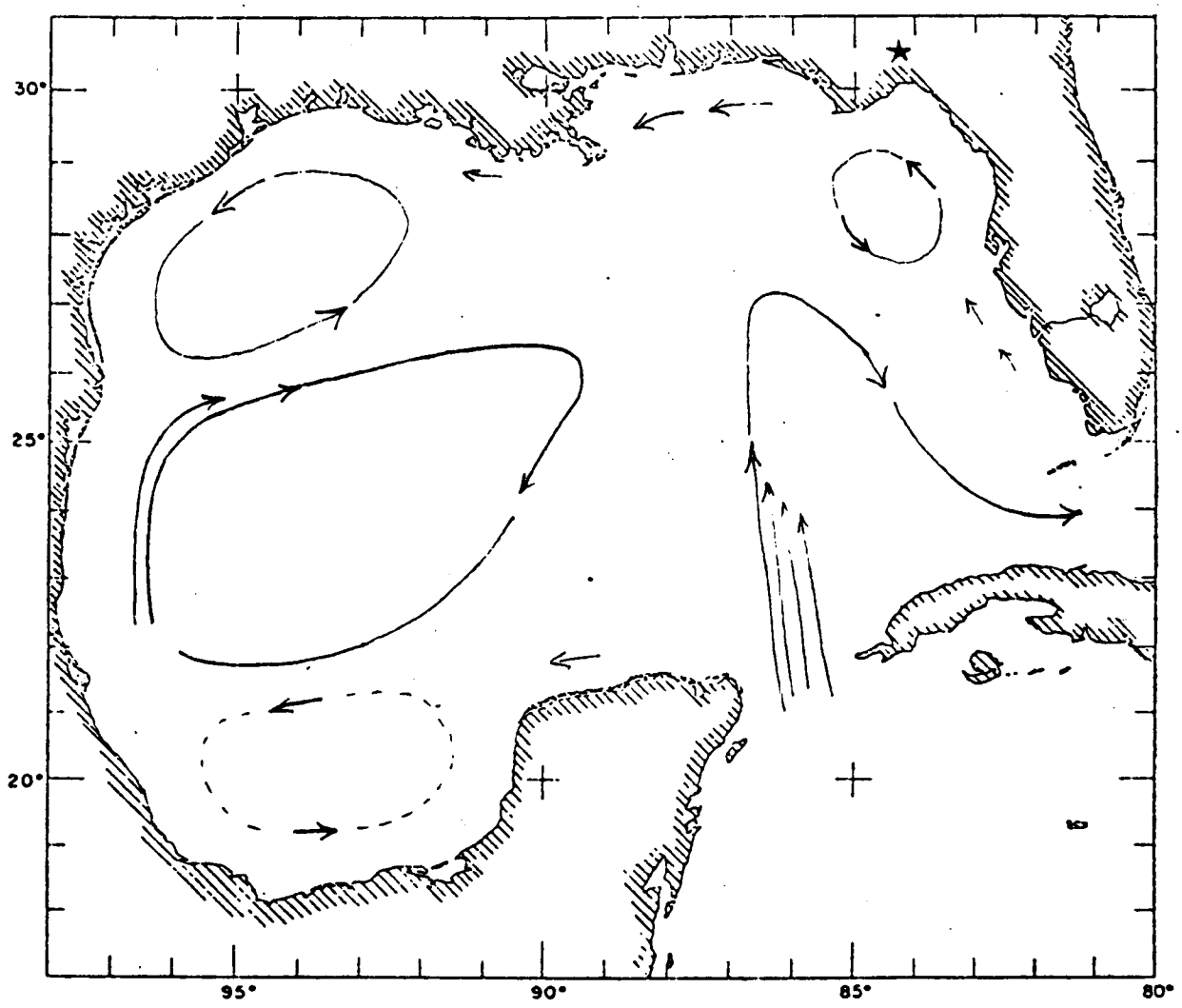

Figure 2.5.5: Eddy circulation suggested by Sturges & Shang (1978).

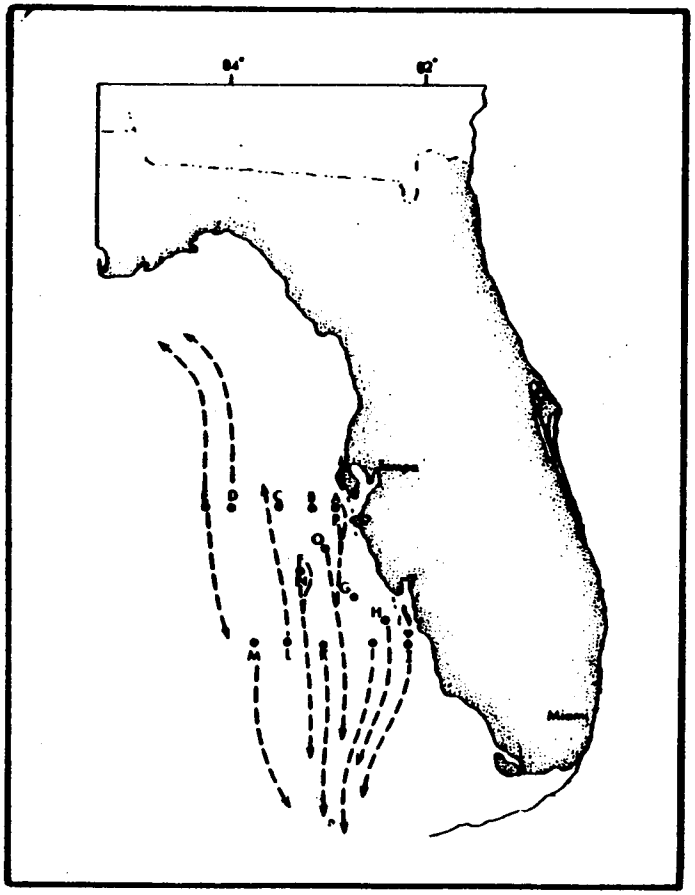

Figure 2.5.6a: Hourglass drift bottle release, November, 1965 (Williams, et al., 1977)

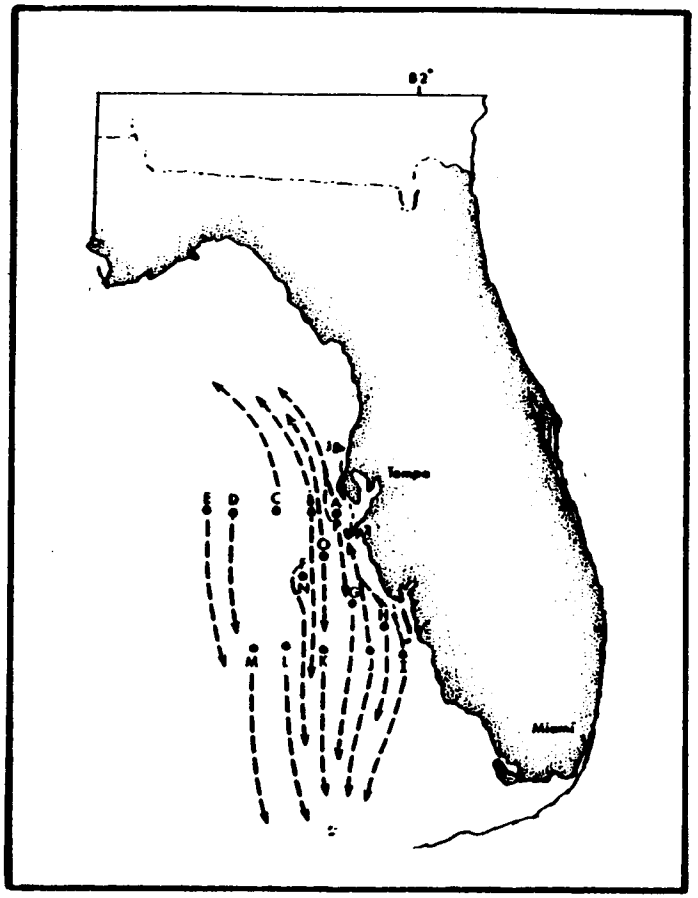

Figure 2.5.6b: Hourglass drift bottle release, April, 1966 (Williams, et al., 1977)

Tolbert and Salsman (1964) reported on surface drift bottle data taken over a 28 month period beginning in September 1960. Daily releases were made from a platform 20 km off Panama City, Florida as shown in Figure 2.4.1. The bottles were released within the land-sea breeze zone where typical diurnal winds could easily advect drifters ashore in less than one-half cycle. As a result most (67%) of the bottles were blown ashore between Apalachicola and Pensacola on the north Gulf coast. Twenty percent of the returns, however, were from the Florida Keys and the east Florida coast, implying speeds up to 35 km day^{-1} and suggesting that the LC was at times also a significant factor in surface water transport from the area. Only five bottles were found on the west Florida coast between Apalachicola and the Keys.

The third major drift bottle study was performed by Gaul (1967) and was graphically summarized by Ichiye, et al. (1973). Releases were made off the Pensacola-Panama City area at two sites shown in Figure 2.4.1. The study period extended from April 1963 to October 1964. Releases typically ended up to the south - on the east Florida coast and Florida Keys. However, during certain periods, a significant number of releases ended up on the Texas and Mexican Gulf coasts. Only a small portion of releases (i.e. 2%) were found along the west Florida coast between the Keys and Apalachicola.

When viewed as a whole the three drifter studies offer some interesting insights into the WFS circulation. Figure 2.5.7 shows the location of the release sites for the three studies and summarizes the results of each of the studies. Three conclusions are apparent:

1. an overwhelming number of drifters were found in Zone 1 during the fall and winter (October-February);

2. substantial numbers of drifters were found in Zone 1 during the remainder of the year; and

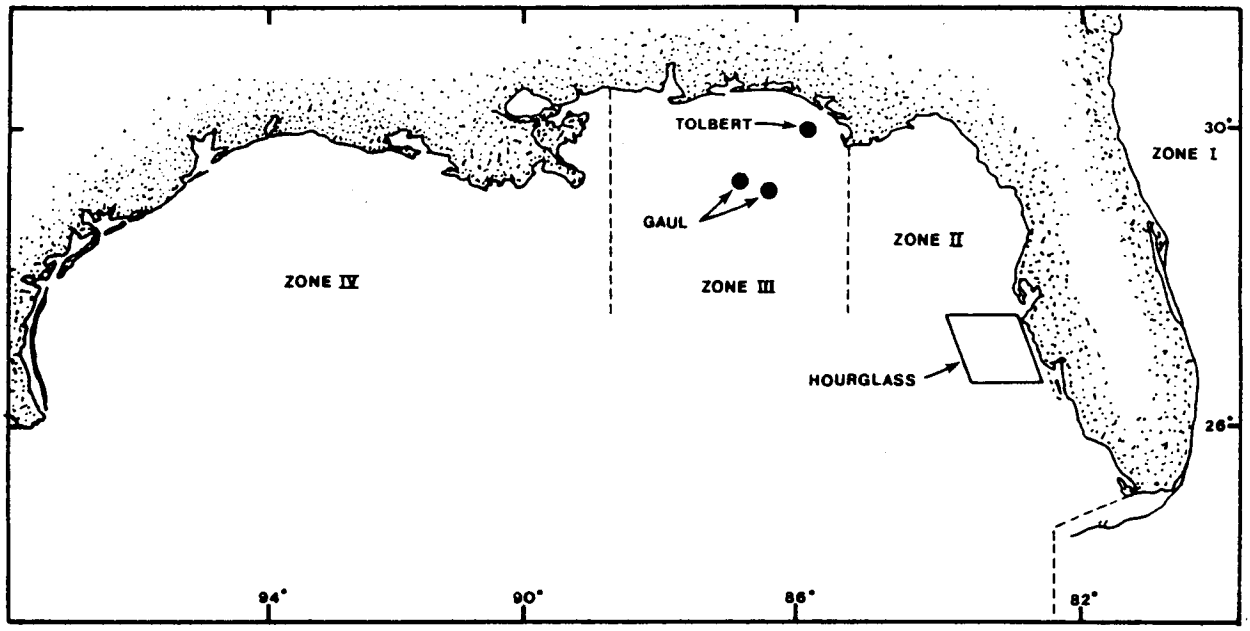

	MONTH OF RELEASE	NO. OF BOTTLES RELEASED	NO. OF BOTTLES RECOVERED	PERCENT OF RECOVERED BOTTLES ZONE I	ZONE II	ZONE III	ZONE IV
TOLBERT	JAN	84	14	64	0	29	7
	FEB	48	24	17	0	83	0
	MAR	48	9	56	0	44	0
	APR	80	43	7	0	93	0
	MAY	78	22	18	5	73	5
	JUN	100	45	2	0	94	4
	JUL	90	40	5	0	78	18
	AUG	88	28	0	0	68	32
	SEP	85	23	30	0	30	39
	OCT	77	8	63	0	0	38
	NOV	71	5	60	0	20	20
	DEC	102	15	87	0	13	0
	TOTAL	951	276	20	0	68	12
GAUL	JAN	240	41	93	0	0	7
	FEB	-	-	-	-	-	-
	MAR	-	-	-	-	-	-
	APR	1200	397	30	3	20	49
	MAY	2304	344	87	3	4	7
	JUN	1344	269	94	1	0	5
	JUL	240	34	62	3	32	3
	AUG	1512	244	57	3	11	29
	SEP	960	66	23	0	0	77
	OCT	240	27	11	0	0	89
	NOV	-	-	-	-	-	-
	DEC	240	30	100	0	0	0
	TOTAL	6919	1452	63	2	9	26
HOURGLASS	JAN	310	73	85	15	0	0
	FEB	320	100	100	0	0	0
	MAR	310	100	62	35	1	2
	APR	320	113	42	41	12	5
	MAY	320	136	38	60	1	1
	JUN	320	126	48	45	1	6
	JUL	320	134	34	57	1	8
	AUG	480	87	35	44	1	13
	SEP	480	124	56	19	1	23
	OCT	480	122	79	14	0	7
	NOV	480	129	88	5	0	7
	DEC	320	103	90	7	0	3
	TOTAL	4460	1347	62	30	1	7

Figure 2.5.7: Drift card release sites and recovery zones for experiments by Tolbert & Salsman (1964), Gaul (1967), and Hourglass (Williams et al., 1977).

3. virtually no drifters were found in Zone 2 at any time except from release sites in Hourglass which were within about 20 km of shore and obviously under the influence of land-sea breezes and other mesoscale effects.

The large number of drifters consistently recovered in Zone I is particularly remarkable because both the Gaul and Tolbert releases were located far to the north in the Gulf of Mexico and close to shore. An inspection of the seasonal wind data (Figure 2.3.2) would seem to indicate that surface drifters should move primarily to the west, especially during spring and summer, and would be recovered in Zone IV. The substantial number of drifters which consistently travel to Zone I indicates that a southerly advective mechanism is also operative. One possibility is that the LC substantially influences a large portion of the WFS, including the northern portion, during all times of the year. This hypothesis is discussed at length in Section 5.3 and Appendix B.3.

OTHER STUDIES

Hsueh and Peng (1973) used a numerical model to investigate circulation in the open bay between Apalachicola and Tarpon Springs. The study is primarily of a theoretical nature, as no attempt was made to force the model with realistic boundary values or to verify the results.

Several investigators from Florida State University have recently published three articles concerning surface elevations and currents on the WFS. Marmorino (1981) investigated the low frequency sea level response along the Florida west coast to atmospheric forcing during the winter 1978. He found the winds and sea levels to be well correlated over the entire shelf. Surface levels followed changes in local wind stress by 18 hours in the north and by 9 hours in the south, implying the southward propagation of a wave excited by the wind. Using a linear steady-state model, Marmorino found the model results to resemble the observed elevations in an average sense. He

also investigated the effect of the LC on coastal elevations using the model. He idealized the effects of the LC as a sea level distribution along the shelf break as derived from steric sea level patterns from Whitaker (1971). The model indicated negligible changes in sea level at the coast due to the LC.

Like Marmorino, Cragg et al. (1974, 1981) investigated low frequency sea level fluctuations but over a much longer duration of three to nine years. Some of their findings were:

1. coherence between wind and surface elevation was a maximum for periods of 4 to 10 days. Lag between wind and sea level in this band varied from 10 to 24 hours;

2. horizontal coherence of wind was high up to a length scale of at least 300 km and horizontal coherence of sea level was high to 500 km;

3. alongshore flows on the order of 100 km wide were implied from the high horizontal coherences of wind and sea level;

4. an alongshore sea level gradient of 6.0×10^{-8} was observed and seemed to be caused by the mean winds.

Mitchum and Sturges (1981) performed extensive analysis and interpretation of three weeks of current meter data taken by Florida State University (marked as "FSU" on Figure 2.4.1) starting in February 1978. They found the low frequency alongshore currents and coastal sea levels to be coherent with the alongshore wind and to lag it by approximately half a day. They found no significant longshore sea level slope during the three week period.

2.6 Summary of present knowledge of the West Florida Shelf

There have been very few historical attempts to form a coherent picture of circulation on the WFS, and these were limited by available data and funding. No study to date has attempted to integrate the more recently available SDE and satellite data into a coherent picture.

High quality observed current data are limited to two studies:

1. the Shelf Dynamics Experiment which provided extensive current and hydrographic data over an extended period. The study focused on a relatively small portion of the shelf near the break and offers little insight into the propagation onto the shelf of LC effects; and

2. the FSU study consisting of two moorings deployed east of Cedar Keys for three weeks during the winter of 1978. Usefulness of the data is limited by the short duration and lack of hydrographic data.

All together, these two sources provide a total of six meter months of current data on the shelf covering three separate time periods. There are no velocity measurements during the spring or summer.

The LC dominates the circulation pattern in the eastern Gulf of Mexico. Its northern boundary varies between roughly 25 and 30°N during a quasi-annual period. Several investigators have suggested an annual period with the maximum northward intrusion occurring in early summer, but it is apparent that this is subject to considerable year-to-year variability.

The LC abuts the lower portion of the WFS during most of the year, and during its northward excursions, abuts nearly the entire length of the shelf..

Given the proximity and magnitude of the LC, it is not surprising that it affects the shelf in a number complex ways.

It is clear from the satellite data that an unstable interface exists between the LC and indigenous shelf waters. This interface is often characterized by a series of wave like undulations of alternating cold shelf and warm LC intrusions as demonstrated in Figure 2.5.8. Warmer waters appear as the darker colored area in the figure. In addition to the wave-like eddies along the interface, there is a large eddy on the order of 200 km wide at the left side of the photo which has recently separated from the LC.

There is good evidence that cyclonic eddies, meanders, and tongues from the LC migrate well onto the shelf. These eddies have length and time scales of 200 km and 15 days, respectively. Such eddies could seriously bias the circulation patterns inferred from indirect measurements such as hydrographic and biological data (i.e. the studies of Austin, 1974 and others). Because these eddies contribute a large portion of the signal, they can also corrupt mean current calculations based on data taken over length scales of the same order as the eddies. A quantitative estimate of the advection due to these eddies does not exist nor is it known what role barotropic and baroclinic forces play in the eddy dynamics. There are no known Lagrangian current measurements and clearly insufficient Eulerian measurements to resolve these issues.

In addition to LC eddies on the shelf, several investigators have suggested that the LC generates currents through a lateral shear mechanism. This mechanism would create shelf-wide circulation with a time scale tied to the seasonal migration of the LC. Chew (1959a, b) has suggested that the lateral shear would generate a cyclonic eddy on the WFS west of Tampa. Other investigators have suggested a similar eddy based on indirect observations.

Our recent knowledge of LC position comes from satellite infrared photos. The satellite photos are of help in quantitatively tracking the path of the

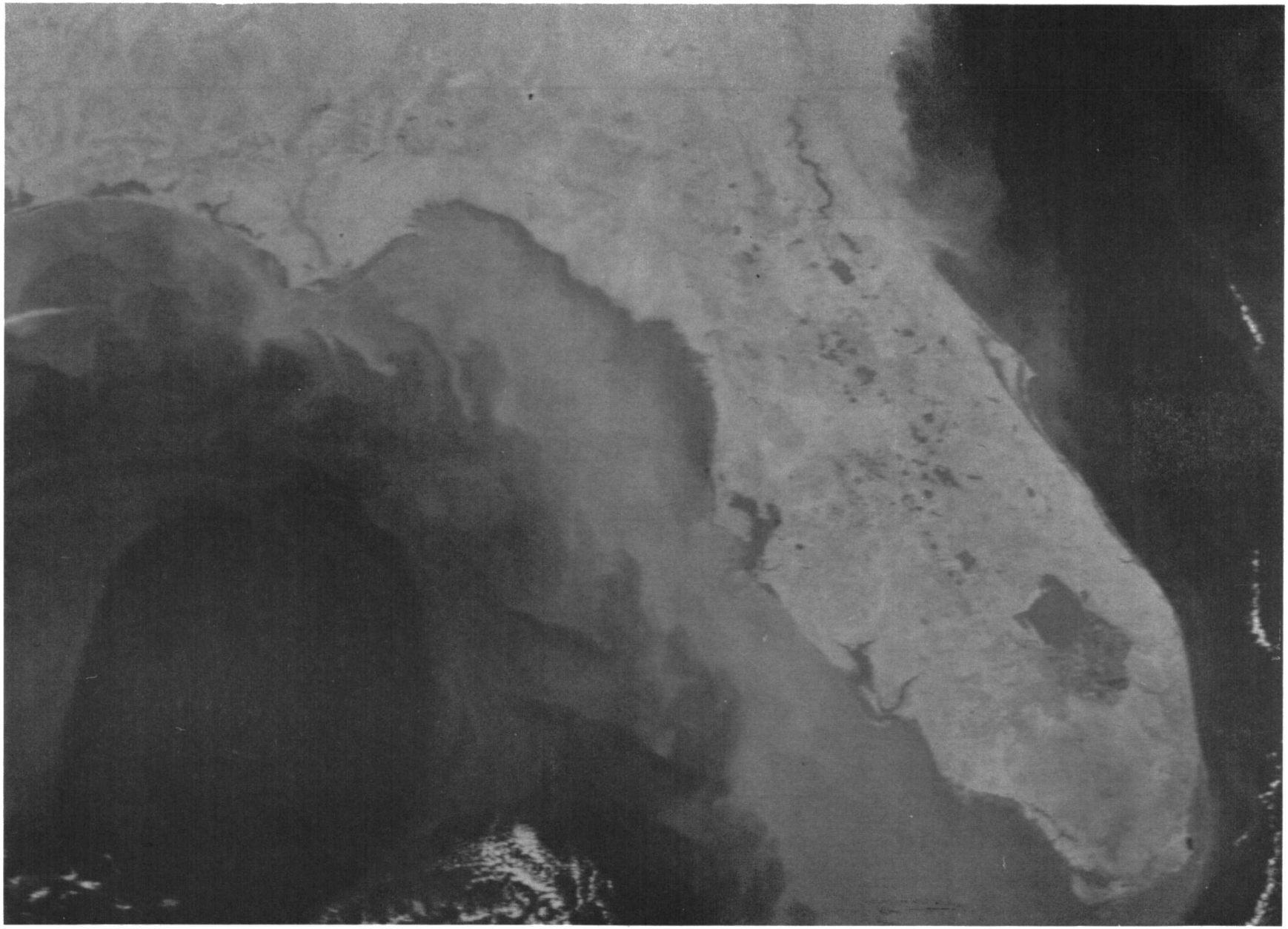

Figure 2.5.8: Satellite image of eastern Gulf of Mexico, 27 February 1981, showing wave-like eddies along WFS break.

LC but otherwise offer mainly qualitative information. When reviewing results based on photos it must be kept in mind that they are not continuous, being unavailable during periods of cloud cover and approximately 50% of the year (i.e. May-September) because of insufficient thermal contrast. In addition, satellite photos give information only about the upper few meters of the water column thus making it difficult to identify such features as shallow lenses, and making interpretation of the photos highly subjective in some cases. These difficulties no doubt have contributed significantly to the rapid temporal change of the LC suggested by some investigators (e.g., Maul, 1981).

Three drift bottle studies have been performed on the WFS. The implication of these observations is that the LC substantially influences a large portion of the WFS including the northern extreme during all parts of the year. This effect is probably in the form of a lateral shear mechanism. Although the migration of eddies and meanders from the LC onto the shelf may also contribute to mixing and advection of shelf waters.

The tidal regime on the shelf has a mean range of 0.3 m. Typical tidal current maxima are 10 cm s^{-1} which cause advection of about 1 km. There is no evidence of residual currents due to tides, nor little theoretical basis to expect any. Thus tidal currents would appear to be an important advective mechanism only when within a few kilometers of the coastline. As a result, the incorporation of tidal forcing into the model is not necessary.

In summary, circulation of the WFS is poorly understood, in large part because of a dramatic absence of high quality in situ data. Existing data indicates a complex flow regime which is strongly influenced by migrating eddies from the LC and by a larger scale lateral shear mechanism.

Chapter 3

Model Formulation

The model, GAL, takes its name from the Galerkin numerical technique upon which the model is based. Model formulation is founded on the description of the vertical variation of the horizontal velocity by a series expansion (Heaps, 1972, 1974). A thorough description of the model is included in Cooper and Pearce (1982), henceforth referred to as PC. Only a brief description will be given here.

3.1 Governing Equations

The model is based on the Navier-Stokes Equations which, after some simplifying assumptions, can be written in the form used in the model as:

$$0 = \frac{\partial u}{\partial t} + \frac{\rho_s}{\rho} g \frac{\partial \eta}{\partial x} - N_h(\nabla^2 u) - \frac{\partial}{\partial z}\left(N_v \frac{\partial u}{\partial z}\right) - fv + \frac{1}{\rho}\frac{\partial P_a}{\partial x} + \frac{g}{\rho}\int_{-\eta}^{z} \frac{\partial \rho}{\partial x}\, d\zeta \qquad (3\text{-}1a)$$

$$0 = \frac{\partial v}{\partial t} + \frac{\rho_s}{\rho} g \frac{\partial \eta}{\partial y} - N_h(\nabla^2 v) - \frac{\partial}{\partial z}\left(N_v \frac{\partial v}{\partial z}\right) + fu + \frac{1}{\rho}\frac{\partial P_a}{\partial y} + \frac{g}{\rho}\int_{-\eta}^{z} \frac{\partial \rho}{\partial y}\, d\zeta \qquad (3\text{-}1b)$$

where:

t	the time variable.
x,y	the horizontal coordinates in a right-handed Cartesian coordinate system.
z	the vertical coordinate, measured as positive downward from the still water surface.
u,v	the horizontal velocity components in the x and y directions, respectively.
ρ_s	the density of the fluid, where the s subscript indicates the value at the surface.
g	the gravitational constant, 9.8 m/sec.
η	the water height of the free surface above datum, z=0.
N_h	the horizontal eddy viscosity coefficient.
N_v	the vertical eddy viscosity coefficient.

f the Coriolis parameter, $2\omega\sin\phi$, where ω is the angular velocity of the earth.

P_a the atmospheric pressure.

∇^2 the Laplacian operator, $\frac{\partial^2}{\partial x^2} + \frac{\partial^2}{\partial y^2}$

Note that the vertical velocity, w, is assumed negligible and this simplifies the Navier-Stokes Equation in the z direction to an expression of the hydrostatic pressure. The other governing equation used in the model formulation is the continuity equation or:

$$\frac{\partial \bar{U}}{\partial x} + \frac{\partial \bar{V}}{\partial y} = \frac{\partial \eta}{\partial t} \qquad (3\text{-}2)$$

where:

$\bar{U}$ the mass flux per unit length in the x direction or $\int_{-\eta}^{H} u\,dz$.

$\bar{V}$ the mass flux per unit length in the y direction or $\int_{-\eta}^{H} v\,dz$.

H the still water depth.

3.2 Boundary Conditions

The surface boundary conditions are:

$$\tau_{sx} = \left[-\rho N_v \frac{\partial u}{\partial z}\right]\Bigg|_{z=0} \qquad \tau_{sy} = \left[-\rho N_v \frac{\partial v}{\partial z}\right]\Bigg|_{z=0} \qquad (3\text{-}3)$$

where τ_{sx} and τ_{sy} are the specified shear stresses at the surface in the x and y direction, respectively.

At the bottom, a linearized friction law is used or:

$$\tau_{bx} = [\rho c_b u]\Big|_{z=H} \qquad \tau_{by} = [\rho c_b v]\Big|_{z=H} \qquad (3\text{-}4)$$

where τ_{bx} and τ_{by} are the bottom shear stresses and c_b is a drag coefficient.

The remaining boundary conditions vary according to the geometric constraints of the water body being modeled. See section 4.1.2 for a listing and explanation of possible boundary conditions.

3.3 Vertical Discretization

It is important to note that the parameters u, v, ρ, and N_v are all functions of (x, y, z, and t), and the parameters N_h, η, c_b, and P_a are functions of horizontal space and time (x, y, and t). Parameters which must be specified are: ρ, N_v, f, P_a, c_b, τ_{sx}, τ_{sy}, and N_h, and the unknowns are u, v, and η.

The governing equations and boundary conditions (i.e. Equations 3-1, 3-2, 3-3, and 3-4) are transformed using the Galerkin technique. This manipulation explicitly eliminates z from the transformed equations and greatly simplifies the eventual solution process. The dependency of u and v on z is implicitly retained in the final equations and the u and v velocity profiles can be regained whenever desired.

Application of the Galerkin technique begins by hypothesizing a vertical distribution of the unknown velocities, u and v, in terms of a series expansion known as the trial functions. The function used in the model is:

$$\hat{u} = \frac{\tau_{sx} z^2 (z-H)}{\rho_s H^2 N_b} + \frac{\tau_{sx}}{\rho_s \alpha} \ln\left(\frac{N_b}{N_v}\right) + \sum_{I=1}^{I=I'} c_I \cos\left(\frac{a_I z}{H}\right) \qquad (3\text{-}5)$$

where:

$\hat{u}$ approximates the x component of the velocity.

N_b vertical eddy viscosity at the bottom, z=H.

α slope of N_v in the surface layer.

I' number of terms used in the cosine series.

a_I constants given by the expression $a_I * \tan(a_I * z / H)$

c_I the undetermined constants.

A similar function exists for $\hat{v}$. The relationships for the y-direction will not be shown here for the sake of brevity. However, the reader should remember that these equations are included in the model. Note that all parameters in (3-5) are specified except the undetermined coefficients, c_I (for the y-direction the undetermined coefficients are d_I).

The trial functions are substituted into (3-1a,b) and, in general, there will be a residual associated with this substitution since the trial functions are not the exact solutions. The residual, γ, is multiplied by a weighting factor, W, to facilitate computation and the product is minimized by integrating over the water depth and setting the result to zero, or for the x-direction:

$$\int_{-\eta}^{H} \gamma W dz = \int_{-\eta}^{H} \{(\frac{\partial \hat{u}}{\partial t} + \frac{\rho s}{\rho} g \frac{\partial \eta}{\partial x} - N_h \nabla^2 \hat{u} - f\hat{v} + \frac{1}{\rho} \frac{\partial pa}{\partial x} + \frac{g}{\rho} \int_{-\eta}^{z} \frac{\partial \rho}{\partial x} d\zeta)\} \cos \frac{a_I z}{H} dz = 0 \quad (3-$$

Again, a similar expression exists for the y-direction.

Before the integration in (3-6) can be performed, it is necessary to specify a distribution for N_v. This is accomplished by assuming N_v to vary in a multi-linear fashion as shown in Figure 3.3.1. Performing the integration in (3-6) yields a set of differential equations in which z has been explicitly eliminated or:

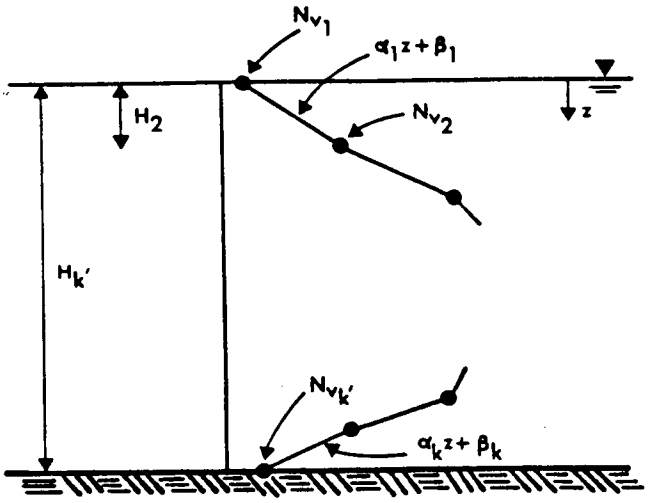

Figure 3.3.1: Functional form of the vertical variation of eddy viscosity in the model.

$$0 = \frac{\partial c_I}{\partial t} - N_h \nabla^2 c_J - f d_I + B_I \frac{\partial \eta}{\partial x} + A_I - \sum_{J=1}^{J=1'} c_J E_{IJ} + P_I + \Gamma_I \qquad (3\text{-}7)$$

where A_I, B_I, and E_I are constants which arise from the integration; Γ_I is a constant associated with density gradients; and P_I is a constant associated with the atmospheric pressure gradient.

Equation3-7and its equivalent in the y-direction represent a set of 2I' equations with 2I'+1 unknowns (i.e. c_I, d_I, d_I, and η). To solve for the unknowns one more equation linking c_I, d_I, and η must be used and this is provided by substituting(3-5)into the continuity equation, (3-2).

3.4 Horizontal Discretization

The existing version of the model uses a finite difference scheme to discretize(3-7), its equivalent in the y-direction, and the transformed continuity equation. While this discretization scheme has proven satisfactory it is not limiting since other schemes such as finite elements could be used.

The "split-time", finite difference scheme has at least two prominent deficiencies. Because it is an explicit scheme, the method requires a smaller time step to maintain stability than might an implicit scheme. In addition, the scheme uses a finite difference method which uses a grid system composed of squares of equal size. Such a grid system is inefficient for water bodies which are long, narrow and contorted. For such problems, a finite element approach is much more appropriate.

To apply the method, the water is discretized in the manner shown in Figure 3.4.1 where the variables c_I, d_J, η, H, $\bar{U}$, $\bar{V}$, and ρ are associated with the spatial points indicated in Figure 3.4.1. Note the subscripts ℓ and m are spatial location counters which are associated with the x and y directions respectively. The time counter is n. There are ℓ' grids in the x direction, m' grids in the y direction, and n' total number of time steps. So, for example, $\bar{U}_{1,2,3}$ would be the mass flux in the x direction associated with element 1,2 at time 3 Δ t, where Δ t is the time step.

Applying the discretization scheme to the x-momentum equation(3-7)yields:

$$c_{I,\ell,m,n+1} = c_{I,\ell,m,n} - \Delta t \left[\frac{-N_H}{\Delta x^2} \left(c_{I,\ell,m+1} + c_{I,\ell+1,m} - 4c_{I,\ell,m} + c_{I,\ell,m-1} + c_{I,\ell-1,}\right.\right.$$

$$+ B_{I,\ell,m} \frac{1}{\Delta x} \left(\eta_{\ell+1,m,n+1/2} - \eta_{\ell-1,m,n+1/2} \right) - f d_{I,\ell,m,n} \qquad (3$$

$$\left. + A_{I,\ell,m} - \sum_{J=1}^{J=I'} c_{J,\ell,m,n} E_{I,J,\ell,m} + \Gamma_{I,\ell,m,n} + P_{I,\ell,m,n} \right]$$

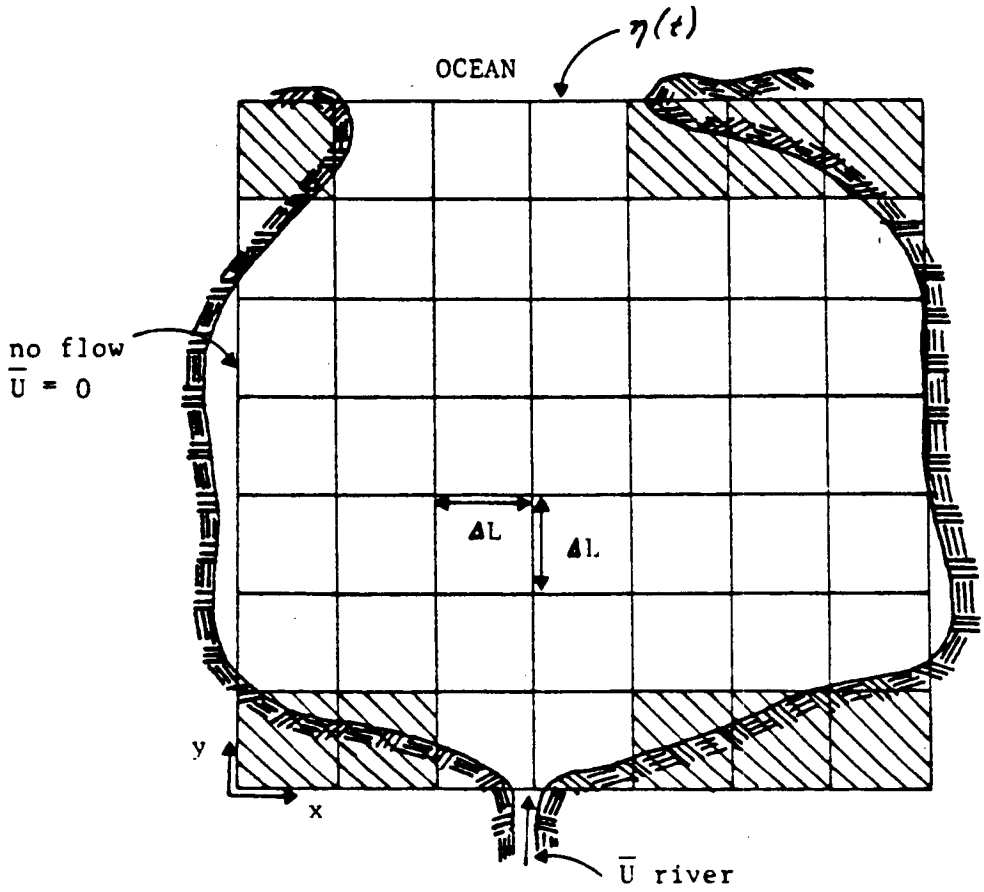

Figure 3.4.1a: Finite difference discretization scheme.

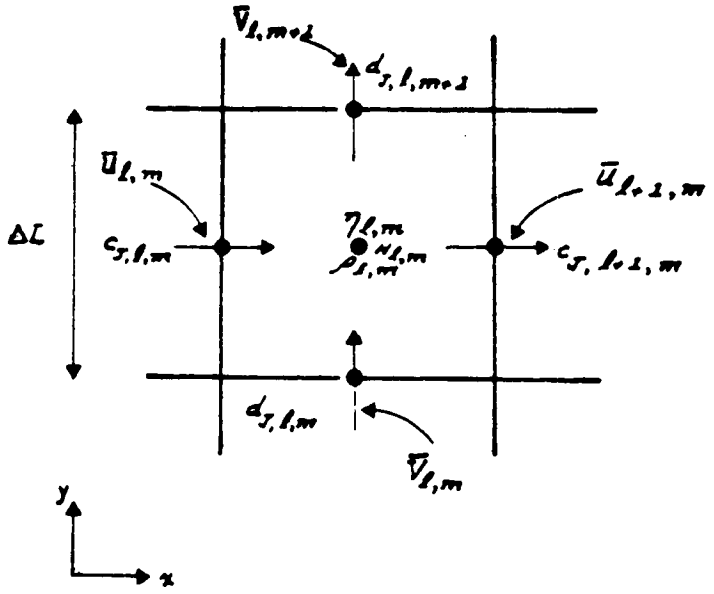

Figure 3.4.1b: Location of critical parameters.

A similar expression exists for the unknown velocity coefficient in the y-direction, d_I.

The continuity equation is discretized in a similar manner yielding:

$$\eta_{\ell,m,n+3/2} = \eta_{\ell,m,n+1/2} + \frac{\Delta t}{\Delta x} \{ \overline{U}_{\ell,m,n+1} - \overline{U}_{\ell+1,m,n+1} + \overline{V}_{\ell,m,n+1} - \overline{V}_{\ell,m+1,n+1} \} \quad (3\text{-}9)$$

where $\overline{U}$ and $\overline{V}$ are the mass fluxes per unit length in the x and y-directions, respectively. The mass fluxes are easily related to the unknown coefficients c_J and d_J by integrating (3-5) and its y equivalent through the water depth. In the x-direction, for example, this yields:

$$\overline{U} = U_*^2 F + H \sum_{I=1}^{I'} c_I \frac{\sin a_I}{a_I}$$

where F is a constant arising from the integration and U_*^2 is the wind shear velocity in the x-direction.

Equation 3-8, its y equivalent and 3-9 represent the equations which are solved in GAL (Program CIRC). Once c_I, d_I and η have been calculated for a given location and time step, the water velocity at any depth, z, can be calculated from 3-5 and its y equivalent (this is done in Program PRTVEL).

3.5 Time Step

Because the model uses an explicit scheme to integrate in time, the time step, Δt, is limited by two stability criteria:

$$\Delta t < \Delta x \, (2 \, g \, H)^{-1/2}$$

$$\Delta t < H^2 (a_j^2 N_v)^{-1}$$

where all terms are as previously defined.

Figure 3.5.1 shows the interactions which take place between the various programs. Each program has the following functions:

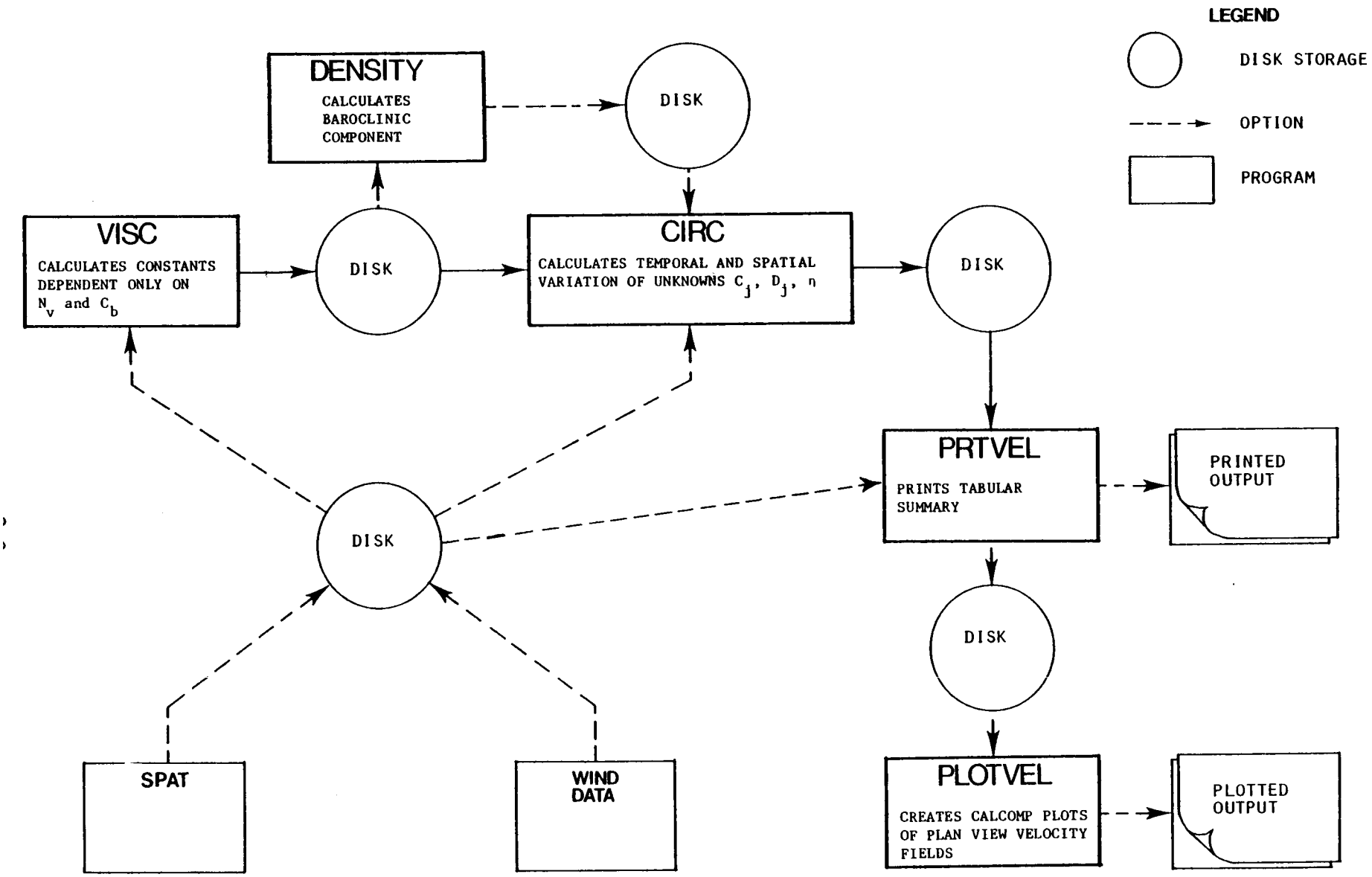

Figure 3.5.1: Flow chart of computer implementation of the model.

VISCOUS calculates all parameters which are functions of the vertical eddy viscosity (N_v), the bottom friction coefficient (C_b), and the grid configuration. If these parameters do not change, then there is no need to rerun VISCOUS. The program writes one disk file which is read by CIRC and PRTVEL.

DENSITY calculates all parameters associated with the horizontal density-driven component of the flow. The program reads the disk file created by VISCOUS and writes one disk file which is read by CIRC and PRTVEL.

CIRC calculates the unknowns in the trial function, c(j,l,m), d(j,l,m) and the surface elevation, eta(l,m). The program reads disk files created by VISCOUS and wind data, and writes a disk file containing the temporal change of various parameters specified by the user, such as horizontal shear stresses c(j,l,m), d(j,l,m), river inflow (U_b(l,m)), etc.

PRTVEL is the main output program. It reads disk files created by VISCOUS and CIRC as well as wind data. It prints tables which summarize the run, consisting of water depth, bottom friction coefficients, surface elevation, eddy viscosity, etc. for each grid element. PRTVEL also prints vertical velocity profiles at specified locations for specified depths, plan views of the velocity at specified depths, surface elevation levels, and mass fluxes.

PLOTVEL creates a series of CALCOMP plots consisting of a plan view of current vectors for a specified depth and time.

WIND generates a spatially uniform wind field which can change in time during initial start-up. The program writes one disk file which is read by VISC, CIRC, and PRTVEL.

SPAT generates a temporally and spatially variable wind field by interpolating observed winds. The program writes one disk file which is read by VISC, CIRC, and PRTVEL. Either SPAT or WIND is run, but not both.

3.6 Model Grid and Lateral Boundaries

Figure 3.6.1 shows the model grid for the WFS. The element size is 30 km and the water depths (in meters) are shown at the center of each element. Also shown are: location of current meter data sites (solid circles), coordinate axis, major isobaths and major cities. Rows are defined as running along the x axis and columns run along the y axis.

Boundary conditions along the horizontal perimeter of the grid must be specified and for the WFS are of three types: land, seaward (i.e. column 1), and lateral open (i.e. row 1, columns 1-6 and row 24, columns 1-5). The boundary between land and sea elements is indicated in the figure by the heavy border.

Figures 3.6.2-4 show examples of the specific assumptions made for each of the three boundary types. Along a land boundary the mass flux normal to the coast is set to zero, and negative reflectional symmetry is assumed for the alongshore component of the velocity. The latter results in a no-slip condition at the coasts. An example is shown in Figure 3.6.2 in which the land boundary is aligned with the y axis.

Open lateral boundaries occur at elements (2,1), (3,1), (4,1), (5,1), (6,1), (2,24), (3,24), (4,24), and (5,24). For these elements a zero slope condition normal to the boundary and positive reflectional symmetry is established. Figure 3.6.3 shows an example along row 1. The zero slope condition is satisfied by setting $eta_{1,1} = eta_{1,2}$.

The seaward boundary occurs along column 1 of the grid. Along this boundary the surface elevation is set to zero and positive reflectional symmetry is

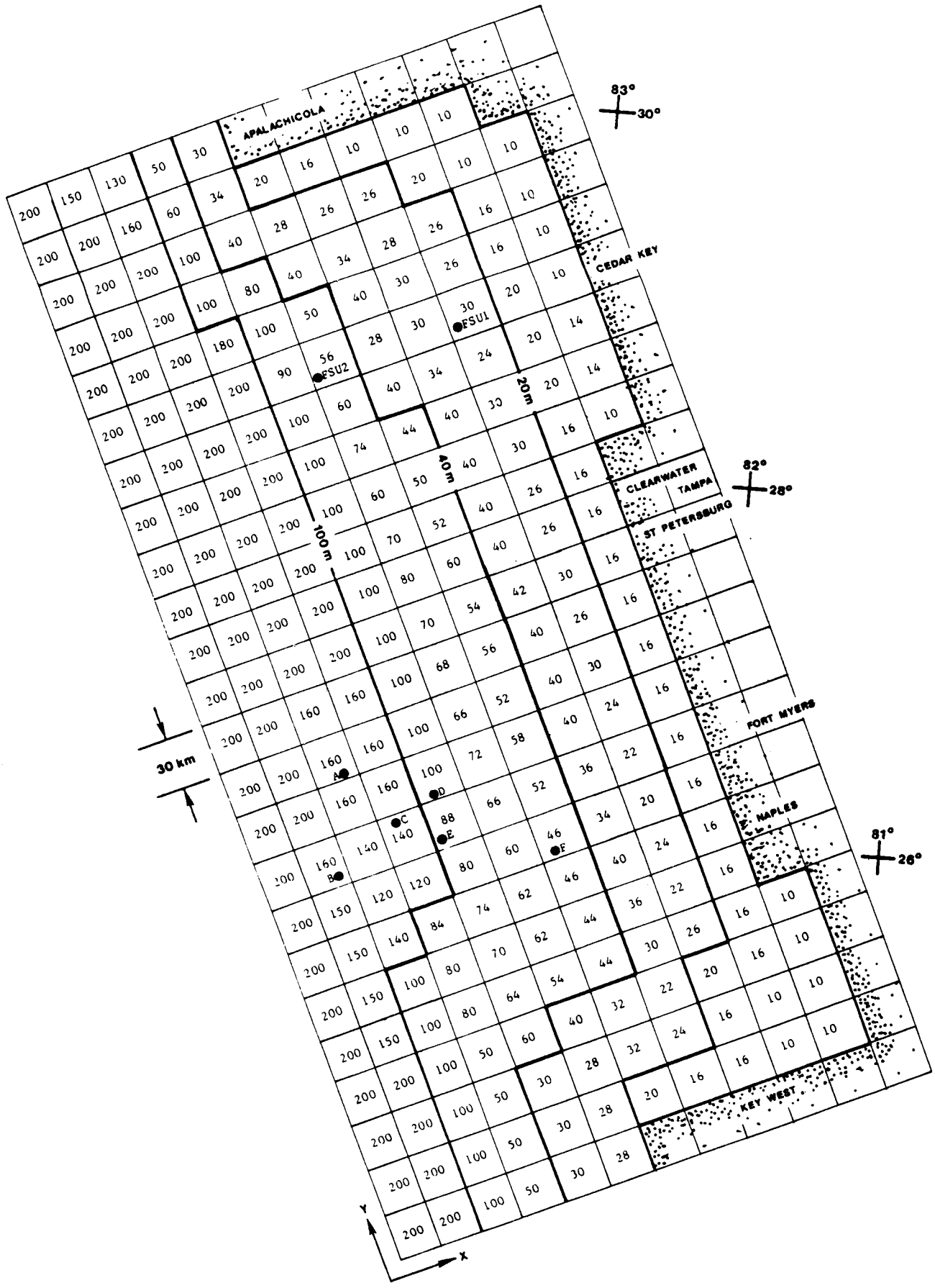

Figure 3.6.1: Model grid configuration (12 x 24) showing: water depth used for each element, coordinate axis, major isobaths, location of FSU data sites, location of winter 1973 SDE data sites, and major cities on the coast.

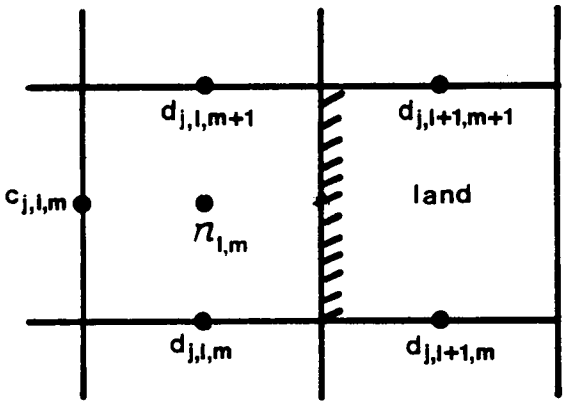

$c_{j,l+1,m} = 0.0$

$d_{j,l+1,m} = -d_{j,l,m}$

$d_{j,l+1,m+1} = -d_{j,l,m+1}$

Figure 3.6.2: Boundary conditions along a land boundary.

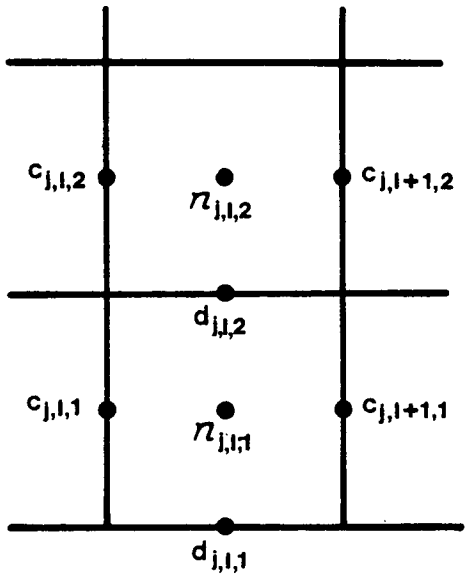

$\eta_{j,l,1} = \eta_{j,l,2}$

$c_{j,l,1} = c_{j,l,2}$

$c_{j,l+1,1} = c_{j,l+1,2}$

$d_{j,l,1} = d_{j,l,2}$

Figure 3.6.3: Boundary conditions along an open lateral boundary.

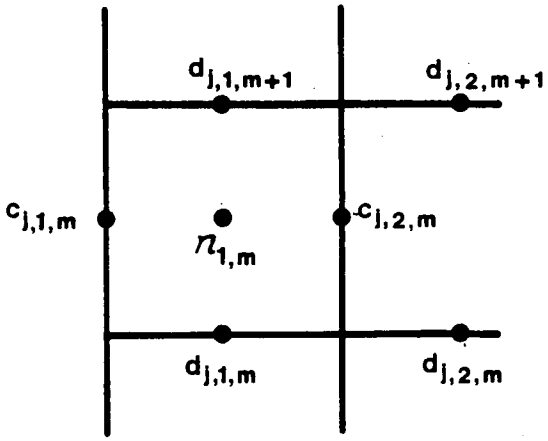

$\eta_{1,m} = 0.0$

$c_{j,1,m}$ = specified

or

$c_{j,1,m} = c_{j,2,m}$

$d_{j,1,m} = d_{j,2,m}$

$d_{j,1,m+1} = d_{j,2,m+1}$

Figure 3.6.4: Boundary conditions along a seaward lateral boundary.

specified. Figure 3.6.4 shows a general element. $Eta_{1,m}$ is set to zero and $c_{j,1,m} = c_{j,2,m}$. The specification of the d's vary according to the specific case. If the Loop Current is included then it is necessary to specify $d_{j,1,m}$. In the absence of Loop Current forcing, positive reflectional symmetry is assumed.

Chapter 4

Model Modifications and Basic Sensitivity Studies

4.1 Selection of Model Parameters

Running the model requires that the following parameters be specified:

1. atmospheric forcing (i.e. wind shear stress, pressure gradients, etc);
2. forcing at the ocean boundary (i.e. boundary shear currents, etc.);
3. density gradients, both vertical and horizontal;
4. bathymetry; and
5. energy dissipation coefficients, i.e. c_b, N_v, and N_h.

Both bathymetry and dissipation coefficients are often treated by modelers as knobs to be twiddled until desired results are obtained. While there is some uncertainty involved, physical considerations should determine the values of these parameters. The modeler who ignores these considerations risks serious errors, including:

1. Covering up inadequacies in the basic model formulation. His model may in fact be little more than a "black box" which has been tuned for a particular hindcast, and since the black box has little physical validity, it is doubtful that forecasts of other situations will be accurate.

2. using an unrealistic combination of parameters in a multi-parameter model. In most models such as GAL, a user can achieve similar currents for a given hindcast using several different combinations of input parameters. But if a certain set is chosen simply because it gives a reasonable hindcast without regard to the physical validity of the parameters, then chances are the model will not correctly model conditions with different environmental forcing.

4.1.1 Bathymetry

The depths used in the model grid are given in Figure 3.6.1 and were based mainly on NOAA chart 411, with two exceptions. These exceptions were associated with grid elements at or near the open boundary and included:

1. insertion of a "false bottom" of 200 m. Columns 1 and 2 of the grid fall beyond the shelf break, and actual depths exceed 200 m in many of these elements. However, use of the actual depths in the model would decrease the permissible model time step by a factor of two, making the model twice as expensive to run. Sensitivity studies indicate that this approximation does not appreciably affect simulated flow <u>on</u> the West Florida Shelf (WFS).

2. modification of the bottom slope in the southwest corner of the grid.

The bathymetry in the vicinity of the southwest corner of the grid (Figure 2.3.1) shows an extreme slope of 10^{-2}. An early attempt was made to duplicate this gradient, but it resulted in severe and unrealistic oscillations in the model. These oscillations were due to the rapid change in the element depths in conjunction with the reflective boundary conditions used in the model. The most preferable method of eliminating the oscillations would be to use either a very small element size or incorporate a radiative boundary condition in the model or a combination of both. The former would increase computer costs substantially and the latter would have required extensive labor. The solution was to decrease the depth gradient of the four elements in the extreme southwest corner of the grid. Since this area is well away from the primary area being modeled the influence of the approximation should be minimal in the area of interest. To verify this, however, would require implementation of one of the approaches described above.

4.1.2 Bottom Friction Coefficient

Water moving along the sea floor creates friction. Kinetic energy is converted to heat energy, and transformed into smaller scale turbulent kinetic energy. This process is simulated in the model primarily through the bottom friction coefficient.

Bottom friction coefficients are commonly used in flow models, including classical open-channel and pipe relationships such as the Manning and Darcey-Weisbach equations. The coefficient is dependent on several factors, including the local Reynolds number, water temperature, small-scale turbulence, and the characteristic roughness height of the bottom. The coefficient can also incorporate some of the numerical and theoretical errors

of the solution technique, particularly when the coefficient is selected based on "best-fit" hindcasts.

GAL uses a linear bottom friction coefficient. Values used in prior applications of the model ranged from 0.025 to 0.1 cm s^{-1}. Two of these applications, located in the Gulf of Mexico, are reported in Cooper and Pearce (1982). While the bottom roughness for these sites is probably very similar to those of the WFS, other conditions such as the Reynolds number and local wave activity, are much different. Accordingly, a somewhat smaller value would be expected for the WFS. Mitchum and Sturges (1981) used a value of 0.02-0.01 cm s^{-1} for their simple barotropic model of the FSU Winter 1978 current data. This constant was derived from wind measurements made at land stations. Because the WFS model uses estimates of offshore winds, the constant should be multiplied by roughly four, yielding values for c_b of 0.08-0.04 cm s^{-1}.

The bottom friction coefficient can also be calculated using a relationship which expresses c_b in terms of the more widely used and studied quadratic bottom friction coefficient:

$$c_b = n^2 * g \, W_b \, H^{-0.33}$$

where: n = Manning's n
W_b = water velocity at the bottom
H = depth

Values for n can be obtained from most hydraulics handbooks. Assuming the bottom to be relatively smooth earth yields n = 0.025. The measured current data on the shelf suggests an average bottom velocity on the order of 10 cm s^{-1}. Substituting these two estimates into the relationship above gives a range of c_b from 0.01 cm s^{-1} in 200 m of water to 0.03 cm s^{-1} in 10 m of water. These values correspond reasonably well to the estimates by Mitchum and Sturges (1981) and Cooper and Pearce (1982).

In summary, previous work indicates a reasonable range of c_b for the WFS to be 0.08 to 0.01 cm s^{-1}.

4.1.3 Vertical Eddy Viscosity

The eddy viscosity coefficient represents the amount of momentum transformed into turbulent eddies. Rather than pay the computational price of fully accounting for these small scale velocities, they are modeled via the eddy viscosity coefficient. If N_v is increased in the model, turbulent energy dissipation increases and current velocities and surface elevations tend to decrease. Physically, N_v is analogous to a second order damping coefficient in a simple spring-mass-damper system. The amplitudes of the mass oscillation and the velocity of the mass decrease more rapidly in time as the damping coefficient increases.

The vertical eddy viscosity will be dependent on a number of parameters including the surface shear stress, the local water depth and vertical density stratification. Including these effects in the estimation of N_v is difficult. In the case of unstratified conditions the following relationship by Townsend (1976) has proven adequate for a number of applications and was used extensively in the WFS study.

$$N_v = W_{*_s} H/R \qquad (4.1)$$

where: W_{*_s} = the wind friction velocity
H = the local water depth
R = the flow Reynolds number

Various researchers suggest values for **R** ranging from 12 to 32. A value of 12 was found to be appropriate in previous applications of the model, and was used in the WFS study.

Stratification normally develops on the WFS in the late spring, summer and early fall and is characterized by a thermocline at about 20 m below the surface. Stratification suppresses vertical momentum exchange. Since N_v is a measure of this process, one would expect the value to decrease near the thermocline. The region above the thermocline is typically referred to as the mixed layer.

Several studies have attempted to find relationships between N_v and stratification. Bowden et al. (1959) and others suggest a relationship originally proposed by Rossby and Montgomery (1935) and further refined by Munk and Anderson (1948). The relationship is:

$$N_{*vt} = N_v (1 + 10 R_i)^{-1/2} \qquad (4.2)$$

where: N_{*vt} = the eddy viscosity in the presence of stratification.
R_i = $g[\partial\rho/\partial z] \bar{\rho}^{-1} (\partial s/\partial z)^{-2}$, the Richardson number.
s = the local current magnitude.

Estimation of R_i for the ocean is an imprecise task that is eased somewhat by defining a bulk R_i as follows:

$$R_i = g D \Delta\rho \bar{\rho}^{-1} \Delta s^{-2} \qquad (4.3)$$

where: D = the effective depth i.e. the ratio of the mixed layer depth to the lower layer depth times the total depth.
Δs = the difference between currents in the mixed and lower layers
$\Delta\rho$ = the difference between density in the mixed and lower layers

Specific application of these equations to the WFS is discussed in Section 4.5.

4.1.4 Horizontal Eddy Viscosity

In the case of nonlinear models incorporating the advective terms, N_h is a measure of the subgrid turbulence, i.e. the velocities with length scales less than an element size. The Galerkin model used in this study is a linear model and so N_h must incorporate not only subgrid turbulence but the error due to neglecting the advective terms. Estimates of N_h based on ocean diffusion studies by Okubo (1971) imply a value for N_h on the order of 10^7 cm^2 s^{-1}. Many of the sensitivity studies described later in this Chapter attempt to refine these estimates specifically for the WFS.

4.2 Lateral Shear Stress

The Loop Current (LC) is known to affect the WFS through a number of complex mechanisms. One of the more important mechanisms is the advection of momentum and turbulence. This mechanism is simulated in the model via the so-called lateral shear stress terms which involve the parameter N_h and the second order horizontal spatial gradients of the velocity field.

Initially the model included a linear parameterization of the lateral shear stress - a satisfactory approach for many fluid flows. However, given the importance of the LC for the WFS, it was decided early in the study to improve the lateral stress parameterization by including a second order relationship. The method in which this was accomplished is described in Appendix E.2.

4.2.1 Comparison to Analytic Solution

To verify the addition of the second order lateral shear stress terms to the model, a simple comparison was made between the model and an analytic solution. A complete derivation of the analytic solution is given in Appendix F.1. The upper portion of Figure 4.2.1 shows the physical configuration and model grid system for the problem. A boundary current of 100 cm s^{-1} is imposed in the y-direction along an open boundary at a distance of 11 km from an infinitely long coastline aligned with the y-axis. The water depth is constant (10 m), N_v = 10 cm^2 s^{-1}, N_h = 10^9 cm^2 s^{-1} and c_b is set very large so that the bottom velocity becomes essentially zero. There is no rotation (i.e. no Coriolis force) so there is no mechanism to establish a surface gradient or velocity component in the x-direction.

A 'no-slip' boundary condition is assumed at the coast so one would expect the velocity to vary monotonically from a maximum at the open boundary (i.e. 100 cm s^{-1}) to zero at the coast. The lower portion of Figure 4.2.1 shows the exact solution to exponentially decrease as one moves from the open boundary to shore. Note that the model and analytic solution compare well.

4.2.2 Sensitivity to Steady Boundary Current

The method in which a boundary current such as the LC imposes a lateral shearing effect on the WFS is poorly defined. Therefore sensitivity studies were performed to investigate the influence of several boundary current configurations which were thought to be feasible.

Figure 4.2.2 shows the steady-state surface currents for Case 13.30 due to a boundary current impinging along the entire length of the shelf break. The boundary current was modeled by specifying a 100 cm s^{-1} y-component of

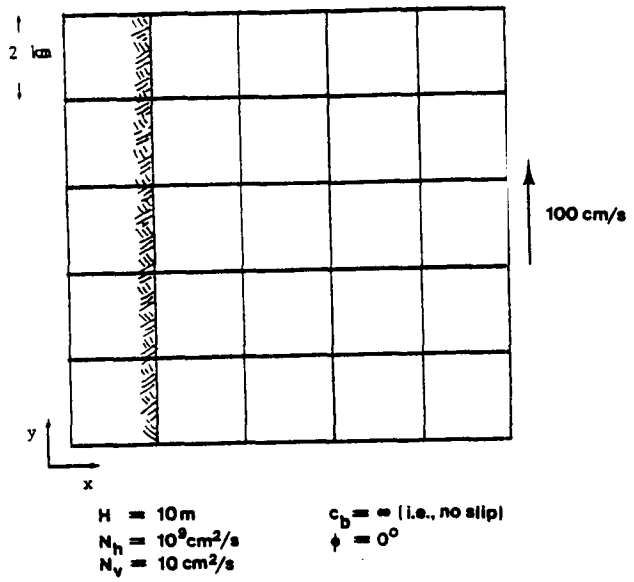

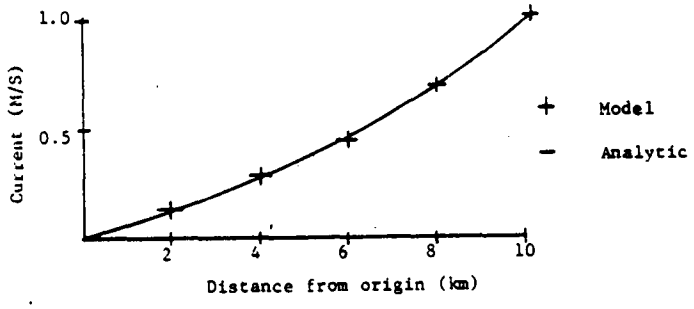

Figure 4.2.1: Comparison between the model and analytic solution for the case of a boundary current along an infinitely long coastline.

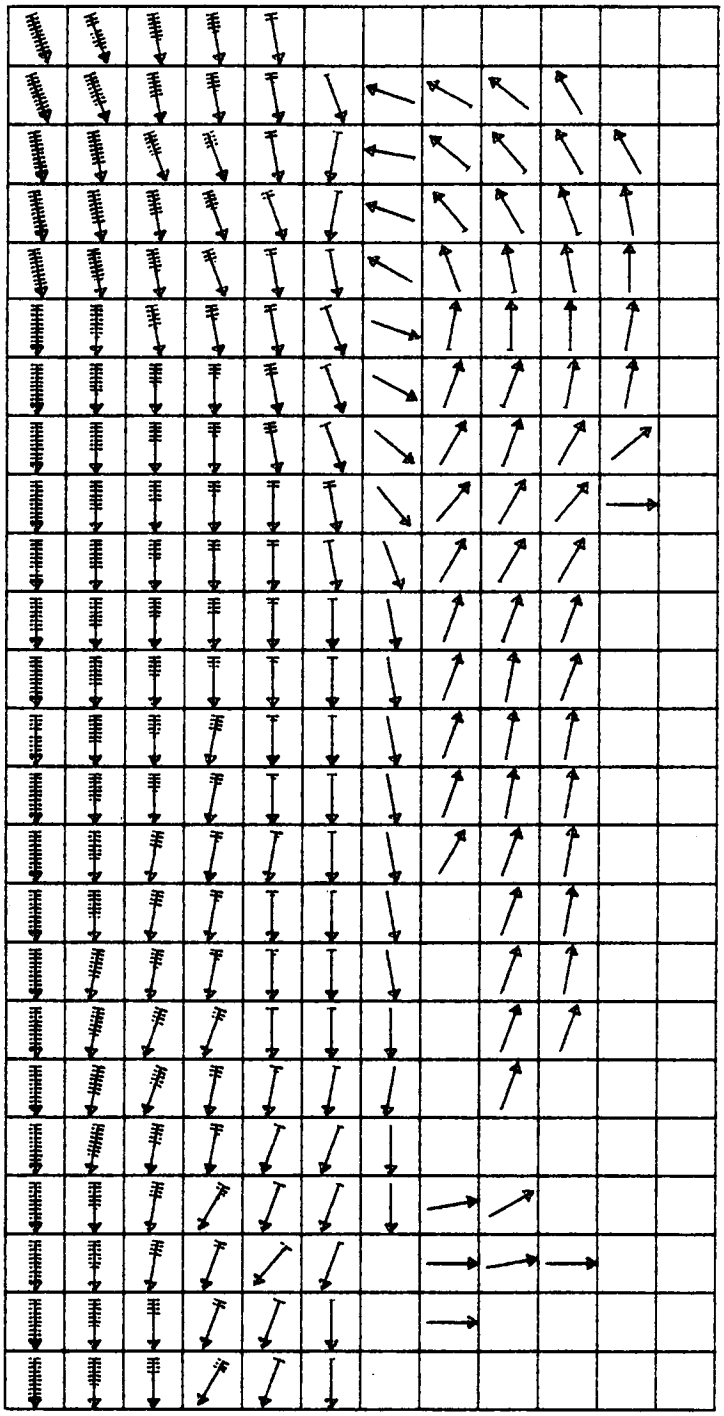

Figure 4.2.2: Steady-state surface currents due to constant boundary current imposed along western boundary of model grid (Case 13-30). Each grid element equals 30 km, each feather equals 10 cm s^{-1}. See Appendix D for listing of model input parameters.

velocity at each of the 24 elements in column 1 of Figure 3.6.1. The velocity at the boundary varies as cosine($0.7z\ H^{-1}$) where z is the distance from the free surface, and H is the local water depth.

Several aspects of Figure 4.2.2 should be noted:

1. the velocity at each element is shown by an arrow with a multiple number of feathers. The velocity at the element is found by multiplying the number of feathers by the scale shown in the figure caption, e.g. current at element x=2, y=1 is 5.7 feathers x 10 cm s^{-1}.

2. a single elongated cyclonic eddy is established on the northeastern portion of the shelf. Velocities in the eddy are too weak to show in the figure but are on the order of 2 cm s^{-1} as derived from the model print-out. It is interesting to note that Chew (1955a,b) and others have proposed a similar eddy based upon various indirect observations.

3. the velocity at a given location is essentially constant with depth.

4. flow is approximately geostrophic in water deeper than 100 m.

5. steady-state is reached in roughly 50 hours.

6. the value for $N_h = 10^9 cm^2\ s^{-1}$.

7. a 'set-down' (i.e. negative surface elevation) occurs at the coast. As indicated in Figure 4.2.3, the set-down is on the order of 30 cm.

8. the eddy shows northward intensification consistent with linear, steady-state theory based on a Stommel (1948)-Munk (1950) vorticity equation (personal communication, R.O. Reid).

Since the model is linear, the velocities and surface elevations that would

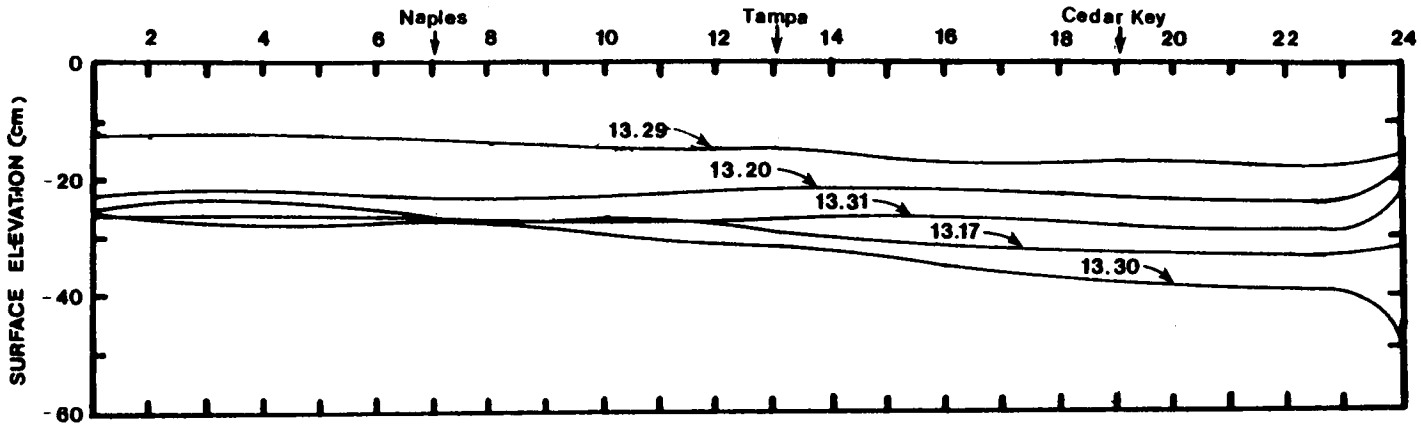

Figure 4.2.3: Steady-state coastal surface elevations for five boundary current configurations (13-30, 13-17, 13-27, 13-20, and 13-31)

result from a boundary current magnitude different than 100 cm s^{-1} can be found by simple scaling. For example, if the boundary current is assumed to be 50 cm s^{-1} instead of 100 cm s^{-1} then the current patterns shown in the figures still apply if the magnitude is divided by two.

Vukovich et al. (1980) and Behringer, et al (1977) have observed that the LC spends most of its time below 27° N. If the LC is assumed to impinge only on the lower half of the western boundary, a pair of cyclonic eddies are generated on the shelf as shown in Figure 4.2.4. This Case (13.17) is set-up identically to 13.30 except that a current of 100 cm s^{-1} is imposed only in column 1, rows 1 through 12 of the model grid (i.e., as a step function). The eddies are quite weak - displaying currents on the order of 1 cm s^{-1} as derived from the actual model print-out.

The influence of N_h on currents is demonstrated in Case 13.26 (Figure 4.2.5) which is the same as 13.17 except that N_h is one order of magnitude less or 10^8 cm^2 s^{-1}. The change in N_h causes the southern eddy observed in the previous case to disappear. The northern eddy remains. Current magnitudes and surface elevations are reduced by about 50%.

In Cases 13.17 and 13.26 described above, a discontinuity in the forcing mechanism is imposed in column 1 between row 12 where the y-component of the current is specified at 100 cm s^{-1} and row 13 where the current is initially zero. Frictional processes lessen the difference in currents at these two elements from 100 cm s^{-1} at model start-up to 40 cm s^{-1} at steady-state. It is this discontinuity in the forcing mechanism which supports the dual eddy system, as shown by Case 13-20, in which the specified y-component current at column 1 is varied linearly (i.e., as a ramp function) from 0 at row 12 to 100 cm s^{-1} at row 1. In this case Figure 4.2.6 shows the eddies are replaced by a simple southerly flushing action.

Unfortunately it is unclear whether the LC does in fact apply a relatively sudden discontinuity at the break and so it is difficult to say at this point

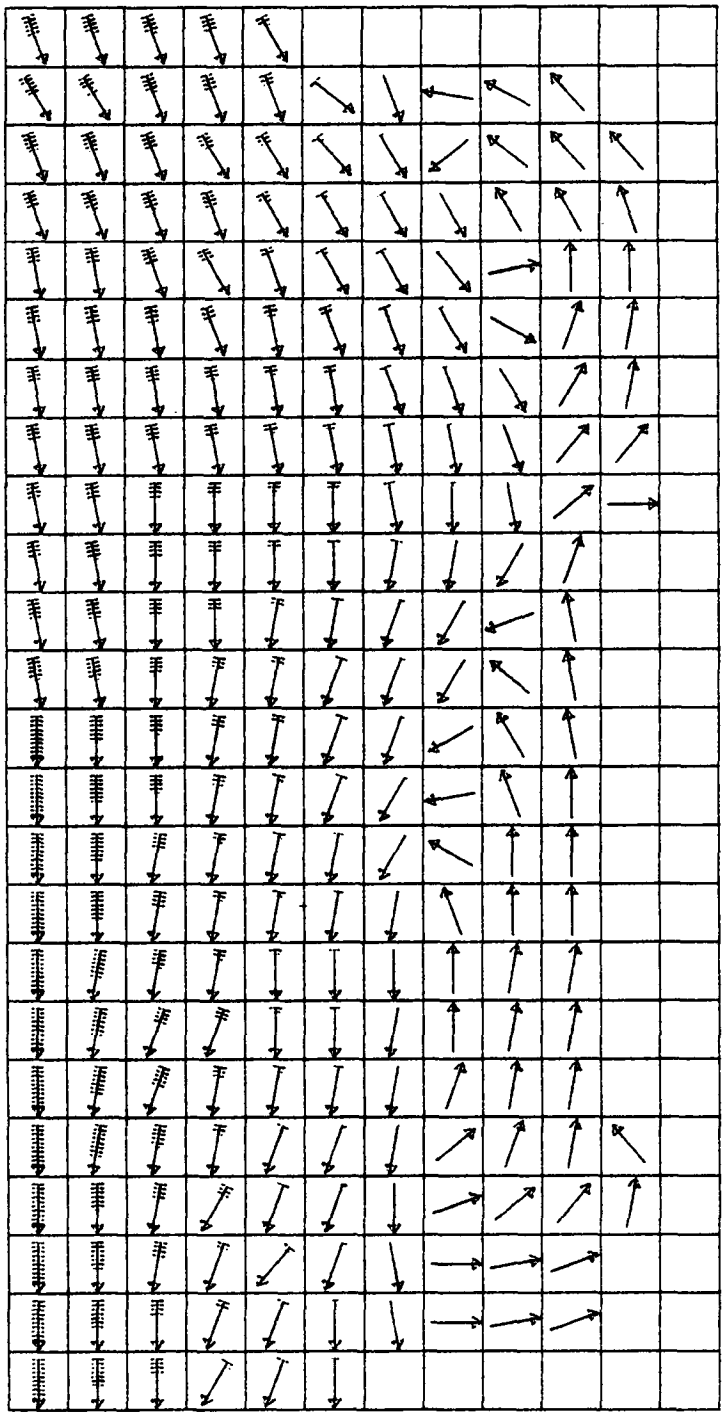

Figure 4.2.4: Steady-state surface currents due to constant boundary current imposed on lower half of western boundary (Case 13-17). Each grid element equals 30 km, each feather equals 10 cm s^{-1}. See Appendix D for listing of model input parameters.

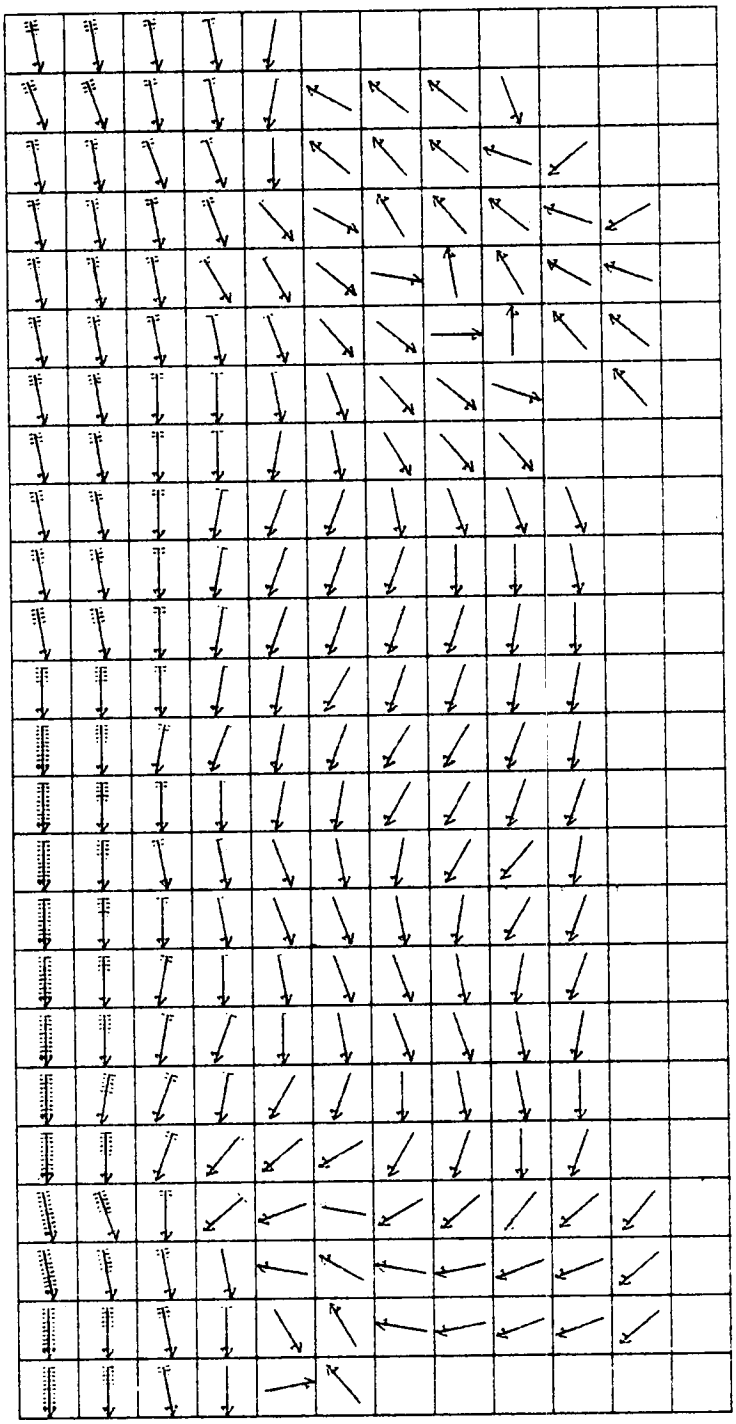

Figure 4.2.5: Steady-state surface currents due to constant boundary current imposed on lower half of western boundary (Case 13-26). Each grid element equals 30 km, each feather equals 10 cm s^{-1}. See Appendix D for listing of model input parameters.

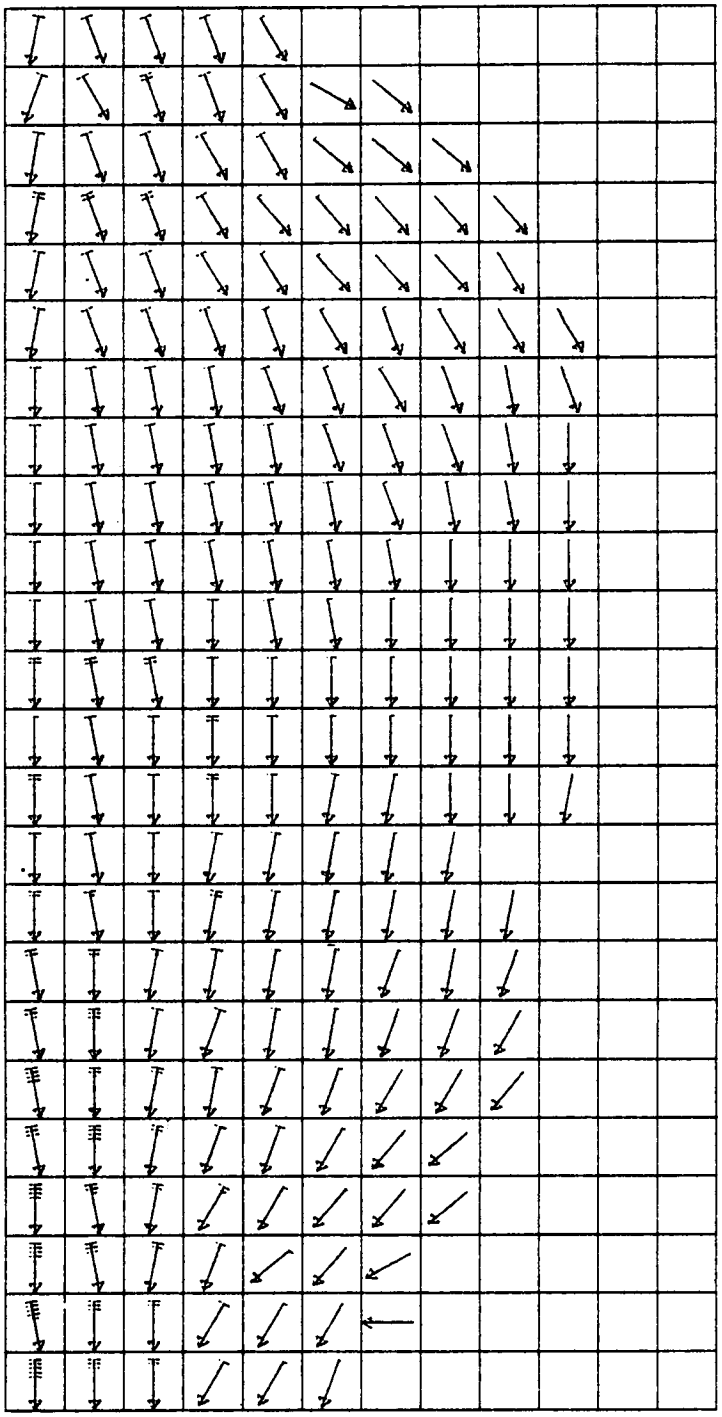

Figure 4.2.6: Steady-state surface currents due to linearly increasing boundary current imposed along lower half of western boundary (Case 13-20). Each grid element equals 30 km, each feather equals 20 cm s^{-1}. See Appendix D for listing of model input parameters.

whether Case 13-20 or 13-17 is more applicable to the WFS.

The cases studied thus far assume the specified boundary current varies as 100 cosine (0.7 z H^{-1}). In other words the velocity is almost uniform with depth. Case 13.29 shown in Figure 4.2.7 is identical to 13-17 except that the boundary current is specified as 100 cm s^{-1} in the upper 50 m and 0 cm s^{-1} from 50 m to the bottom. Figure 4.2.3 shows the surface elevation. When these results are compared to Case 13.17, it is apparent that the currents and surface elevations are significantly affected by the vertical variation of the boundary current.

4.2.3 Sensitivity to Time Varying Boundary Current

Niiler's Eddy Wave Field

Niiler (1976) has suggested that one of the most dominant influences of the LC on the deeper portions the WFS circulation is the propagation of eddies from the LC onto the shelf. He suggests that the eddy field has a characteristic wavelength of 600 km and period of 16 days.

Several runs were made to investigate the effect of eddy fields on the model circulation. Case 13-21 incorporates a time and space variation of the y-component of the velocity along column 1 of the form:

$$v_{1,m} = A \text{ SIN } (k \text{ m DL} - w \text{ t})$$

where:

A = the current magnitude

$v_{1,m}$ = the y-component of the velocity at element (1,m) referenced to the origin shown in Figure 3.6.1. m is the index in the y direction and has integer values between 1 and 24.

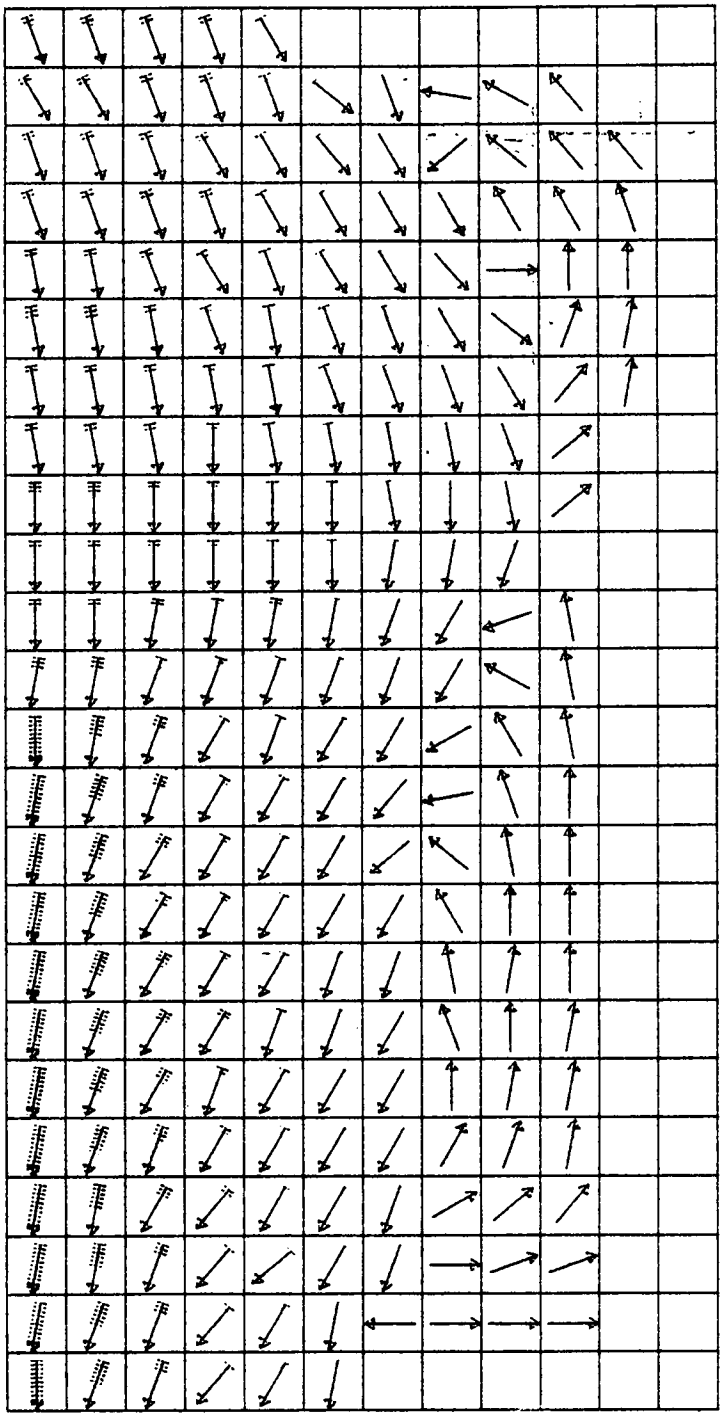

Figure 4.2.7: Steady-state surface currents due to linearly increasing boundary current imposed along lower half of western boundary (Case 13-29). Boundary current is imposed on upper 50 m of water column only. Each grid element equals 30 km, each feather equals 10 cm s^{-1}. See Appendix D for listing of model input parameters.

DL = the grid size (30 km)

k = the wave number or 2 pi / L, where L is the wavelength.

w = the phase speed, 2 pi / T, where T is the wave period (in hours)

t = the time in hours.

This forcing at the western boundary generates a series of barotropic waves which migrate onto the shelf and progress northward. Figures 4.2.8a-j show the resulting velocity fields at 2 day increments (T=16 days, L=600 km). The barotropic waves are clearly evident as the center of either cyclonic (trough of wave) or anticyclonic (crest of wave) eddies.

Of particular interest in the figures is the northward movement of divergence and convergence zones associated with the eddies. A divergence zone is seen in the first frame at 48 hours located at row 12. During the next three frames spanning 6 days, the zone can be seen to move progressively to the northwest corner where it disappears on about the 8th day. At 10 days (i.e. 240 hours) a convergence zone appears at the same area as the initial divergence zone. During the next three frames, the convergence zone can be followed as it propagates to the northwest corner. At 16 days, the cycle repeats, with the divergence zone reappearing.

Figure 4.2.9 shows the surface elevation as a function of time at Cedar Keys and Naples. The order of magnitude of the amplitude is 20 cm. Further sensitivity studies indicated that this amplitude was reduced by about 6 cm if N_h was reduced from the value of 10^9 used in Figures 4.2.8-9 to 10^8 cm^2 s^{-1}. Coastal surface elevations were reduced by only a few cm if the wave forcing was restricted to the southern half of the western boundary.

The propagation of barotropic waves onto the shelf is known to be dependent on the wavelength of the initial wave as shown by Kroll and Niiler (1976). An additional Case (13.24) was made to study the effect of decreasing the wavelength to 300 km. The propagation of both kinetic and potential energy

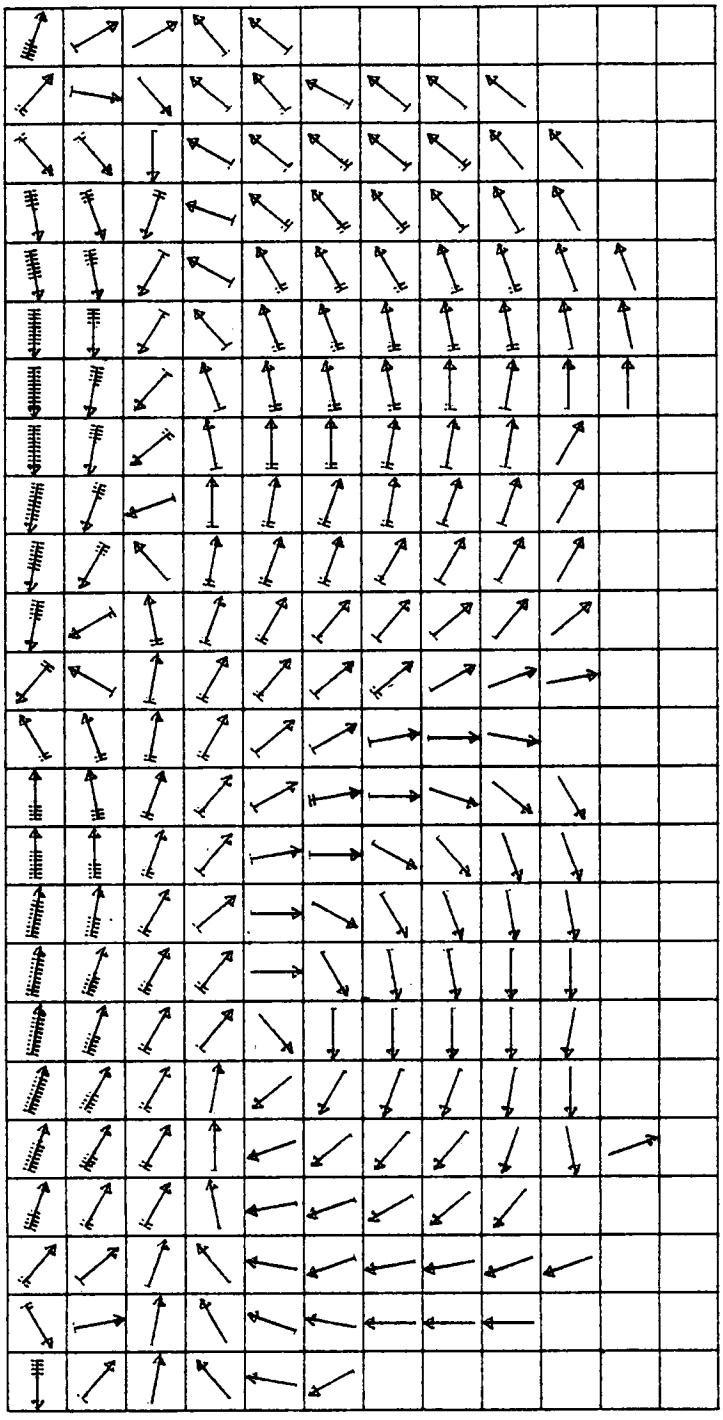

Figure 4.2.8a: Surface currents due to time-varying boundary current with wave-length of 600 km and period of 16 days (13-21). Each grid element equals 30 km, each feather equals 10 cm s^{-1}. See Appendix D for listing of model input parameters.

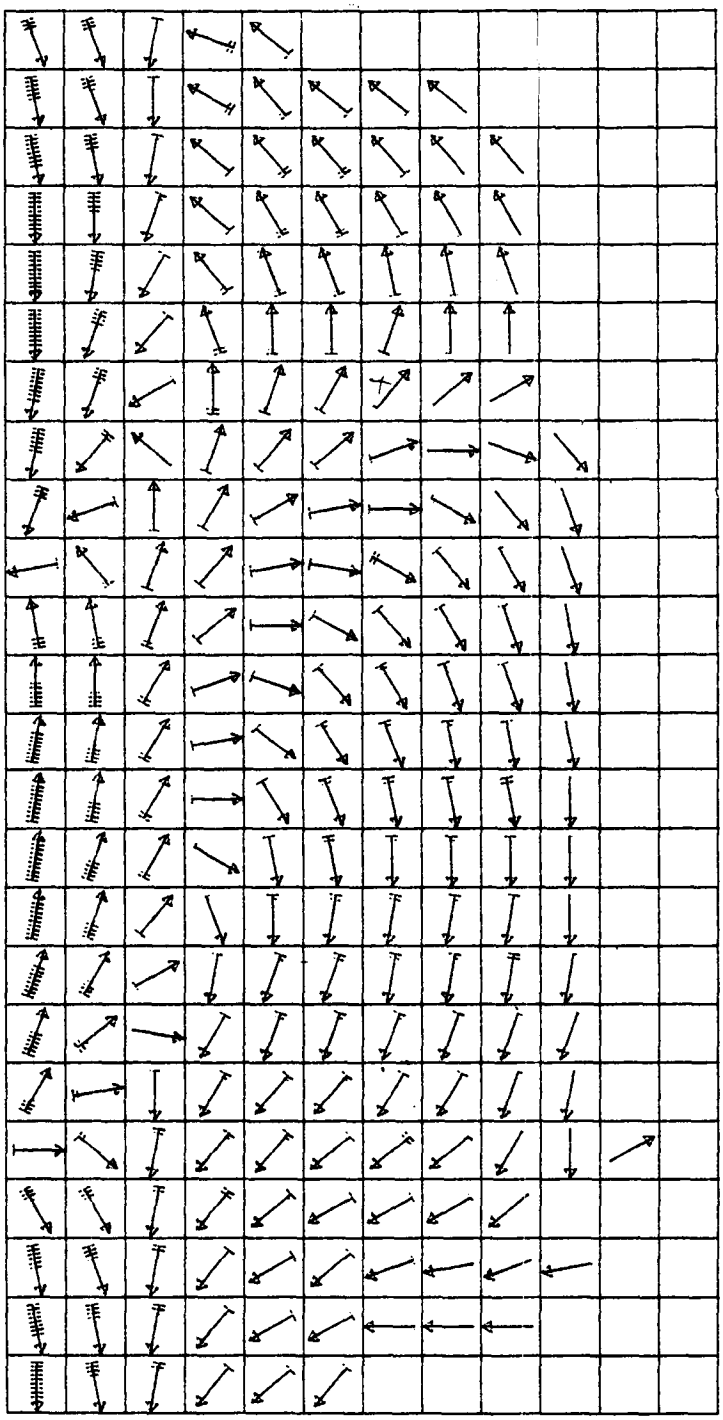

Figure 4.2.8b: Surface currents due to time-varying boundary current with wave-length of 600 km and period of 16 days (13-21). Each grid element equals 30 km, each feather equals 10 cm s^{-1}. See Appendix D for listing of model input parameters.

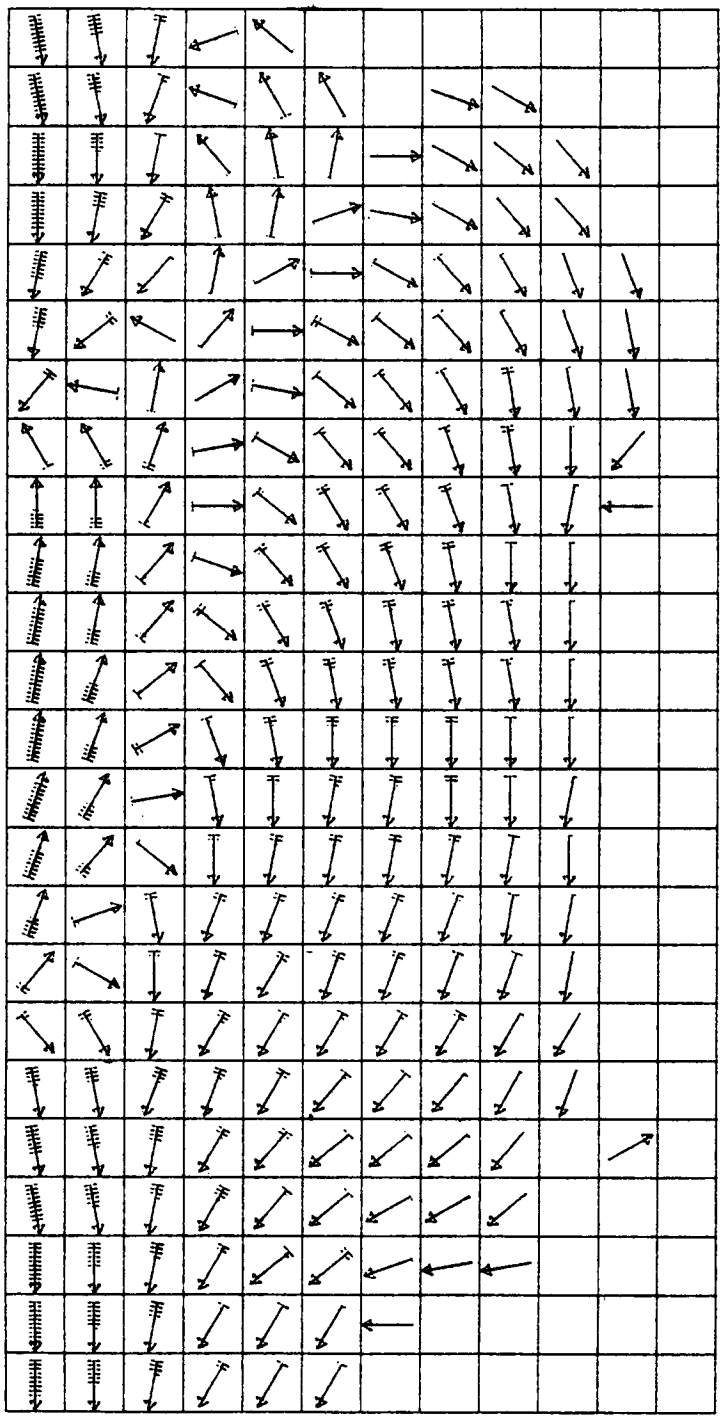

Figure 4.2.8c: Surface currents due to time-varying boundary current with wave-length of 600 km and period of 16 days (13-21). Each grid element equals 30 km, each feather equals 10 cm s^{-1}. See Appendix D for listing of model input parameters.

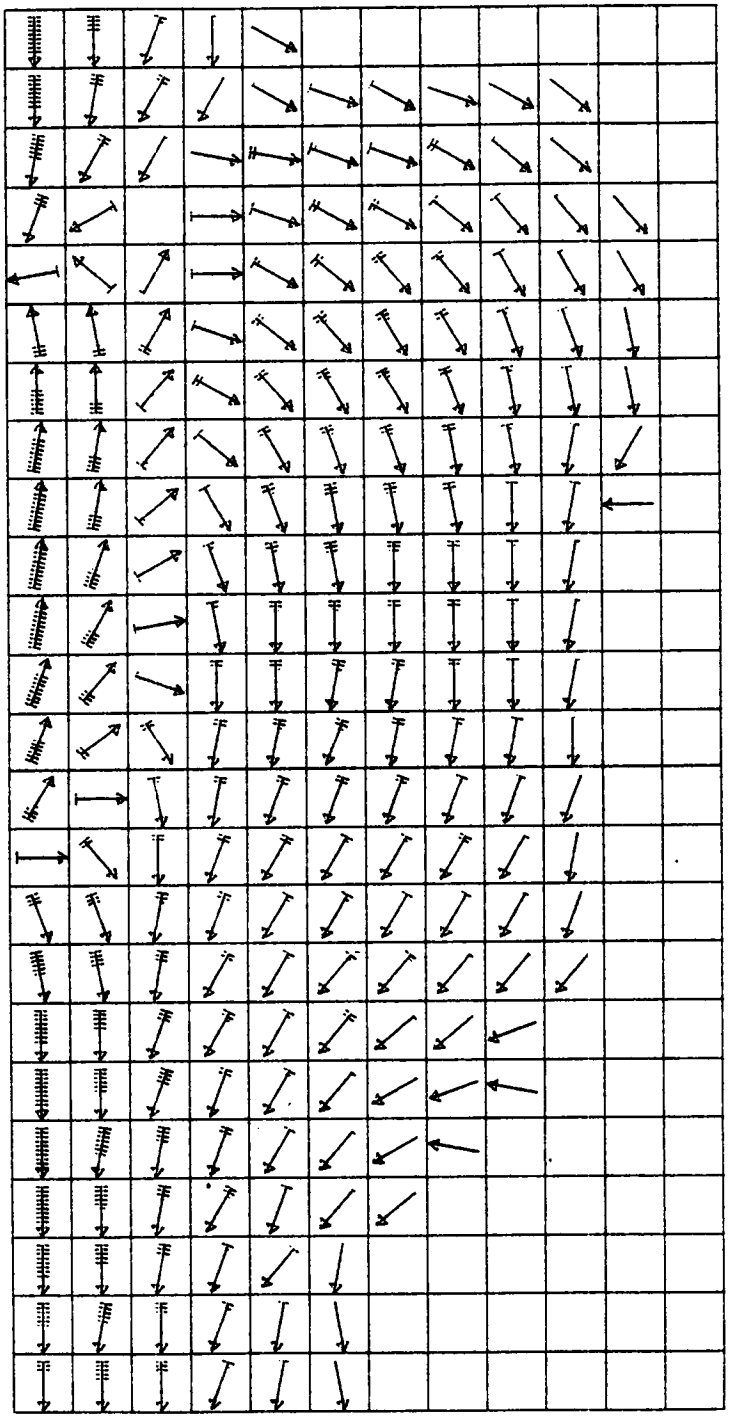

Figure 4.2.8d: Surface currents due to time-varying boundary current with wave-length of 600 km and period of 16 days (13-21). Each grid element equals 30 km, each feather equals 10 cm s^{-1}. See Appendix D for listing of model input parameters.

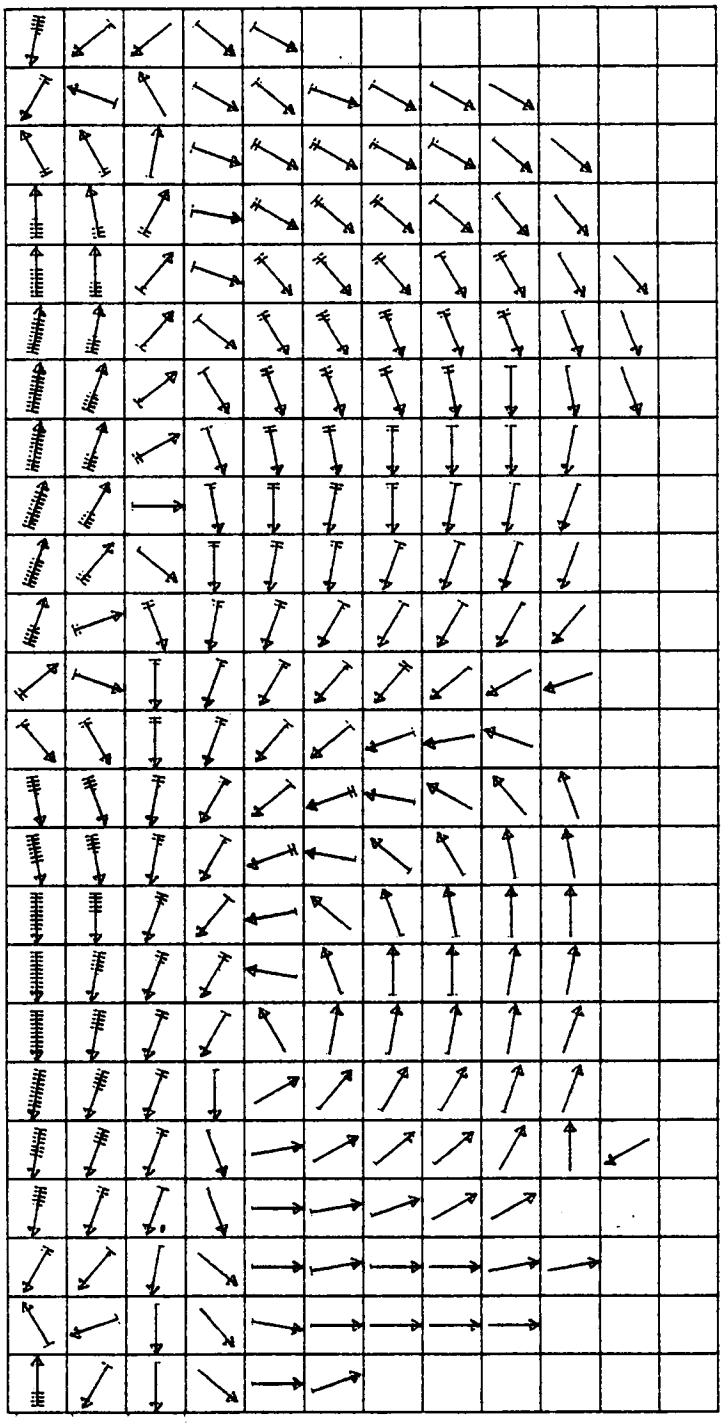

TIME =240.00 H

Figure 4.2.8e: Surface currents due to time-varying boundary current with wave-length of 600 km and period of 16 days (13-21). Each grid element equals 30 km, each feather equals 10 cm s^{-1}. See Appendix D for listing of model input parameters.

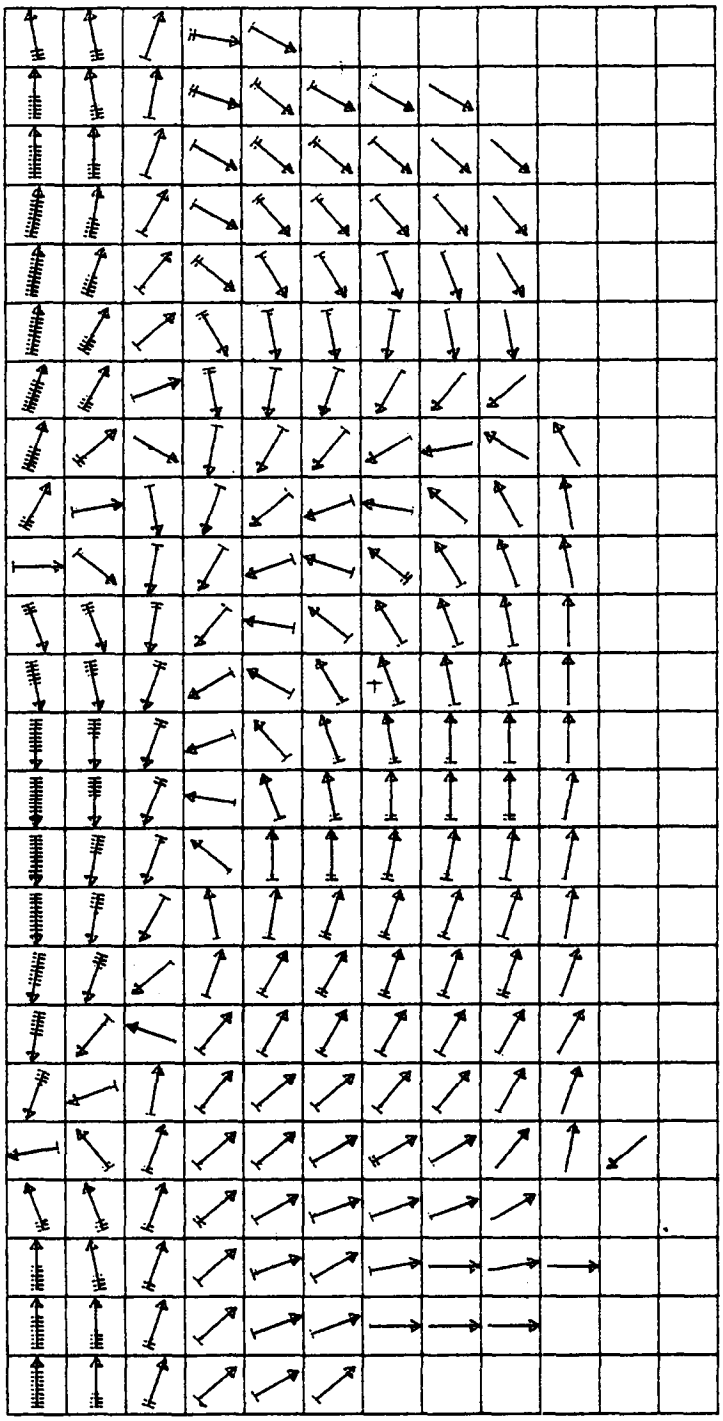

Figure 4.2.8f: Surface currents due to time-varying boundary current with wave-length of 600 km and period of 16 days (13-21). Each grid element equals 30 km, each feather equals 10 cm s^{-1}. See Appendix D for listing of model input parameters.

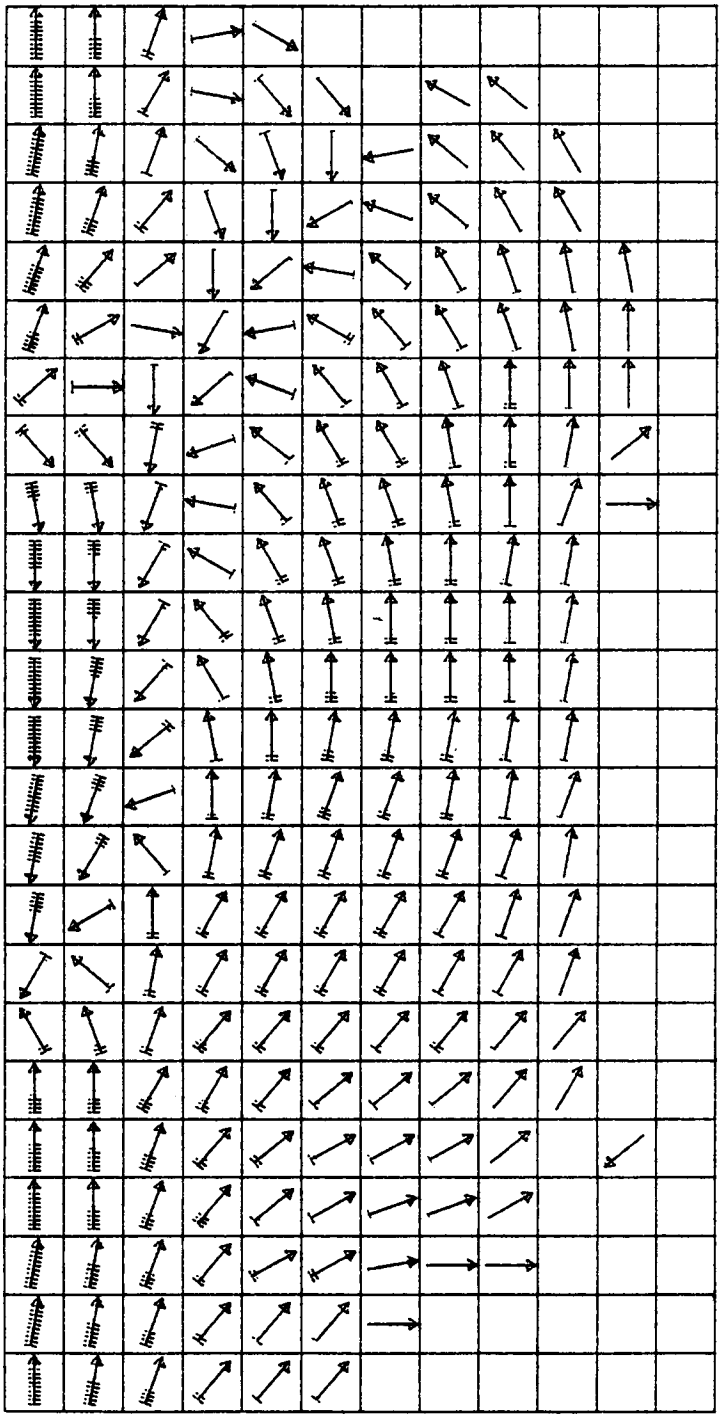

TIME =336.00 H

Figure 4.2.8g: Surface currents due to time-varying boundary current with wave-length of 600 km and period of 16 days (13-21). Each grid element equals 30 km, each feather equals 10 cm s^{-1}. See Appendix D for listing of model input parameters.

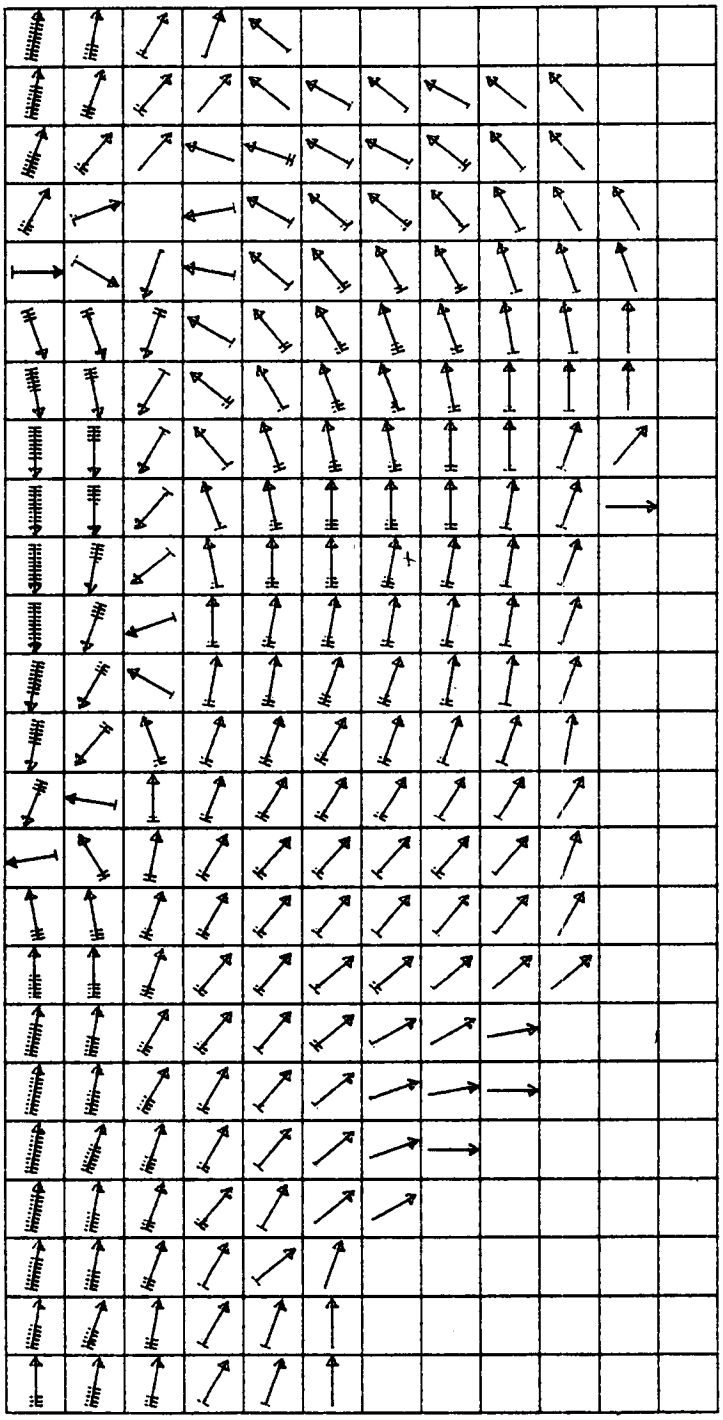

Figure 4.2.8h: Surface currents due to time-varying boundary current with wave-length of 600 km and period of 16 days (13-21). Each grid element equals 30 km, each feather equals 10 cm s^{-1}.

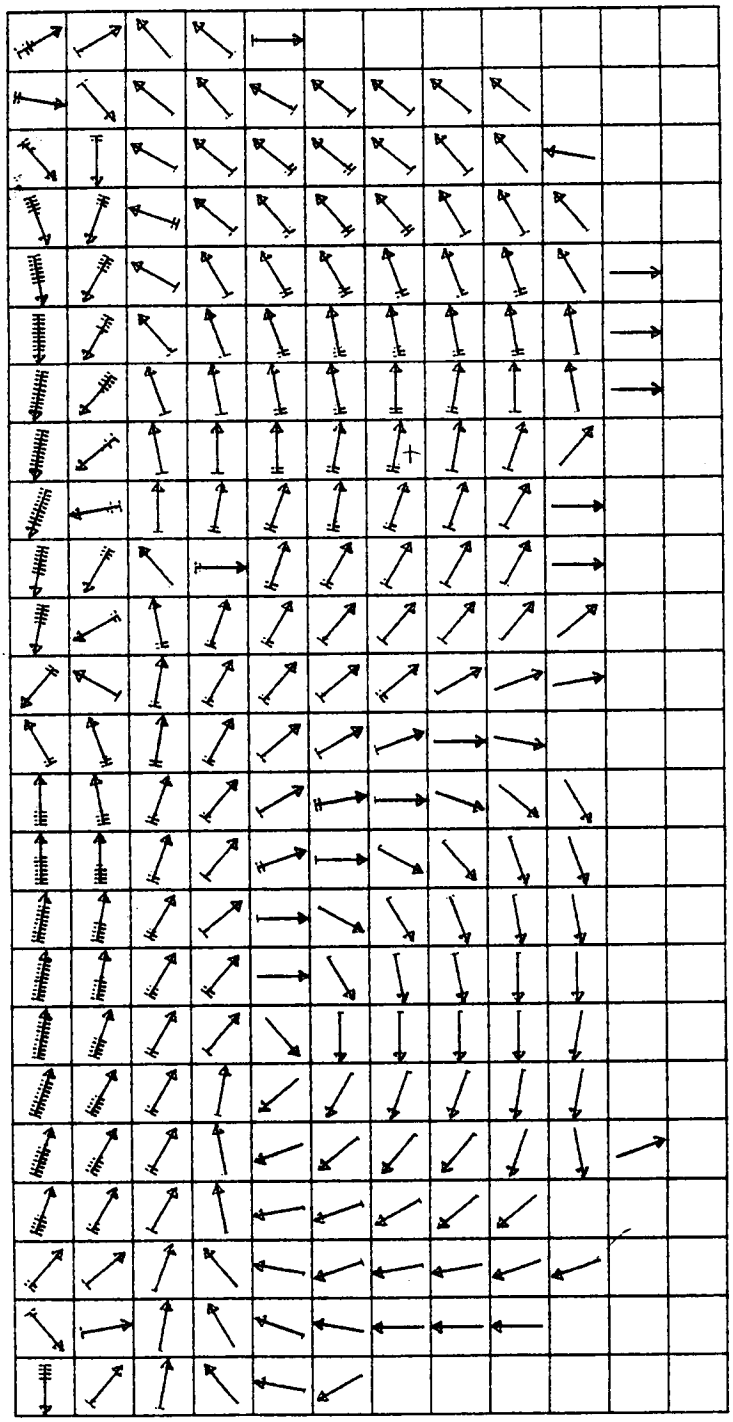

TIME =432.00 H

Figure 4.2.8i: Surface currents due to time-varying boundary current with wave-length of 600 km and period of 16 days (13-21). Each grid element equals 30 km, each feather equals 10 cm s^{-1}. See Appendix D for listing of model input parameters.

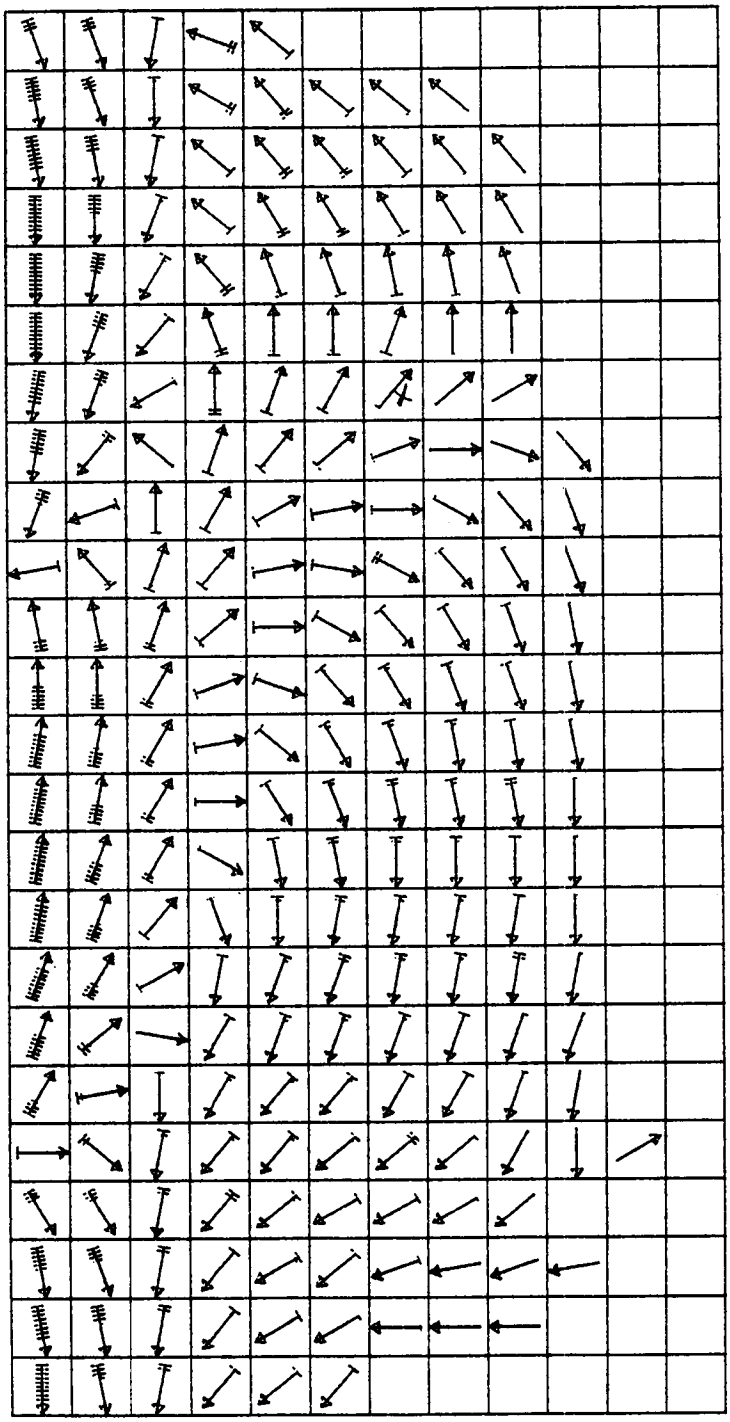

Figure 4.2.8j: Surface currents due to time-varying boundary current with wave-length of 600 km and period of 16 days (13-21). Each grid element equals 30 km, each feather equals 10 cm s^{-1}. See Appendix D for listing of model input parameters.

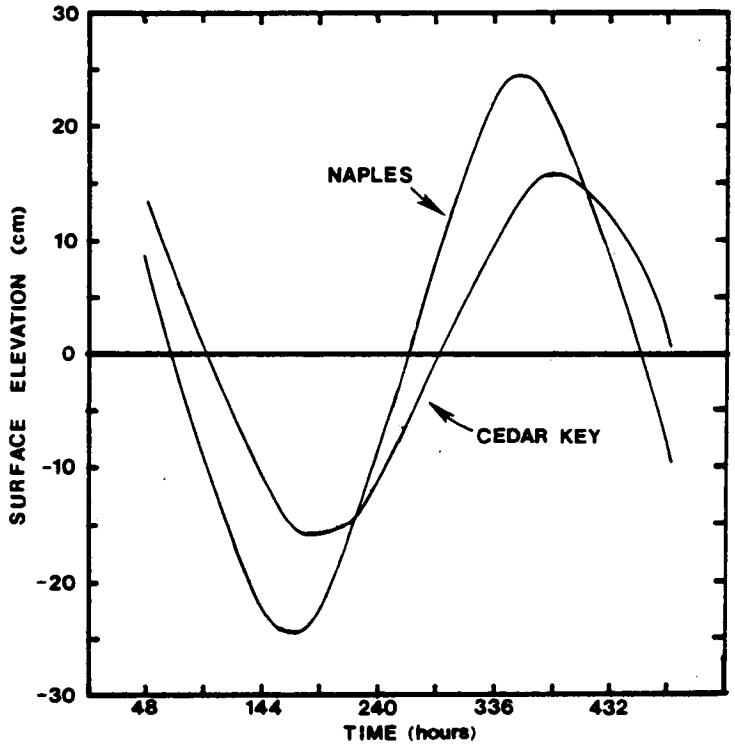

Figure 4.2.9: Surface elevations at Naples and Cedar Keys due to time varying boundary current (13.21).

onto the shelf was found to be substantially reduced. In the case of coastal surface elevations, the amplitudes for the 300 km wavelength at Naples and Cedar Keys are 15 and 11 cm, respectively, which compares to 24 and 16 cm for the 600 km wavelength. Currents display a similar decrease.

Vukovich et al. (1978) have suggested that the meanders they observed are of the same nature as the eddy wave Niiler (1976) observed. However, there are a number of differences between the two processes including the sign of the phase speed, which suggest that the two processes are fundamentally different. Nevertheless, at this point it is a simple matter to point out that if we assume the Vukovich-Niiler waves are identical except for the phase speed, the Vukovich et al. wave can be expected to generate essentially the mirror image (about row 12) of Case 13-21. This is due to the linear nature of the model and the symmetry of the WFS topography.

The importance of the model behavior displayed in Figures 4.2.8 is three-fold. First, the cyclic reversals are qualitatively similar to those observed in much of the Shelf Dynamics Experiment (SDE) data. Second, the divergence zones offer a mechanism to explain the large divergence seen in the drifter data noted in Section 2.5. Third, the coastal surface elevation fluctuations are on the order of 20 cm, a value which is not corroborated by the available observations.

Temporal Variations in Northward Penetration of Loop Current

The northward limit of the LC is known to vary by almost 500 km during a period on the order of one year. The model was used to test the sensitivity of currents on the WFS to changes in the LC position. Figures 4.2.2-4 and 4.2.10 show results for three positions of the LC: Case 13-30 (Figure 4.2.2), LC impinging along entire shelf; Case 13-17 (Figure 4.2.4), LC impinging on lower one-half; and Case 13-31 (Figure 4.2.10), LC impinging on lower one-fourth. In all three cases the LC has been assumed to vary as a step function. The results show that the LC is remarkably effective in

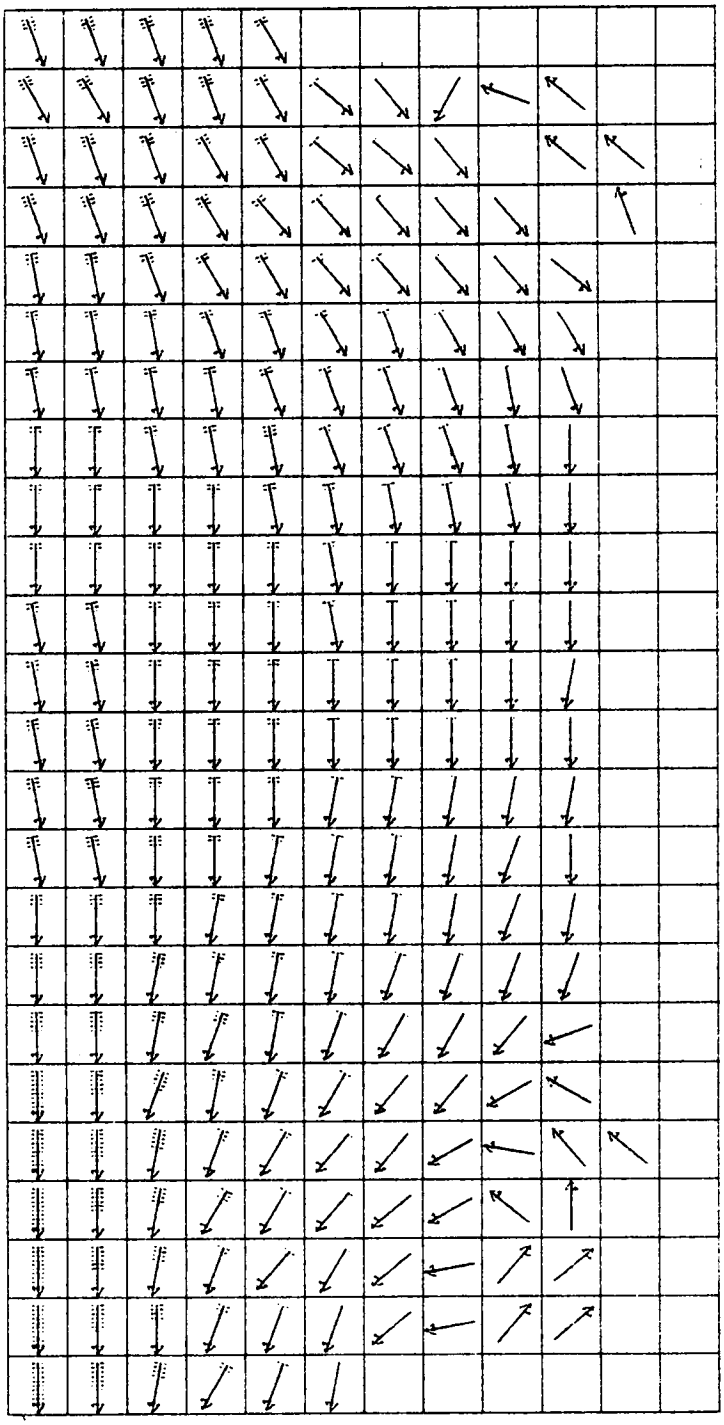

Figure 4.2.10: Steady-state surface currents due to constant boundary current imposed on lower one-fourth of western boundary (13.31). Each grid element equals 30 km, each feather equals 10 cm s^{-1}. See Appendix D for listing of model input parameters.

transferring momentum to the northern shelf even when it is tangent only in the lower one-fourth of the shelf as evidenced by the surface elevations along the northern coast which are only 10 cm less for case 13.31 than for case 13.30 (Figure 4.2.3).

4.3 Sensitivity to Changes in Bottom Friction and Eddy Viscosity

The sensitivity of water motion on the WFS to changes in c_b and N_v was investigated for two forcing mechanisms: the wind and a boundary current. In all the results which follow the surface elevations were set to zero at the western boundary and the surface gradient was set to zero at the northern and southern water boundary. A value for N_h of 10^9 cm^2 s^{-1} was used and all results were for steady-state.

4.3.1 Wind Forcing

Figures 4.3.1-4 show results in which the forcing consists of a spatially constant wind increasing from 0 to 10 m s^{-1} during the initial 20 hours of the run. Figure 4.3.1 shows a plan view of the surface velocities for Case 5.5 which serves as a basis for comparisons. Case 5.7 shown in 4.3.2 is the same as Case 5.5 except that c_b is 0.1 cm s^{-1} or four times c_b used in 5.5. A comparison of Figures 4.3.1 and 4.3.2 indicates that the surface velocities are essentially identical for the two cases as are the coastal elevations (see Figure 4.3.3). Velocities beneath the surface become progressively more affected as one moves into shallower water and/or deeper into the water column. For example, near bottom velocities at the 40 m isobath for Case 5.7

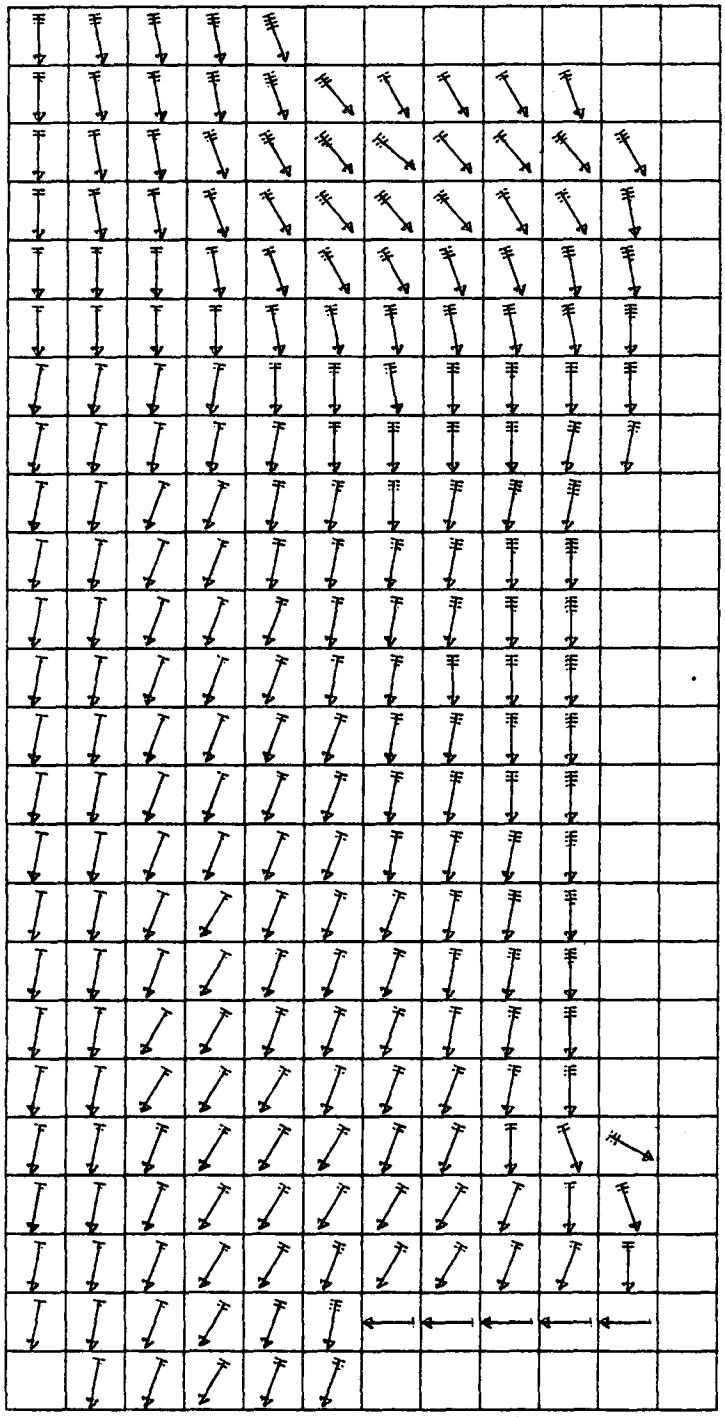

Figure 4.3.1: Steady-state surface velocities due to steady alongshore wind of 10 m s^{-1} (Case 5.5). Each grid element equals 30 km, each feather equals 10 cm s^{-1}. See Appendix D for listing of model input parameters.

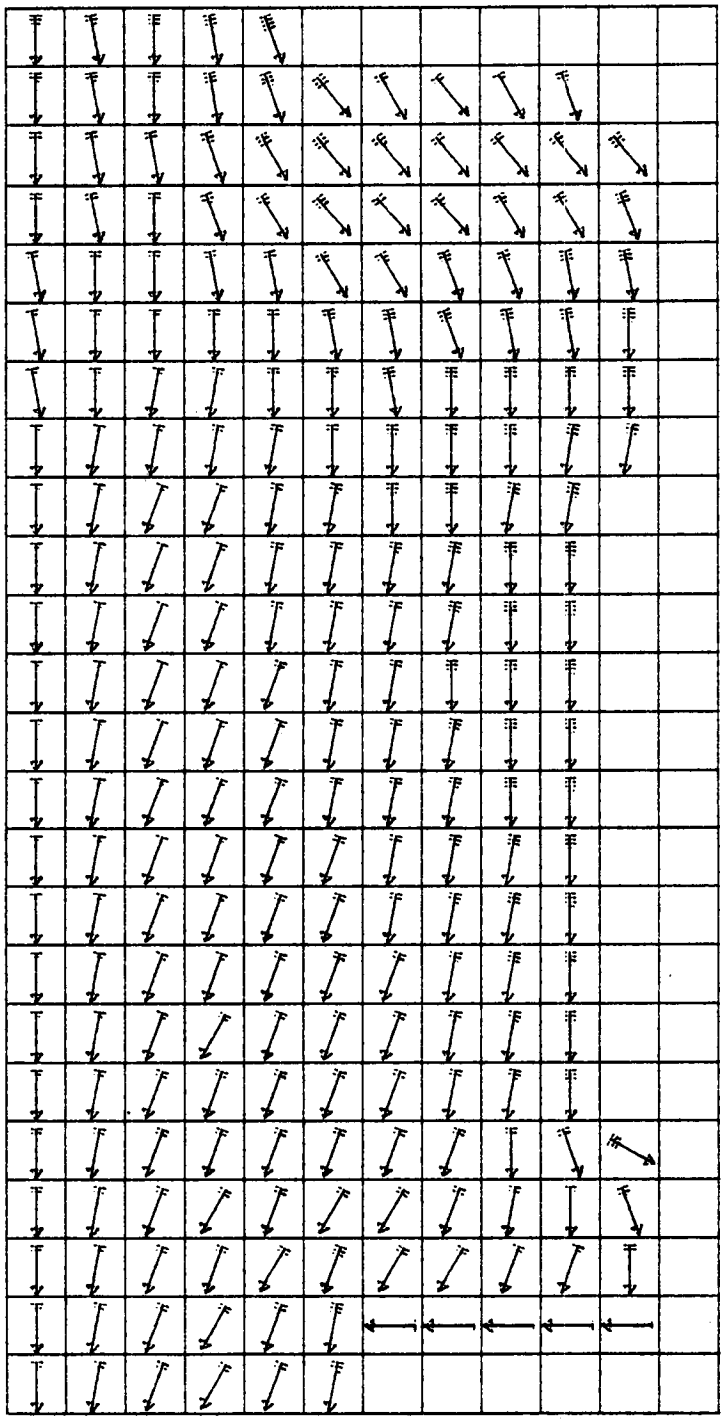

Figure 4.3.2: Steady-state surface velocities due to steady alongshore wind of 10 m s^{-1} (Case 5.7). Each grid element equals 30 km, each feather equals 10 cm s^{-1}. See Appendix D for listing of model input parameters.

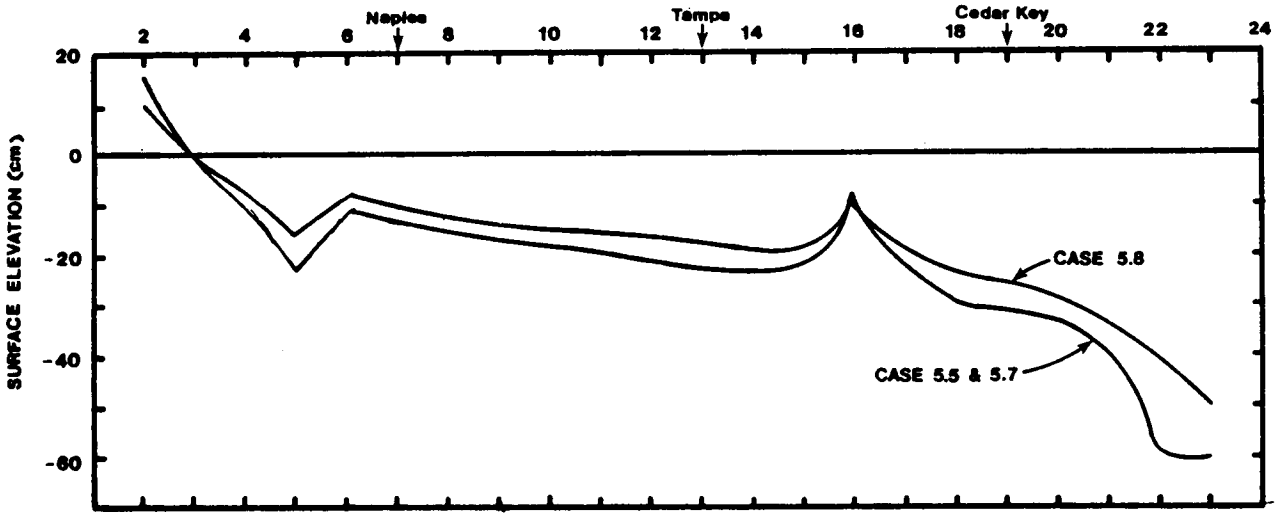

Figure 4.3.3: Comparison of surface elevations along the coast for various values of c_b and N_v (Cases 5.5, 5.7, and 5.8).

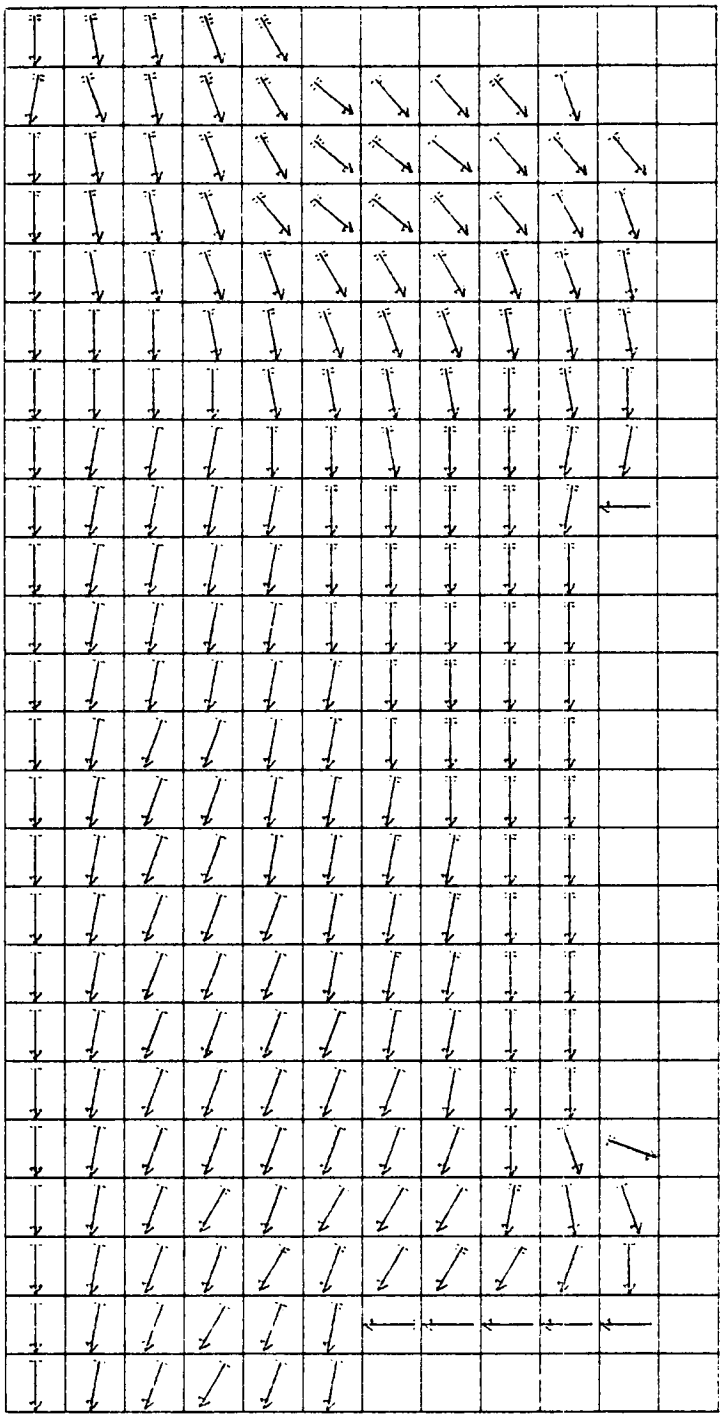

Figure 4.3.4: Steady-state surface velocities due to steady alongshore wind of 10 m s^{-1} (Case 5.8). Each grid element equals 30 km, each feather equals 10 cm s^{-1}. See Appendix D for listing of model input parameters.

are approximately 50% of those for Case 5.5. The reduction becomes progressively less as one moves seaward and totally disappears in about 100 m of water. These observations are not surprising when one considers that the Ekman depth of frictional influence is about 30 m.

Case 5.8 is the same as 5.5 except that N_v is twice the value used for 5.5. A comparison of Figures 4.3.1 and 4.3.4 demonstrates that surface velocities are noticeably affected by the change in N_v as are the coastal surface elevations shown in Figure 4.3.3. Velocity directions remain largely unchanged but the magnitudes for Case 5.8 tend to be smaller than 5.5. The difference between the two cases is a strong function of water depth, varying from 50% in the shallowest water to 0% in water depths exceeding 100 m. Surface currents are more dramatically affected by changes in N_v than are bottom currents. As a consequence the vertical shear in the water column is larger in case 5.5 than 5.8.

Two peaks in the coastal surface elevations are evident at grids (11,5) and (11,16) in Figure 4.3.3. These are partially numerical in origin and result from the staggered finite difference scheme used with the lateral eddy viscosity term. The peaks can be removed but a significant computational burden is imposed. This was not felt justified because sensitivity studies indicated the phenomenon was very local and is at its worst when the winds are alongshore and from the north(i.e. the peaks are never worse than those shown in Figure 4.3.3).

4.3.2 Boundary Current Forcing

As indicated in Section 4.2, it has been suggested that the LC generates eddies which propagate onto the shelf. The eddies studied in 4.2 were barotropic in nature and the vertical current shear was quite small (i.e., current velocity was nearly constant with depth). One would expect bottom

friction to play a more important role for such currents than was evident for the case of wind-driven currents examined above. Sensitivity studies support this reasoning.

Figure 4.3.5 shows the surface elevations as a function of time for Naples for Cases 13.24, 13.25, and 13.27. Case 13.24 serves as the basis for comparison and was originally described in Section 4.2. A sinusoidal forcing was applied at the southern half of the western boundary with T = 16 days and L = 300 km. The values for c_b, W_{*s} and N_h were 0.025 cm s^{-1}, 0.5 cm s^{-1} and $10^9 cm^2$ s^{-1}, respectively. Case 13.25 is the same as 13.24 except c_b was increased by a factor of four to 0.1 cm s^{-1}. Likewise, 13.27 is identical to 13.24 except N_v was increased by a factor of two. As indicated in Figure 4.3.5, the increase in N_v has no appreciable affect on surface elevations but the increase in c_b decreased the coastal surface elevations by about 20%. Similar changes apply to the velocities on the shelf. Therefore, LC induced flows are sensitive to input values of c_b.

4.4 Spatially Variable Coriolis Parameter

Several low frequency shelf wave phenomena such as Kelvin and Rossby waves are affected by spatial variation in the Coriolis parameter, becoming totally dependent upon the Coriolis differential in the absence of topographic variation. The boundaries of the WFS stretch from roughly 24^oN latitude in the south to 30^o in the north, resulting in a variation in the Coriolis parameter of 5.8×10^{-5} to $7.4 \times 10^{-5} s^{-1}$. This variation is not insignificant, and at the suggestion of Drs. Reid, Niiler and Sturges (personal communication, May 1981), the model was modified to include a spatial variation in the Coriolis parameter. The modifications were straight

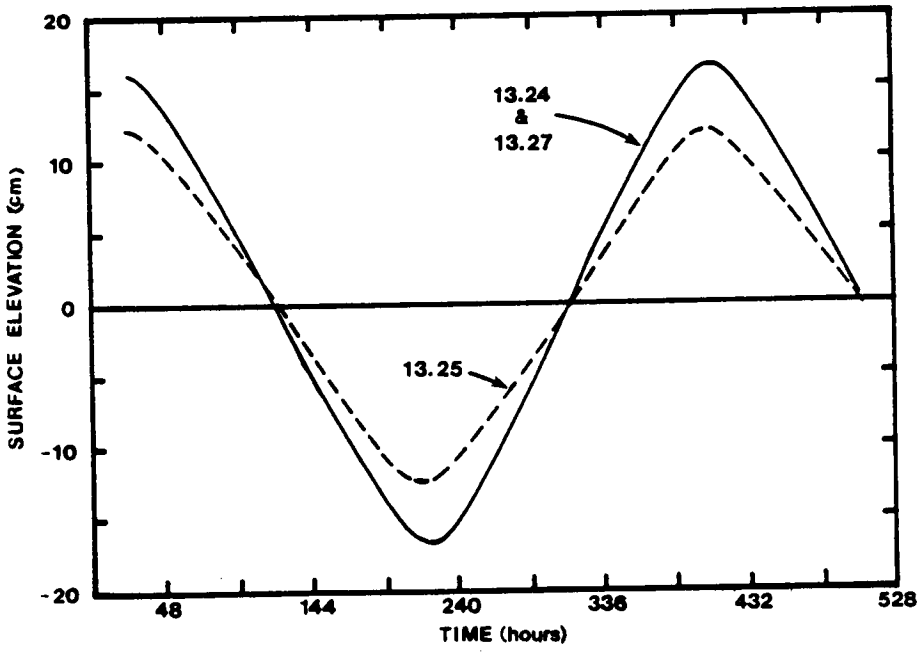

Figure 4.3.5: Temporal changes of surface elevation at Naples for various boundary current configurations (13.24, 13.25, and 13.27).

forward and details are included in Appendix E.1. The model implementation is analogous to the Beta Plane approximation often incorporated in analytic methods used to investigate shelf wave phenomena (e.g., Pedlosky, 1979).

Some simple sensitivity studies were performed to investigate the importance of the Coriolis differential in the model. An alongshore wind of 10 m s^{-1} was uniformly imposed on the model grid with a ramp function of 20 hours (i.e. the same wind forcing function used in Case 5.5) and the model results were compared to Case 5.5 in which the Coriolis parameter was assumed constant. The modeled surface elevations for both runs were within 1 cm of each other at all times. Likewise, the velocities compared to within 1 cm s^{-1}.

Based on the above findings it can be argued that the Coriolis differential is not very significant when compared to topographic effects. However, the case studied is simple and for more complicated situations the Coriolis differential may be more substantial. Because of this possibility and because the cost of including the Coriolis differential is negligible, it is included in all production runs.

4.5 Vertical Stratification

Vertical density stratification is evident on the shelf from April to October (see Section 6.1). The effect of stratification can be included in the model via the vertical eddy viscosity coefficient (N_v) as discussed in Section 4.1.3. In general, stratification will greatly suppress local turbulence as well as the transfer of turbulence through the shear zone surrounding the thermocline. In the case of flow which is primarily driven by surface winds, stratification will suppress the transfer of turbulence from the mixed layer

to the underlying layer. This means that N_v in the lower layer will tend to be smaller than the mixed layer, suggesting a distribution for N_v as shown in Figure 4.5.1.

The choice of the layer depths, H_1 and H_2, is not simple. Niiler (1976) states that the thermocline rarely is lower than 30 m from the surface. For this study, we have specified the two depths to be 20 and 40%, respectively, of the total depth, e.g. at the 50 m isobath, the thermocline is placed between 10 and 20 m.

Equations 4.1-3 can be used to estimate N_v. Values for the parameters needed to calculate the bulk R_i were estimated as follows: (1) $\Delta\rho$ = 0.002 g cm^{-3} as suggested by the statistical analysis of long term hydrographic data for the summer described in Section 6.1, (2) average mixed layer and total depths of 20 m and 50 m, respectively, and (3) s = 0.4-0.2 cm s^{-1} = 0.2 cm s^{-1}, and. Estimation of s is particularly difficult because there are no summer current data on the shelf in which measurements were simultaneously made in the mixed and lower layers. In lieu of actual data, Reid (personal communication, 1982) has suggested that the ratio of mixed layer to bottom layer velocity be taken as two.

When substituted into equation 4.3, the parameters yield a R_i of approximately 15. Substituting this into 4.2 suggests that N_{vl} (the N_v in the lower layer) should be approximately a factor of ten less than N_{vm} (the N_v in the mixed layer). This value compares nicely to the factor used by Forristall (1980).

The surface value for N_{vm} can be estimated from 4.1 using the mixed layer depth, $H_1 + H_2$ /2, instead of the total depth. Assuming W_{*s} = 0.5 cm s^{-1} and R = 12 as in Section 4.1.3 indicates a value for N_{vm} of 0.3 cm s^{-2} at the 200 m isobath. It follows from the previous paragraph that N_{vl} = 0.03 cm s^{-2}. Both N_{vl} and N_{vm} decrease in proportion to the local water depth as one moves into shallower water (i.e., N_{vm}= 0.3H/200, N_{vl}=0.03H/200).

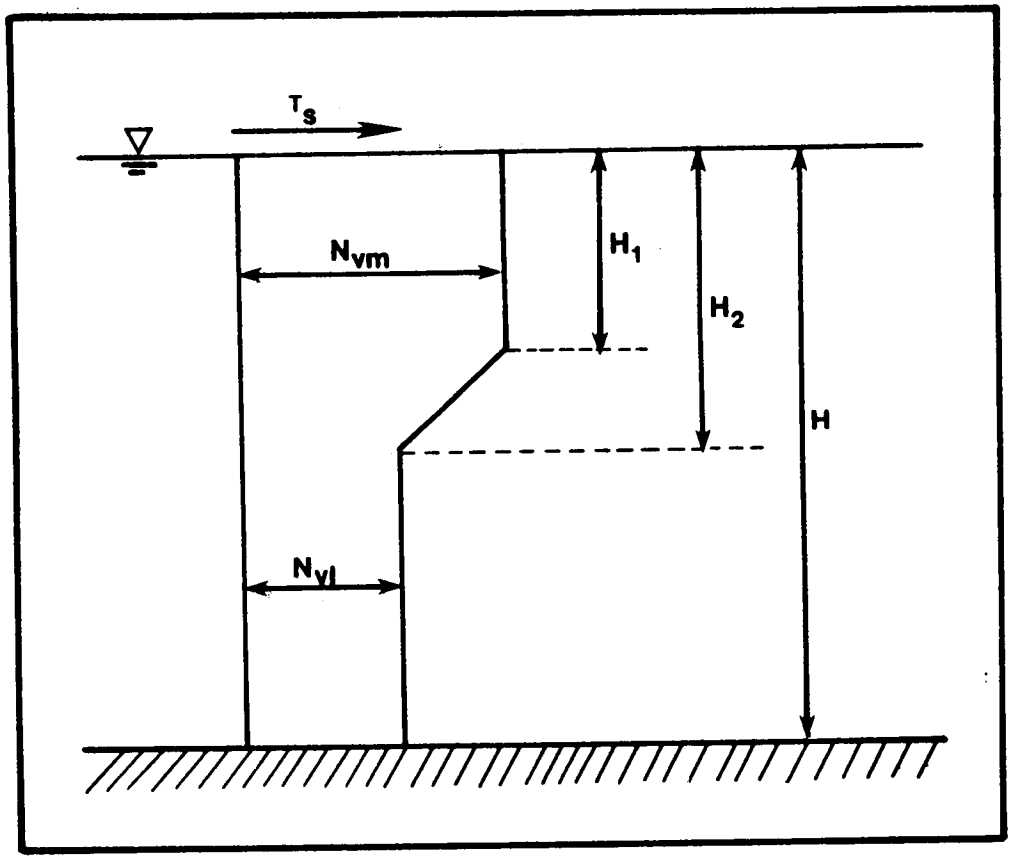

Figure 4.5.1: Variation of N_v appropriate for typical summer stratification on the WFS.

Figures 4.5.2-3 show the surface elevations and plan views of velocities at surface, mid-depth, and the bottom (Case 19.7). Forcing is due to alongshore, northerly winds at 10 m s^{-1}. A somewhat simplified bathymetry was used to be consistent with that used in Section 4.6.2. The input parameters for this case are identical to Case 5.5 except that vertical stratification has been included by varying N_v in the vertical as described above. As can be seen by comparing Figures 4.5.3 to 4.3.1, surface currents for the stratified case are generally higher than for the homogeneous case while currents at mid-depth and bottom are lower. Surface elevations for the stratified case (19.7) are about 10% higher than Case 5.5 (compare Figures 4.5.2 and 4.3.3). These features are consistent with classical two layer flow theory. Note that Figure 4.5.3c shows the velocity at 100% of the depth (i.e., the "bottom"). This depth is actually a few cm above the physical bottom and would correspond to the velocity at the top of the bottom log layer. This comment applies to all subsequent figures with depth shown as 100%.

4.6 Horizontal Density Gradients

4.6.1 Verification of Model Modifications

As part of the WFS study, the model was modified to include flow driven by horizontal density gradients. Appendix E.3 gives the details of the implementation used in the model. To verify model coding, stability and convergence, the model was set up for a simple test case and compared agast the analytic solution. Derivation of the analytic solution is given in

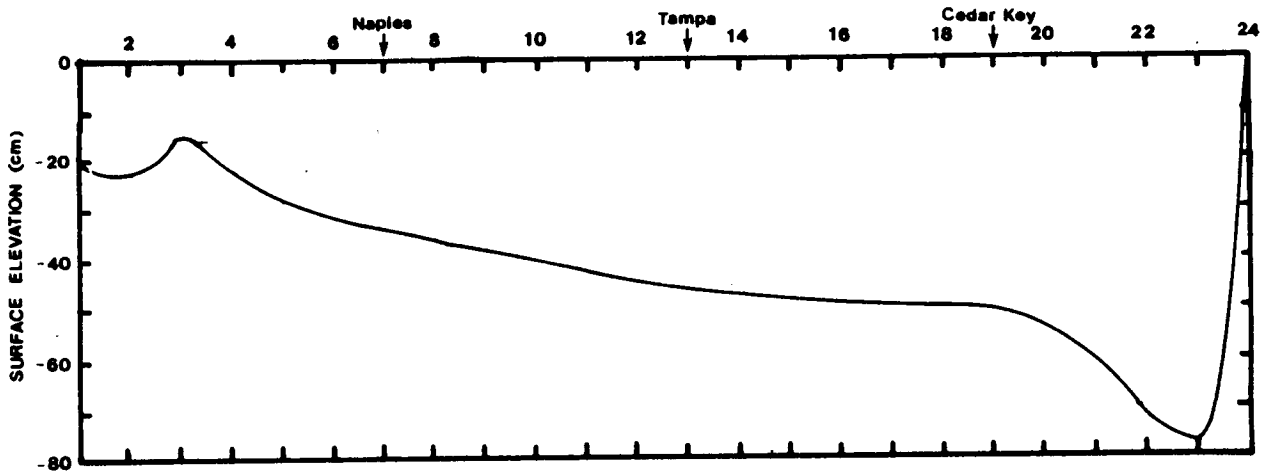

Figure 4.5.2: Steady-state coastal surface elevations due to alongshore, northerly winds of 10 m s^{-1}, with typical summer stratified conditions (19.7).

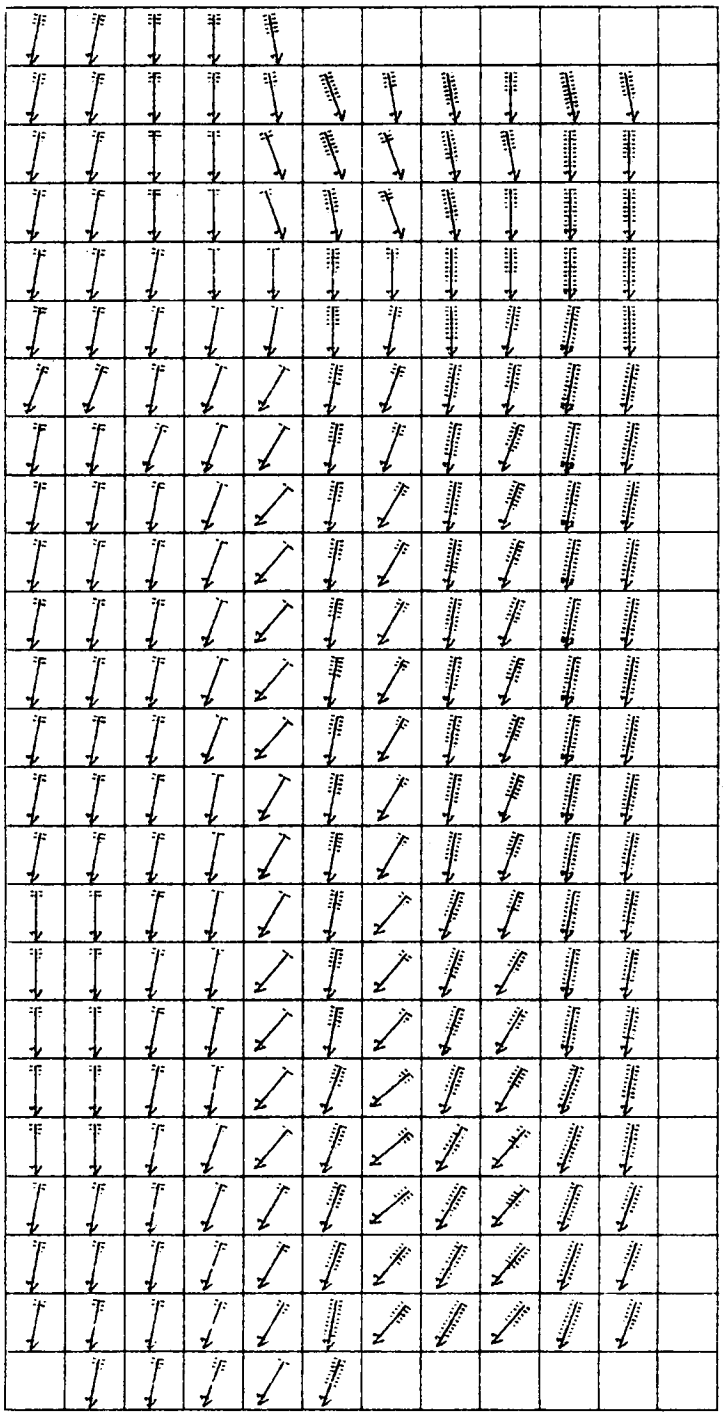

Figure 4.5.3a: Steady-state currents at surface due to alongshore winds of 10 m s^{-1} with typical summer stratified conditions (19.7) Each grid element equals 30 km, each feather equals 10 cm s^{-1}. See Appendix D for listing of input parameters.

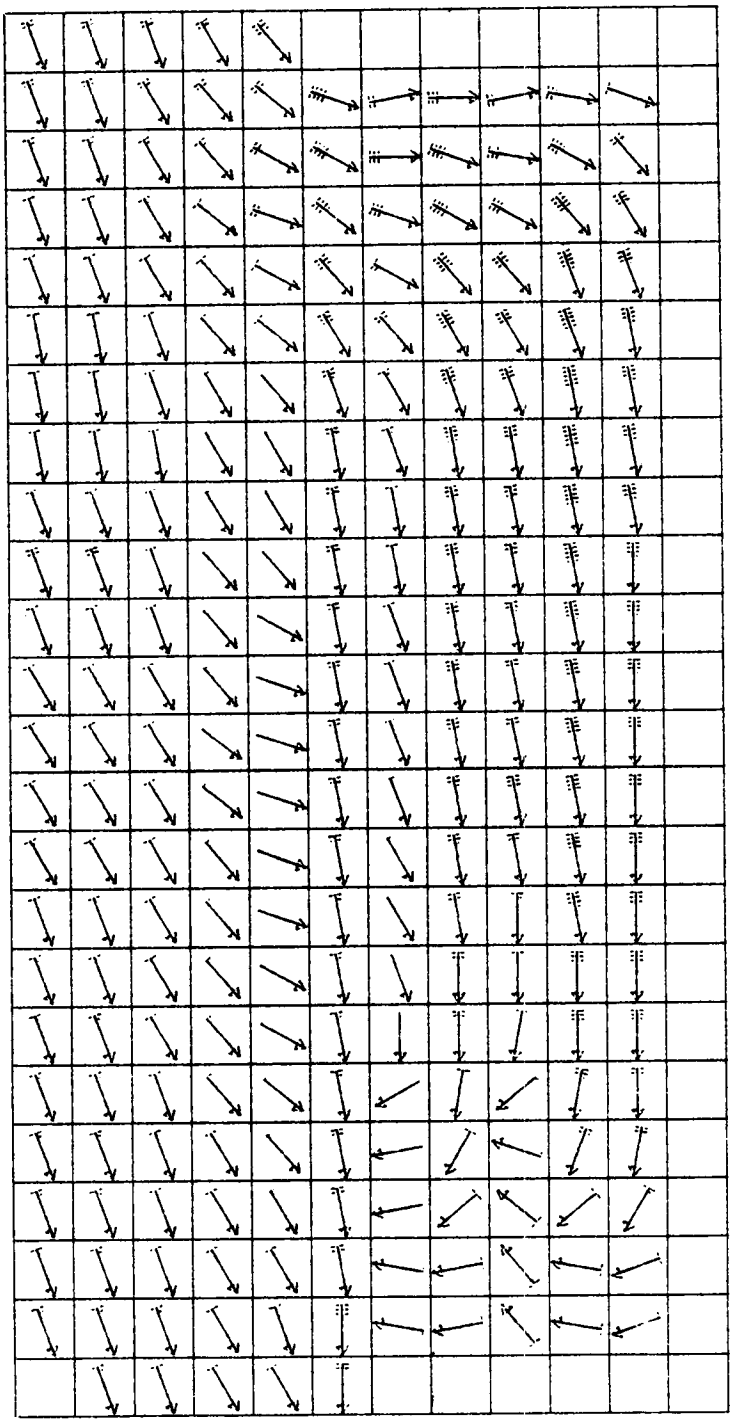

Figure 4.5.3b: Steady-state currents at mid-depth due to alongshore winds of 10 m s^{-1} with typical summer stratified conditions (19.7) Each grid element equals 30 km, each feather equals 10 cm s^{-1}. See Appendix D for listing of input parameters.

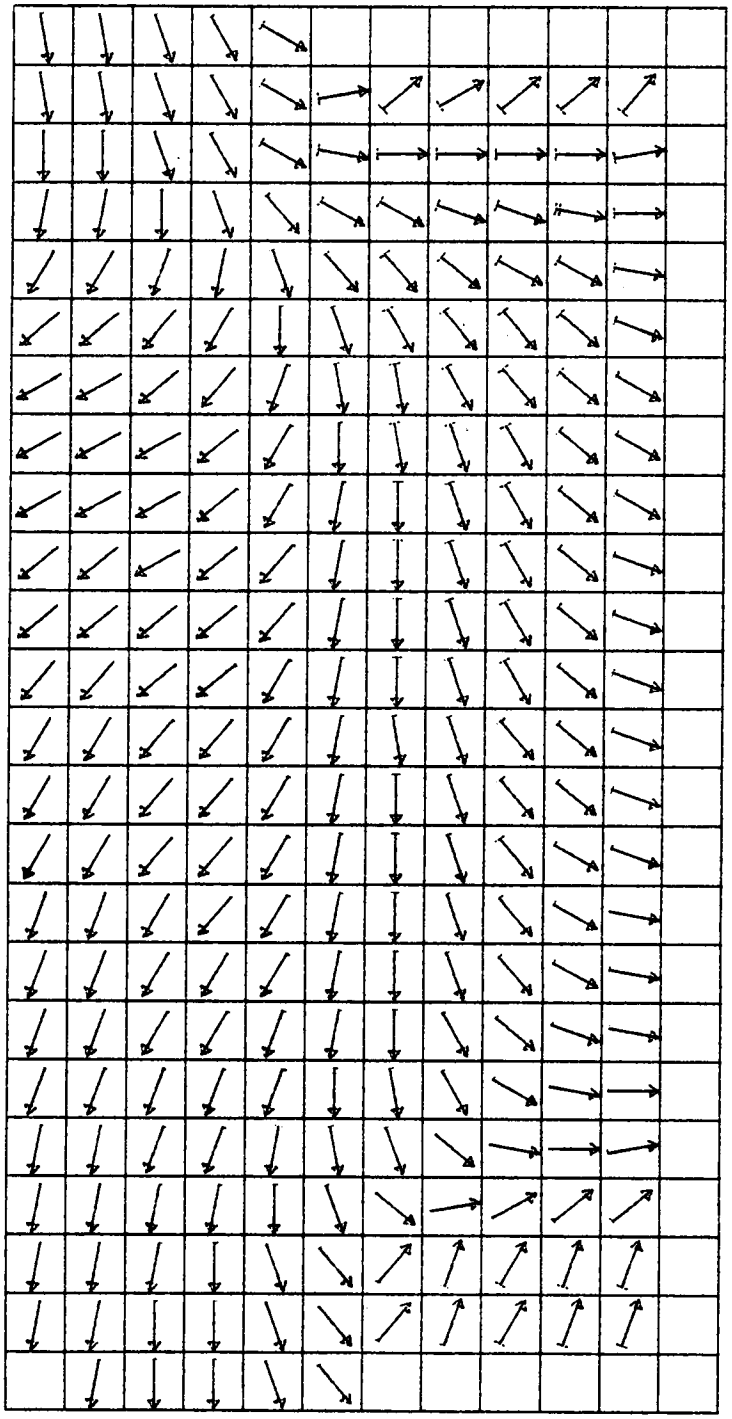

Figure 4.5.3c: Steady-state currents at bottom due to alongshore winds of 10 m s^{-1} with typical summer stratified conditions (19.7) Each grid element equals 30 km, each feather equals 10 cm s^{-1}. See Appendix D for listing of input parameters.

Appendix F.2.

The test case consisted of a 10 m deep, infinitely long channel with unidirectional flow. An upper and lower layer are established with density gradients of equal magnitude (2.525×10^{-3} kg $m^{-3}m^{-1}$, or 2.525×10^{-3} g cm^{-3} km^{-1}) but opposite sign. The value for N_v was constant at 10 cm^2s^{-1}, and a no slip bottom boundary condition was specified. Figure 4.6.1 shows the resulting steady-state current profile as calculated by both the model and analytic solution. The comparison between the two solutions is excellent.

4.6.2 Sensitivity to Horizontal Density Gradients

Review of the existing hydrographic data base on the WFS as described in Section 6.1 suggests a maximum cross-shelf density gradient on the order of 1×10^{-5} g cm^{-3} km^{-1}. Note that this gradient exists only during the summer, so that vertical stratification must also be considered.

Based on analytic investigation of density-driven flow in shelf areas, Niiler (personal communication, 1981) stated that it is essential to keep the isopycnals parallel with the isobaths. This was substantiated by initial model runs using the standard bathymetry shown in Figure 3.6.1. The velocity field which resulted was chaotic. The local divergence of the density field from the isobaths clearly dominated the larger scale effects of interest.

In order to eliminate this problem the model bathymetry was simplified so that the depth varied primarily in the x-direction. This required surprisingly little change from the standard model bathymetry. The modified depths for column 1 to 12 were: 200, 200, 150, 140, 90, 60, 50, 30, 25, 15, 10, and 0 m. This variation applied to all rows except 1 and 24 which contained land elements in columns 5-12 and columns 6-12, respectively.

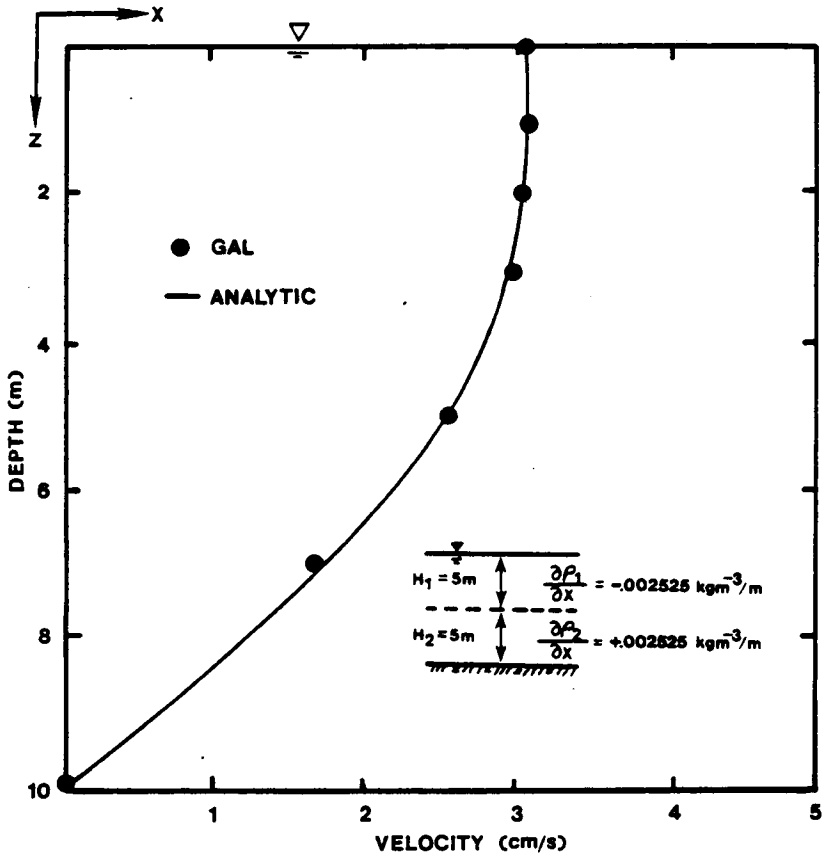

Figure 4.6.1: Comparison between model and analytical solution for two-layer density driven flow in an infinitely long channel.

The density field given in Table 6.1.1 was used to force the model with the modified bathymetry. The density specified in the mixed layer columns 1-12 was: 1.0235, 1.0235, 1.0235, 1.0235, 1.0234, 1.0233, 1.0232, 1.0231, 1.0230, 1.0220, 1.0215, 1.0210 g cm^{-3}. The density in the lower layer was 1.025 g cm^{-3}. Stratification was included as described in the previous section. Figure 4.6.2 shows the velocity flow field for this case (20.9). Velocities are quite small, being less than 1 cm s^{-1}.

4.7 Summary of Model Tuning and Sensitivity Studies

EFFECTS OF MODEL INPUT COEFFICIENTS

1. Previous studies in combination with generalized relationships suggest that reasonable values for c_b and N_h range from 0.02 to 0.08 cm s^{-1} and 10^7 to 10^9 cm^2 s^{-1}, respectively. A generalized relationship for N_v in unstratified waters is suggested by Townsend that relates N_v to the wind velocity and the Reynolds number which has been found to vary between 12 and 32.

2. In the case of wind-induced flow, surface velocity and coastal surface elevations are insensitive to changes in c_b, but velocities lower in the water column in the shallower elements are sensitive. For flow driven by barotropic waves originating from a boundary current, the circulation and surface elevations are sensitive to c_b, decreasing roughly 40% due to an increase of four in c_b.

3. In the case of wind-induced flow, surface elevations along the coast are inversely proportional to N_v as are simulated velocities in shallow

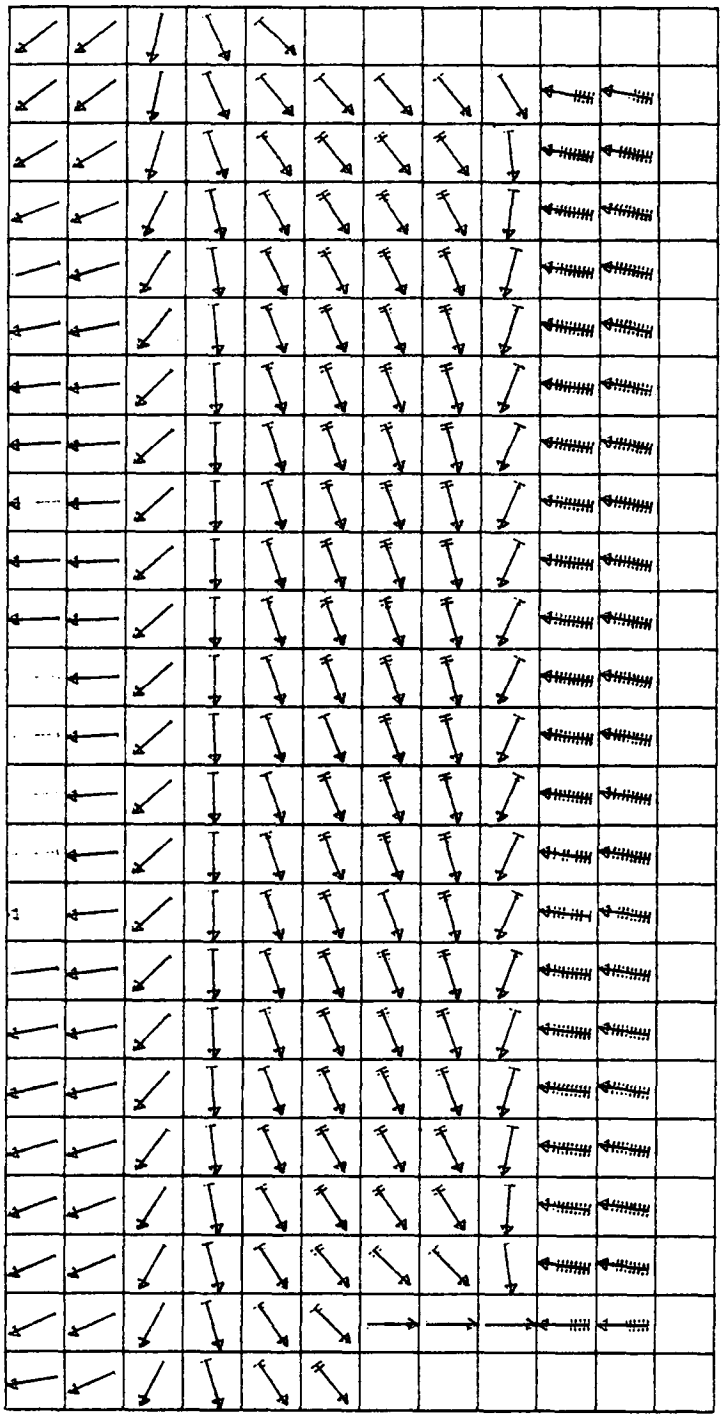

Figure 4.6.2a: Steady-state currents at surface due to typical horizontal density gradient with stratification (Case 20.9). Each grid element equals 30 km, each feather equals .05 cm s^{-1}. See Appendix D for listing of input parameters.

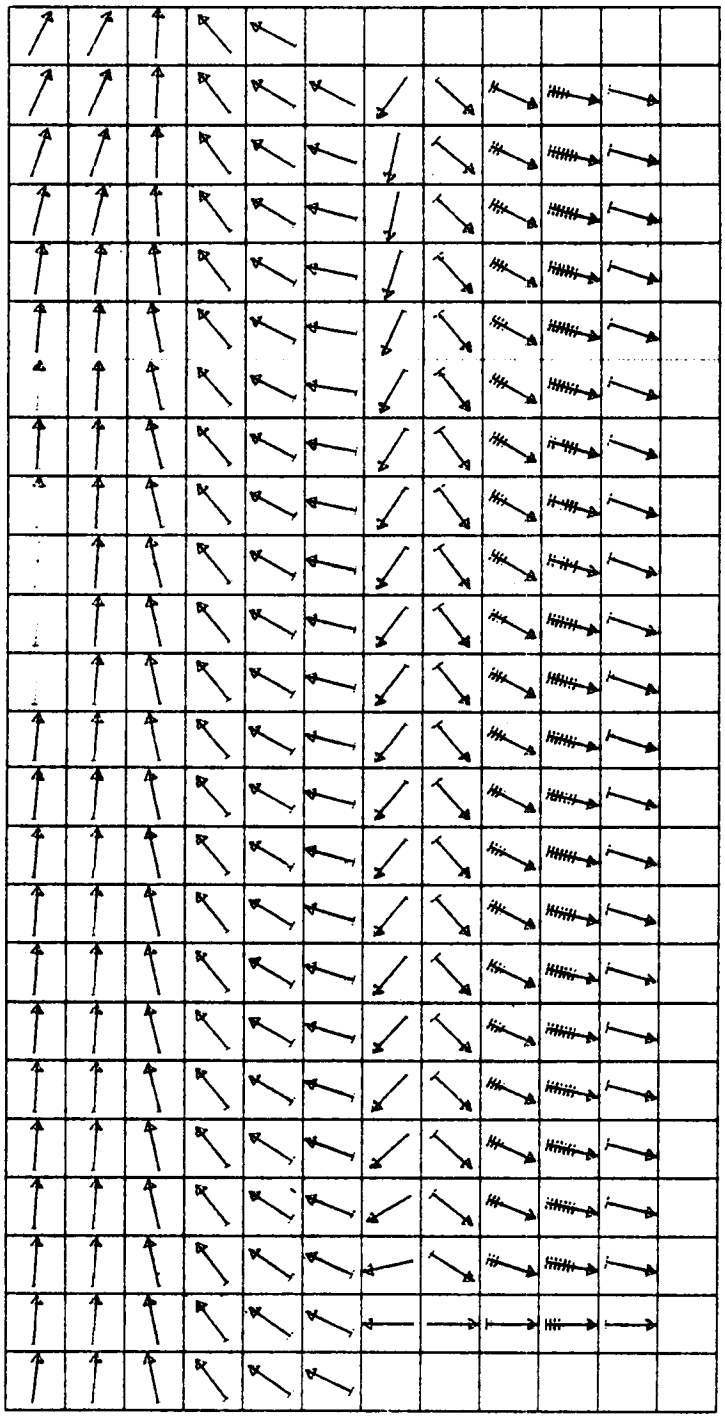

Figure 4.6.2b: Steady-state currents at mid-depth due to typical horizontal density gradient with stratification (Case 20.9). Each grid element equals 30 km, each feather equals .05 cm s^{-1}. See Appendix D for listing of input parameters.

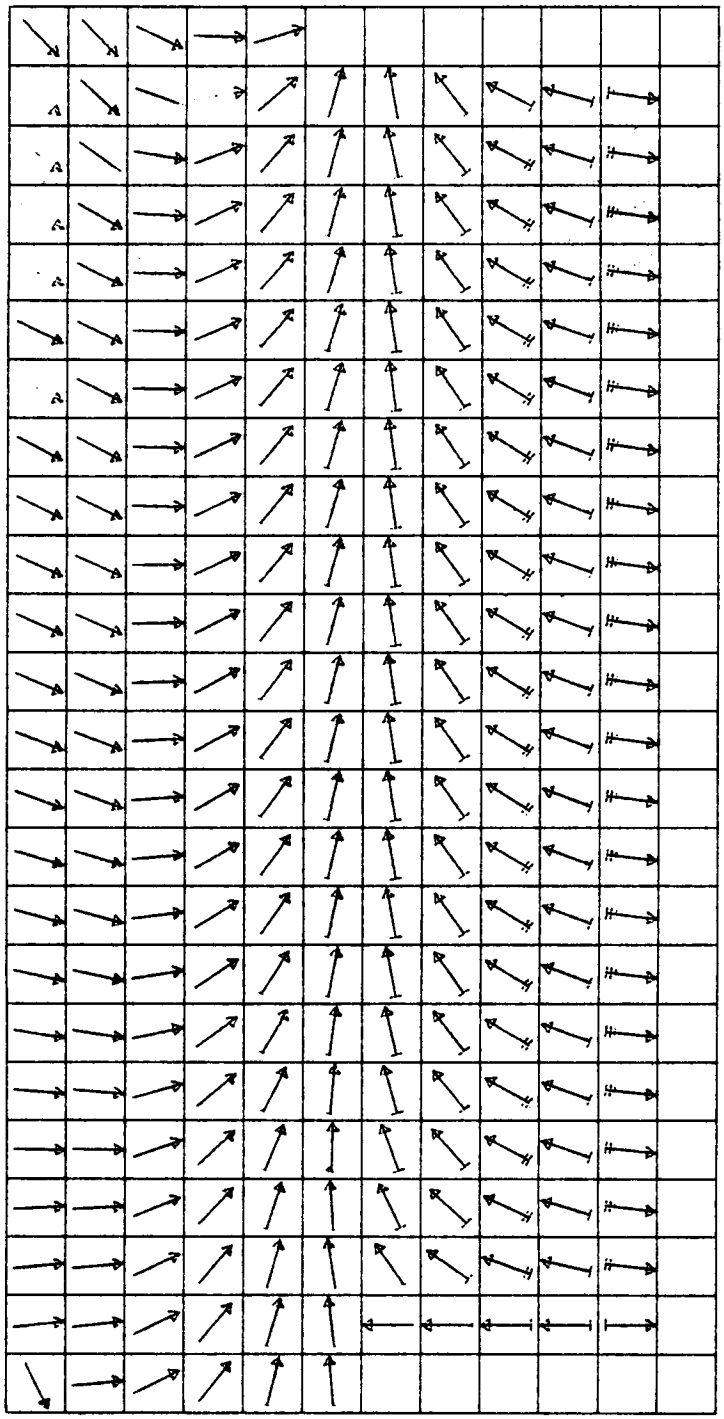

Figure 4.6.2c: Steady-state currents at bottom due to typical horizontal density gradient with stratification (Case 20.9). Each grid element equals 30 km, each feather equals .05 cm s^{-1}. See Appendix D for listing of input parameters.

water. The effect of N_v on velocity decreases in deeper water and is absent in water depths exceeding 100 m. The barotropic waves from a boundary current are insensitive to changes in N_v.

4. Changes in N_h substantially affect the energy transferred from a boundary current to the shelf. For example a change from 10^9 to $10^8 cm^2 s^{-1}$ reduces shelf current and surface elevations magnitudes by a factor of two. In addition, the existence of eddies on the eastern shelf is very dependent on the value of N_h. As N_h drops below 10^8 cm^2 s^{-1}, the eddies totally disappear.

5. Neither surface elevations or velocities for the cases studied appear to be sensitive to spatial variation of the Coriolis parameter, but a Coriolis variation is included in all production runs because of its potential importance and the negligible computational cost.

EFFECTS OF A BOUNDARY CURRENT

1. The effect of a boundary current (e.g. LC) on the WFS was investigated by imposing an alongshore current component at the western boundary of the grid. A magnitude of 100 cm s^{-1} was assumed but all plots can be scaled to account for different magnitudes because of the linearity of the model.

2. Imposition of a steady boundary current along the entire western boundary generates a single weak cyclonic gyre with northward intensification consistent with a simple analytic solution (for the range of N_v explored in the study).

3. Imposition of a steady boundary current along the southern half of the western boundary generates a dual eddy system if the boundary current is assumed to be suddenly imposed at its northern tangent to the shelf. If the boundary current is assumed to be imposed more

gradually, say, linearly increasing in a southerly direction, the dual eddy system is replaced by a much simpler southerly flow aligned with the isobaths.

4. Coastal surface elevations are substantially affected by imposition of a steady boundary current. Elevations are depressed and depend on the northward extent of the boundary current. These results imply a permanent set-down along the coast of on the order of 10 cm, with a seasonal variation of the same order.

5. A temporally varying boundary current generates barotropic waves which migrate northward on the shelf. The resulting circulation exhibits the cyclic reversals observed in the SDE data, and strong zones of divergence which offer a mechanism to explain the divergent drift directions observed in some of the drift bottle data.

6. Effects of an oscillatory boundary current on coastal surface elevations are substantial. Changes of the model input parameters within reasonable ranges indicate a minimum range of 20 cm at the coast should be expected. The surface elevations are not sensitive to the value for N_v, but are sensitive to the wavelength of the oscillation (L), N_h, c_b, the magnitude of the boundary current, and the vertical variation of the boundary current.

EFFECTS OF VERTICAL STRATIFICATION

1. The sensitivity of wind-driven currents to stratification was briefly studied and indicated that typical summer stratification on the shelf will tend to increase currents in the mixed layer and decrease currents in the lower layer. Surface elevations are not greatly affected.

EFFECTS OF HORIZONTAL DENSITY GRADIENTS

1. Large scale density-driven currents were studied using the modifications implemented for this study. When calculating density-driven circulation care must be taken to see that the isopycnals are parallel with the local isobaths otherwise a chaotic velocity field results. A slightly simplified model bathymetry was used to calculate the circulation which would result from a typical density distribution on the WFS and the results suggest southerly surface currents less than 1 cm s^{-1}.

Chapter 5

Model Tuning and Verification

The model was tuned and verified using three data sets collected on the west Florida Shelf (WFS). For two of the data sets, current velocity and surface elevation data were available; current measurements were taken in the winter of 1978 by Florida State University (FSU) and in the winter of 1973 during the Shelf Dynamics Experiment (SDE) by the University of Miami (see Figure 2.4.1 for site locations). It would also have been desirable to verify the model for summer conditions, but velocity data at sites in water depths less than 100 m were not available for this season. Therefore, the third data set from the summer of 1974 was much less extensive than the two winter sets - comparisons were limited to surface elevations at two coastal stations. Table 5.1.1 summarizes the available data for the three periods.

The objective of modeling is of course to predict currents, not surface elevations. Unfortunately, it was necessary to do some tuning and verification using surface elevation data simply because of the paucity of velocity observations. There is good reason to believe that the two are closely related, particularly for the shallower portions of the WFS (e.g., see Cragg et al., 1981).

Ideally, the process of model tuning and verification proceeds in two distinct phases. The available data base is partitoned so that part of the data are used for tuning and the remainder is used for error assessment or verification of the model results. This procedure was followed to some extent in this study, but full compliance with the ideal approach was

DATA TYPE & LOCATION	1973	1974	1978
	29 JAN - 3 MAR	1 JUL - 29 AUG	14 FEB - 27 MAR
METEOROLOGICAL			
MET BUOY	—	—	*
PENSACOLA	*	—	—
APALACHICOLA	—	*	*
TAMPA	*	*	*
FORT MYERS	*	*	*
KEY WEST	*	*	*
INTERPRETED	—	*	—
TIDE			
PENSACOLA	—	*	—
CEDAR KEYS	*	—	*
CLEARWATER	—	*	*
ST. PETERSBURG	*	—	—
NAPLES	*	*	*
KEY WEST	—	*	*
CURRENT VELOCITY			
FSU INSHORE	—	—	*
FSU OFFSHORE	—	—	*
SDE F1	*	—	—
SDE F2	*	—	—

* DATA ON HAND

\- DATA NOT AVAILABLE

Table 5.1.1: Summary of data availability for three hindcast periods.

impossible given the small data base available. For the FSU simulation, extensive tuning was performed, including modification of input parameters (i.e., c_b, N_v and N_h) and boundary conditions. These were parameters were not varied for the other two hindcasts. However, in the case of the winter 1973 data, some further combined tuning and sensitivity studies involving model forcing of the open ocean boundary were performed. These were essential, since this was the only data in which Loop Current (LC) effects were obvious.

The discussion below has been condensed to accommodate readers who are not interested in details. Appendix B gives a more complete discussion.

5.1 Winter 1978

5.1.1 Data Analysis

Florida State University deployed four Aanderaa recording current meters for approximately 30 days at two sites to the west of Cedar Keys. Figure 2.4.1 shows the location of the two sites and Table 5.1.2 gives deployment details for each of the four meters.

The FSU sites are well north of the region of primary interest to MMS on the WFS. Nevertheless, a hindcast was justified because the data represent one of only two high quality current meter data sets on the WFS (the other being the SDE). Also, unlike most of the SDE sites, the FSU sites were located in shallow water well onto the WFS, and so were not greatly affected by the complexities of the LC. The FSU data were made available through the

generosity of Dr. Wilton Sturges.

Table 5.1.2: Deployment details for FSU winter 1978 experiment

2/24/78 to 3/20/78

Meter	Location	Depth(m)	Distance Offshore	Name
00840	28.3 N 84.3 W	9/44	150 km	"upper offshore"
01317	"	39/44	150 km	"lower offshore"
00921	29.1 N 83.8 W	12/22	75 km	"upper inshore"
00922	"	17/22	75 km	"lower inshore"

Other data besides the current meter measurements are available including: surface elevation measurements at approximately 10 stations along the coast, and wind measurements from four coastal stations and NDBO weather buoy 42003. Appendix B.1 presents the data, analysis and discussion in detail. In summary, the FSU data indicate:

1. the strongest atmospheric forcing is associated with large high pressure systems which migrate into the area every 7 to 10 days;

2. winds in the alongshore direction are two to three times those in the cross-shelf direction;

3. low frequency currents at the FSU sites are strongly influenced by the passage of cold fronts occurring every 7 days or so;

4. current changes follow wind changes by about 12 hours;

5. the water column is essentially unstratified but an average 3^{o} C horizontal temperature gradient did exist between the two sites (75 km apart)

6. average currents during the 22 days were about 2 cm s^{-1}. Current direction at the upper offshore and both inshore meters was west-southwest while direction at the lower offshore meter was north; and

7. the northerly limit of the LC was at 27^{o} N latitude.

5.1.2 Model Comparisons

Figures 5.1.1-4 show comparisons between various model runs and the current data, and Figure 5.1.5 shows comparisons between the simulated and observed surface elevations at Cedar Keys, Naples, and Key West. All data have been filtered using a Doodson filter to eliminate tidal frequencies, and surface elevation data have been corrected for atmospheric pressure effects. Values for the model input parameters are as follows: c_b = 0.025 cm s^{-1}, W_{*s} = 0.5 cm s^{-1}, and N_h = 10^9 cm^2 s^{-1}. A spatially variable Coriolis parameter is included (i.e. the Beta plane approximation) and the lateral boundary conditions are: surface elevation equals zero on the western boundary, the surface gradient in the y-direction is set to zero on the northern and southern water boundaries, and the mass fluxes perpendicular to the coast are set to zero.

COMPARISONS USING SPATIALLY CONSTANT WIND FIELD

As a first pass at simulating the currents, a spatially constant wind field was used in the model. Winds recorded at the NDBO weather buoy were specified at each grid location of the circulation model. The results using

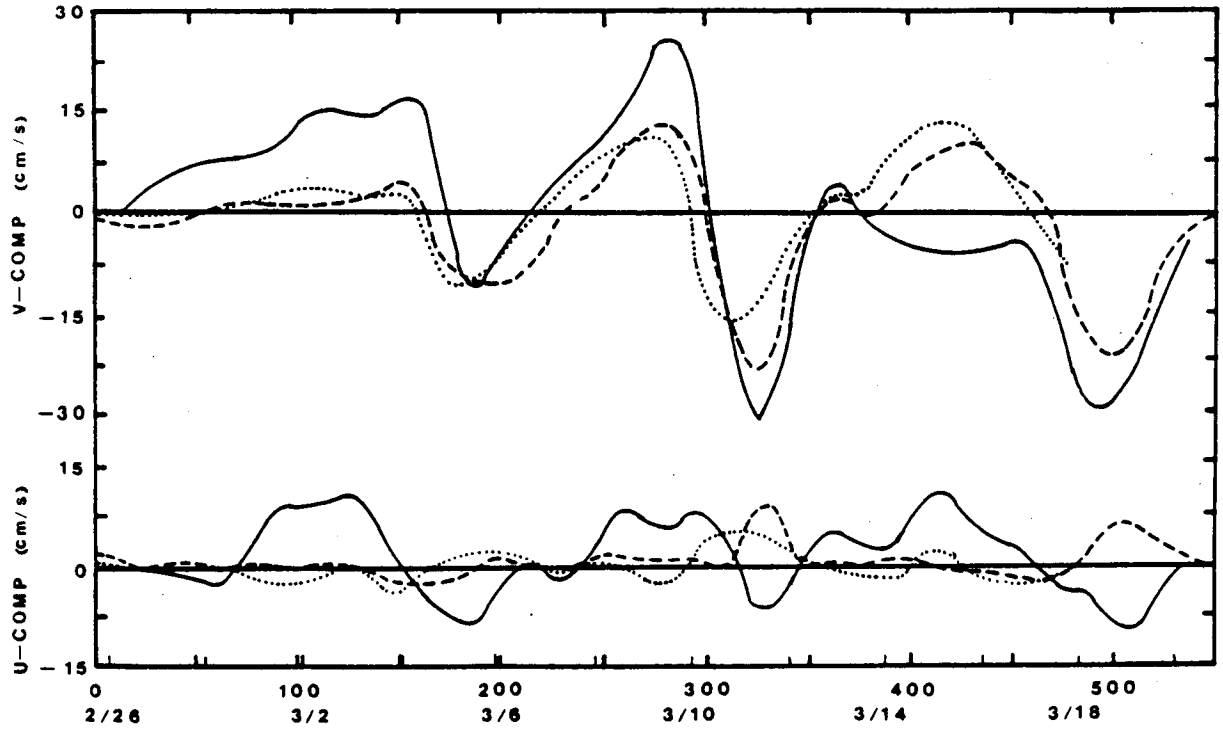

Figure 5.1.1: Comparison of model results (dashed and dotted lines) and observed currents (solid line) at upper offshore meter for winter 1978 hindcast.

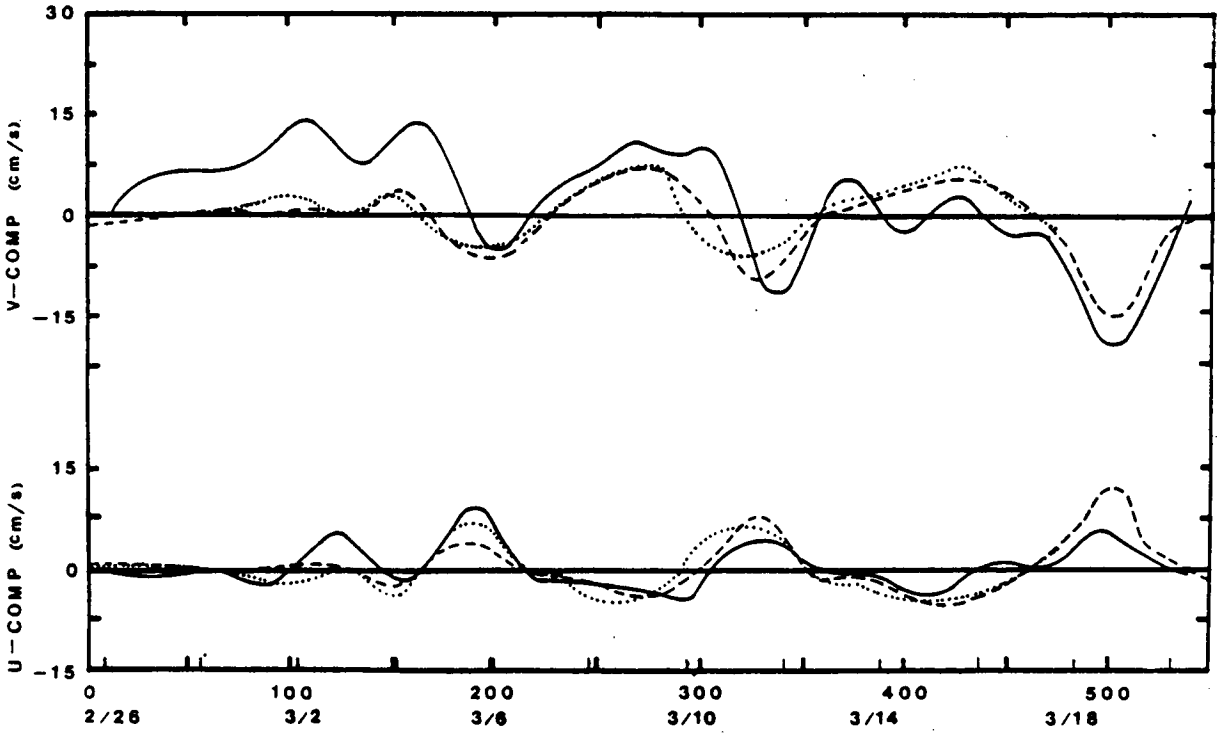

Figure 5.1.2: Comparison of model results (dashed and dotted lines) and observed currents (solid line) at lower offshore meter for winter 1978 hindcast.

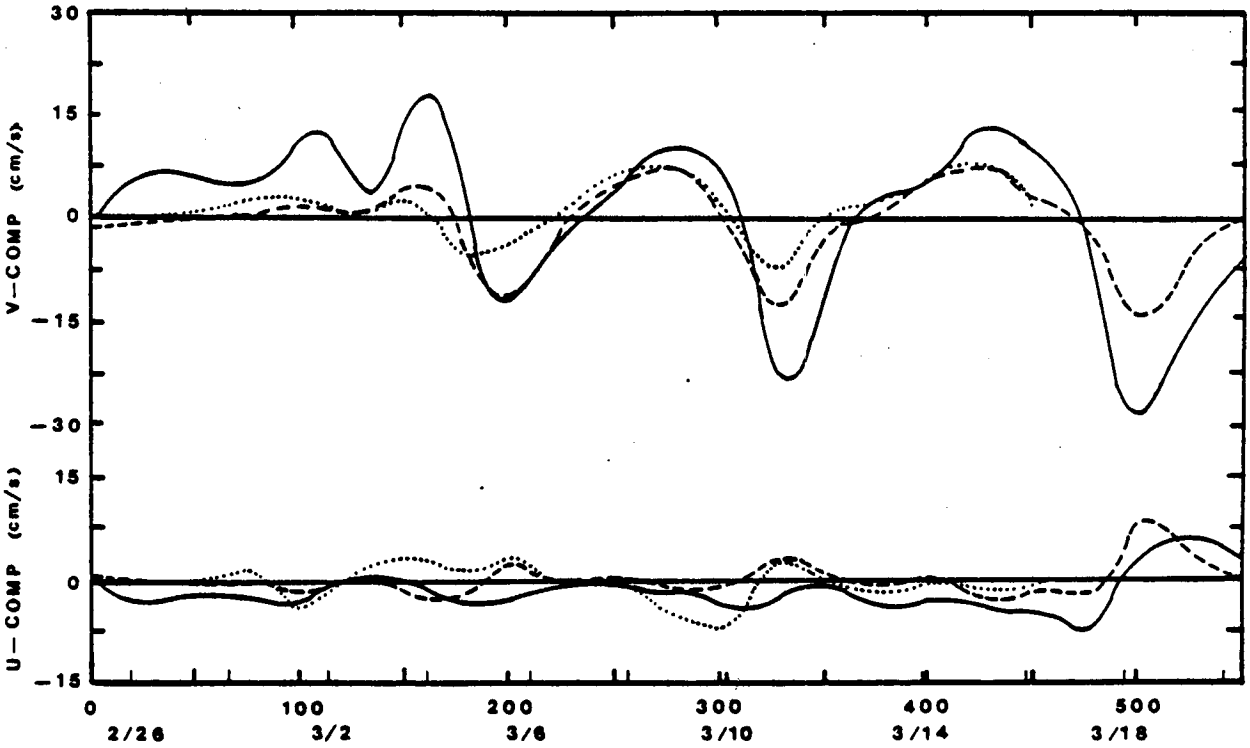

Figure 5.1.3: Comparison of model results (dashed and dotted lines) and observed currents (solid line) at upper inshore meter for winter 1978 hindcast.

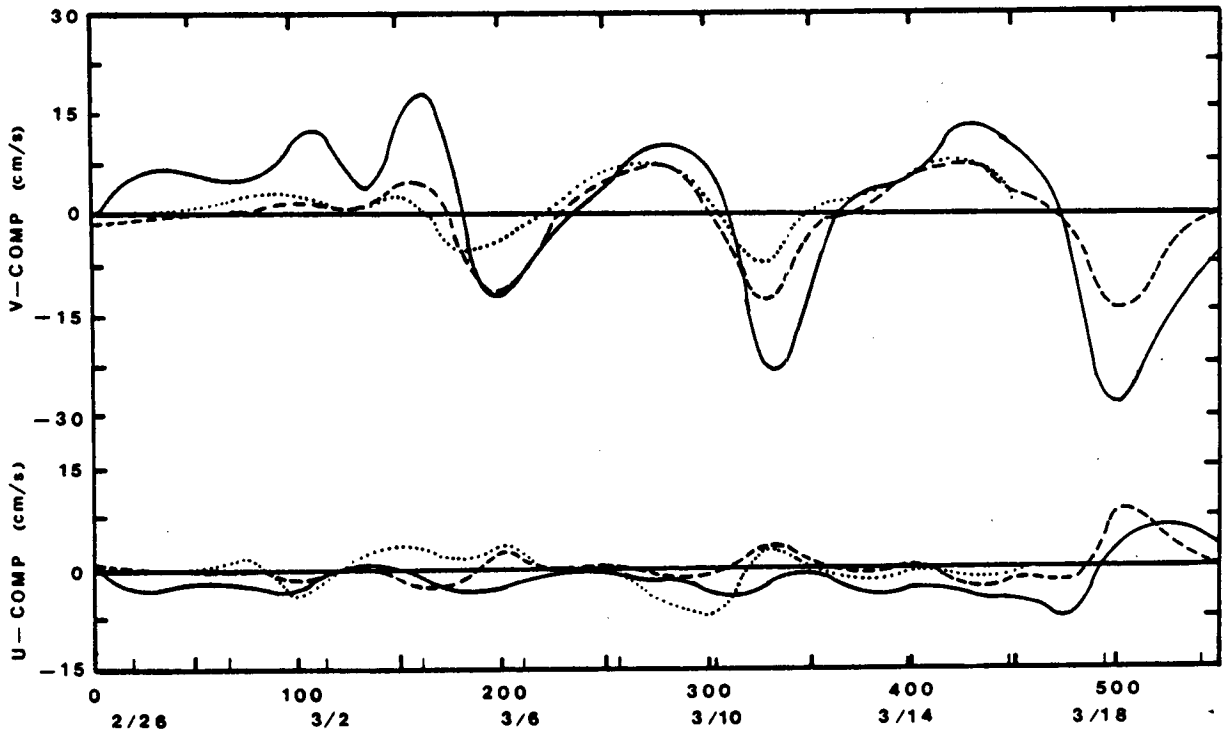

Figure 5.1.4: Comparison of model results (dashed and dotted lines) and observed currents (solid line) at lower inshore meter for winter 1978 hindcast.

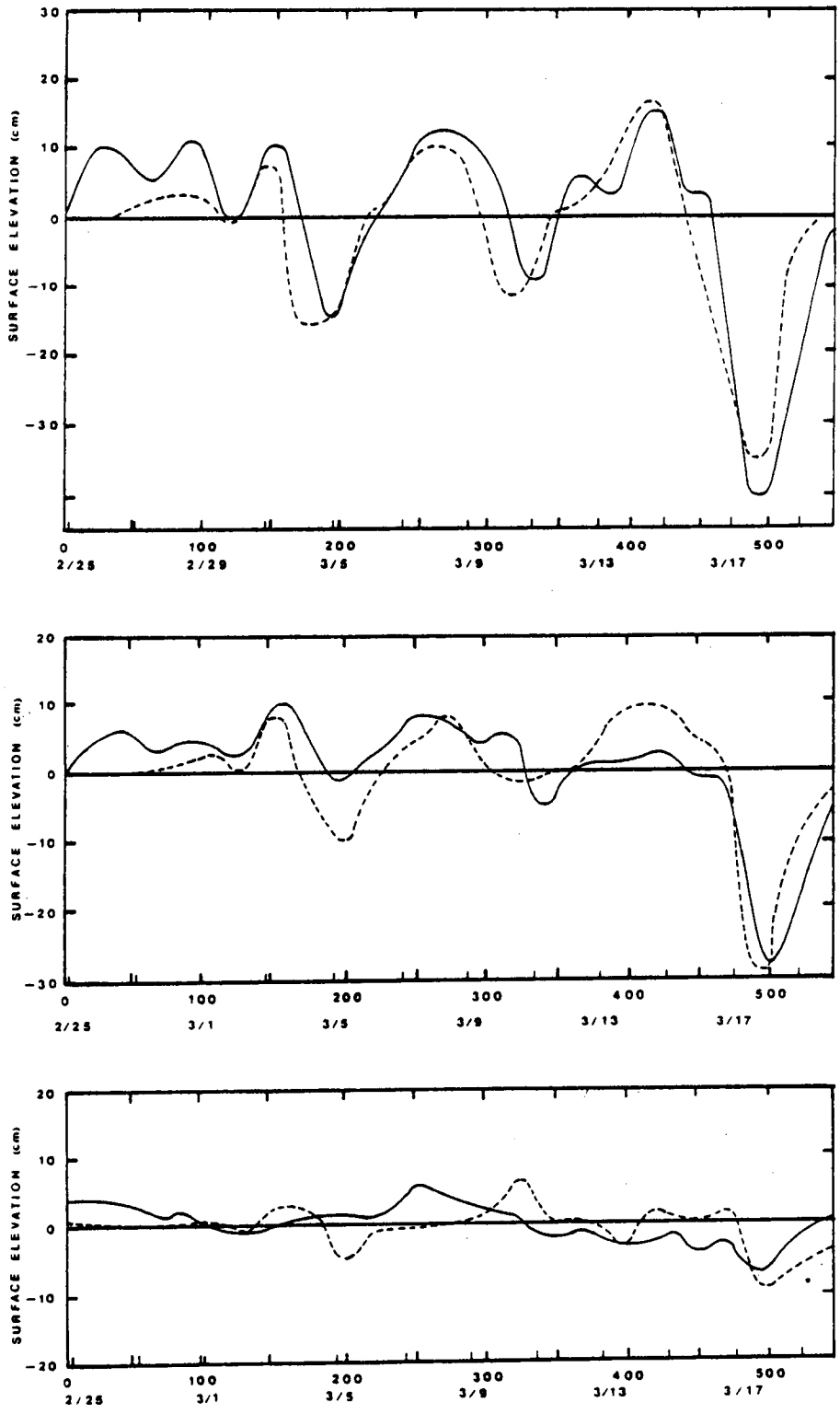

Figure 5.1.5: Comparison of model results (dashed line) and observed (solid line) surface elevations at Cedar Keys (top), Naples (middle) and Key West (bottom) for winter 1978 hindcast. Atmospheric pressure effects have been removed from the data

this wind field are plotted with a dotted line in Figures 5.1.1-4.

The model predicts the surface elevations at Cedar Keys and Naples very well. At Key West the comparison is not nearly as good although the model does predict elevations in the correct range of +/-5 cm. There are several probable reasons for the poor comparison at Key West:

1. discretization error, i.e. the bathymetry in the Key West region changes rapidly and cannot be adequately represented except with a much smaller element size than that used in the present model grid;

2. reflective lateral boundary conditions are used in the model. Reflected waves are most strongly felt at the boundary ; and

3. the signal variation at Key West is much smaller than the other stations and much less coherent (private communication, W. Sturges, 1982).

The alongshore currents at the FSU sites compare reasonably well with the simulations. A phase lag is apparent and is due to the geographical distance between the wind and current measuring sites (recall the wind forcing is spatially constant and is taken from the measured buoy time series). The model generally underpredicts the four extremes that occurred.

The cross-shelf current comparisons vary from one meter to the next. The most serious discrepancy occurs at the upper offshore meter where the model predicts the wrong direction more often than not. At the lower offshore meter the comparison is the best, despite the rather small variation of the signal.

COMPARISONS USING SPATIALLY VARIABLE WIND FIELD

To investigate the importance of the spatial variability of the wind, the

wind interpolation program described in Appendix H.7 (Volume II) was used to interpolate between the buoy data and the data from the four land stations. The factors used to amplify the land stations were: 2.04, 1.94, 2.11, and 1.2 for Apalachicola, Tampa, Fort Myers, and Key West respectively. The factors were found by dividing the average wind magnitude at the buoy by the average at the station in question during the February-March period. A more sophisticated approach was later used to derive the amplification factors. This method involved constructing a scatter plot of buoy speed vs the lagged speed at the land station in question and calculating the linear regression equation as described in Appendix B.1. This method suggested that the station amplification factor is indeed independent of wind speed. The method did yield somewhat larger factors than the previous method based on averages but subsequent modeling using the revised factors did not change the water velocity comparison appreciably.

Case 15.15 (dashed line) in Figures 5.1.1-5 shows the model results using the spatially varying wind field. The phase differences are generally improved, but the net improvement in magnitude is only about 10% on average. The improvement is probably due to bettering the estimate of the local wind.

FACTORS AFFECTING COMPARISONS OF MODELED AND OBSERVED CURRENTS

Other factors were considered in an attempt to improve the model comparisons with the real time data. The most puzzling aspect is the model's consistent underestimate of the current extremes, particularly in the alongshore direction. This is clearly evident during the February 28 to March 3 period. The real time comparisons were not substantially improved by factor of 10 changes in c_b and N_v - a finding consistent with the results from Chapter 4. Including the Coriolis differential had little influence on the alongshore current components or the surface elevation, but it did affect the cross-shelf component, though it did not improve the comparison appreciably.

One possible reason for the discrepancy in real time currents is measurement

error. A comparison of Aanderaa and VACM (a vector averaging meter by AMF) data taken during the SDE study (Koblinsky and Niiler, 1980) shows that the two instruments moored at the same location and time period correlate reasonably well but a discrepancy on the order of 5 cm s^{-1} is not unusual. Since the VACM is generally considered the more accurate of the two, this would imply the error bars on the FSU data are on the order of 5 cm s^{-1}, which represents a significant portion of the current signal particularly in the cross-shelf component. Hence, measurement error may dominate much of the lower magnitude data signal and an exact comparison between the model and the data may not be appropriate during the time periods of especially small currents.

The measurement error described above is somewhat of an average error. At times the error may be higher due to certain quirks in the instrument. It is well known that the Aanderaa current meters used in the FSU study are susceptible to rotor pumping when used in shallow water and subjected to strong surface wave activity (Halpern, 1976). Rotor pumping can increase the recorded speed over and above what actually existed by a factor of two or more. Since rotor pumping is dependent on surface wave activity which is in turn dependent on wind speed, it follows that during periods of strong winds the Aanderaas will have a tendency to record artificially larger speeds. Mitchum and Sturges (1981) briefly investigated this possibility and their analysis indicates that rotor pumping was not a problem during the study although the basis for their method is not clear nor do they reference any previous work justifying their technique.

Another possible reason for the differences observed between the model and the real time data could be LC effects recorded by the current meters but not included in the model forcing. As will be seen in Section 5.3, the SDE data show that the LC effects, particularly in the form of eddies, can migrate over 100 km onto the WFS. These eddies have length and velocity scales on order of 100 km and 10 cm s^{-1}, respectively, lasting for 10 days. Eddies

would only have to migrate on the order of 100 km from the furthest northerly position of the LC during March 1978 to affect the FSU study area. Temperature variations during these time periods may only be 1^{o} C. Such temperature variations are evident in the FSU temperature record (Figure B.1.19).

One other possibility for the discrepancy in currents is that significant horizontal density gradients may have existed during the study. As noted above, the water temperature at the inshore meters was an average of about 3^{o} C lower than at the offshore site. If it is assumed that the salinity is the same at both sites, then the density gradient could potentially drive flows on the order of 10 cm s^{-1}, clearly substantial when compared to the measured currents. However, given the lack of hydrographic data during the FSU study it is not possible to include the density driven components in the modeling.

5.1.3 Summary Of Winter 1978 Hindcast

The model comparisons with the FSU data set demonstrate the following:

1. the model predicts alongshore currents to within about 20%, although the model results consistently underestimate the peak alongshore values. The model does not hindcast the small cross-shelf component as well, probably because the signal to noise ratio is quite high;

2. the sensitivity studies imply that the discrepancy between the modeled and observed currents is not due to an inadequate choice of the various model parameters. The discrepancy may be due to any number of other factors such as measurement error, unmodeled effects of the LC or horizontal density gradients. There are not sufficient hydrographic data to model the latter two possibilities. Another source of error

may be short term non-linear effects (i.e., advective mechanisms) which may be important but will not be precisely simulated using the present model formulation; and

3. the model hindcasts the surface elevations at the coast quite well, peaks being predicted to about +/- 2 cm over a range of 40 cm. Phase discrepancies of about five hours are sometimes observed. The hindcast of Key West elevations is poor, but there are several characteristics of the site which make it a difficult one to model.

5.2 Summer 1974

5.2.1 Data Analysis

A data base that includes good quality current measurements on the WFS during the summer months does not exist. The only good summer current data were taken during the SDE on the shelf break. However, some verification of the model during summer conditions was felt to be desirable and so a hindcast of surface elevations at various coastal sites was performed. The summer of 1974 was chosen in part because of the availability of calculated offshore winds from the SDE.

Wind data are available at four coastal stations (Key West, Fort Myers, Tampa, and Apalachicola) during the July-August time period of interest. These data are augmented by Partagas (1973a,b) who calculated the offshore winds at 86° W and 26° N using barometric pressure maps in conjunction with the observed coastal winds. Surface elevation data are available at a number

of stations including Naples, Key West, and Clearwater.

Spectral analysis and coherences were performed on the data and results are given in Appendix B.2. The major findings of the analysis can be summarized as follows:

1. the low frequency summer winds are much less energetic than the winter winds - maximum offshore summer winds are 7 m s^{-1} as compared to winter maximums of 15 m s^{-1}. The alongshore and cross-shelf components during summer are roughly equal. No dominant low frequency is evident for the summer winds.

2. coastal, non-tidal surface elevations are small, experiencing a range of +/- 5 cm. No dominant period is evident for the surface elevations.

3. the spatial coherence of the low frequency wind is appreciably less than during the winter 1978 with typical r^2 (correlation coefficients squared) values of 0.6 for summer vs 0.9 for winter between Key West and Tampa (350 km apart).

4. coherence between the low frequency wind and surface elevations is generally weak. Of the two components, the cross-shelf is somewhat better correlated than the alongshore component.

5.2.2 Model Comparisons

Figure 5.2.1 shows a comparison between the modeled surface elevations (dashed line) and observed elevations (solid line) at Clearwater and Naples. A spatially varying wind was used in the modeling. Interpolation between the five observation points was performed using the interpolation program

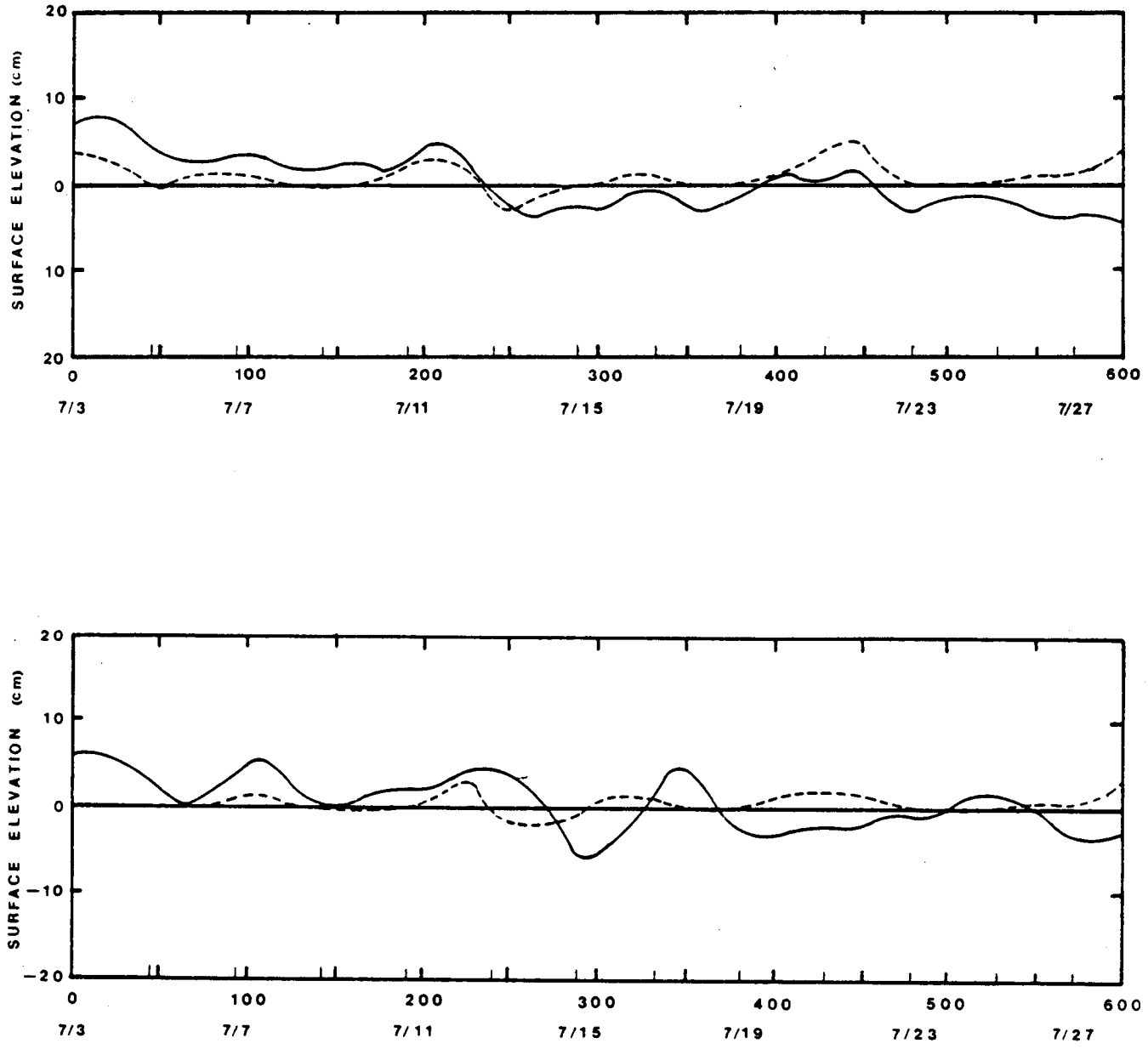

Figure 5.2.1: Comparison of Clearwater (upper) and Naples (lower) surface elevations (solid line) with model results (dashed line) for summer 1974 hindcast. Atmospheric pressure effects have been removed from the data.

described in Appendix H.7 (Volume II). The amplification factors were recalculated so as to crudely account for the differences in the typical summer and winter wind characteristics. The factors used were: 1.2, 1.94, 2.11, and 2.04 for Key West, Fort Myers, Tampa and Apalachicola. These were found by dividing the average wind magnitude during the summer of 1978 at the buoy by the average at the station in question during the same period. Values used for the input parameters in the model were identical to those used in the winter of 1978 simulation, as were the boundary conditions.

The dashed curve in the figure considers only wind forcing. The water density is assumed homogeneous. As is evident from the comparison, the model hindcasts the correct range for the surface elevation, but there is no apparent correlation between the maximum and minimum of the modeled and observed signal.

The most likely explanations for the discrepancies between modeled and observed surface elevations are:

1. poor specification of the wind field. The spatial correlations indicate that substantial variations in the wind field between stations exist for the summer, yet this variability can not be adequately modeled with the wind data available;

2. accumulated errors in recording and processing the data contributing to a high signal to noise ratio;

3. the possible presence of topographic waves on the shelf which are dampened in the model due to N_h. This problem, if it exists, cannot be resolved without including non-linear terms in the model; and

4. the possible existence of a northerly coastal flow due to the LC.

5.2.3 Summary Of Summer 1974 Hindcast

Verification of the model for summer conditions is hampered by the absence of appropriate current data, the spatial variability of winds, and the low amplitude of coastal surface elevation fluctuations. Because of the low frequency and intensity of regional weather systems, the inability to use satellite imagery to locate the LC due to the lack of thermal contrast, and the low intensity of overall WFS processes, the ability of numerical modeling techniques to adequately resolve summer time WFS circulation will be seriously impaired.

5.3 Winter 1973

5.3.1 Data Analysis

The source of much of the data for this time period is the SDE. Most of the velocity data gathered during the SDE were taken on or near the WFS break within a 100 km radius of 84 ^{o} W and 26 ^{o} N. These data are located near the open ocean boundary of the model and they are useful in specifying the open ocean boundary condition for the model, but the data are not very helpful for comparison with model results. There are two periods, October-December 1973 and February-March 1973, when data were taken at a site on the 50m isobath (stations F and V in Figure 2.4.2). Current data were also taken during these time periods at stations A, B, C, D, and E. More current and hydrographic data were taken in February-March, so these data were chosen for modeling.

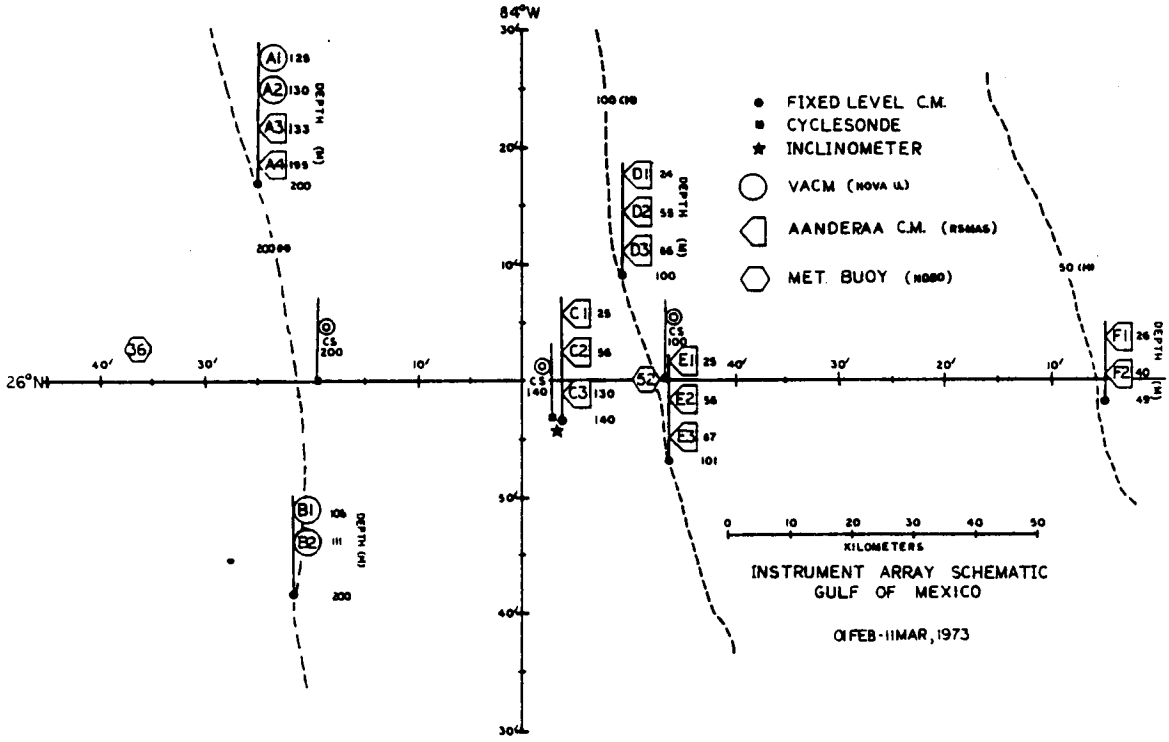

Figure 5.3.1: Location of Shelf Dynamics Experiment sites for the winter 1973 study.

Figure 5.3.1 summarizes the site locations for the Winter experiment. Note that meters A1 and B2 did not return useable data.

In addition to the extensive velocity and hydrographic data available from the SDE, there are also surface elevation data from government installations at Naples, Cedar Keys and St. Petersburg and wind data from four stations at Key West, Tampa, Fort Myers, and Pensacola. Estimates of the wind at 86° W and 26° N are also available from Partagas (1973a,b).

A good deal of analysis of the current and hydrographic data has been performed and is reported in Price and Mooers (1974c, 1974d) but little interpretation of low frequency components has been made, with the exception of Niiler (1976) who reviewed the entire SDE study and made some general interpretations which are relevant to the February-March data set.

In addition to the previous analyses available in the literature, further analyses were performed during the course of the WFS study and are included in Appendix B.3 along with a more complete discussion. In general, the conclusions which can be drawn from the data are severely limited by the short duration of the current meter record at the shallow water sites. Nevertheless, our analyses and those of Niiler (1976) suggest the following:

1. Offshore winds are dominated by the passage of cold fronts every 7 to 10 days as is typical for the winter season on the shelf.

2. Currents near the shelf break are apparently dominated by eddy fields shed from the LC consisting of alternating cyclonic and anticyclonic eddies. The eddies induce currents with a period on the order of 15 days and maxima of 50 cm s^{-1}. Temperature fluctuations associated with passage of the eddies are approximately 4°C.

3. Niiler suggests flow on the shelf is dominated by eddies similar to those observed at the break, the difference being that the shelf

filters some of the eddy frequencies. The eddies would result in no net advection over climatological (i.e., on the order of months) time periods.

4. An alternative interpretation of the shelf stations suggests that a net southerly flow is induced on the shelf by the large scale effect of the LC. Eddies occasionally separate from the LC and migrate onto the shelf causing significant flow reversals of the order 10 cm s^{-1}.

5. Currents at sites with water depths in excess of 100 m are negligibly correlated with wind. Currents at sites in shallower water are only weakly correlated to the wind.

6. It is probably not feasible to infer net long term drift from a vector average of the data unless the duration of the measurement period is on the order of many months. Averages based on shorter measurement durations will likely be biased by a few extreme events or by measuring a non-integral number of eddy cycles.

5.3.2 Model Comparisons

The major difference between the 1978 and 1973 verification periods is the location of the LC relative to the current measuring location. While the 1978 FSU data was only marginally, if at all, affected by the LC, the 1973 SDE data was taken primarily to observe LC/shelf water interaction (compare Figures B.1.23 and B.3.2). Thus attempts to model the 1973 SDE data must include both wind and LC forcing mechanisms.

WIND DRIVEN COMPONENT

Initial modeling of the data focused on only the wind-driven component of the shelf circulation, ignoring LC effects. The wind forcing was varied

spatially using the interpolation technique described in Appendix H.7 (Volume II). Amplification factors applied to the land station data were the same as those used in the Winter 1978 hindcast. Values for N_v, c_b and the boundary conditions were the same as in the previous hindcasts and the Coriolis differential was included.

Figure 5.3.2 shows the comparison of the model with surface elevation data at three coastal sites for the case of wind forcing only (Case 18-6). The comparison is good, typically being within 5 cm in amplitude and 5 hours in phase.

Figures 5.3.3-4 show the comparison of modeled to observed currents at location F. Recall that the model includes wind forcing only and though the winds obviously are the cause of some of the modulation in the data, LC effects are also significant. The model generally underestimates the current observations substantially. The poor comparison between the wind-driven simulated currents and those observed is not surprising in light of the poor statistical correlation found between the current and wind data (see Figure B.3.8).

LOOP CURRENT COMPONENT: EDDY WAVE FIELD

Considerable labor was spent attempting to derive a reasonable parameterization of the forcing imposed by the LC at the western boundary of the model. It is apparent from studying the current data at F that a realistic forcing parameterization must generate a southerly current of about 7 cm s^{-1} for the first 15 days of the record, followed by a northerly current of the same magnitude for the remaining 10 days. If this were the only criteria, it could be satisfied by forcing the model boundary with a simple sinusoid as described in Section 2.3, using a period of roughly 30 days. Such a forcing mechanism would approximate the eddy wave field suggested by Niiler (1976). This forcing function is fairly consistent with the observed currents but it does not give realistic coastal surface elevations. This

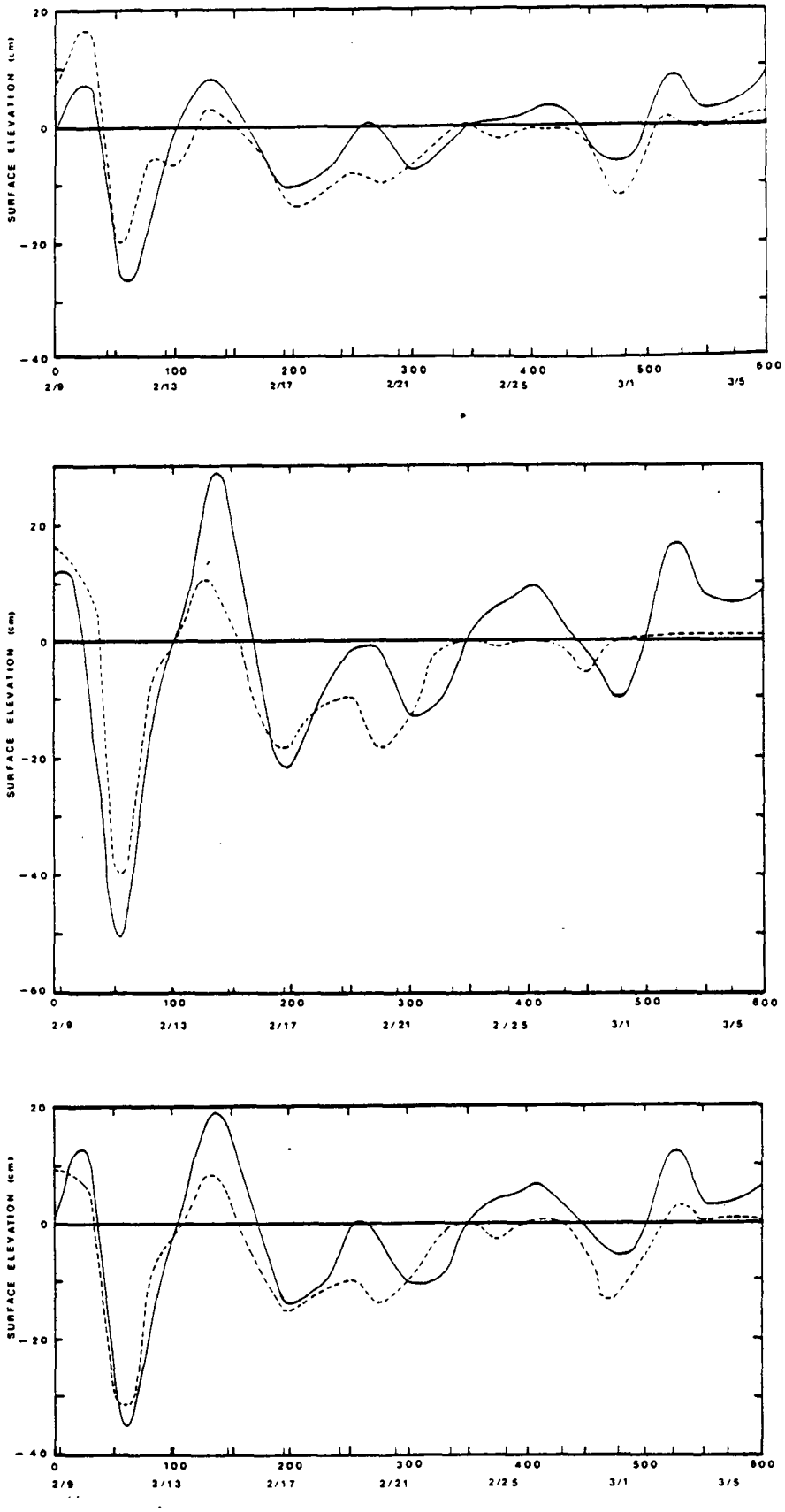

Figure 5.3.2: Comparison of modeled (dashed line) and observed (solid line) surface elevations at St. Petersburg (lower), Cedar Keys, (middle) and Naples (top) for winter 1973 hindcast. Atmospheric pressure effects have been removed from the data.

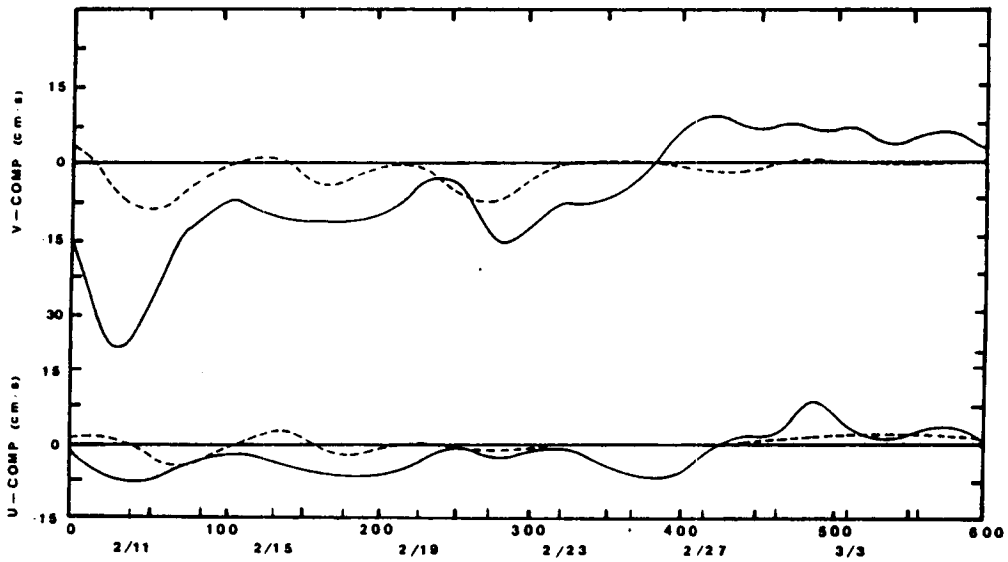

Figure 5.3.3: Comparison of modeled wind-induced (dashed line) and observed (solid line) currents at site F1 for winter 1973 experiment.

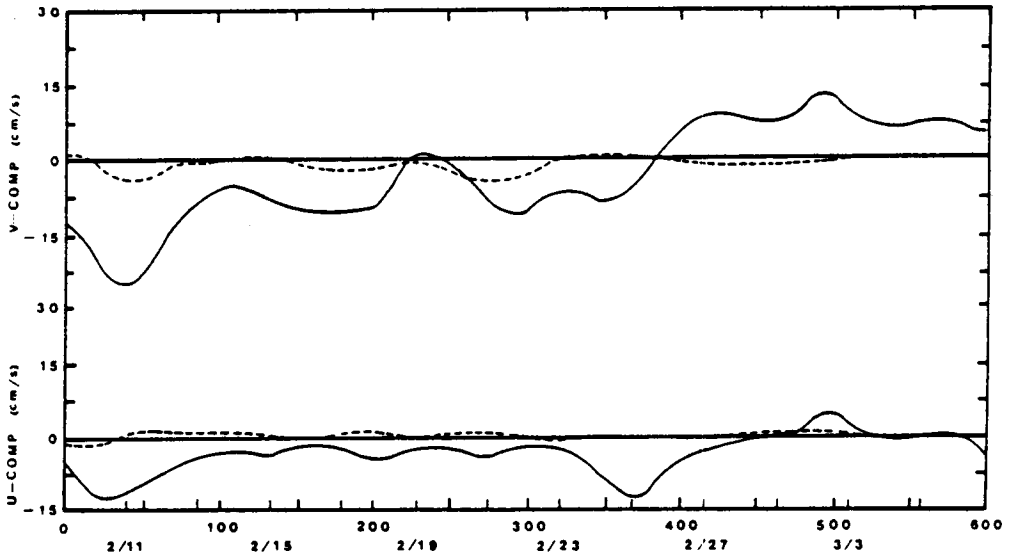

Figure 5.3.4: Comparison of modeled wind-induced (dashed line) and observed (solid line) currents at site F2 for winter 1973 hindcast.

problem is discussed more fully in Appendix B.3.

There are a number of potential reasons why the eddy wave field suggested by Niiler does not reproduce the data:

1. the baroclinic component of the eddies has been ignored yet the hydrographic data show that substantial baroclinicity is often associated with the eddies;

2. a monochromatic wave was implemented in the model to simulate the eddy wave forcing at the western boundary but spectral data indicate the eddies contain a broad band of energy;

3. it can be argued that the eddy wave field suggested by Niiler is really applicable only to the shelf break, and that circulation on the shelf is dominated by a net southerly drift which is occasionally altered by the intrusion of eddies (with perhaps one or two weak stationary eddies near the coast) with length and time scales comparable to those suggested by Niiler;

4. the currents at the model boundary used to drive the flow have been assumed to vary as 100 cosine$(0.7\ z\ H^{-1})$, where H is the local water depth, z is the distance from the surface and the units of velocity are cm s^{-1}. This simple function does not describe the complex vertical variations sometimes observed in the current data especially during summer conditions;

5. stations are located near the shelf break. The sharp bathymetric gradient near the break may be inadequately simulated in the model because of discretization error resulting from the rather large element size of 30 km used in the model. This may ultimately cause errors in the modeled velocities since some of the data do indicate a strong dependence of velocity on topography; and

6. eddy advection onto the shelf is approximated in the model via a linear lateral eddy viscosity term. It is probable that the nonlinear advective terms which are neglected in the model are frequently important when attempting to model the eddies and thus neglect of these terms may be a source of error.

Of the six reasons cited, the first three are due to possible inadequacies in Niiler's suggested wave field and the last three are linked to the model implementation. Items 1-2 and 4-6 could be investigated with the model if the appropriate modifications were made, but these would be extensive and beyond the present scope of work. In several cases (i.e. item 1) model modifications would not be justified at this point because the existing data base is insufficient for verification of model modifications.

LOOP CURRENT COMPONENT: LATERAL SHEAR STRESS

Niiler (1976) has hypothesized that the dominant LC effect on the shelf is the propagation of a barotropic eddy wave. An alternative hypothesis is suggested in item 3 above and discussed in detail in Appendix B.3. This hypothesis suggests that the primary influence of the LC on the shelf is through the transfer of momentum to shelf waters from the LC. The result is a generally southward flowing pattern on the shelf with perhaps one or two quasi-stationary, weak cyclonic eddies near the coast. This pattern is occasionally affected by the migration of eddies and tongues from the LC.

Support for this hypothesis can be found in the current and hydrographic data from the shelf stations of the SDE discussed in Appendix B.3. The data imply that for the first 12 days or so, the shelf sites were not affected by migrating eddies as indicated by the very static hydrography in the area. Flow during this time period is relatively constant and to the south. Following the 12th day, an eddy begins to invade the sites from the west, generating a sudden shift in currents and hydrography.

Further support for the lateral shear hypothesis is indirectly supplied by model sensitivity studies (i.e., cases 13-17, 13-20 and 13-26), and by the drift bottle data on the shelf, which will be discussed in Chapter 6.

Although the lateral shear hypothesis appears reasonable given the available data, the fact remains that the supporting data are of very short duration relative to the time scales in question. The only other SDE data which could conceivably be used as a further check were taken during the Fall 1973 Experiment in which one current meter at station V (roughly the same location as F) returned useable data. Unfortunately, the synoptic hydrographic data during that time period are too sparse to provide an adequate check.

For the sake of argument let us proceed and assume that there is a net southerly drift over most of the shelf. We can estimate the net southerly drift due to the large scale influence of the LC by subtracting the modeled wind component from the observed data at station F during the 8-20 February period when the hydrographic data indicate the region was unaffected by eddies. Referring to Figure 5.3.3 and subtracting the modeled wind-induced current from the total observed currents gives a mean alongshore and cross-shelf drift of 9 cm s^{-1} (standard deviation = 7) and 3 cm s^{-1} (standard deviation = 2), respectively.

The residual current calculated above can be compared to the modeled LC residual. To do this we need to know the position of the LC. Satellite infrared photos (Figure B.3.2), located the northward extent of the LC at about mid-shelf. Model runs 13.17 or 13.20 described in Section 4.2 are appropriate for this LC position. Recall that case 13.17 was forced on the lower half of the model grid using a constant southern alongshore velocity of 100 cm s^{-1}. Case 13.20 was identical except the forcing was linearly increased from 0 cm s^{-1} at mid-shelf to 100 cm s^{-1} at the southern end.

Modeled LC-induced circulation for 13.20 at station F are 7 and 2 cm s^{-1} for the two components, comparing closely to the residual components (9 and 3 cm

s^{-1}) calculated from the data above. Currents from 13.17 are smaller than the calculated residual - 3 and 1 cm s^{-1} for the two components and this perhaps implies that the sudden imposition of the LC forcing used in 13.17 is somewhat unrealistic.

To state these results in another way, the average observed currents of 10 cm s^{-1} alongshore and 5 cm s^{-1} cross-shelf can be viewed as the sum of the modeled wind-induced components (Case 18-6, 3 cm s^{-1} alongshore and 2 cm s^{-1} cross-shelf) plus the modeled LC component (Case 13-20, 7 cm s^{-1} alongshore and 2 cm s^{-1} cross-shelf). Thus the modeled and observed comparison is quite good for the 8-27 February period. The period following the 27th is dominated by the intrusion of an eddy or tongue which cannot be simulated without significant modification of the model formulation.

The primary factor affecting the accuracy of this comparison is the absence of long term current data from anywhere on the WFS. The lateral shear hypothesis does not preclude the existence of LC eddies migrating onto the shelf, but proposes that net long term advection is due primarily to lateral shear effects. In order to confirm this, current measurements on the shelf with time scales many times longer that the eddy time scales are required.

5.3.3 Summary Of Winter 1973 Hindcast

In summary, coastal surface elevations are hindcasted reasonably well by the wind forced model, displaying about the same order of error as for the Winter 1978 hindcast.

The current data at the SDE sites clearly show the domination of the LC even at sites as shallow as 50 m. Niiler (1976) has done extensive analysis of the sites in depths of 100 m and greater and suggests that the LC influences these sites via eddies traveling northward along the 150 m isobath. He

further suggests that these eddies propagate onto the shelf to approximately the 40 m isobath. The model was forced at the shelf break using the Niiler eddy wave and the results were compared to the current data at three stations. A reasonable hindcast of the current data can be made for several of the stations including the shallowest at F using a somewhat slower moving wave field than that suggested by Niiler. However, the model predicts fluctuations of the surface elevations at the break which are about a factor of two too large, and at the coast, fluctuations which are an order of magnitude too large.

Another hypothesis is that the primary influence of the LC on the shelf is not through the intrusion of barotropic waves but rather via large scale transfer of momentum from the LC to the shelf which generates southerly currents over much of the shelf. This flow field is occasionally interrupted by the intrusion of tongues and eddies which migrate eastward from the LC and eventually retract and/or dissipate on the shelf.

This lateral shear hypothesis is supported by hydrographic data taken during the February-March period, model results, some previous investigations, and drift bottle studies. Incorporation of this hypothesis into the hindcast of the SDE data is encouraging but final resolution of the issue is hampered by the lack of long term data on the shelf.

Chapter 6

Seasonal Circulation

The literature review indicates three mechanisms should be included in a realistic model of the shelf: density gradients (both horizontal and vertical), wind, and the Loop Current (LC). These mechanisms are discussed in the three following sections. Each section includes: (1) a derivation of the seasonal representation from available data and (2) model circulation due to the mechanism acting by itself. The fourth section presents combined circulation patterns resulting from all three forcing mechanisms.

6.1 Density Gradient Effects

DATA ANALYSIS

Density gradients on the shelf can originate from two sources: differential thermal heating and the LC. The latter appears to affect the shelf primarily via intrusions of warm, high salinity tongues and eddies with length scales on the order of 100 km. Also, because the LC is nearly always tangent to the southern portion of the West Florida Shelf (WFS), it is possible that the LC may provide a large scale source (in a dispersive sense) of high salinity warm water. Further discussion of the first LC effect is postponed to the third section of this chapter.

Differential thermal heating generates two important effects on the shelf: vertical stratification and horizontal density gradients. Vertical stratification is characterized by two layer flow. The upper layer is the so called mixed layer. Underlying the mixed layer is a colder, generally less dynamic layer which usually extends to the bottom. Separation of the two layers is marked by a thermocline and velocity shear. Vertical stratification is evident on the WFS during the summer, and sensitivity studies described in Section 4.5 suggest that stratification should be included in the circulation modeling.

Horizontal density gradients are established on the shelf through differential heating and perhaps the LC. The former effect occurs because the shallower water heats and cools more rapidly than the deeper water of the shelf. An example of differential heating is shown in the FSU winter 1978 data set described in Section 5.1.

The characteristic length and time scales associated with density gradients can range over several orders of magnitude. Because of our interest in residual currents, we will focus on changes on the order of weeks and months. This is also a practical limitation from the standpoint of availability of shelf wide data.

All STD data available for the eastern Gulf from NODC as of October 1980 were catalogued and analyzed. Over 35000 data points are available spanning roughly 30 years. The data base was reduced by eliminating all stations located off the WFS. The remaining data were then broken into two seasons: the summer season encompassing 1 April to 30 September, and the winter season encompassing 1 December to 31 March. A total of 5424 and 4149 data points on the WFS were available for winter and summer, respectively.

STD data were converted to sigma-t values for various levels. Tables 6.1.1-2 summarize the density distribution on the WFS for the two seasons at two

SIGMA-T STATISTICS FOR DEPTHS 0 -10 M 1 APR TO 30 SEP									
MEAN	22.55	22.01	21.49						
STD.DEV.	1.95	1.55	1.47						
MINIMUM	20.86	20.40	19.56						
MAXIMUM	24.24	24.10	23.16						30°
NO. OBS.	4	11	10						
MEAN	22.21	22.11	22.31	21.36					
STD. DEV.	0.96	1.55	1.04	1.20					
MINIMUM	20.77	19.52	21.17	18.80					
MAXIMUM	23.18	24.04	23.55	23.00					
NO. OBS.	12	21	12	18					
MEAN	22.42	24.69	22.71	22.16					
STD. DEV.	0.86	1.62	0.88	0.77					
MINIMUM	21.42	21.35	21.71	20.96					
MAXIMUM	23.57	26.21	24.14	23.64					
NO. OBS.	20	60	21	23					
MEAN	22.60	22.85	22.60	21.89	21.84				
STD. DEV.	1.67	0.68	0.70	0.86	0.83				
MINIMUM	19.30	21.70	21.25	20.35	21.18				
MAXIMUM	24.42	23.75	24.16	22.56	23.36				
NO. OBS.	16	29	29	21	10				
MEAN	22.34	23.23	23.32	23.28	22.53				
STD. DEV.	1.76	1.24	1.28	1.10	1.03				
MINIMUM	18.26	20.11	20.71	21.33	20.61				
MAXIMUM	24.42	25.99	26.02	26.05	24.52				28°
NO. OBS.	21	66	71	146	91				
MEAN	23.23	23.15	23.60	23.43	23.06				
STD. DEV.	0.82	1.17	1.13	1.20	0.99				
MINIMUM	22.18	21.60	22.06	20.92	20.52				
MAXIMUM	24.53	24.74	25.79	25.61	24.59				
NO. OBS.	16	20	26	80	43				
MEAN	22.93	23.35	23.00	23.24	23.32	22.44			
STD. DEV.	0.55	0.85	1.07	1.09	0.87	1.38			
MINIMUM	21.99	21.93	20.87	21.51	21.71	19.45			
MAXIMUM	23.80	24.68	24.36	24.42	24.97	24.52			
NO. OBS.	21	18	24	14	45	52			
MEAN	23.56	23.67	23.55	23.55	23.27	22.65	20.48		
STD. DEV.	0.57	0.40	0.44	0.89	0.97	1.23	2.47		
MINIMUM	22.60	22.03	21.00	22.00	21.51	18.63	15.53		
MAXIMUM	24.96	25.09	25.81	25.74	25.35	25.03	23.55		
NO. OBS.	26	181	296	57	60	90	9		
MEAN	23.20	23.40	22.97	23.17	23.54	22.91	23.07		
STD. DEV.	0.77	0.73	0.48	0.79	0.62	0.34	0.61		
MINIMUM	22.16	22.74	22.40	22.21	22.80	22.30	22.05		
MAXIMUM	24.71	24.55	24.17	24.45	24.21	24.01	24.00		26°
NO. OBS.	28	8	76	29	19	93	26		
MEAN	23.31	23.32	23.24	23.08	23.50	23.48	23.12	22.71	
STD. DEV.	0.57	0.54	0.75	0.64	1.01	0.60	0.92	0.48	
MINIMUM	22.55	22.49	22.12	22.55	21.77	22.37	22.14	21.92	
MAXIMUM	24.22	24.20	25.15	25.25	25.23	25.18	24.96	23.80	
NO.OBS.	18	32	42	136	39	173	28	186	
	86°				83°				

Table 6.1.1a: Statistical summary of summer density gradients, 0-10 m.

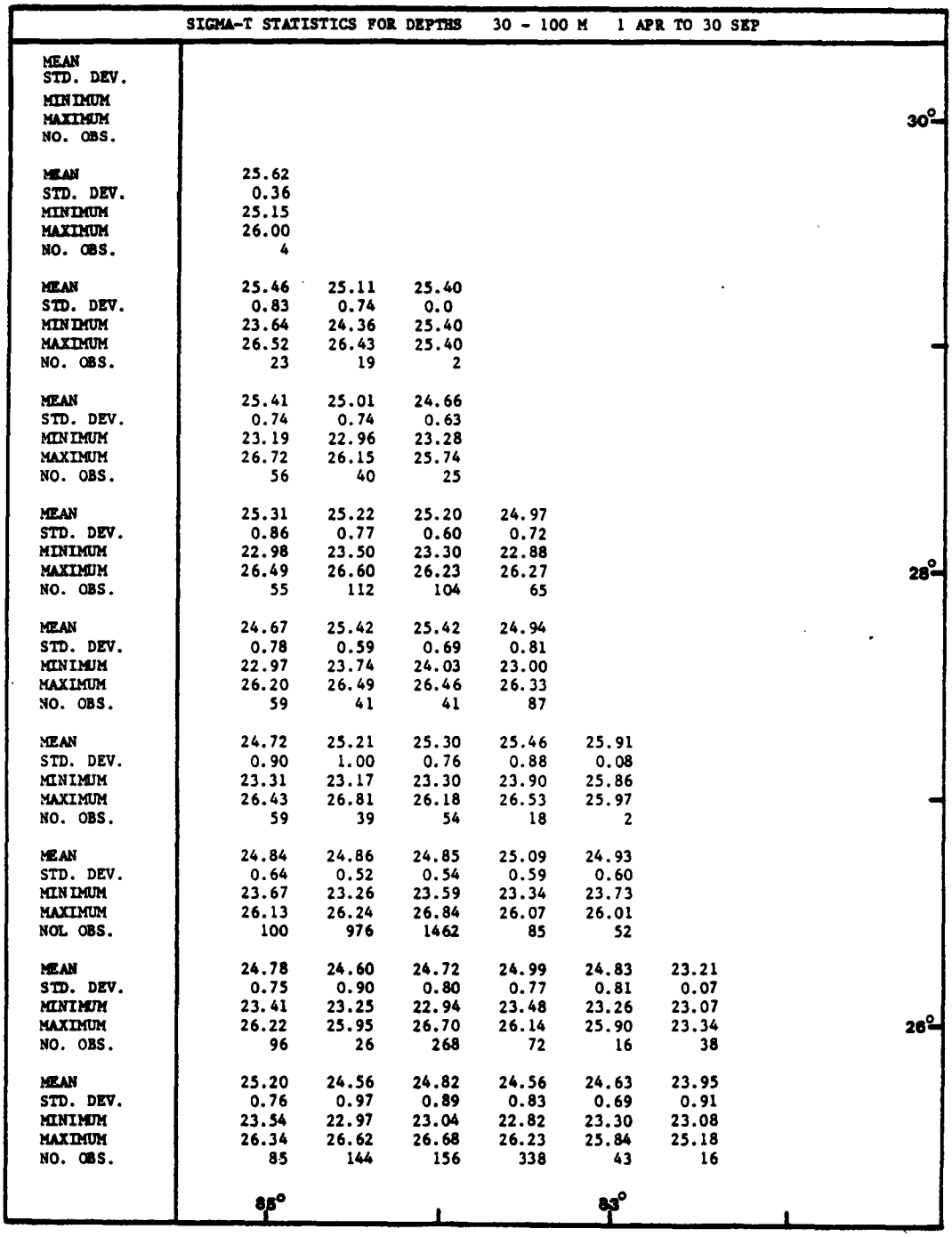

Table 6.1.1b: Statistical summary of summer density gradients, 30-100 m.

SIGMA-T STATISTICS FOR DEPTHS 0 -10 M 1 DEC TO 31 MAR									
MEAN	25.34	25.59	25.10						
STD. DEV.	0.0	0.53	0.71						
MINIMUM	25.34	24.92	24.62						30°
MAXIMUM	25.34	26.00	26.13						
NO. OBS.	2	6	7						
MEAN	25.73	25.62	26.34	24.89					
STD. DEV.	0.19	0.28	0.01	0.70					
MINIMUM	25.57	25.32	26.33	24.16					
MAXIMUM	25.90	25.94	26.35	25.76					
NO. OBS.	4	6	3	12					
MEAN	25.49	25.97	26.37	25.45					
STD. DEV.	0.10	0.76	0.46	0.69					
MINIMUM	25.41	25.32	26.03	24.50					
MAXIMUM	25.58	27.03	27.10	26.20					
NO. OBS.	4	7	8	10					
MEAN	26.03	26.10	25.83	25.67	24.05				
STD. DEV.	0.67	0.62	0.26	0.76	1.07				
MINIMUM	25.28	25.54	25.48	23.96	23.13				
MAXIMUM	26.85	26.89	26.13	26.21	25.25				
NO. OBS.	8	9	8	14	9				
MEAN	25.49	25.70	25.53	25.54	24.39				
STD. DEV.	0.20	0.52	0.43	0.54	0.61				
MINIMUM	25.18	24.69	24.67	24.62	23.51				28°
MAXIMUM	25.66	26.73	26.01	26.41	25.69				
NO. OBS.	8	29	20	47	34				
MEAN	0.0	25.79	25.88	25.73	25.50				
STD. DEV.	0.0	0.55	0.52	0.41	0.58				
MINIMUM	0.0	25.15	25.34	24.98	24.49				
MAXIMUM	0.0	26.39	26.45	26.44	26.46				
NO. OBS.	0	8	8	31	21				
MEAN	25.41	25.45	25.61	25.98	25.44	24.87			
STD. DEV.	0.46	0.56	0.58	0.72	0.54	0.38			
MINIMUM	24.78	24.68	24.98	25.36	24.43	24.50			
MAXIMUM	25.98	26.33	26.43	26.60	25.85	25.66			
NO. OBS.	16	12	12	4	10	18			
MEAN	25.07	25.06	25.22	25.31	25.64	25.12	26.16		
STD. DEV.	0.30	0.46	0.37	0.47	0.46	0.43	0.0		
MINIMUM	24.57	24.55	24.58	24.51	24.89	24.32	26.16		
MAXIMUM	25.34	25.66	25.67	26.13	26.47	25.69	26.16		
NO. OBS.	9	10	21	23	19	35	1		
MEAN	24.80	24.77	24.99	25.52	25.82	25.21	25.70		
STD. DEV.	0.46	0.38	0.46	0.37	0.59	0.26	0.13		
MINIMUM	24.42	24.26	24.51	25.12	25.31	24.98	25.56		26°
MAXIMUM	25.38	25.28	25.89	25.94	26.33	25.48	25.81		
NO. OBS.	6	14	14	6	4	5	5		
MEAN	0.0	24.39	25.08	25.34	25.02	25.06	24.80	23.80	
STD. DEV.	0.0	0.33	0.61	0.39	0.38	0.46	0.55	0.0	
MINIMUM	0.0	23.94	24.51	25.05	24.31	24.31	23.77	23.80	
MAXIMUM	0.0	24.69	26.09	26.17	25.79	25.53	25.27	23.80	
NO. OBS.	0	8	9	13	37	19	11	2	
	88°				83°				

Table 6.1.2a: Statistical summary of winter density gradients, 0-10 m.

SIGMA-T STATISTICS FOR DEPTHS 30 - 100 M 1 DEC TO 31 MAR

MEAN							
STD. DEV.							
MINIMUM							30°
MAXIMUM							
NO. OBS.							
MEAN	25.83	25.98					
STD. DEV.	0.37	0.0					
MINIMUM	25.56	25.98					
MAXIMUM	26.24	25.98					
NO. OBS.	5	2					
MEAN	25.64	26.44					
STD. DEV.	0.31	0.39					
MINIMUM	25.40	26.09					
MAXIMUM	26.12	26.99					
NO. OBS.	8	7					
MEAN	25.89	26.49	26.06				
STD. DEV.	0.56	0.52	0.37				
MINIMUM	25.30	25.68	25.78				
MAXIMUM	26.94	26.88	26.59				
NO. OBS.	26	11	7				
MEAN	25.66	25.89	25.66	25.83			
STD. DEV.	0.30	0.56	0.52	0.46			
MINIMUM	25.21	24.69	24.58	24.92			28°
MAXIMUM	26.32	26.85	26.27	26.43			
NO. OBS.	38	51	30	24			
MEAN	0.0	25.83	25.92	25.87			
STD. DEV.	0.0	0.52	0.70	0.50			
MINIMUM	*****	25.17	25.33	24.91			
MAXIMUM	*****	26.68	26.91	27.01			
NO. OBS.	0	39	23	36			
MEAN	25.61	25.68	25.75	26.02			
STD. DEV.	0.37	0.37	0.50	0.62			
MINIMUM	24.95	24.93	25.08	25.44			
MAXIMUM	26.33	26.36	26.80	26.60			
NO. OBS.	48	50	41	6			
MEAN	25.41	25.35	25.57	25.67	25.79		
STD. DEV.	0.47	0.37	0.46	0.46	0.45		
MINIMUM	24.58	24.57	24.55	24.49	24.97		
MAXIMUM	26.25	26.07	26.35	26.23	26.47		
NO. OBS.	25	58	59	35	17		
MEAN	25.64	25.22	25.59	25.67	25.85		
STD. DEV.	0.51	0.46	0.51	0.46	0.53		
MINIMUM	24.68	23.98	24.40	25.19	25.35		26°
MAXIMUM	26.46	25.96	26.25	26.23	26.39		
NO. OBS.	18	57	56	14	8		
MEAN	0.0	25.13	25.51	25.60	25.28	25.42	
STD. DEV.	0.0	0.63	0.48	0.36	0.43	0.05	
MINIMUM	*****	23.88	24.70	25.17	24.42	25.35	
MAXIMUM	*****	25.99	26.19	26.19	25.89	25.47	
NO. OBS.	0	21	34	20	44	4	
	85°				83°		

Table 6.1.2b: Statistical summary of winter density gradients, 30-100 m.

levels - 0-10 meters and greater than 30 meters. Levels between 10 and 30 meters are not shown since this tends to be the interface region between the mixed and lower layers. The interface varies in time so including data from this transition zone could have biased the average data.

The tables show the mean, standard deviation of the mean and range of the sigma-t values at 0.5° squares with the upper left hand corner of each table corresponding to $85^{\circ}W$, $30^{\circ}N$. The summer density means display a lower density along the coast probably due to the intense thermal heating which occurs in the shallow water during the summer season. However, the standard deviation of many of the squares is quite high and raises questions concerning the significance of the trend implied by the means.

To test significance levels, the standard Duncan test (1975) available as part of the Statistical Analysis System (SAS) was used. At the 95% confidence level there was no significant difference in the horizontal variations for the winter (all levels) or for the summer (at the 30-100 m level). The test did indicate significance for the summer surface level and the resulting density gradient is depicted in Figure 6.1.1.

These finding can be explained as follows. Because of the close vicinity of the LC, the deeper shelf waters (i.e., 70 m) tend to experience less of a seasonal change and also tend to be more saline than the shallower portions of the shelf. Thus if the shallower waters are at the same temperature as the deeper water, the shallower, less saline waters will be less dense. This situation might exist in the summertime when satellite images indicate that there is very little temperature difference in surface waters on the shelf. During the winter, shallow waters on the shelf become considerably colder that the deeper shelf waters (at the same level), and hence become denser than during the summer. This increase in density due to temperature tends to compensate for the salinity deficit of the shallow water, resulting in a nearly homogeneous density field in the horizontal.

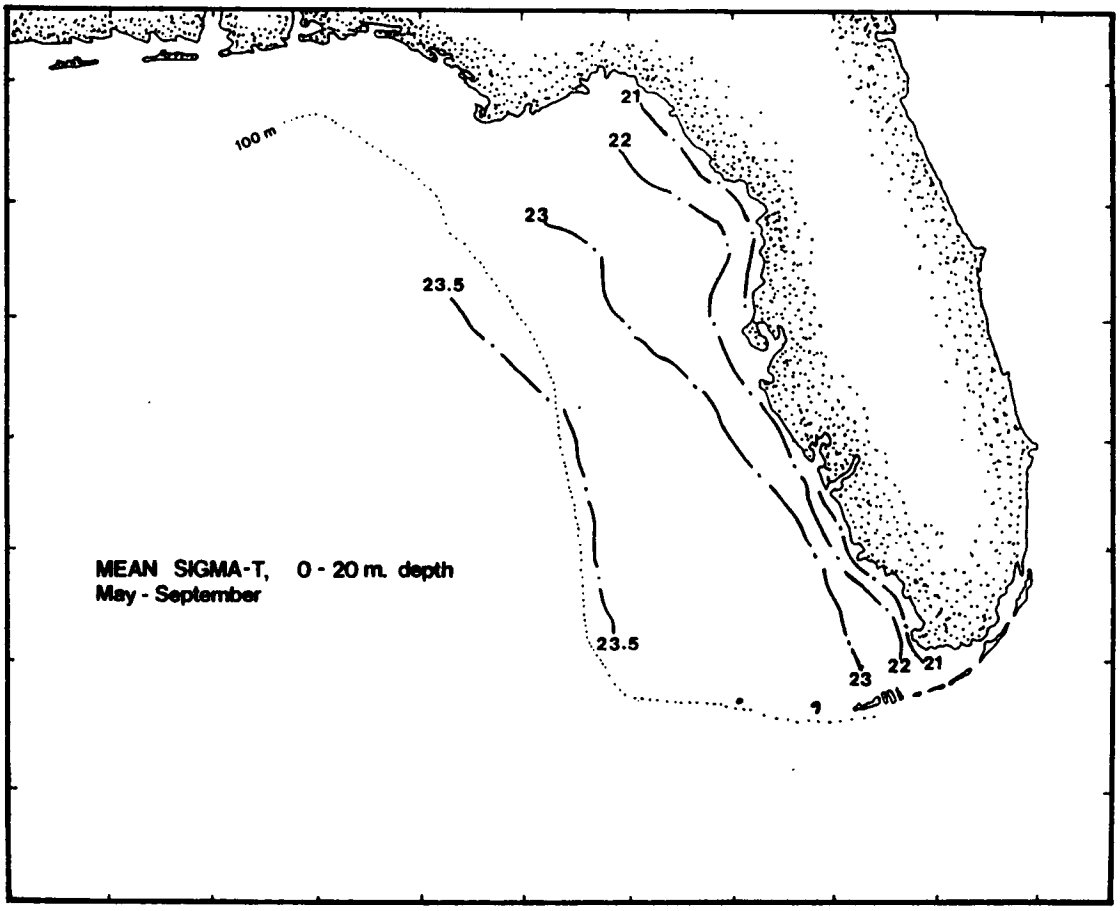

Figure 6.1.1: Typical surface horizontal density gradient - summer.

The above explanation is quite simplistic, but it does appear to explain the observed results, i.e., no density gradient during the winter and a negative gradient (relative to the model grid x-axis) in the summer. However, upon further study of Tables 6.1.1-2, it is apparent that there are very few samples at many of the boxes. Inspection of the actual data reveals that individual hydrographic cruises cover only a third of the shelf at most. There have been no synoptic, shelf-wide cruises. These factors tend to smooth the data and render any final conclusions tentative, at best.

MODEL RESULTS

The summer density gradient was used in the model to estimate the density driven current. The resulting flows (see Figure 4.6.2) are generally in a southerly direction at the surface, onshore at mid-depth in shallow water, and northerly at the bottom. The significance of the density driven flow on overall circulation is very low - the currents are all less than 1 cm s^{-1}.

Since a significant vertical gradient is evident during the summer, its effect was included in the modeling by varying the vertical eddy viscosity coefficient in the manner suggested in Section 4.5. A value of 1.025 g cm^{-3} was used for the density in the lower layer.

6.2 Wind-Driven Currents

DATA ANALYSIS

Historical wind data are available from the Naval Weather Service (Federal Building, Asheville, North Carolina) in reports known as "Summaries of Meteorological Observations, Surface" (SMOS). The wind data are presented in

these reports in a tabular format giving the percentage of total observations occurring in 16 direction categories and 11 wind velocity classes. Wind summaries on a monthly basis are available at Key West for the period 1973-77 and Pensacola for the period 1952-72.

Monthly wind stress resultants were calculated for these two stations by converting the wind velocity classes to wind stress classes, utilizing the equation suggested by Wu (1980):

$$K = (0.95375 + 0.0775\ U)10^{-6}$$

$$\tau = K\ U^2$$

where τ is the wind shear stress and U is the wind speed in m s^{-1}.

The magnitude of the stress in each direction category was calculated by summing the product of the midpoint of each stress category in the SMOS by the percent of observations in each category. The total stress magnitude for each direction was then resolved into u and v components. These components were summed for each direction and the overall monthly resultant calculated.

In order to compare net wind stress resultants which were unbiased by land effects, the entire available wind record from the NDBO weather buoy (July 1977-September 1979) was processed to yield results similar to those described above. The raw wind data were converted to u,v stress components, summed, and monthly resultants were calculated.

To determine seasonal groupings, the monthly resultants from Key West, Pensacola and NDBO weather buoy 42003 were plotted. Results in all cases were similar to those shown for Key West in Figure 6.2.1. The monthly resultants suggest three seasonal groupings: a winter season extending from October through February with winds blowing toward the southwest, a summer

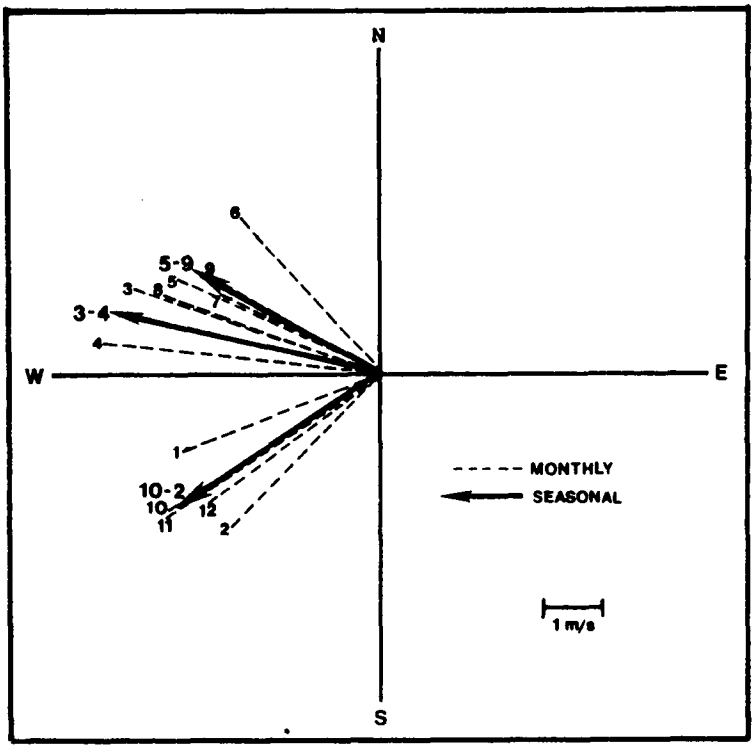

Figure 6.2.1: Mean monthly and seasonal winds at Key West as as derived from mean monthly wind stress using Wu (1980).

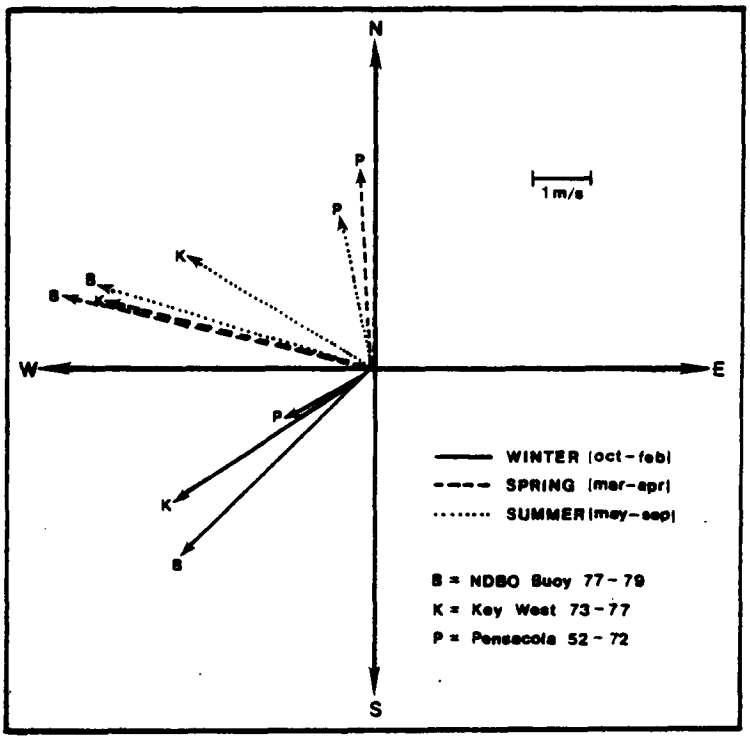

Figure 6.2.2: Seasonal winds at Key West, NDBO data buoy 42003 and Pensacola, Florida as derived from mean monthly wind stress using Wu (1980).

season extending from May through September with winds blowing toward the northwest, and a transitional spring period in March and April with winds blowing toward the west-northwest.

The seasonal resultants at the buoy and Key West compare quite well as demonstrated in Figure 6.2.2. Key West winds are consistently lower in magnitude ranging from 6% during spring, 15% for winter and 36% for summer. With the exception of summer, these factors are quite similar to those found earlier for the real time data during the winter 1978 and summer 1978. A review of the tropical cyclone deck (NOAA, 1981) reveals that at least three tropical depressions passed within approximately 100 km of the buoy during the three year period for which data are available. Simple sensitivity studies demonstrated that removal of the months in which the tropical storms passed the buoy significantly affected the buoy's resultant summer wind. Thus the buoy summer resultant was unduly biased by the passage of tropical depressions. Tropical storms no doubt affected the Key West data but their effect was smoothed because of the longer period of record.

The wind resultants at Pensacola differ substantially from Key West and the buoy. These differences are thought to be due largely to topographic affects though some may be due to characteristic differences in the meteorologic phenomena dominating the region. For the purposes of calculating residual wind-induced currents, we have ignored Pensacola and used the seasonal winds at Key West with an amplification factor of 10% to approximate offshore sites. Winds are assumed spatially uniform. Key West winds were used over those at the buoy because the time series at Key West was substantially longer than at the buoy and hence the Key West resultants are statistically more significant. This appears to be particularly important during the summer for reasons explained above.

The primary shortcoming of this approach is that it excludes wind curl affects in the resulting wind-driven currents. This was felt justified for several reasons:

1. the good comparison between seasonal winds at the NDBO buoy and Key West suggests a very small wind curl in the area of principal concern to MMS. Recall that these two sites were located 400 km apart, and yet the difference in seasonal wind resultants is quite small.

2. No offshore wind data are available on the WFS other than at the buoy (and Key West which closely approximates offshore winds). Extensive analysis would have been needed to remove topographic effects from the only other available data at shore based stations. Such analysis was beyond the time and budget constraints of this study.

MODEL RESULTS

The wind-induced residual currents for the three seasons are shown in Figures 6.2.3-5. Stratification has been included in the currents for the summer season as described in the previous section. The currents are generally quite weak, less than 5 cm s^{-1} in almost all locations. Flow patterns are relatively simple, with an Ekman spiral evident in the deeper water. Surface currents are typically about 20^{o} to the right of the seasonal wind vector.

6.3 Loop Current

DATA ANALYSIS

The Shelf Dynamics Experiment (SDE) data indicate that the LC is the most important forcing mechanism for approximately the southern half of the WFS, from the shelf break to at least the 50 m isobath. Model results imply an even wider effective range. The data base is sufficient to demonstrate the

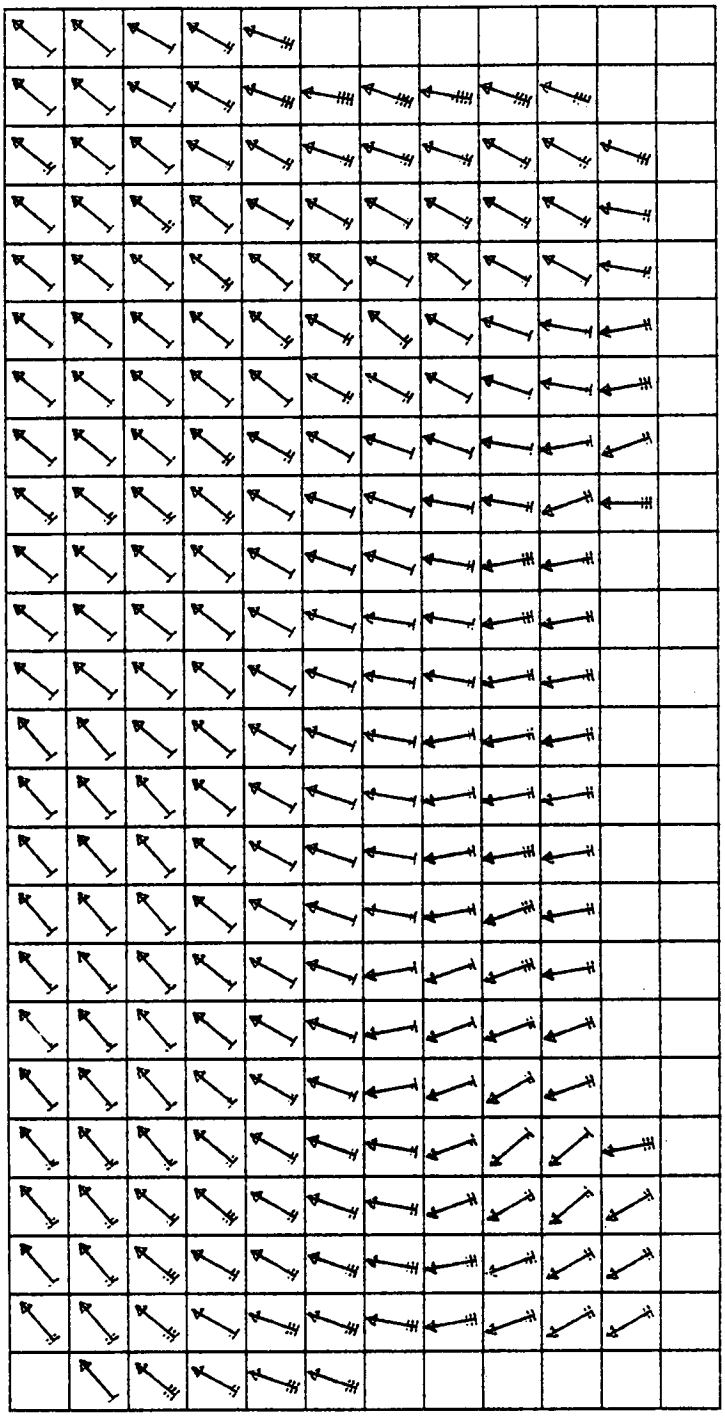

Figure 6.2.3a: Fall-winter residual currents at the surface due to winds ($\underline{18}_{1}4$)
Each grid element equals 30 km, each feather equals 1.0 cm s^{-1}
See Appendix D for list of model input parameters.

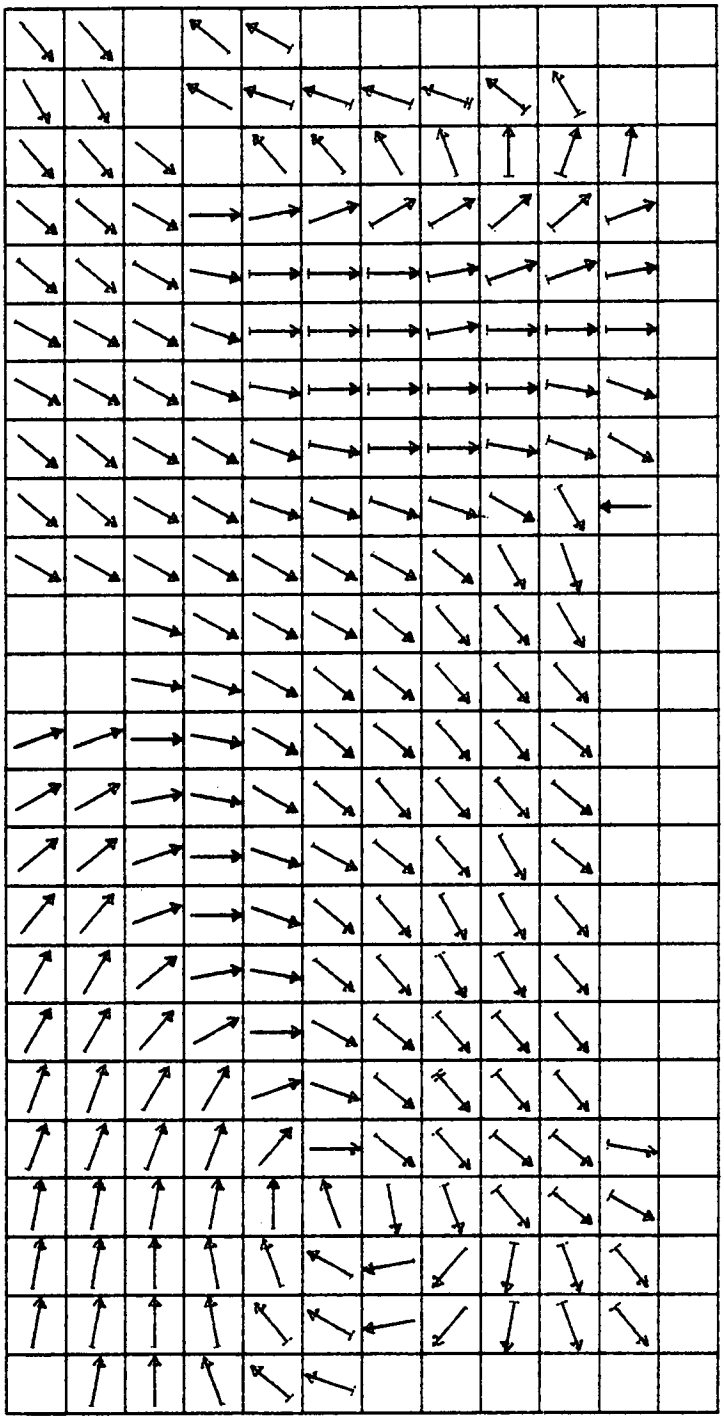

Figure 6.2.3b: Fall-winter residual currents at mid-depth due to winds (18.4)
Each grid element equals 30 km, each feather equals 1.0 cm s^{-1}
See Appendix D for list of model input parameters.

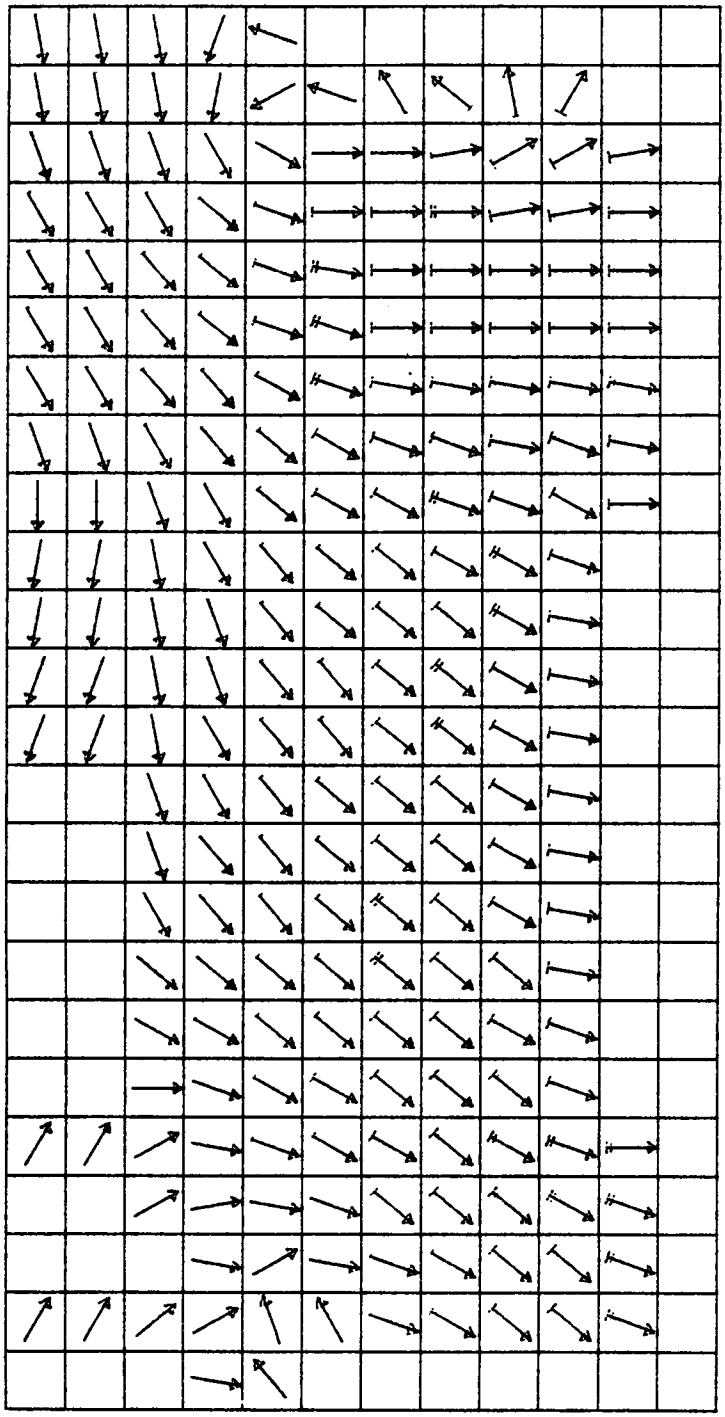

Figure 6.2.3c: Fall-winter residual currents at the bottom due to winds (18.4) Each grid element equals 30 km, each feather equals 1.0 cm s^{-1} See Appendix D for list of model input parameters.

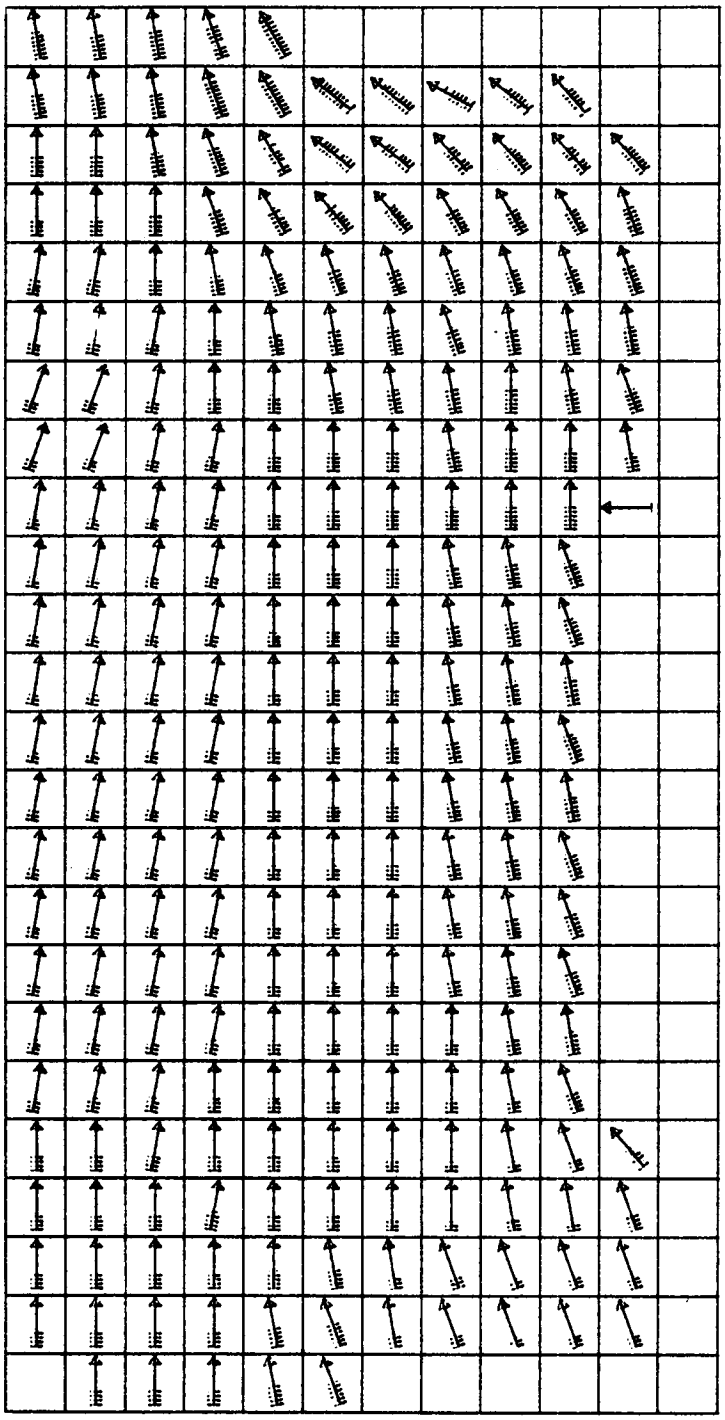

Figure 6.2.4a: Spring residual currents at the surface due to winds (18.5). Each grid element equals 30 km, each feather equals 1.0 cm s^{-1} See Appendix D for list of model input parameters.

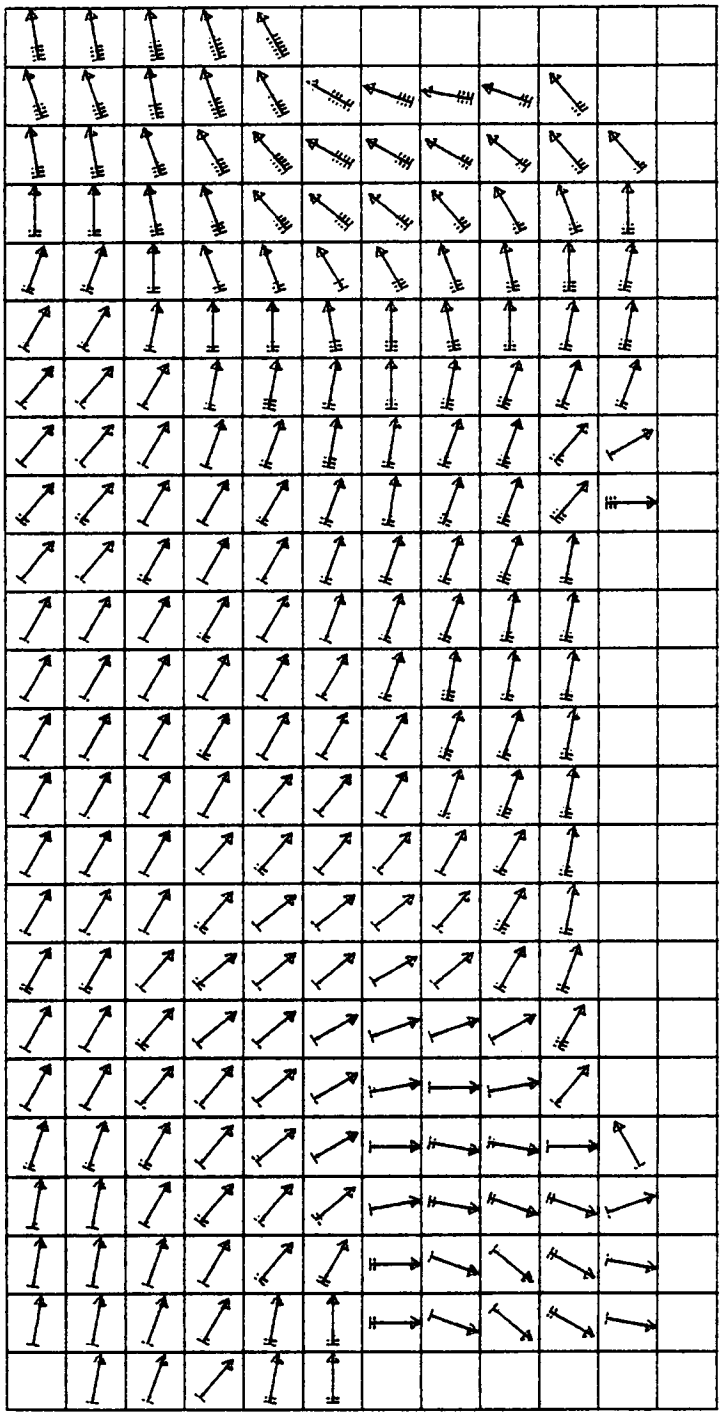

Figure 6.2.4b: Spring residual currents at mid-depth due to winds (18.5). Each grid element equals 30 km, each feather equals 1.0 cm s^{-1} See Appendix D for list of model input parameters.

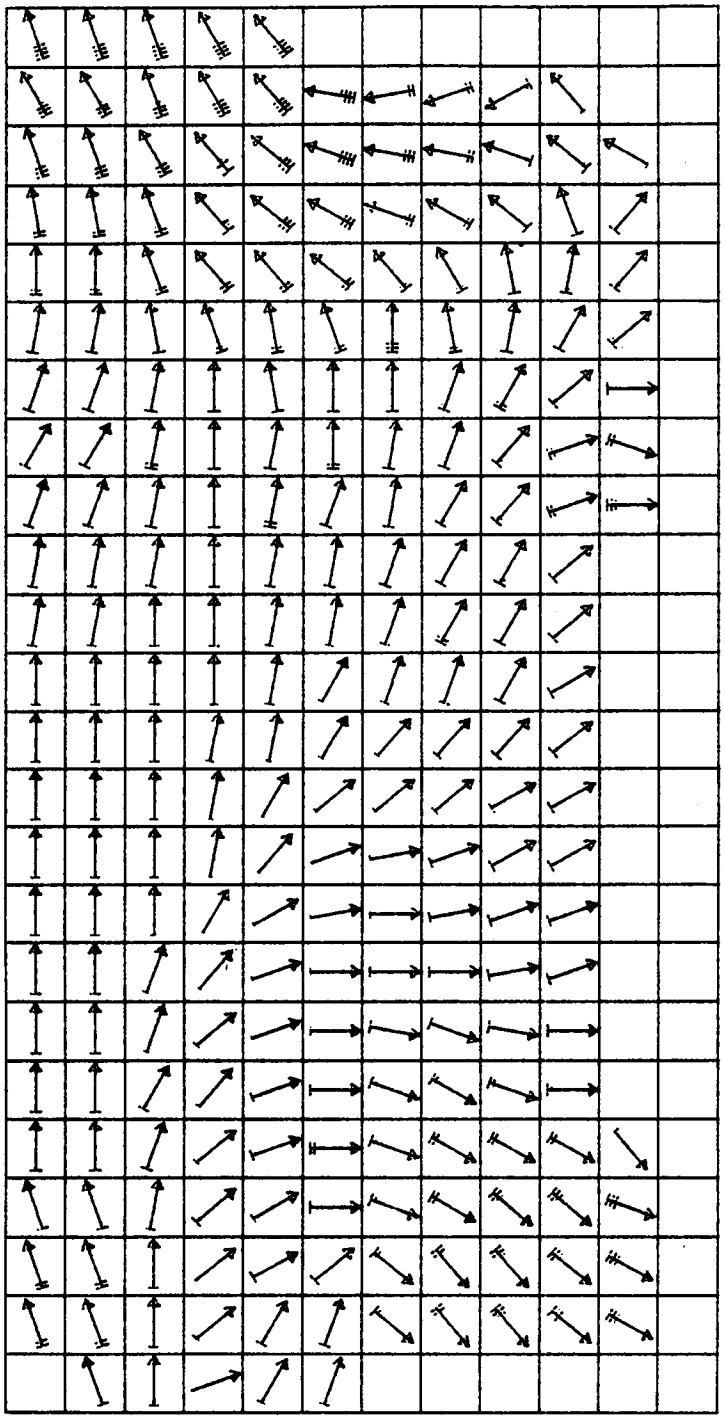

Figure 6.2.4c: Spring residual currents at the bottom due to winds (18.5). Each grid element equals 30 km, each feather equals 1.0 cm s^{-1} See Appendix D for list of model input parameters.

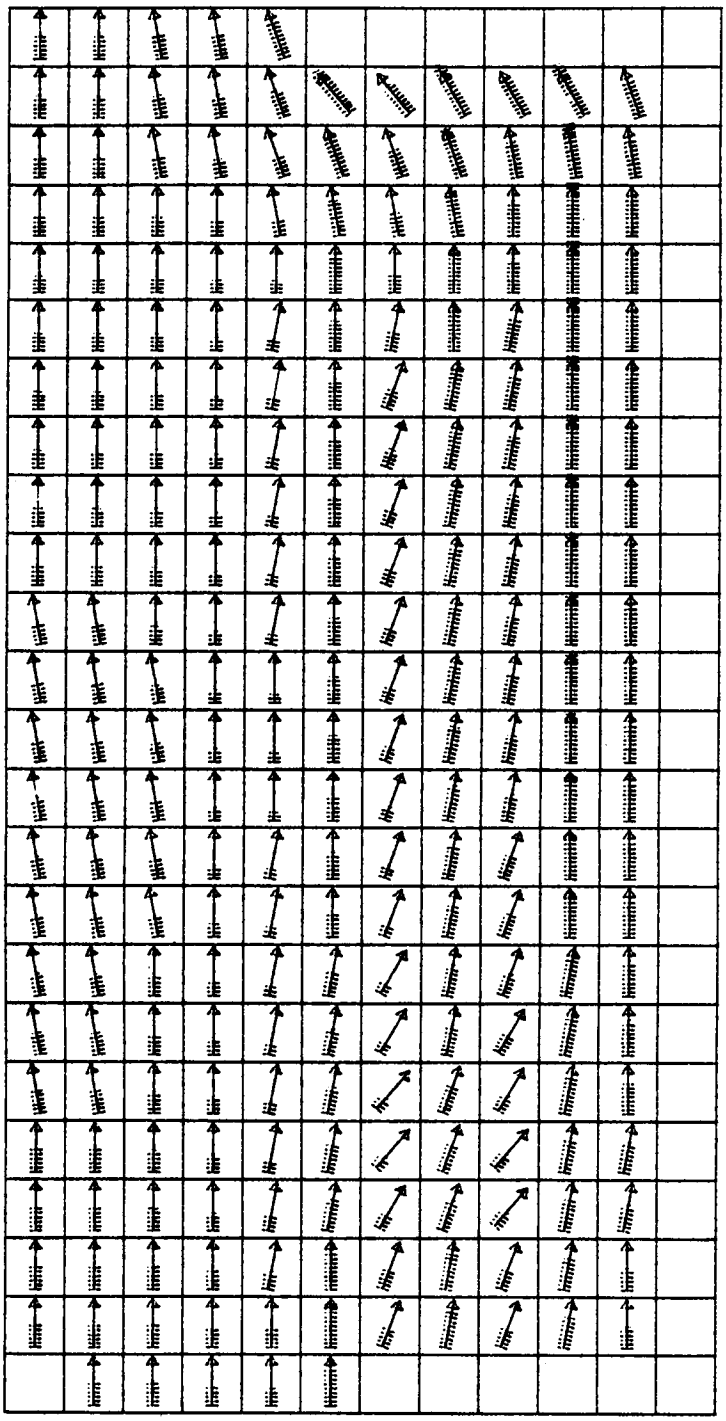

Figure 6.2.5a: Summer residual currents at the surface due to winds including stratification (18-6). Each grid element equals 30 km, each feather equals 1.0 cm s^{-1}. See Appendix D for list of model input parameters.

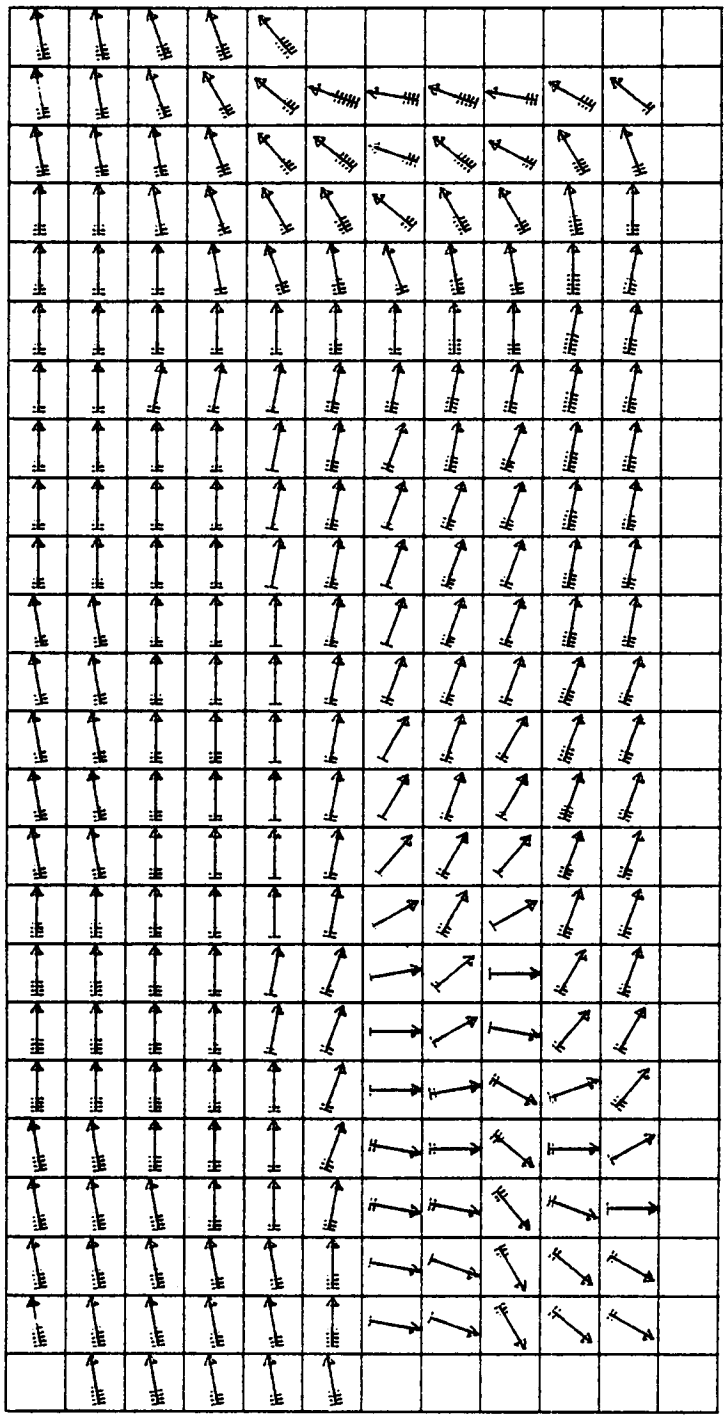

Figure 6.2.5b: Summer residual currents at mid-depth due to winds including stratification (18-6). Each grid element equals 30 km, each feather equals 1.0 cm s^{-1}. See Appendix D for list of model input parameters.

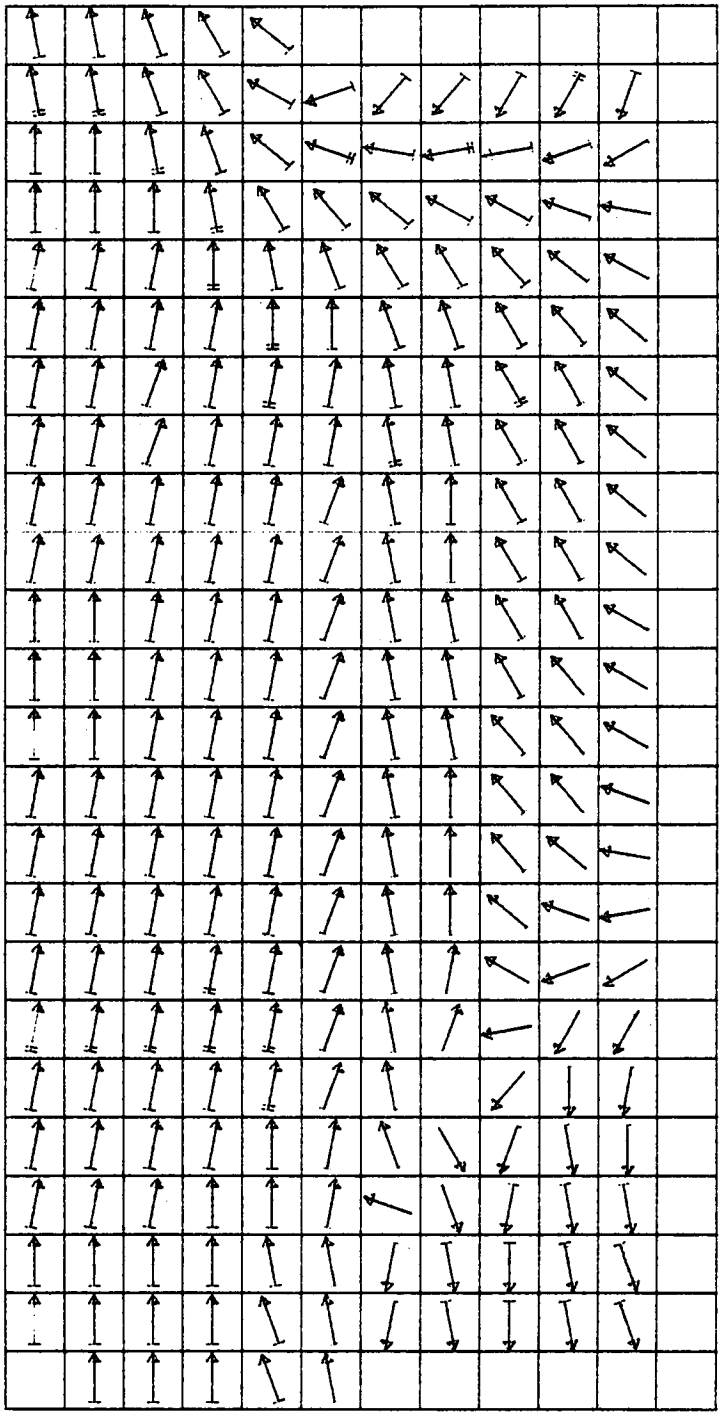

Figure 6.2.5c: Summer residual currents at the bottom due to winds including stratification (18-6). Each grid element equals 30 km, each feather equals 1.0 cm s^{-1}. See Appendix D for list of model input parameters.

importance of the LC and to offer teasing glimpses of the complex processes at play, but is insufficient to quantify the processes with any confidence.

The two most likely theories of how the LC affects shelf circulation have been outlined in chapter 4: (1) a simple lateral shearing mechanism as characterized by Case 13.20 (Figure 4.2.6) in conjunction with occasional intrusions of eddies from the LC, and (2) an eddy wave phenomena suggested by Niiler (1976) (Figure 4.2.8). Both theories are reasonably consistent with the limited velocity data available from the SDE. The two theories are examined in light of some of the other data available on the WFS below.

SURFACE ELEVATIONS

One negative aspect of the eddy wave theory becomes apparent when it is investigated with the model. If the model is driven with an eddy wave, it predicts coastal surface fluctuations which are an order of magnitude too high at the coast and a factor of two too large at the 160 m isobath (see Appendix B.3 for details). Sensitivity studies demonstrate that the problem cannot be resolved by adjusting the model input parameters. A number of weaknesses in the model and the eddy wave concept could explain the large surface elevations. The most likely appear to be the neglect of: the nonlinear terms in the model formulation, and the baroclinic (i.e. density-driven) component associated with the eddies.

Forcing the model with the eddy wave field does not simulate surface fluctuations very well even at a location only 120 km from the western model boundary where the forcing is specified. It is doubtful that such a substantial error could accumulate in this short a distance due to neglect of the nonlinear terms in the model. It seems more likely that the eddies contain a significant baroclinic component (recall that the eddy wave suggested by Niiler and implemented in the model considers only a barotropic forcing mechanism). Hence in order to obtain the observed SDE flow using only barotropic forcing we must over-force the boundary and this shows up in

the modeling as excessive surface elevation fluctuations.

The lateral shear mechanism can generate temporal changes in surface elevations on the shelf in two ways: (1) through the intrusion of eddies or tongues, and (2) through seasonal changes in the position of the LC along the WFS break. The eddies proposed here are strongly baroclinic and are rapidly dissipated as they propagate into the shallower waters of the shelf. Their effect would be minimal at the coast. Seasonal changes in the LC were studied in Section 4.2. These studies showed that when the northward extent of the LC ranged from 30°N to 25°N the coastal surface elevation changed by about 5-10 cm. This is a reasonable range based on recent observations of long-term variations in coastal sea levels (personal communication, W. Sturges, 1982).

DRIFT BOTTLE STUDIES

Figure 2.5.7 summarizes the results of the three drift bottle studies performed on the shelf. Though drifter data is subject to many uncertainties, two important conclusions relevant to this discussion are:

1. the majority of drifters released more than 20 km from shore migrate to the south and land on the Keys or the east coast of Florida; and

2. the migration to the south is overwhelming during the winter months - November, December, January, and February (with the exception of Tolbert and Salsman's February data). During the spring and summer months the destination varies, with a substantial number still found to the south although many are deposited on the northern and western Gulf coasts.

Drifter results can be biased by a number of factors, most notably coastal population density and relatively high energy, high frequency processes (i.e., 2 to .1 cycles per day) such as land-sea breezes and astronomical

tides.

It might be argued, for instance, that because the beaches on the east coast of Florida are more densely populated than those on the west coast, a higher percentage of landed drifters would be recovered from the east coast than the west. However, close inspection of the Hourglass results reveals that drifters released within a few km of the west Florida coast are consistently recovered from the west Florida coast. This obviously suggests that land-sea breezes and/or astronomical tides tend to dominate all other advection processes in this zone. More importantly, the nearshore release results suggest that there are sufficient people on the west coast of Florida to find drifters once they land. Had drifters released near shore consistently not been found, then it could reasonably be argued that all the drifter data were biased. However, this is not the case.

The second factor which can bias drifter data is high frequency events such as land-sea breezes. If a drifter is released close to shore, then such processes can quickly advect the drifter to shore before other, longer term residual currents (which are of primary interest to this study) have time to work. The drifter results on the WFS are particularly remarkable in that many of the release sites were quite close to the coast, yet a significant percentage of the drifters were recovered many hundreds of km away. This suggests that the residual currents in the region are relatively strong, especially the southerly currents.

The drift bottle results are consistent with the LC lateral shear mechanism. Model results indicate the lateral shear-induced current is of the same order as the residual wind-induced current. Hence, during the fall-winter months the LC-induced drift combines with the westerly residual wind drift (e.g. Figure 6.2.3.a) to virtually insure southerly advection and deposition in the Keys or entrainment in the LC. Once entrained in the LC, a drifter will almost surely be deposited on the Keys or Atlantic seaboard. During spring and summer the residual wind vector becomes northerly and counteracts the

southerly lateral shear mechanism. The drifter destination becomes more random, depending to a greater degree on the specific time series of: (1) the total wind and (2) eddy intrusions from the LC.

Additional support for the lateral shear mechanism is found by considering the characteristic travel times involved with the two northernmost drift studies by Tolbert and Salsman (TS) and Gaul and Boykin (GB). Their results show a substantial number of southern retrievals consistently throughout the year. This persistence is easily explained by the lateral shear mechanism in conjunction with either weak wind activity or a fairly brief period of strong northerly winds.

If the lateral shear mechanism is ruled out, the only remaining processes to drive the TS-GB drifters south are:

1. direct entrainment in the LC,
2. northerly winds, or
3. the eddy wave.

Historically, the northwardmost extent of the LC has reached the TS-GB release sites but observations by Behringer et al. (1977), and Vukovich et al. (1978) indicate these extreme northward extensions are rare. For instance Vukovich et al. reports only 6 months out of 31 in which the LC extended above 28^{o} N. Roughly translated this means that the northward edge of the LC is over 200 km from the TS site for 80% of the time. Thus it seems improbable that direct entrainment in the LC was responsible for the majority of the southerly drifters.

As for item (2), the seasonal wind patterns for two of the three seasons drive a net northerly drift and so any net southerly drift would have to come from abnormal northerly winds. What magnitude and duration would these

northerly winds have to be to drive the drifters sufficiently far south to reach the LC? Behringer et al. suggest the average northwardmost edge of the LC is 26°N or over 400 km from the TS-GB release sites. Assuming a 3% wind drift factor, it would require about 13 days of consecutive northerly winds of average 10 m s^{-1} to drive the drifters to 26°N. Even if the LC is located at 28°N, it would take about 7 days of northerly winds. Such extended periods of strong northerly winds are extremely unlikely particularly in the spring-summer.

As for item (3), the eddy waves cause no net long term advection by themselves because of their oscillatory nature. But, they can cause advection over time scales less than a full period. For the 16 day period eddy wave suggested by Niiler, the maximum advection will occur during a 4 day period (1/4 of an eddy wave cycle). Based on an average 40 cm s^{-1} speed (which is consistent with observations from SDE data and model runs shown in Figures 4.2.8), the net advection during this period would be about 150 km. Hence the eddies suggested by Niiler are insufficient to consistently advect drifters to the LC by themselves.

There are two final characteristics of the Hourglass drift bottle studies which are worth noting and comparing with model results. First, the releases often display rather dramatic divergence in direction as indicated in Figure 2.5.6a at stations E and L. Such rapid changes in the flow field are probably due to eddies and suggest that the eddies can be important in determining the ultimate destination of drifters.

The second characteristic is the northerly coastal current which is often observed, e.g. Figure 2.5.6b. Such a feature is evidently not due to the local wind according to Williams et al (1977) but is consistent with the model investigations of the lateral shear mechanism as shown in Figure 4.2.2. A persistent northerly coastal current is not readily explained using the eddy wave concept.

SUMMARY OF LOOP CURRENT DATA ANALYSIS

1. Both the eddy wave and lateral shear mechanism are consistent with the SDE velocity data on the shelf.

2. When investigated with the model, the eddy wave mechanism substantially over predicts surface level fluctuations suggested by observations. This may be partially due to neglecting the nonlinear terms in the model but some of the data imply that this shortcoming is more likely due to neglecting the baroclinic component of the eddies.

3. Surface fluctuations due to the seasonal migration of the LC are apparent in the offshore surface elevation data. These variations are simulated quite well by the model by varying the position of a ramp or step forcing function along the western boundary.

4. Drifter releases consistently show retrievals to the south throughout the year. During the winter the majority of drifters are found to the south. These results are consistent with an lateral shear mechanism which generates a net southerly drift over most of the shelf. The drifter results are not easily explained without the lateral shear mechanism.

5. The drifter data from the Hourglass study imply the existence of a weak northerly coastal current which is consistent with the model results using a lateral shear type forcing mechanism. The northerly current is difficult to explain with any other mechanism.

6.3.1 Modeling Loop Current Induced Residual Currents

Based on the data at hand it is recommended that the effect of the LC on

shelf circulation be included primarily via the lateral shear mechanism. This is implemented by imposing a steady velocity along column 1 of the model grid in the negative y-direction. The velocity varies from 0 at the northward extent to 100 cm s^{-1} at row 1.

In the vertical the velocity is applied over the upper 50 m of the water column. Earlier sensitivity studies with lateral shear forcing had assumed the current to extend uniformly over the entire water column. However, when this configuration is combined with the other seasonal parameters, the northerly coastal jet suggested in the data is eliminated in the northern portion of the shelf. Thus no mechanism for drifters to consistently escape to the western Gulf would have been provided. In addition, seasonal coastal surface fluctuations would have been in excess of 10 cm, a value thought to be on the higher end of reasonable values.

The seasonal migration of the LC is roughly accounted for by varying the northward extent of the specified boundary velocity. Three positions are proposed: 24^{o}, 26^{o}, and 28^{o}N.

At this time it is not possible to include any eddy processes in the modeling. This applies both to the eddy wave mechanism and the tongues or eddies suggested as part of the lateral shear mechanism. Omission of eddies is due to: (1) the uncertainty regarding the nature of the eddy wave mechanism, (2) the lack of synoptic data describing the density field of the eddies, and (3) the inability of the present model formulation to simulate certain aspects of the eddies which are suspected to be important.

MODEL RESULTS

Figures 6.3.1-3 show the modeled currents generated by the lateral shear mechanism for the three LC positions. Plan views of currents are shown for the surface only, there being no significant variation of velocity with depth on the shelf. For the so called 'northerly' position (i.e. 28^{o}N) shown in

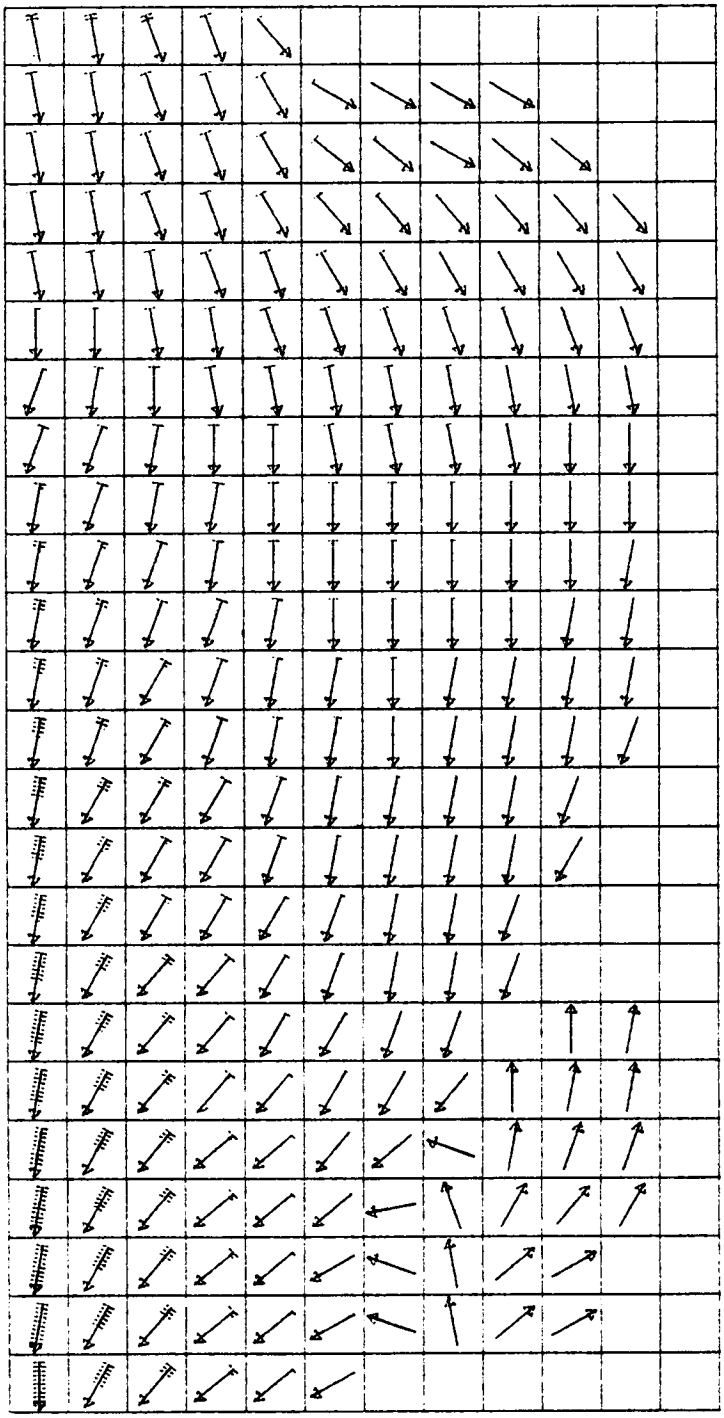

Figure 6.3.1: Surface currents due to northerly position of LC, including stratification (13-35). Each grid element equals 30 km, each feather equals 10 cm s^{-1}. See Appendix D for list of model input parameters.

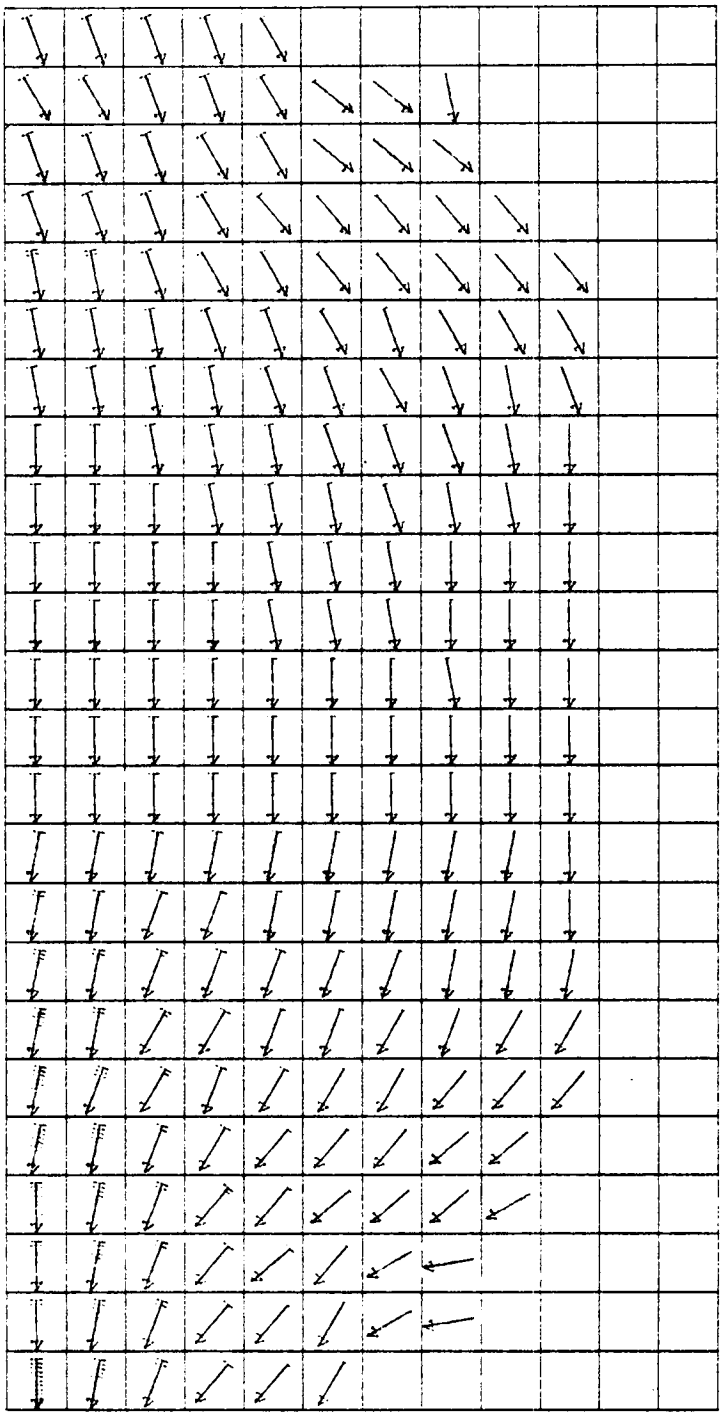

Figure 6.3.2: Surface currents due to mid-position of LC (13.36). Each grid element equals 30 km, each feather equals 10 cm s^{-1}. See Appendix D for list of model input parameters.

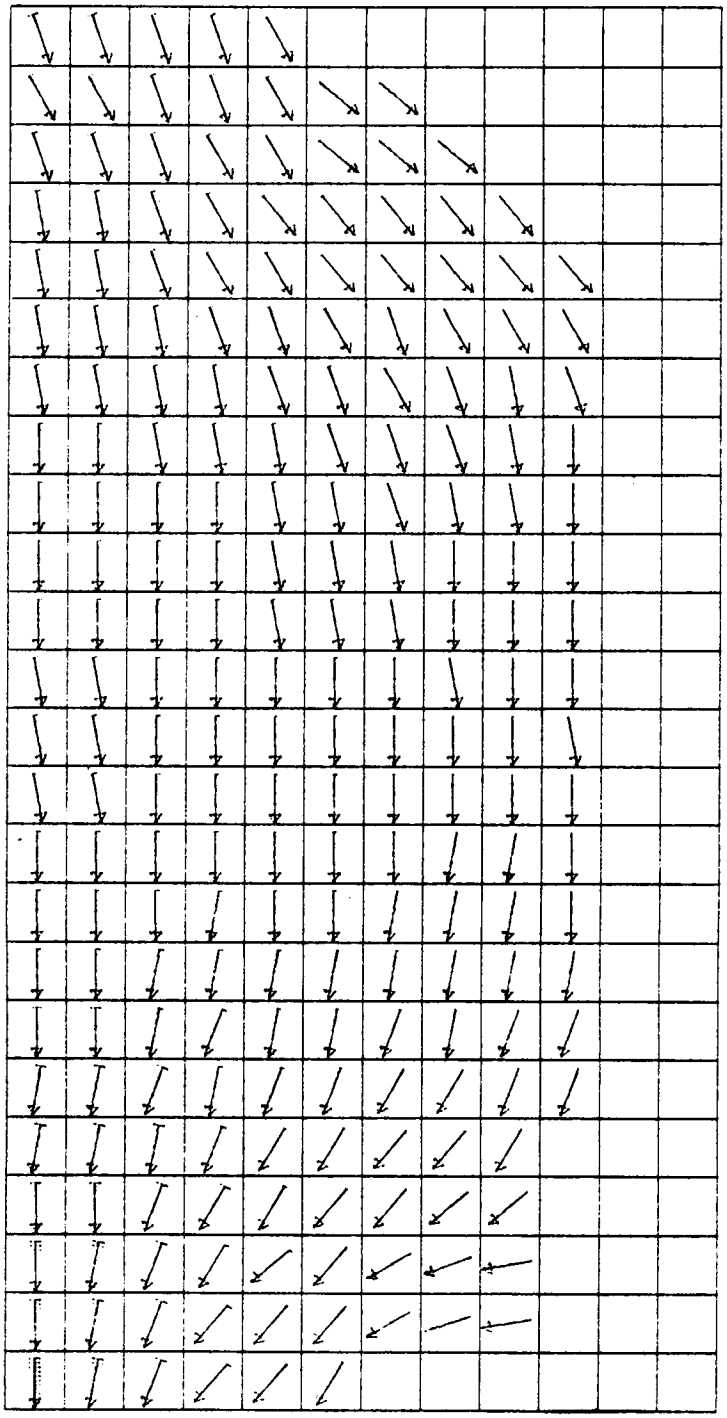

Figure 6.3.3: Currents due to southerly position of LC (13.37). Each grid element equals 30 km, each feather equals 10 cm s^{-1}. See Appendix D for list of model input parameters.

Figure 6.3.1, the velocity is specified in column 1, rows 1-19; for the 'mid' position (i.e., 26°N), rows 1-11; and for the 'southerly' position (i.e., 24°N), rows 1-3. Values for c_b, W_{*s}^2, and N_h are consistent with the other flow fields shown in this chapter. Vertical stratification has been included for the summer season.

6.4 Modeling Combined Effects of WFS Forcing Mechanisms

A central issue in deriving the total seasonal circulation is the method of accounting for the LC effects. If it is assumed that the northward extent of the LC varies yearly as suggested by Leipper (1970), Behringer et al. (1977) and others, then combining flow fields becomes quite simple. For example, Behringer et al. suggest the variation shown in Figure 2.3.10 which indicates: (1) the 'northerly' position of the LC defined above would be appropriate for summer, (2) the 'southerly' for fall-winter, and (3) the 'mid' for spring. Once the three positions of the LC are related to season, one need only linearly superimpose plan view plots for the appropriate seasons (recall that the model is linear so superposition is legitimate). For instance, the total summer circulation can be found by combining Figures 4.6.2, 6.2.5 and 6.3.1.

More recent studies by Hurlburt and Thompson (1980) and Vukovich et al. (1978) suggest the cycle of the LC is not yearly. The model of Hurlburt and Thompson found a 8-10 month cycle. Vukovich et al. avoid the issue of cycle. Instead they show a mean monthly position of the LC based on five years of infrared satellite observations. These positions display no clear cycle and in fact reveal substantial exceptions to the cycle suggested by Behringer et al. and others.

If it is assumed that the LC is independent of season then combining the LC with the seasonal wind and density fields would have to be handled in a probabilistic manner. One simple method of accomplishing this would be to assume the probability of occurrence for each of the three LC positions is roughly equal. This assumption is consistent with the data from Vukovich et al. and Behringer, et al. Using this assumption, LC position could be treated as a uniformly distributed random variable and combined with seasonal and real time winds in the Department of the Interior's trajectory analysis. Computationally this would require roughly a factor of three more time than assuming a seasonal cycle in the LC.

The ultimate answer to whether the LC has an annual cycle remains unknown. At this point it is recommended that the LC be regarded as seasonal. The evidence supporting this assumption is admittedly not overwhelming but the additional expense of treating the LC in a probabilistic manner seems unecessary until the temporal variation of the LC is better understood.

Figures 6.4.1-3 show the combined residual currents for the fall-winter, spring, and summer seasons, respectively. Currents are shown at three levels: surface, mid-depth, and bottom.

The winter circulation is primarily southerly at all levels except within 60 km of the coast where: (1) a weak cyclonic eddy is apparent in the lower levels in the northeast corner of the shelf, and (2) weak up-welling is implied along the coast. Velocities are small along the coast: about 2 cm/s at the surface and about one-half that at lower levels. The net southerly drift on the shelf is consistent with the observed drifter studies.

The spring circulation is considerably more complex than the winter. Again, a weak clockwise eddy is seen in the northeast corner and up-welling is apparent at the coast. A northerly coastal jet forms in the surface waters along the coast and extends from Key West to Apalachicola. Typical surface currents are 5 cm/s. This jet is consistent with the Hourglass drift results

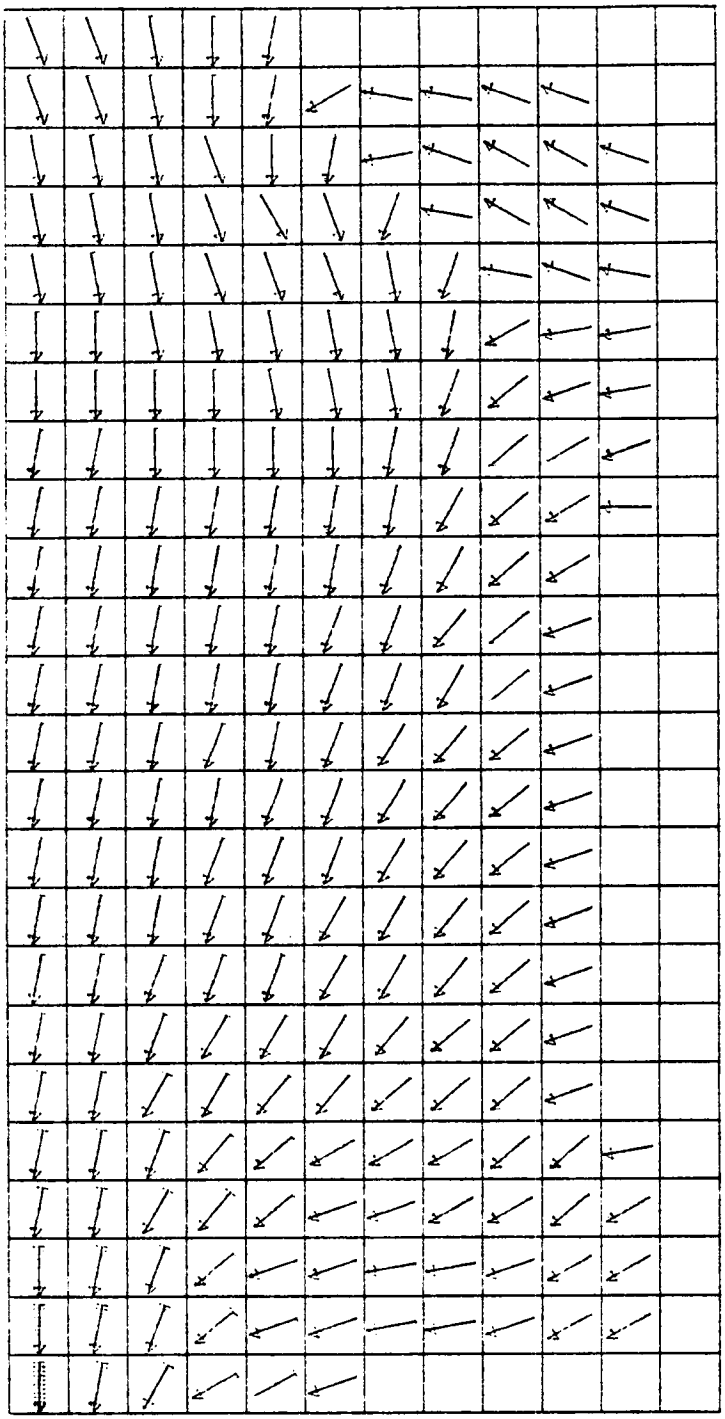

Figure 6.4.1a: Fall-winter residual currents at the surface due to wind and LC (21-6). Each grid element equals 30 km, each feather equals 10 cm s^{-1}. See Appendix D for list of model input parameters.

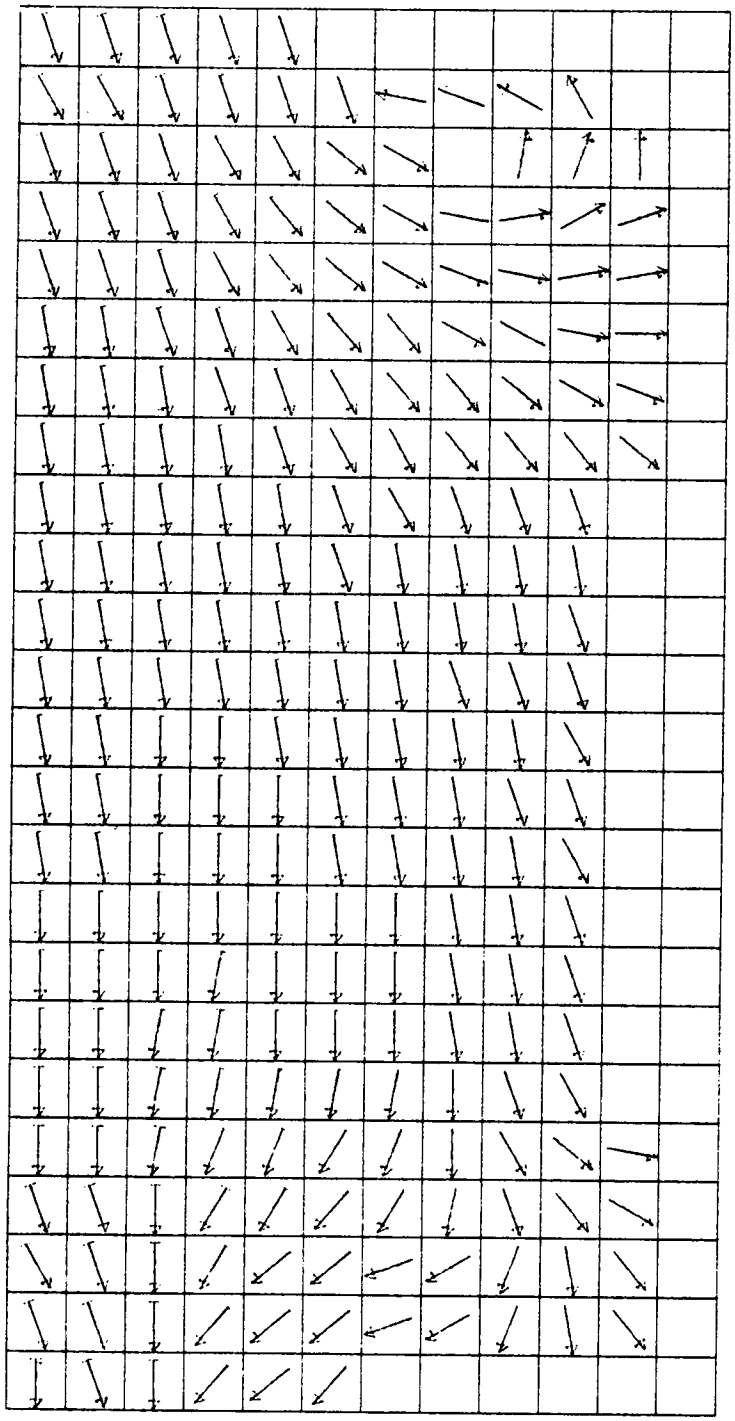

Figure 6.4.1b: Fall-winter residual currents at mid-depth due to wind and LC (21-6). Each grid element equals 30 km, each feather equals 10 cm s^{-1}. See Appendix D for list of model input parameters.

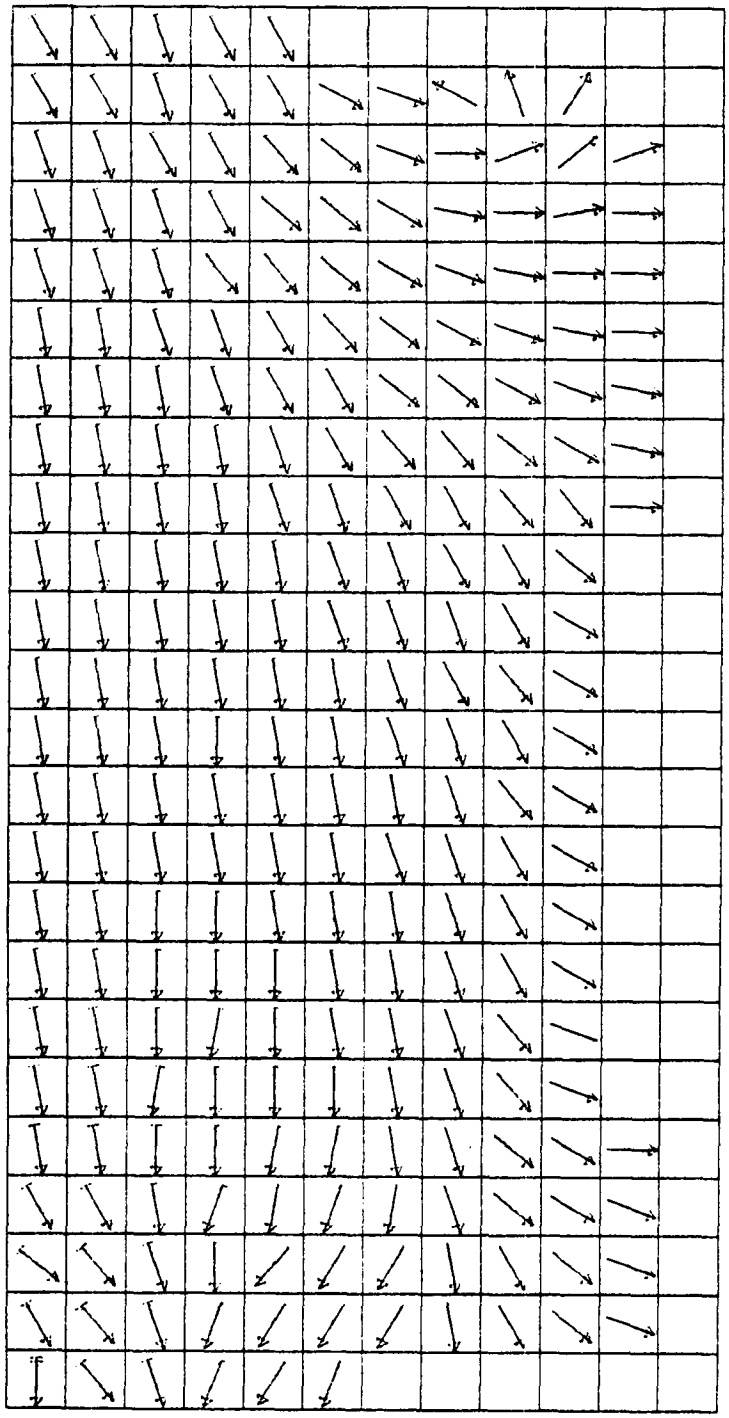

Figure 6.4.1c: Fall-winter residual currents at the bottom due to wind and LC (21-6). Each grid element equals 30 km, each feather equals 10 cm s^{-1}. See Appendix D for list of model input parameters.

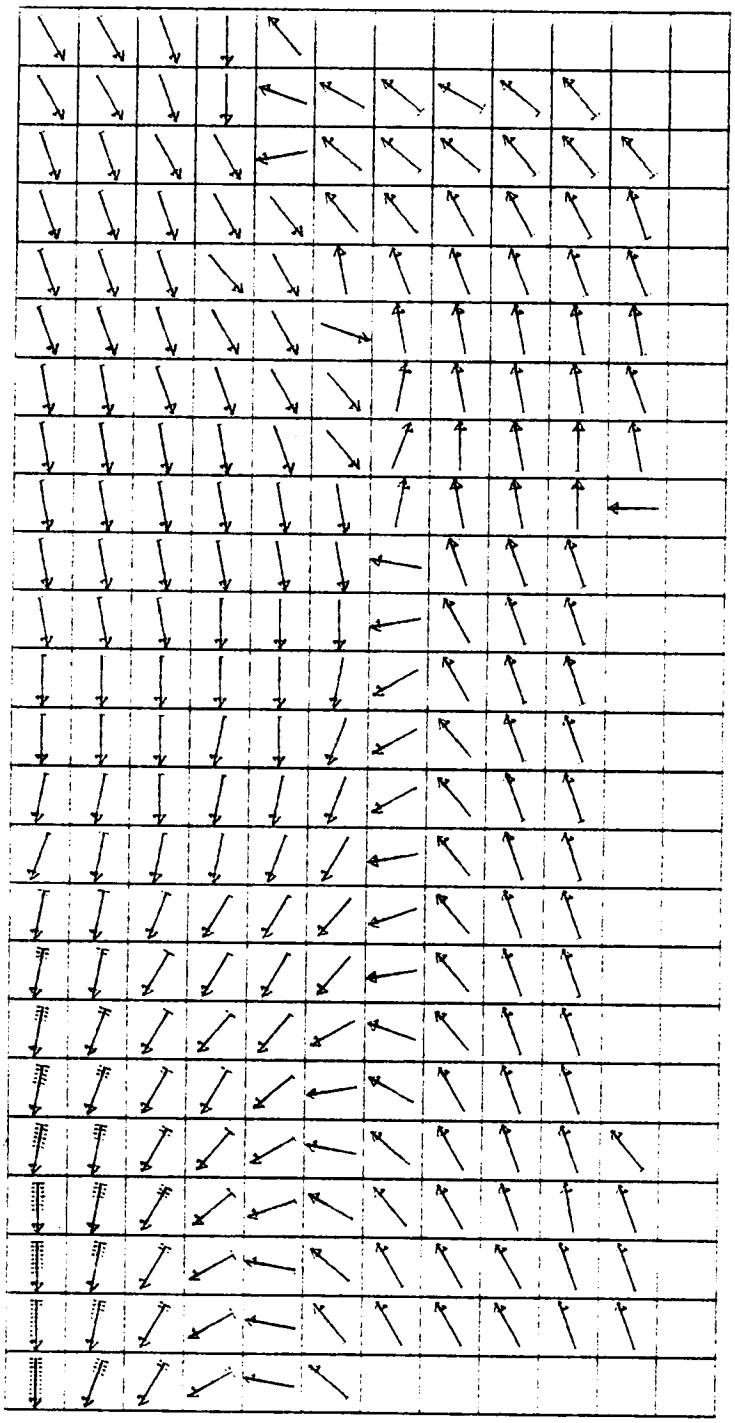

Figure 6.4.2a: Spring residual currents at the surface due to wind and LC (21-4). Each grid element equals 30 km, each feather equals 10 cm s^{-1}. See Appendix D for list of model input parameters.

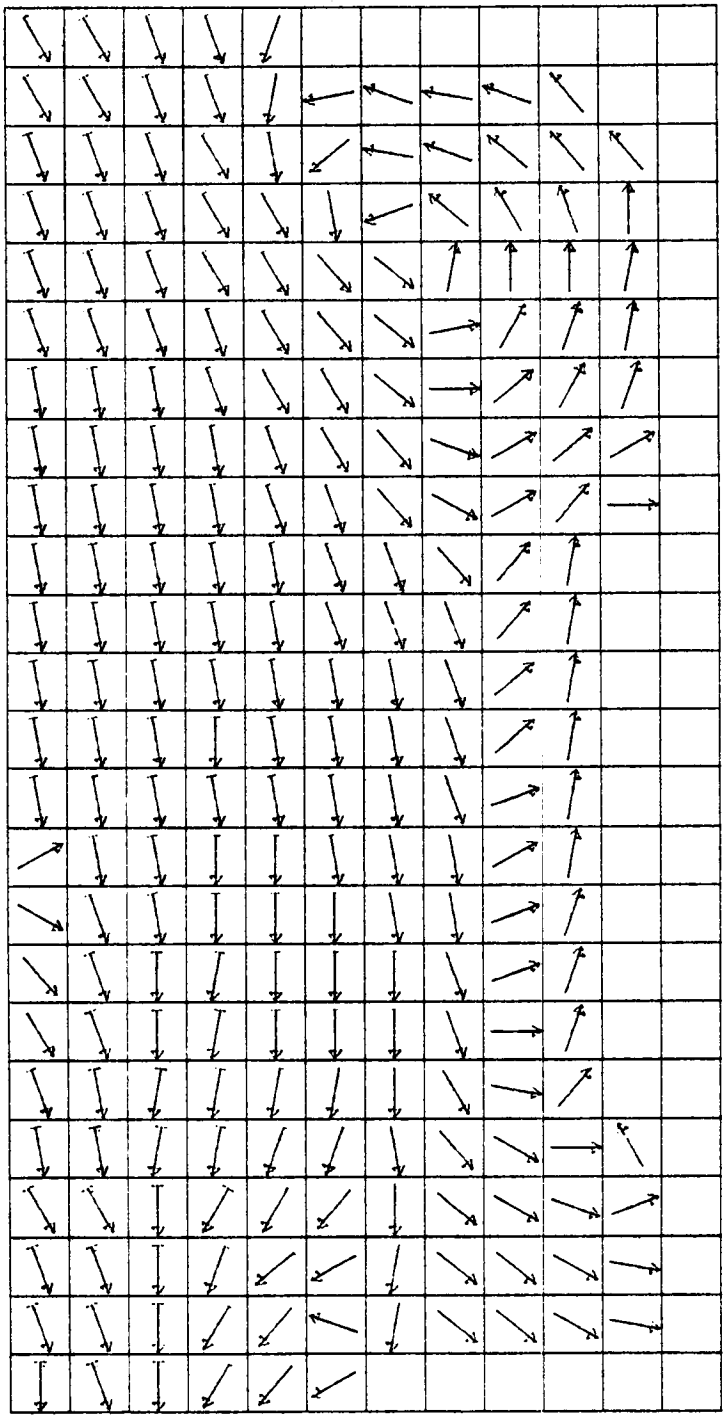

Figure 6.4.2b: Spring residual currents at mid-depth due to wind and LC (21-4). Each grid element equals 30 km, each feather equals 10 cm s^{-1}. See Appendix D for list of model input parameters.

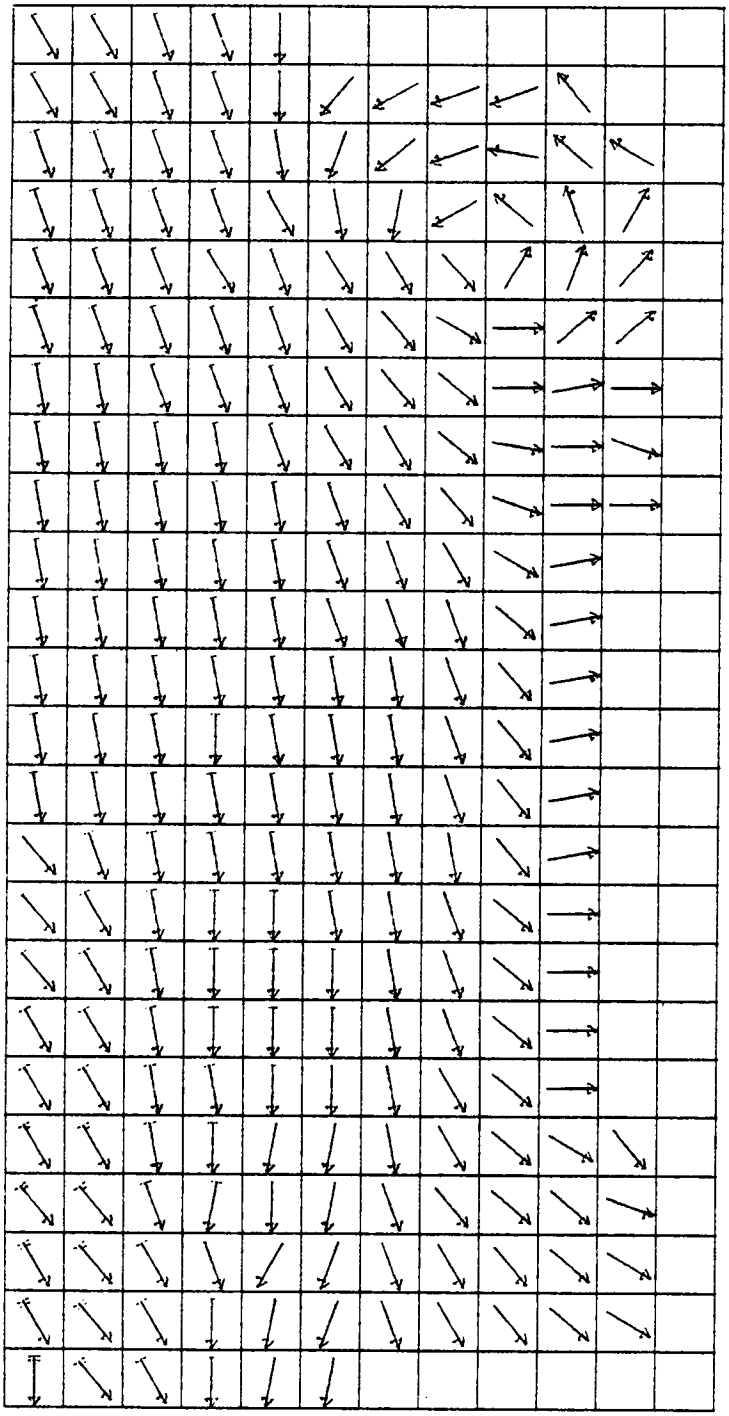

Figure 6.4.2c: Spring residual currents at the bottom due to wind and LC (21-4). Each grid element equals 30 km, each feather equals 10 cm s^{-1}. See Appendix D for list of model input parameters.

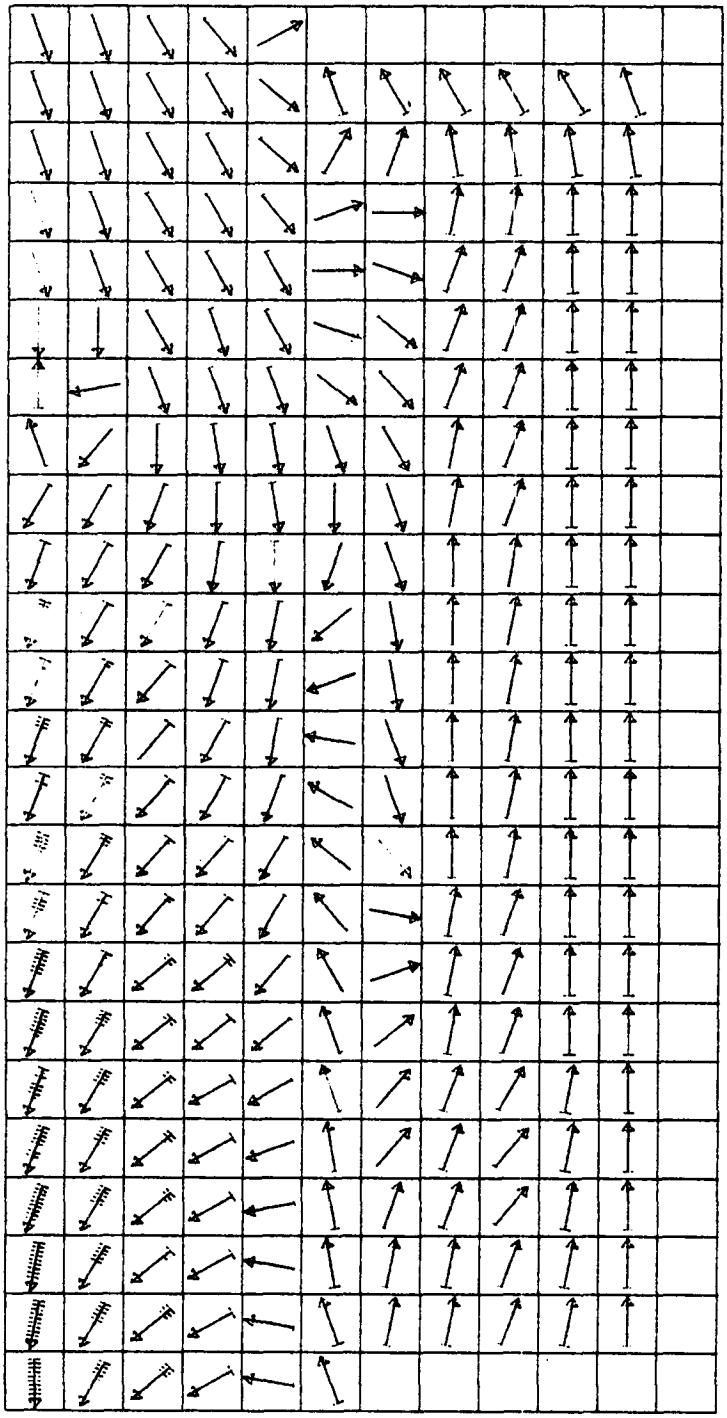

Figure 6.4.3a: Summer residual currents at the surface due to wind, horizontal density gradients, and LC, including stratification (21.5). Each grid element equals 30 km, each feather equals 10 cm s^{-1}. See Appendix D for list of model input parameters.

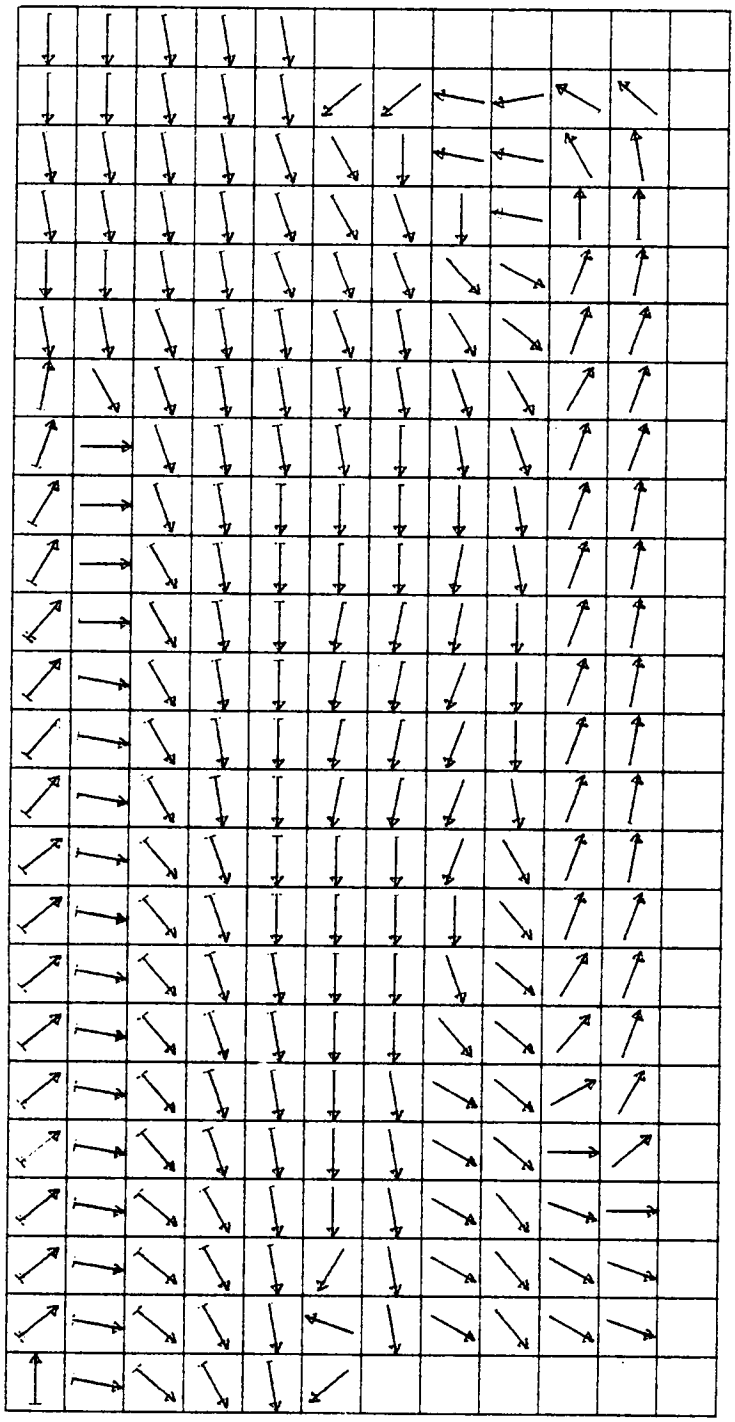

Figure 6.4.3b: Summer residual currents at mid-depth due to wind, horizontal density gradients, and LC, including stratification (21.5). Each grid element equals 30 km, each feather equals 10 cm s^{-1}. See Appendix D for list of model input parameters.

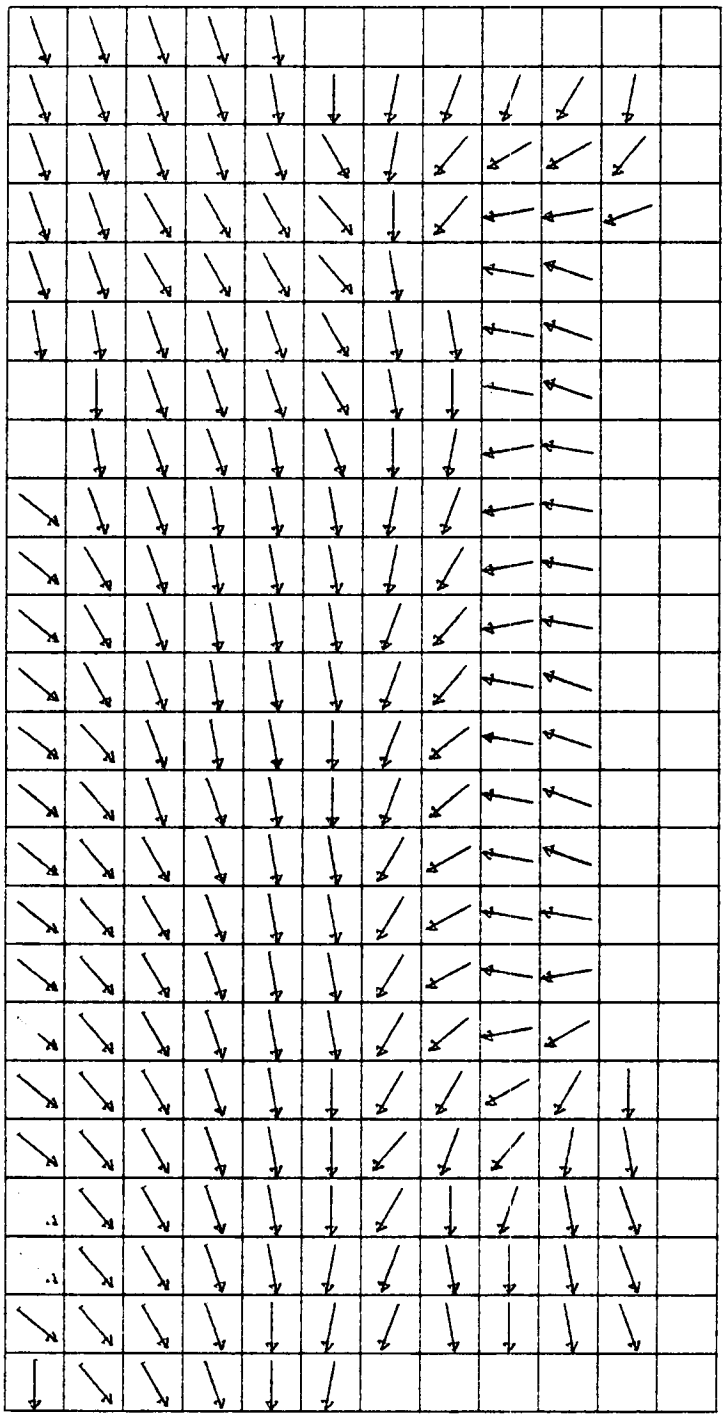

Figure 6.4.3c: Summer residual currents at the bottom due to wind, horizontal density gradients, and LC, including stratification (21.5). Each grid element equals 30 km, each feather equals 10 cm s^{-1}. See Appendix D for list of model input parameters.

which indicated a northerly coastal current during the spring and summer. Also, the northerly current provides a mechanism to transport drifters off the shelf and to the western Gulf.

Summer surface circulation is qualitatively similar to the spring. Stratification effects during the summer cause surface currents in the northerly jet to be about double those in the spring. Summer bottom currents along the coast are offshore and much smaller than their spring counterparts. Weak down-welling is implied by the summer currents at lower levels along the coast. As in the spring, the summer circulation provides a mechanism for drifters to escape LC entrainment and end up in the western Gulf. This is consistent with the drifter data. When reviewing the summer results it should be recalled that a somewhat simplified bathymetry was needed in order to include horizontal density gradients.

Figure 6.4.4 shows the coastal surface elevation changes during the three seasons. The biggest change in elevation during a year (7 cm) occurs between winter and spring-summer in the northeast corner of the shelf. Approximately 4 cm of this is due to the shift in the LC and the remaining 3 cm is due to the change in the seasonal wind stress. The change due to the LC appears to be within a factor of 2 of the change recently suggested by Sturges (personal communication, 1982) based on his preliminary correlation between LC position and observed coastal elevations.

When combining the residual circulation with real time wind data, it should be remembered that the residual currents already include the winds in an average sense. Therefore to superimpose the real time wind-induced currents (e.g. via a 3% rule) on the residual currents would count the residual wind twice. To avoid this, the real-time wind stresses used in the trajectory analysis should have the residual wind stress subtracted from them.

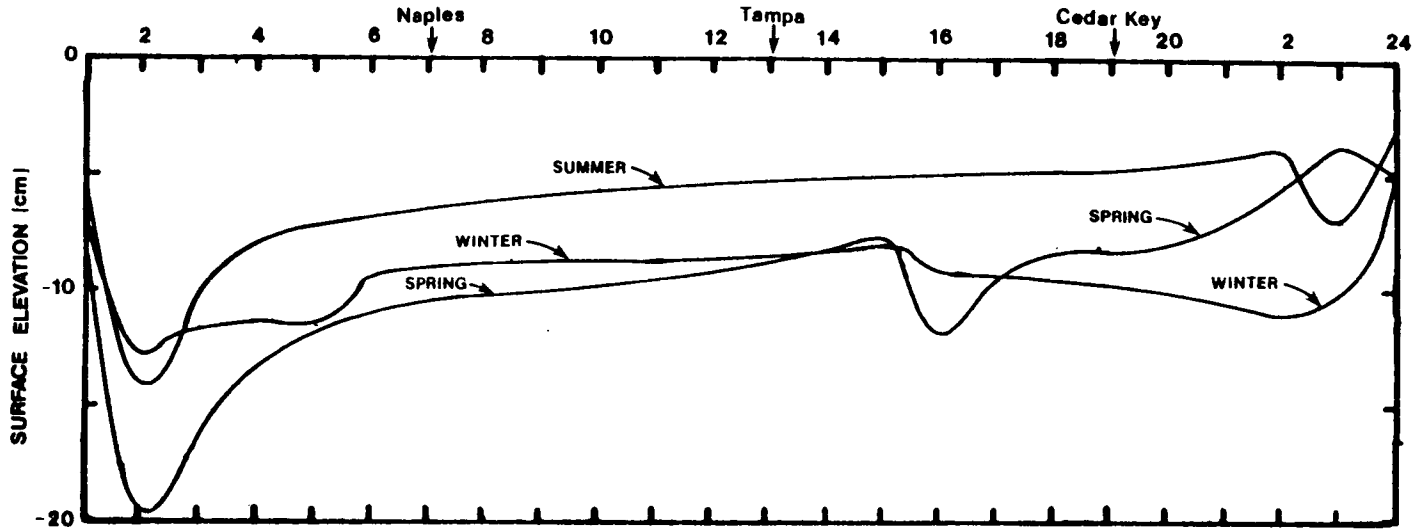

Figure 6.4.4: Seasonal changes in coastal surface elevations.

Chapter 7

Recommendations for Further Work

Model verification, tuning and production runs were severely limited by the lack of high quality in situ current and coincident hydrographic data on the West Florida Shelf (WFS). Further modeling with the existing data sets is limited for this reason, but some topics worth investigating are:

1. real time hindcasts of the Hourglass drifter data,
2. analysis of long term coastal surface elevations to determine possible Loop Current (LC) effects,
3. investigation of the nature of the eddies observed on the shelf during the Winter 1973 Shelf Dynamics Experiment (SDE), and
4. hindcasting of the Florida "Middle Ground" current meter data.

These have been listed in order of their perceived merit to improving the WFS circulation model.

MODELING HOURGLASS DRIFTER DATA

The first topic would involve hindcasting of the Hourglass drift bottle data in real time. The other drift bottle release sites were located outside the present model grid and simulation would require expansion of the model grid, a task difficult to justify given the inherent quality of drifter data.

Simulation of the Hourglass data could be performed in a straight forward manner using the model alone, or more appropriately, by combining the seasonal currents (as reported in this study) with the local winds via a wind factor (e.g. 3% rule). The latter approach would be fundamentally identical to the methodology employed in the final Department of the Interior trajectory modeling. The purpose of these hindcasts would be to:

1. allow further, albeit indirect, tuning of the model;
2. estimate the importance of eddies on long term advection on the shelf; and
3. assess the probable error associated with the Department of the Interior's trajectory modeling by measuring the discrepancy between a modeled drifter and an actual one.

LOOP CURRENT EFFECT ON COASTAL SURFACE ELEVATIONS

The second topic of potential interest would be an estimate of the change in surface elevation due to the seasonal movement of the LC. This information would be useful in indirectly testing possible LC forcing mechanisms in the model. Work in this area was begun several years ago by Professor Wilton Sturges at Florida State University (personal communication, 1982), and it would be to MMS's best interest to follow that work.

ANALYSIS OF SDE DATA

The third topic is the most direct method of investigating the nature of the major eddies and tongues which propagate onto the shelf. SDE data from the shelf strongly imply these eddies are an important mechanism in determining advection and dispersion on the shelf. Kroll and Niiler (1976) explored some aspects of the eddies, but their study considered only the barotropic component. Additional work should be started to more thoroughly explore

other characteristics of these eddies including the baroclinic component. The state-of-the-art nature of the problem suggests that it is ideally suited as a thesis topic which could be funded for relatively little cost by MMS.

Data covering at least one of these eddies exist from the winter 1973 SDE experiment (Appendix B.3), but these data are clearly insufficient to resolve the many complex issues concerning the eddies. Nevertheless, the work is still justified since:

1. there appear to be sufficient data available to at least start the process of model conceptualization and testing;

2. it would aid in the design and interpretation of data to be taken in the near future as part of the MMS data collection program; and

3. it would serve as the basis for future incorporation of the eddies into the model should they prove to be as important as the data presently suggest.

ANALYSIS OF MIDDLE GROUND DATA

The fourth area of potential interest involves current meter data taken on the so called west Florida "Middle Ground". Two meters were deployed for a summer in the late 70's for several months. The data have not been catalogued at NODC but have recently been located at the University of Alabama. The data are of interest because they are the only in situ current meter data on the shelf taken during the summer. It is uncertain, without further review, whether a hindcast is justified. Several factors argue against a simulation. For instance, one of the meters was positioned at 1 m off the bottom and is probably affected to a significant degree by local topography. In addition there is no concurrent hydrographic data. In essence, the data set consists of a single measurement source, i.e. data from one meter located near the surface.

A FINAL WORD

Present results of the model should be regarded as preliminary and should be upgraded as new data become available. Within the next two years a number of new data sets will exist including:

1. current data from meters deployed at four sites by Florida State University east of Cedar Keys during the winter of 1981-82;
2. hydrographic data taken on the southwest Florida shelf for MMS by Woodward-Clyde; and
3. oceanographic data on the shelf taken as part of MMS's Gulf-wide long-term data collection program.

Guidelines for the latter study have already been offered as part of the Gulf Circulation Workshop (1981) conducted by NECE. Though the modeling effort in this study generally supports that plan, it is strongly recommended that the study include a specific attempt to measure the surface elevations, currents and hydrography of migrating eddies on the shelf. This is probably best accomplished by using Lagrangian drifters or by frequent relocation (i.e. 2-4 weeks) of Eulerian devices to continuously monitor eddy circulation, migration and decay processes.

Chapter 8

Acknowledgements

Professor R. O. Reid of Texas A & M University and Professor Wilton Sturges of Florida State University served as consultants for the study and offered many helpful criticisms and insights. Particular thanks is extended to Professor Reid for his patient guidance and contributions which extended well beyond the normal obligations of a consultant. The occasional comments of Professor P.P. Niiler of Oregon State University are also acknowledged and appreciated. Dr. C. Koblinski of Scripps provided a tape of the SDE data and Dr. G. Marmorino of FSU provided additional tidal data.

Chapter 9

References

Austin, H.M., 1974. The physical characteristics of the west Florida estuarine gyre, with notes on the distribution of selected plankton during May 4-11, 1979. Proceed. Marine Envir. Implications of Offshore Drilling in the Eastern Gulf of Mexico.

Behringer, D.W., R.L. Molinari, and J.F. Festa, 1977. The variability of anticyclonic current patterns in the Gulf of Mexico, J. Geophys. Res., 82, 34, 5469-5476.

Bowden, et al., 1959. The distribution of shearing stresses in a tidal current, J. Geophys. R., 2, 288, pp305.

Chew, F., 1955a. On the offshore circulation and a convergence mechanism in the red tide region off the west cost of Florida, EOS Trans. Am. Geophys. Union, 36, 6, 963-974.

Chew, F., 1955b. The summer circulation of the Florida west coast offshore water as deduced from the pattern of thermocline depths and a non-geostrophic equation of motion, U. of Miami, Mar. Lab TR 55-12, 6 pp.

Chew, F.C., 1974. The Turning Process in Meandering Currents: A Case Study, Journal of Physical Oceanography, 4, 7.

Cochrane, J.D., 1965. The Yucatan Current and equatorial currents of the western Atlantic, unpubl. rept., Dept. of Ocean., Texas A&M, College

Station, TX, Ref 65-17T.

Cochrane, J.D., 1972. Separation of an anticyclone and subsequent developments in the LC, 1969, in Contributions on the Physical Oceanography of the Gulf of Mexico, Vol II, L.R.A. Capurro and J.L. Reid, eds., Gulf Publishing CO, Houston, Texas, 3-51.

Cooper, C.K. and B.R. Pearce, 1977. A three-dimensional numerical model to calculate currents in coastal waters utilizing a depth varying vertical eddy viscosity. R. M. Parsons Lab., MIT, TR 226,

Cooper, C.K. and B.R. Pearce, 1982. Numerical simulation of storm generated currents, J. of Physical Oceanography, accepted for publication, in press.

Cragg, J., and W. Sturges, 1974. Wind-induced currents and sea surface slopes in the eastern Gulf of Mexico, Dept. of Ocean., Florida State U., TR #123.

Cragg, J., G. T. Mitchum, and W. Sturges, 1981. Wind-induced sea-surface slopes on the west Florida shelf, Dept. of Ocean., Florida State U., submitted to J. Phys. Ocean., Sept.

Duncan, D.B, 1975. t-tests and intervals for comparisons suggested by the data. Biometrics, 31, June, pp 339-359.

Forristall, G.Z., 1980. A two layer model for hurricane-driven currents on an irregular grid., J. Phys. Ocean., 10, 9, 1417-1438, Sept.

Gaul, R.D., 1967. Circulation over the continental margin of the northeast Gulf of Mexico, PhD Diss., Dept. of Ocean., Texas A&M, College Station, 156 pp.

Halpern, D., 1976. Influence of surface waves on subsurface current measurements in shallow water, Notes in Limnology & Ocean., 611-616.

Heaps, N.S., 1974. Development of a three-dimensional model of the Irish Sea.

Rapp. P.-V. Reun., Cons. Int. Explor. Mer., Dec. , 147-162.

Heaps, N.S., 1972. On the numerical solution of the three-dimensional hydrodynamic equations for tides and storm surges. Mem. Soc. R. Sci. Liege, 6, 2, 143-180.

Huh, O.K., W.J. Wiseman, Jr., and L.J. Rouse, Jr., 1981. Intrusion of Loop Current waters onto the west Florida continental shelf, J. Geophys. Res., 86, C5, May 20, 4186-4192.

Hurlburt, H.E. and J.D. Thompson, 1980. A numerical study of Loop Current intrusions and eddy shedding. NORDA TR 64, NSTL Station, MS, May, 121 p.

Hsueh, Y. and C.Y. Peng, 1973. A numerical study of the steady circulation in an open bay, J. of Phys. Ocean., 3, April, 220-225

Ichiye, T., H. Kuo, and M.R. Carnes, 1973. Assessment of currents and hydrography of the eastern Gulf of Mexico, Dept. of Ocean., Texas A&M, College Station, Contribution. 601.

Koblinsky, C.J. and P.P. Niiler, 1980. Direct measurement of circulation on west Florida continental shelf, School Ocean., Oregon State U., TR 79-13, March, 102 pp.

Kroll, J. and P.P. Niiler, 1976. The transmission and decay of barotropic topographic Rossby waves incident on a continental shelf. J. of Phys. Ocean., 6, 432-450.

Leipper, D.F., 1970. A sequence of current patterns in the Gulf of Mexico. J. of Geophys. Res., 75, 3, 637-657.

Marmorino, G. O., 1981. Wind-forced sea level variability along the west Florida shelf, submitted to Journal of Physical Ocean., Dept. of Ocean., Florida State U., Tallahassee, Dec.

Maul, G.A., 1977. The annual cycle of the Gulf Loop Current. Part I. Observations during a one-year time series, J. Mar. Res., 35, 29-47.

Molinari, R.,L., 1978. An overview of the circulation in the Gulf of Mexico, Summary Report: Working conference on the Circulation in the Gulf of Mexico, Florida State U., Tallahasse, W. Sturges and S. L. Shang, eds, 29-30.

Molinari, R.L., J.B. Hazelworth, and D.A. Ortman, 1979. Data from OTEC site characterization studies in the Gulf of Mexico and tropical South Atlantic. NOAA TM ERL AOML-39, Sept.,

Mitchum, G.T and W. Sturges, 1981. Wind-driven currents on the west Florida shelf, Dept. of Ocean., Florida State U., submitted to J. of Phys. Ocean., Sept.

Munk, W.H., 1950. On the wind-driven ocean circulation. J. Meteorol., 7, 79-83.

Munk, W.H., and E.R. Anderson, 1948. Notes on a theory of the thermocline. J. Mar. Res., 7, 276-295.

Niiler, P.P.,1976. Observations of low-frequency currents on the West Florida continental shelf. Mem. Soc. R. Sci. Liege, X, 6, 331-358.

Nowlin, W.D.,Jr., J.M. Hubertz, and R.O. Reid, 1968. A detached eddy in the Gulf of Mexico, J. of Mar. Res., 26, 2, 185-186.

Okubo, A., 1971. Deep Sea Res., 18, 789

Partagas, J.J.F., 1973a. A note on special meteorological studies for the eastern Gulf of Mexico (February-March, 1973), unpublished manuscript, U. of Miami, RSMAS.

Partagas, J.J.F., 1973b. A meteorological study for the eastern Gulf of Mexico (January 16 - March 15, 1973), unpublished manuscript, U. of Miami,

RSMAS.

Pearce, B.R. and C.K. Cooper, 1981. Numerical circulation model for wind induced flow. ASCE, March, 107, HY3, 285-302.

Pedlosky, J., 1979. Geophysical Fluid Dynamics, Springer-Verlag, NY.

Plaisted, R.O., K.M. Waters and P.P. Niiler, 1975. Current meter data report, Shelf Dynamics Program, 1973-1974. Nova U., Phys. Ocean. Lab., Jan.

Price, J.F. and C.N.K. Mooers, 1974a. Shelf dynamics fall experiment, October-December 1973, Current Meter Data Report, RSMAS, U. of Miami.

Price, J.F. and C.N.K. Mooers, 1974b. Shelf dynamics fall experiment, October-December 1973, Hydrographic Data Report, RSMAS, U. of Miami.

Price, J.F. and C.N.K. Mooers, 1974c. Shelf Dynamics Winter Experiment, February-March 1973, Current Meter Data Report, RSMAS, U. of Miami.

Price, J.F. and C.N.K. Mooers, 1974d. Shelf Dynamics Winter Experiment, February-March 1973, Hydrographic Data Report, RSMAS, U. of Miami.

Okubo, A., 1971. Deep-Sea Research, 18, 789

Rinkel, M.O., 1971. Results of cooperative investigations -pilot study of the eastern Gulf of Mexico, Gulf Caribb. Fish. Inst. Proc., 23, 91-108.

Rinkel, M.O., and J.I. Jones, 1973. An oceanographic survey of the Florida territorial sea of Escambia and Santa Rosa Counties, St. Univ. Syst. Inst. of Oceanogr, 1-366.

Rossby, C.G., and R.B. Montgomery, 1935. the layer of frictional influence in wind and ocean currents. Pap. Phys. Oceanog. Meteor., 3, 1-101.

Stommel, H., 1948. The westward intensification of wind-driven ocean currents. Trans. Am. Geophys. U., 29, 2, 202-206.

Sturges, W. and S.L. Shang,, 1978. Appendix B: Mean circulation. Summary Report: Working conference on the Circulation in the Gulf of Mexico, Dept. of Ocean., Florida State U., Tallahasse, W. Sturges and S. L. Shang, eds.

SUSIO, 1975. Compilation and summation of historical and existing physical oceanographic data from the eastern Gulf of Mexico in support of the creation of a MAFLA sampling program, Appendix IV, BLM Contract No. 08550-CT4-16.

Tolbert, W.H. and G.G. Salsman, 1964. Surface circulation of the eastern Gulf of Mexico as determined by drift-bottle studies. J. of Geophys. Res., 69, Jan., 223-230.

Townsend, A.A., 1976.The Structure of Turbulent Flow. Cambridge U. Press, 429 p.

Van Leer, J.C., W.R. Johnson, and E. Mehr, 1974. Shelf Dynamics winter experiment February-March 1973 - cyclesonde data report, U. of Miami, RSMAS 74033, Miami, 27 pp.

Vukovich, F.M., B.W. Crissman and D. Erlich, 1980. Sea surface temperature variability analysis of potential OTEC sites in the eastern Gulf of Mexico utilizing satellite data. Interim Report, NOAA contract No. 3-78-B01-72, Research Triangle Inst., Res. Triangle. Park, NC, 36pp.

Vukovich, F.M., B.W. Crissman, M. Bushnell, and W.J. King, 1979. Some aspects of the oceanography of the Gulf of Mexico using satellite and in situ data. J. Geophys. Res., 84, C12, 7749-7768.

Vukovich, F.M., B.W. Crissman, M. Bushnell, and W.J. King, 1978. Sea-surface temperature variability analysis of potential OTEC sites utilizing satellite data. final report, DOE contract EG 77-C-05-5444, Research Triangle Inst., Res. Triangle. Park, NC, 154 pp.

Whitaker, R.E., 1971. Seasonal variations of steric and recorded sea level of

the Gulf of Mexico, Dept. of Ocean. TR 71-14T, Texas A&M U., College Station, 110p.

Williams, J., W.F. Grey, E. B. Murphy, and J.J. Crane, 1977. Memoirs of the Hourglass cruises, report by the Marine Research Lab, Florida Dept. of Nat. Res., St Petersburg, **IV**, Part III, Aug., 134 pp.

Wu, J., 1980. Wind-stress coefficients over sea surface near neutral conditions - a revisit. J. Phys. Ocean., **10**, May, pp 727-740.

APPENDIX A

Data Availability

DATA SUMMARY - SOUTHWEST FLORIDA SHELF

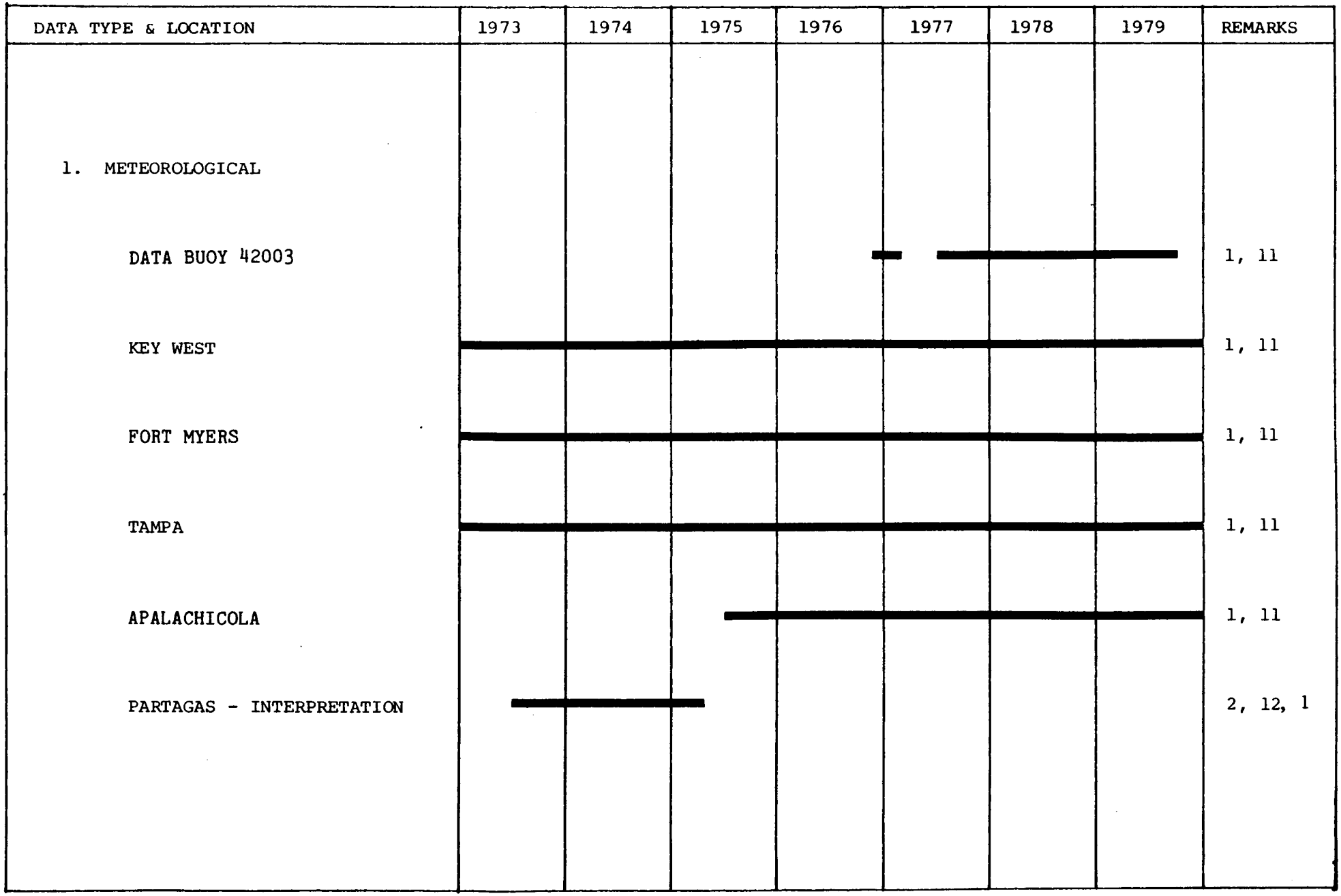

DATA SUMMARY - SOUTHWEST FLORIDA SHELF

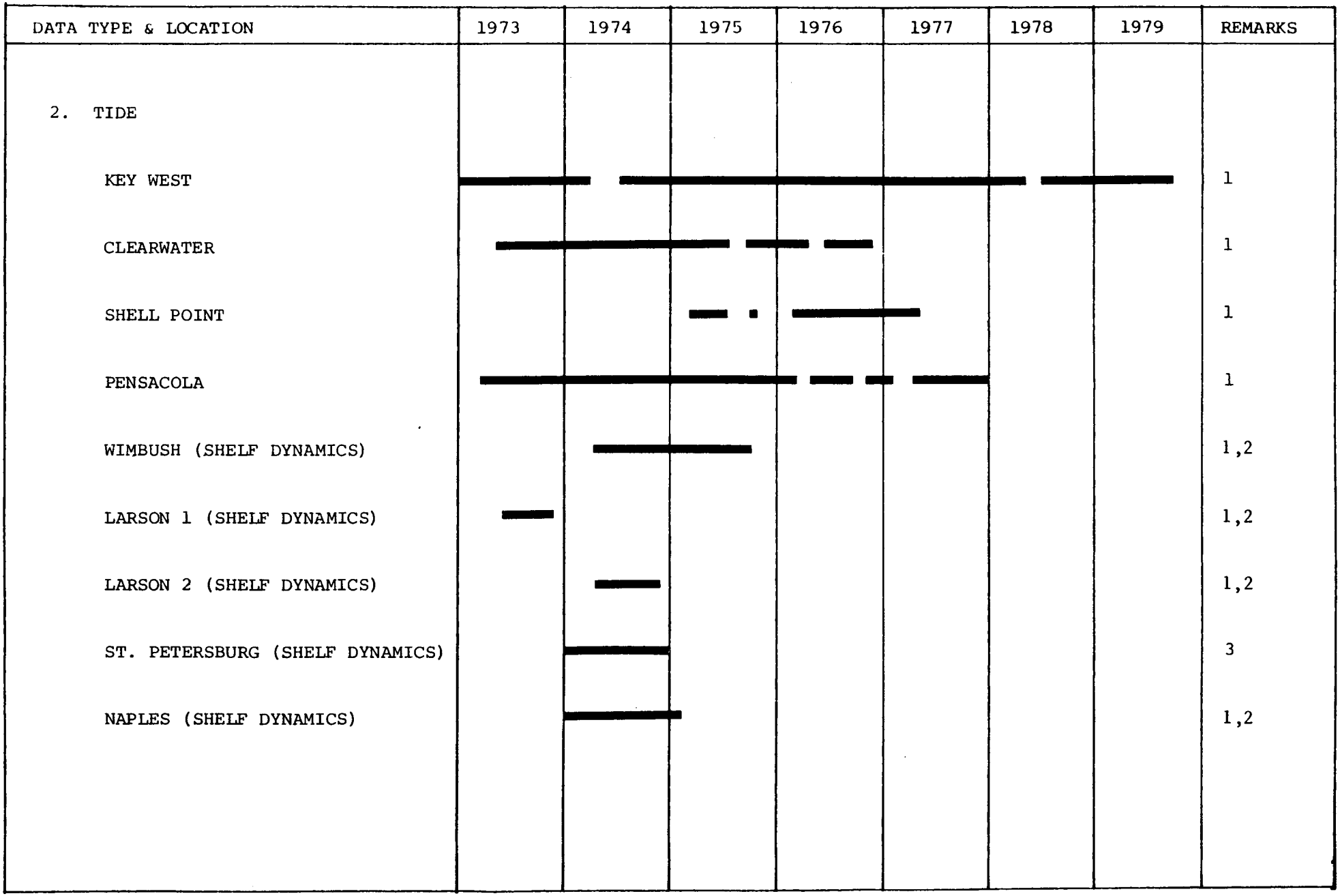

DATA SUMMARY - SOUTHWEST FLORIDA SHELF

DATA TYPE & LOCATION	1973	1974	1975	1976	1977	1978	1979	REMARKS
3. CURRENT								
NIILER, MOOERS, PRICE								
ARRAY 1	▬							1, 31
ARRAY 2	▬							2, 32
ARRAY 3	▬							33
ARRAY 4	▬	▬						2, 34
ARRAY 5		▬	▬					2, 35
ARRAY 6			▬					2, 36
STURGES (29°N, 84°W)						▬		1
MOLINARI (27.5°N, 85.5°W)						▬	▬	1

DATA SUMMARY - SOUTHWEST FLORIDA SHELF

DATA TYPE & LOCATION	1973	1974	1975	1976	1977	1978	1979	REMARKS
4. SALINITY/TEMP								
NODC	━	━	━	━				1
STURGES (29°N, 84°W)						▬		1, 41
NIILER, MOOERS, PRICE	━	━	━					1, 2, 42
MOLINARI (27.5°N, 85.5°W)							▬	1

DATA SUMMARY - SOUTHWEST FLORIDA SHELF

REMARKS

1. Data tape held at NECE

2. Tape sent by Koblinski 2/20/81

3. Information not contained on Koblinski tape.

11. Record assumed to be continuous for indicated periods

12. 700 day record - Interpreted from synoptic charts for shelf dynamics program.

31. 2/73 - 3/73	Analysis by		Price & Mooers
32. 8/73 - 10/73,11/73	"	"	Plaisted, Waters & Niiler
33. 10/16/73 - 11/30/73	"	"	Price & Mooers
34. 11/30/73 - 4/2/74	"	"	Plaisted, Waters & Niiler
35. 4/6/74 - 11/16/74	"	"	Koblinsky & Niiler
36. 11/22/74 - 2/75	"	"	Koblinsky & Niiler

41. Temperature only

42. Temperature only. Record 3 months longer than velocity data.

NOTE: Charts indicate data available on magnetic tape. National Ocean Survey and National Climatic Center have paper records of tide and wind data for many more stations and much longer time periods than indicated here. Contact them directly to determine availability of specific information.

APPENDIX B

Verification Details

Appendix B

Verification Details

B.1 Winter 1978

WIND DATA ANALYSIS

Wind data during the FSU current meter deployment were available at five sites: NDBO weather buoy 42003 at 86° W and 26° N and land stations at Key West, Apalachicola, Tampa, and Fort Myers. Figure B.1.1 shows the temporal variation of the cross-shelf and alongshore components of the buoy wind. The components are aligned with the x and y axis of the grid (Figure 3.6.1).

Stick plots showing the temporal variation of winds relative to true north for all five stations are given in Figures B.1.2-6. The raw wind data were originally collected at three-hour intervals. For this report, the data were expanded (see Appendix G) to generate a one-hour interval time series. In most cases, the data were then filtered using a Doodson filter which removes processes with diurnal and semidiurnal frequencies such as land-sea breezes. Unless otherwise stated, the data shown in the figures in this report have been Doodson filtered.

As noted in Section 2.3, the winter winds on the West Florida Shelf (WFS) are

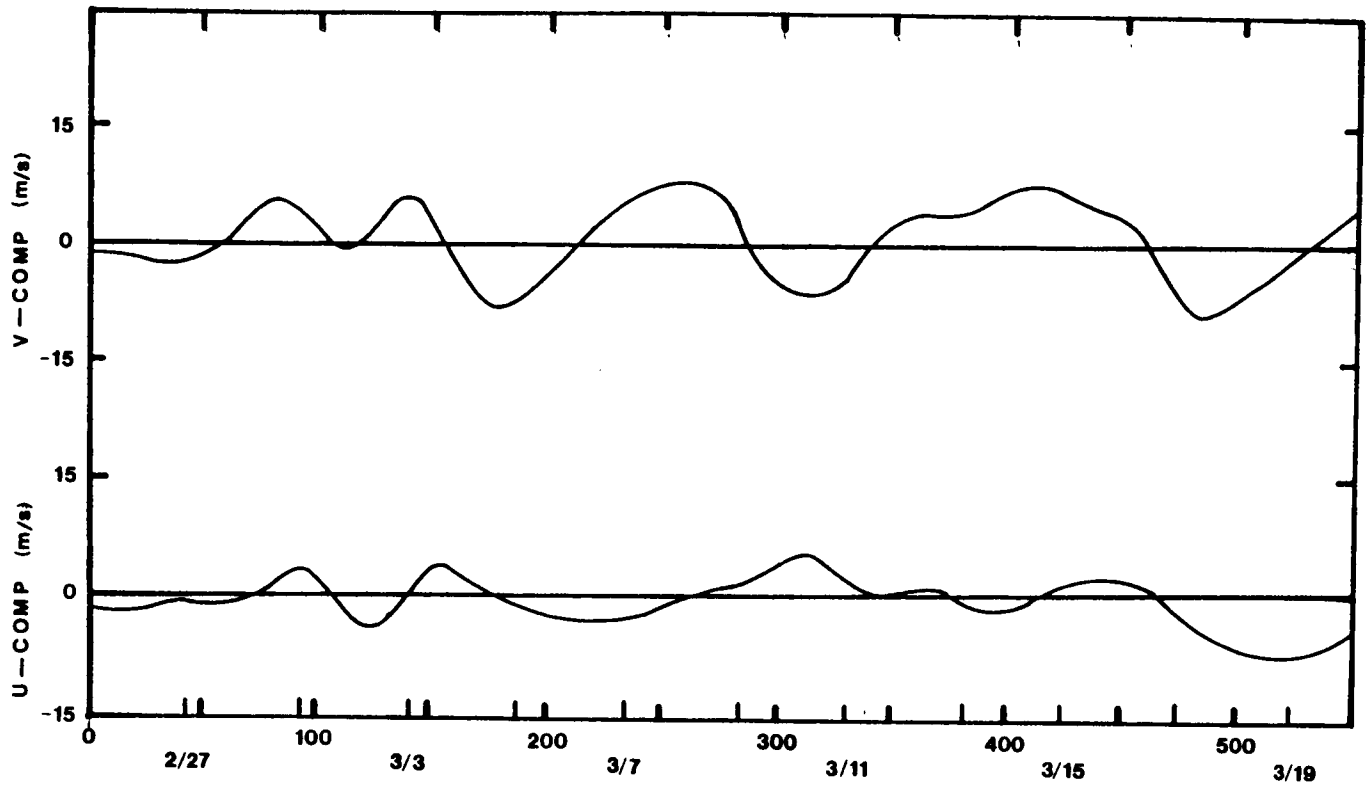

Figure B.1.1: Wind components at NDBO weather buoy 42003 during winter 1978 hindcast.

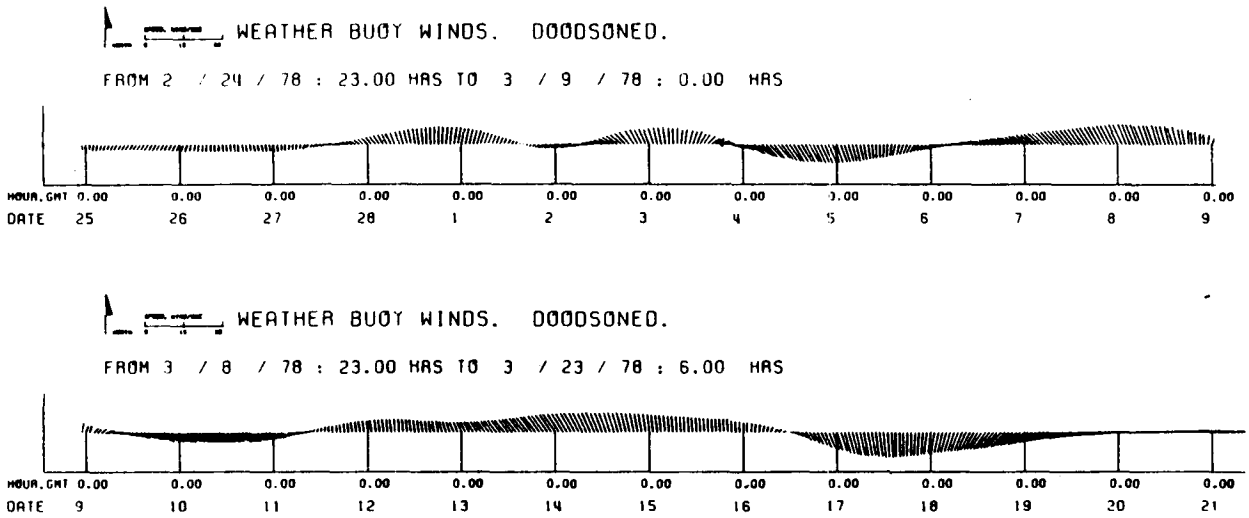

Figure B.1.2: Vector plots of winds at NDBO weather buoy during 1978 hindcast.

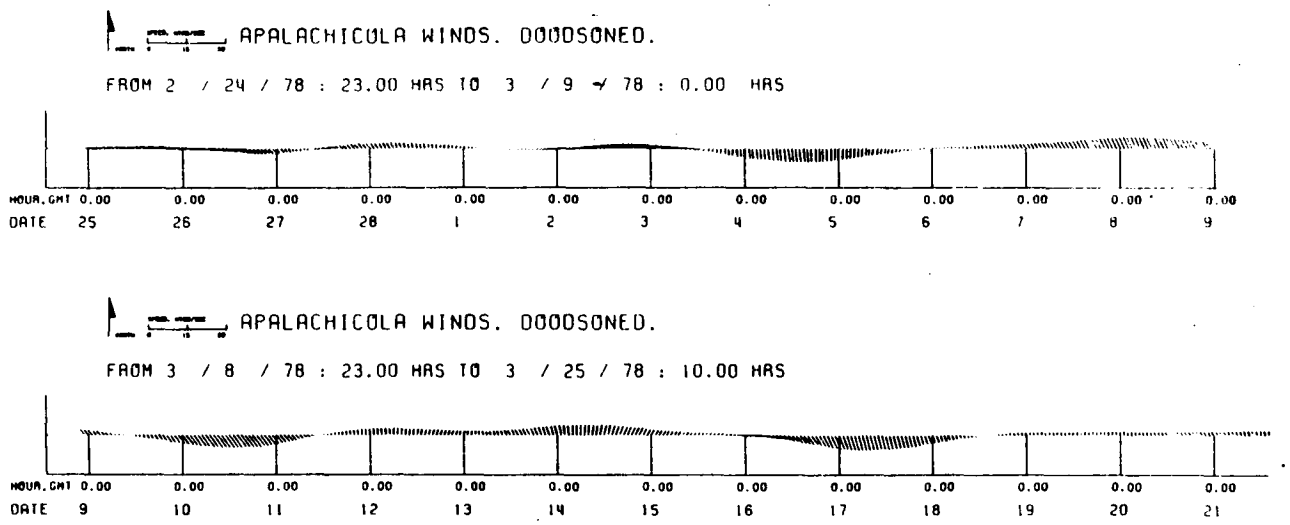

Figure B.1.3: Vector plots of winds at Apalachicola during 1978 hindcast.

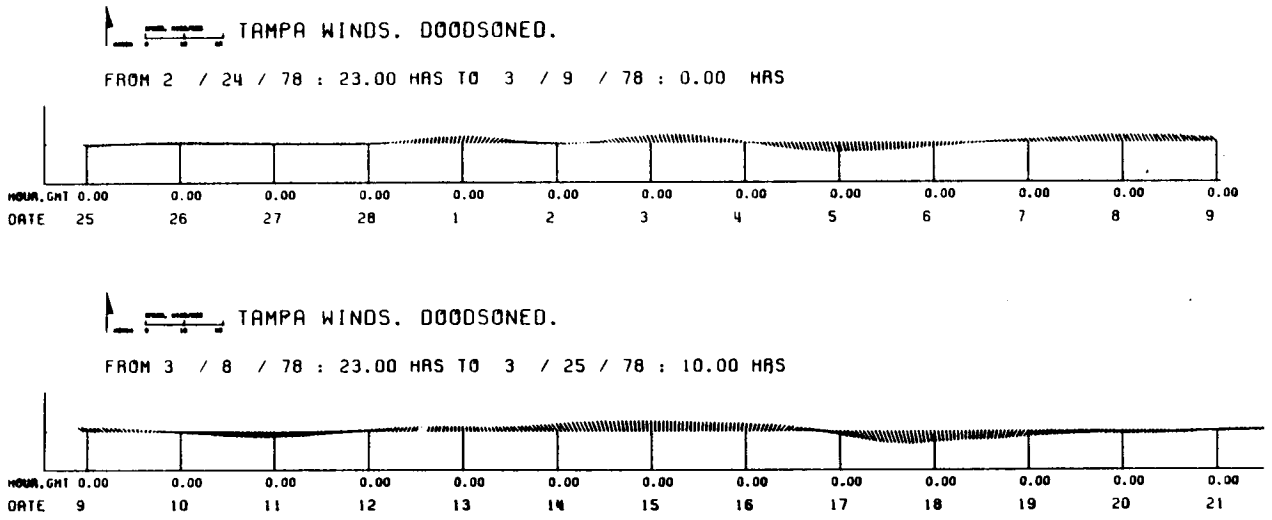

Figure B.1.4: Vector plots of winds at Tampa during 1978 hindcast.

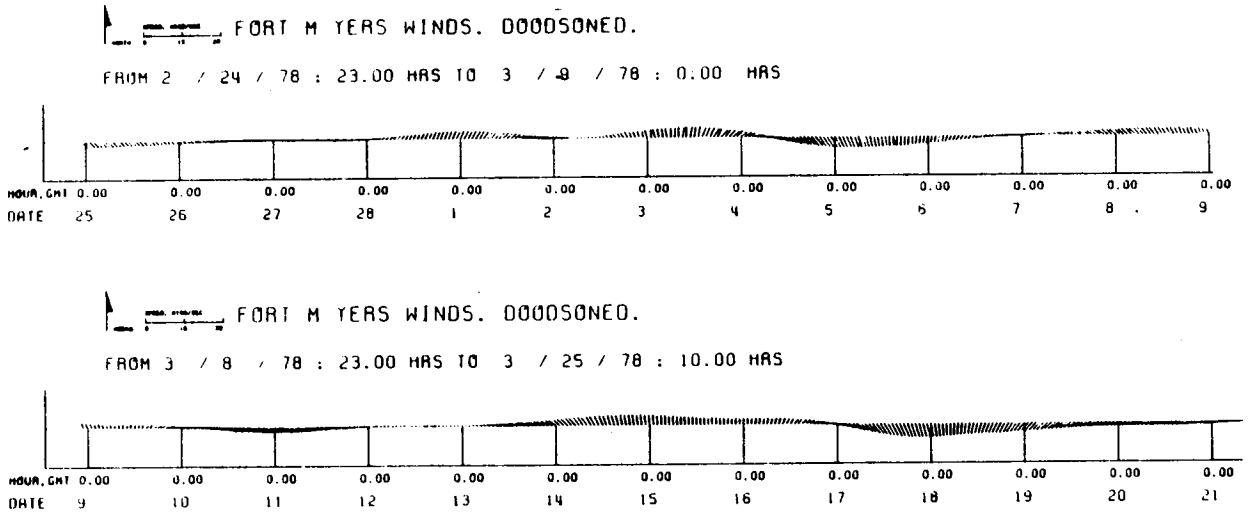

Figure B.1.5: Vector plots of winds at Fort Myers during 1978 hindcast.

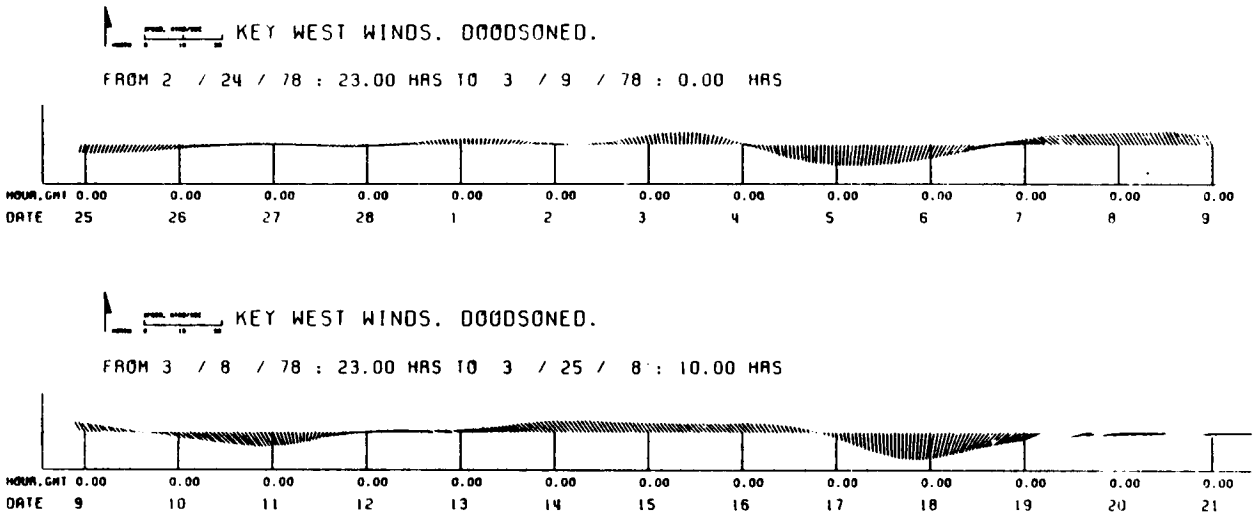

Figure B.1.6: Vector plots of winds at Key West during 1978 hindcast.

dominated by the passage of cold fronts. These are plainly evident in Figures B.1.2-6 in the form of strong northerly to southerly shifts in the wind data about every seven days. A seven day (as well as a less energetic three day) period is evident in the alongshore component of the unfiltered wind spectra at the buoy (Figure B.1.7). Note that the alongshore component contains more energy than the cross-shelf component. Also, the low frequency energy dominates all high frequency energy sources.

A spectral plot of the unfiltered Key West winds (Figure B.1.8) is similar to the buoy in the low frequency range, but there is generally much more energy in the higher frequency range at Key West than at the buoy. There is no land-sea breeze evident at Key West.

Spectra of the unfiltered winds at the other land stations show a further reduction in low frequency energy from the level observed at the buoy or Key West, see for example, Tampa (Figure B.1.9). A land-sea breeze at the diurnal frequency is evident in the Tampa spectrum as well as a relative increase in the high frequency energy.

Table B.1.1 shows the optimal correlations between various wind stations which were obtained by iteratively varying the time lag of the wind records. The decimal numbers shown are the correlation coefficient squared and are based on Doodson filtered wind magnitudes. The phase lags demonstrate that the more southerly stations follow the more northerly, indicating that the weather fronts move into the area from the north - an observation consistent with the pattern described in Chapter 2. These observations are confirmed in frequency coherence plot between Tampa and Key West unfiltered winds shown in Figure B.1.10.

To incorporate the spatial variability of the wind field into the model, a simple interpolation program was written and is described in Appendix H.7. The program calculates the wind at a model grid element by multiplying the wind from each meteorological station by a weighting factor which is

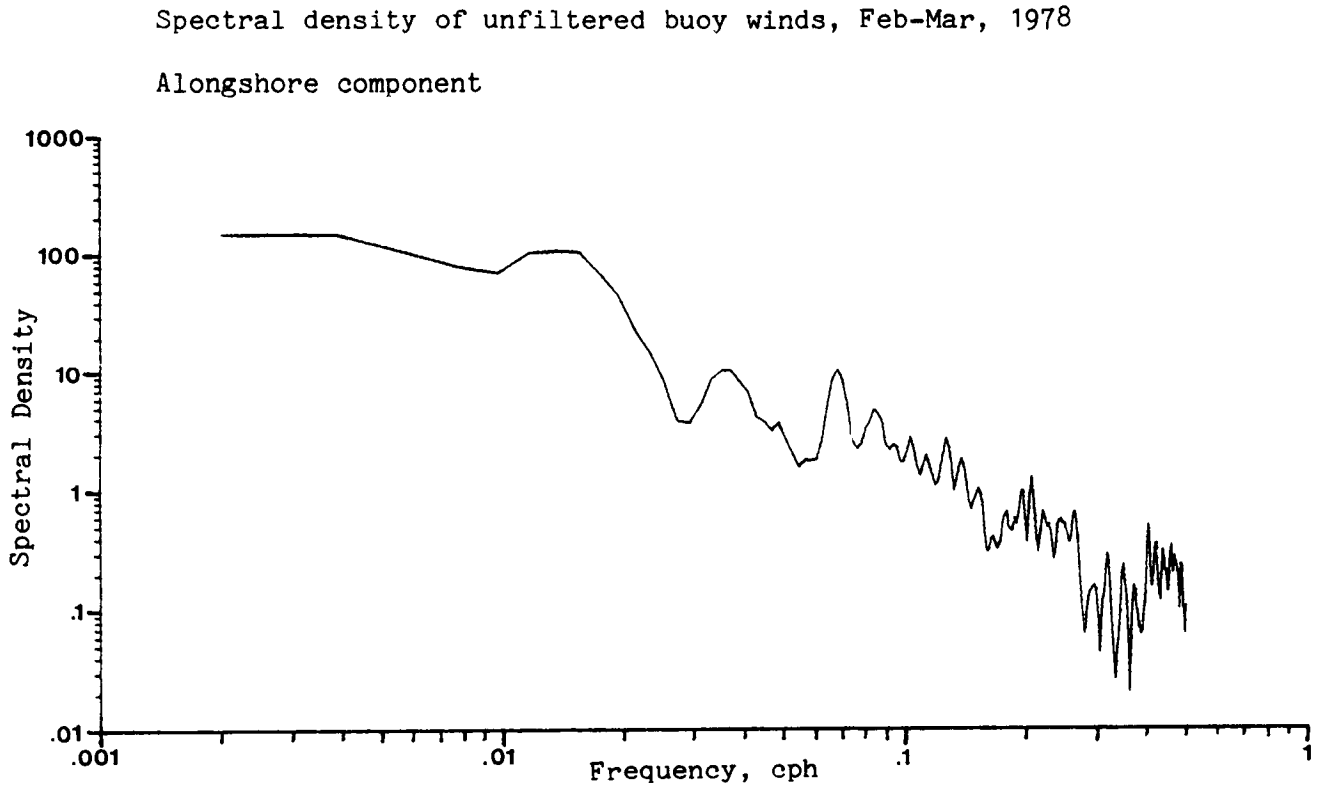

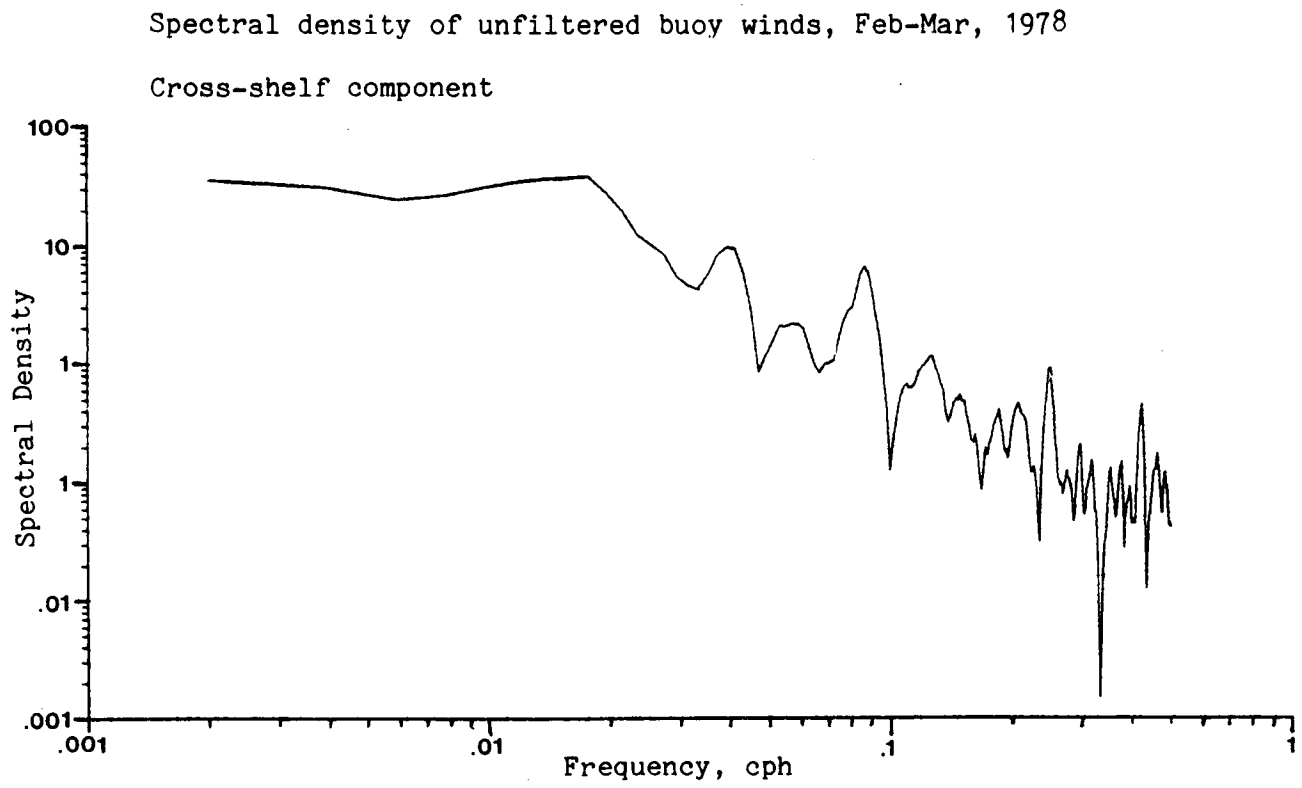

Figure B.1.7: Spectra of unfiltered NDBO buoy winds during 1978 hindcast.

Spectral density of unfiltered Key West winds, Feb-Mar, 1978

Alongshore component

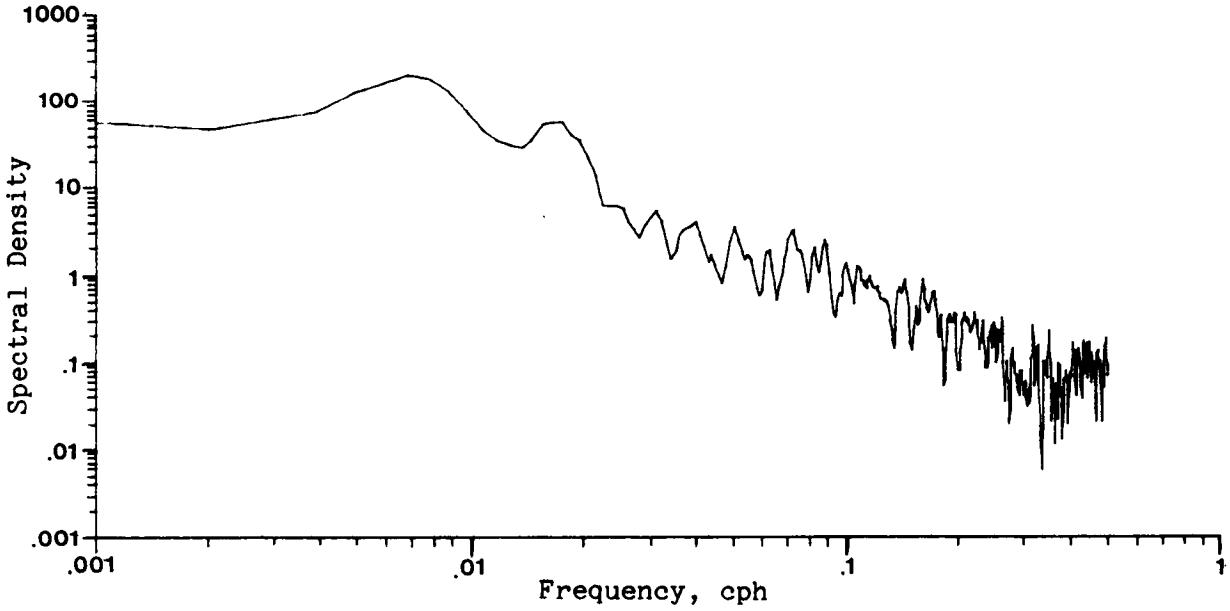

Spectral density of unfiltered Key West winds, Feb-Mar, 1978

Cross-shelf component

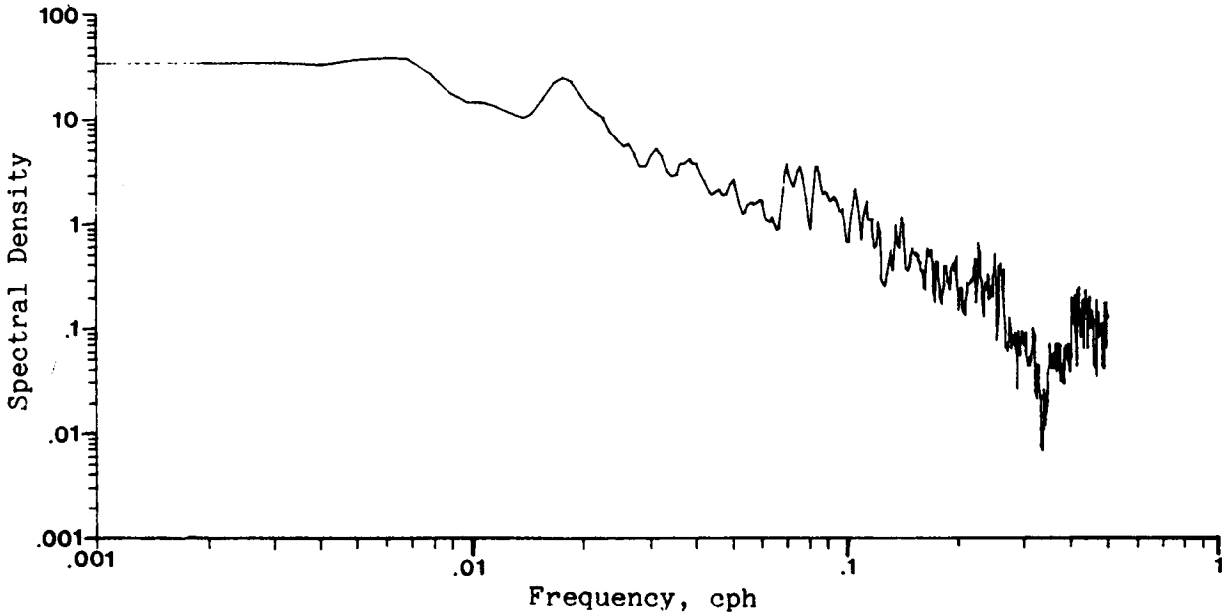

Figure B.1.8: Spectra of unfiltered Key West winds during 1978 hindcast.

Spectral density of unfiltered Tampa winds, Feb-Mar, 1978

Alongshore component

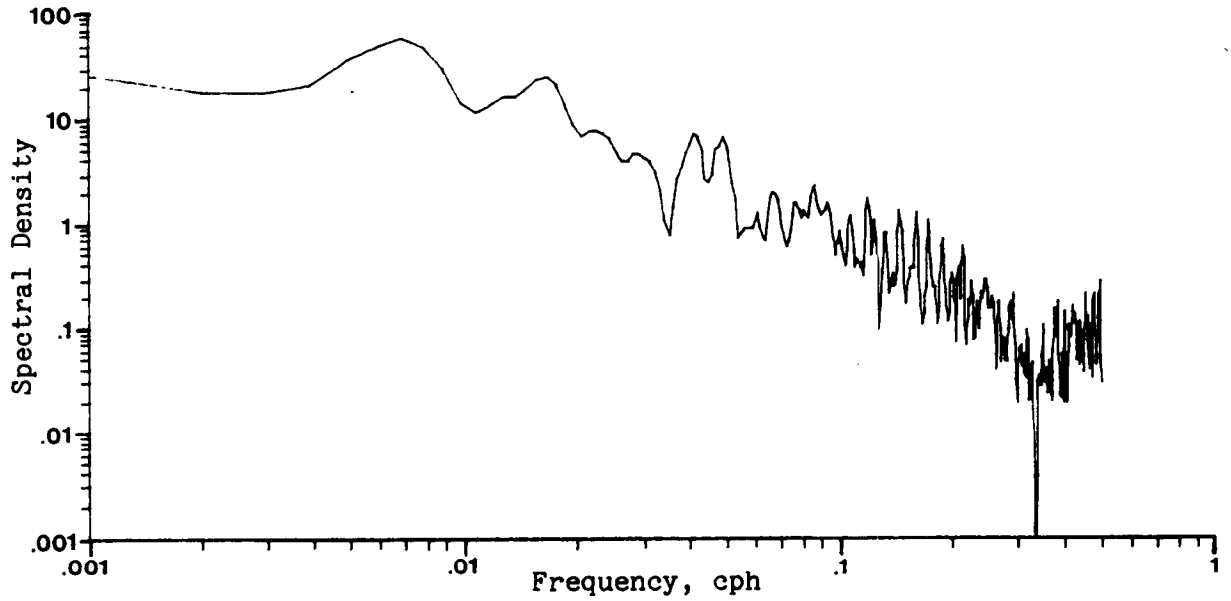

Spectral density of unfiltered Tampa winds, Feb-Mar, 1978

Cross-shelf component

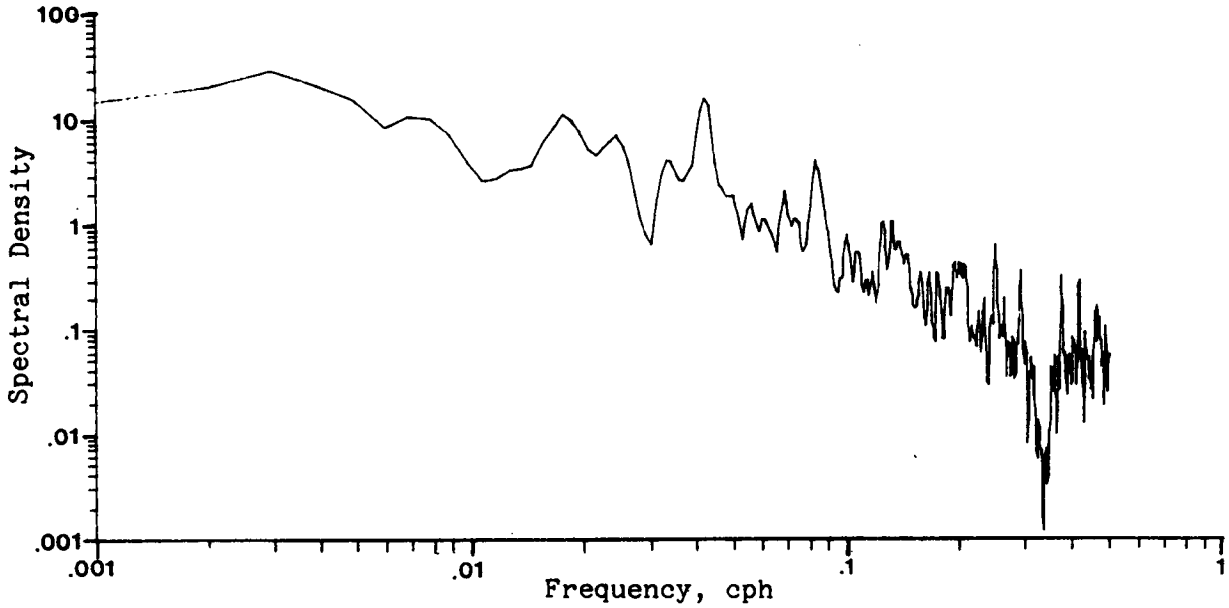

Figure B.1.9: Spectra of unfiltered Tampa winds during 1978 hindcast.

BEST APPALACHICOLA WIND MAGNITUDE CORRELATIONS

	A palachicola	Lag
Buoy	0.59	+ 1 hour
Tampa	0.76	+ 9 hours
Fort M yers	0.62	+ 11 hours
Key West	0.57	+ 12 hours

Table B.1.1: Summary of cross correlations for wind stations.

Coherence of unfiltered Key West and Tampa winds, Feb-Mar, 1978

Alongshore component

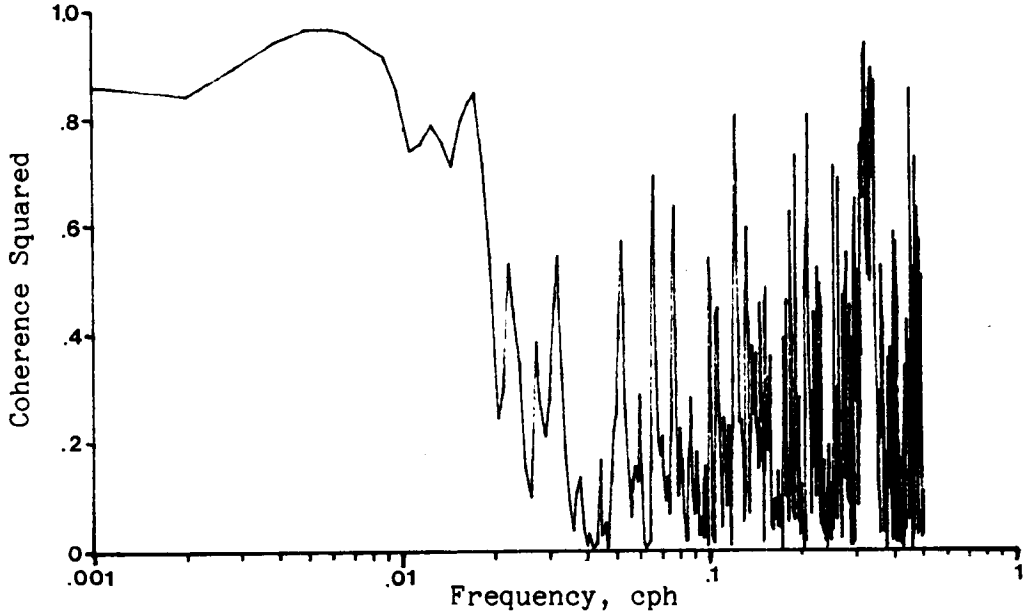

Coherence of unfiltered Key West and Tampa winds, Feb-Mar, 1978

Cross-shelf component

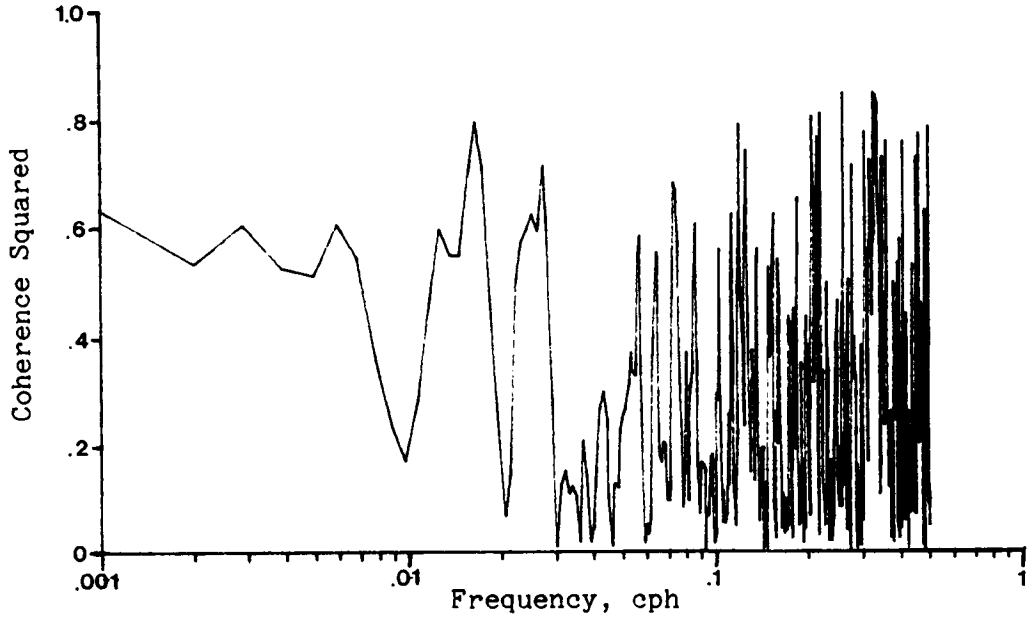

Figure B.1.10: Coherence of unfiltered Tampa and Key West winds during 1978 hindcast.

dependent on the distance from the element to the meteorological station. Data from the meteorological stations can also be multiplied by an amplification factor to account for the tendency of land stations to underestimate the open water wind velocity. In general, the amplification factor is a complex function of wind speed, direction, and the frequency of meteorological phenomena generating the wind. The factor was initially determined by simply dividing the average wind at the land station by the buoy wind. This gave amplification factors of 1.2, 1.94, 2.11 and 2.04 for Key West, Ft Myers, Tampa, and Apalachicola, respectively. The averaging period was the 22 days in February-March during which the FSU current data were collected. In its present form, the program does not account for any distortion of wind directions or magnitudes caused by topography adjacent to the land stations.

The speed dependency of the amplification factor was investigated by plotting the speed at the buoy vs the lagged speed at each land station. The lagging factor varied for each station according to Table B.1.1. Figures B.1.11-14 show the scatter plots for each station as well as the line from a linear least-squares regression. Though there is some scatter, the linear relationship appears to fit the data satisfactorily, at least to the extent that there is no other obvious nonlinear relationship which would substantially improve the fit.

A linear correlation implies that the amplification factor is independent of wind speed and the factor can be found by taking the reciprocal of the slope of the line. Calculating the amplification factors in this ways gives: 1.37, 2.09, 2.53, and 2.54 for Key West, Fort Myers, Tampa, and Apalachicola. These factors are consistently higher by about 20% than those calculated with the averaging technique. Sensitivity studies with the circulation model indicate that errors of this magnitude do not substantially improve model comparisons with the measured current data. This is no doubt due to the strong influence the buoy data play in the interpolation scheme by virtue of its central

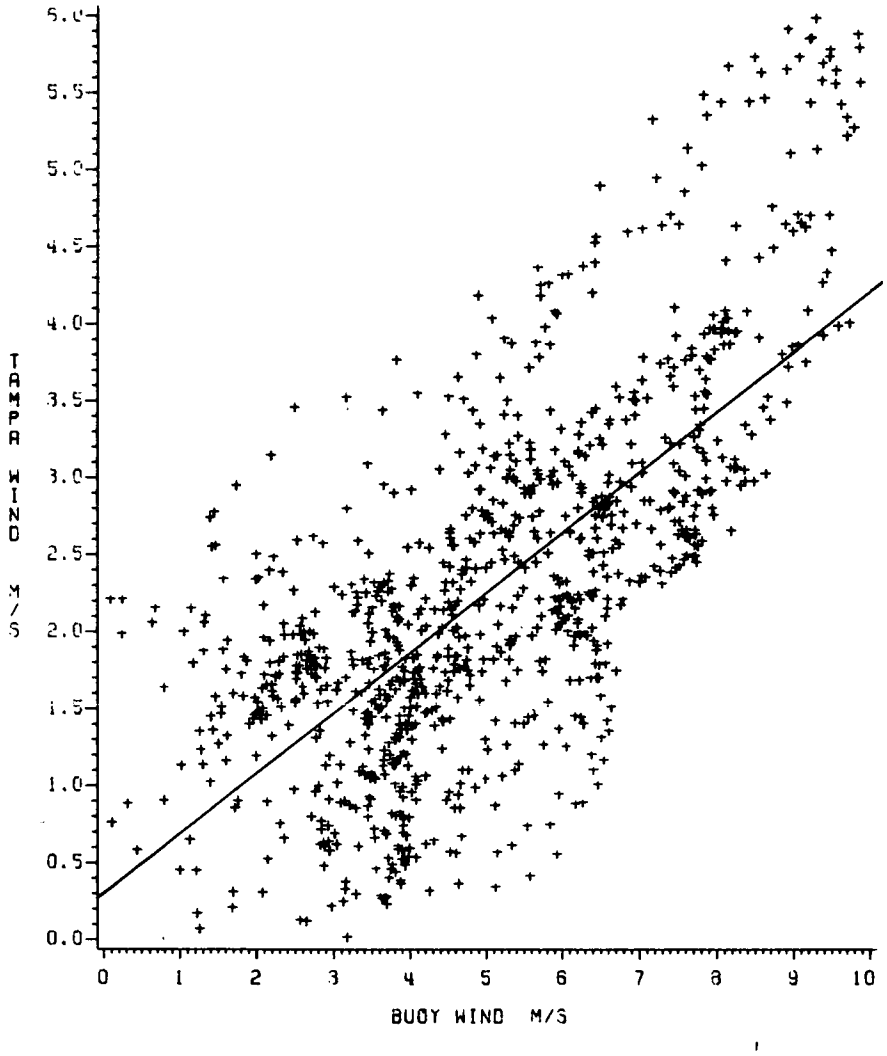

Figure B.1.11: Scatter plot of buoy wind vs lagged Tampa wind.

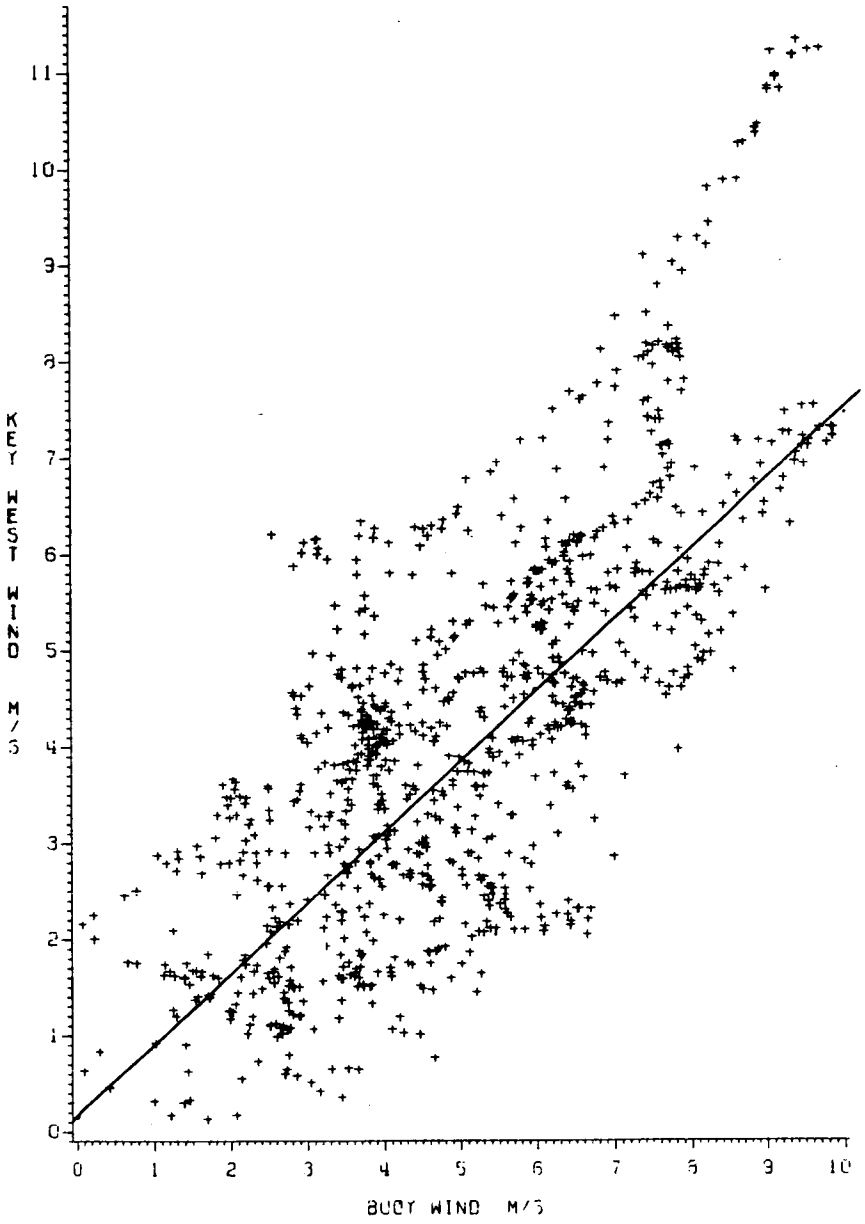

Figure B.1.12: Scatter plot of buoy wind vs lagged Key West wind.

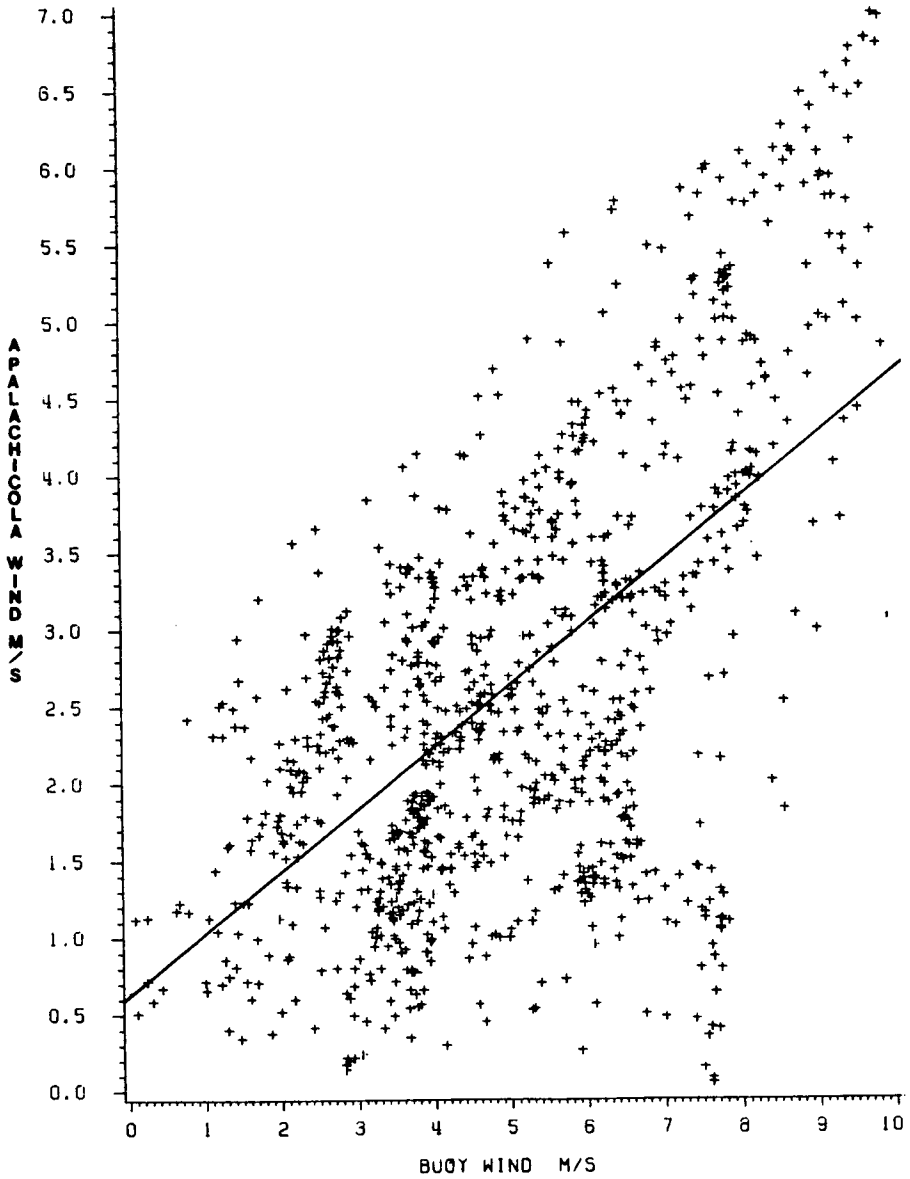

Figure B.1.13: Scatter plot of buoy wind vs lagged Apalachicola wind.

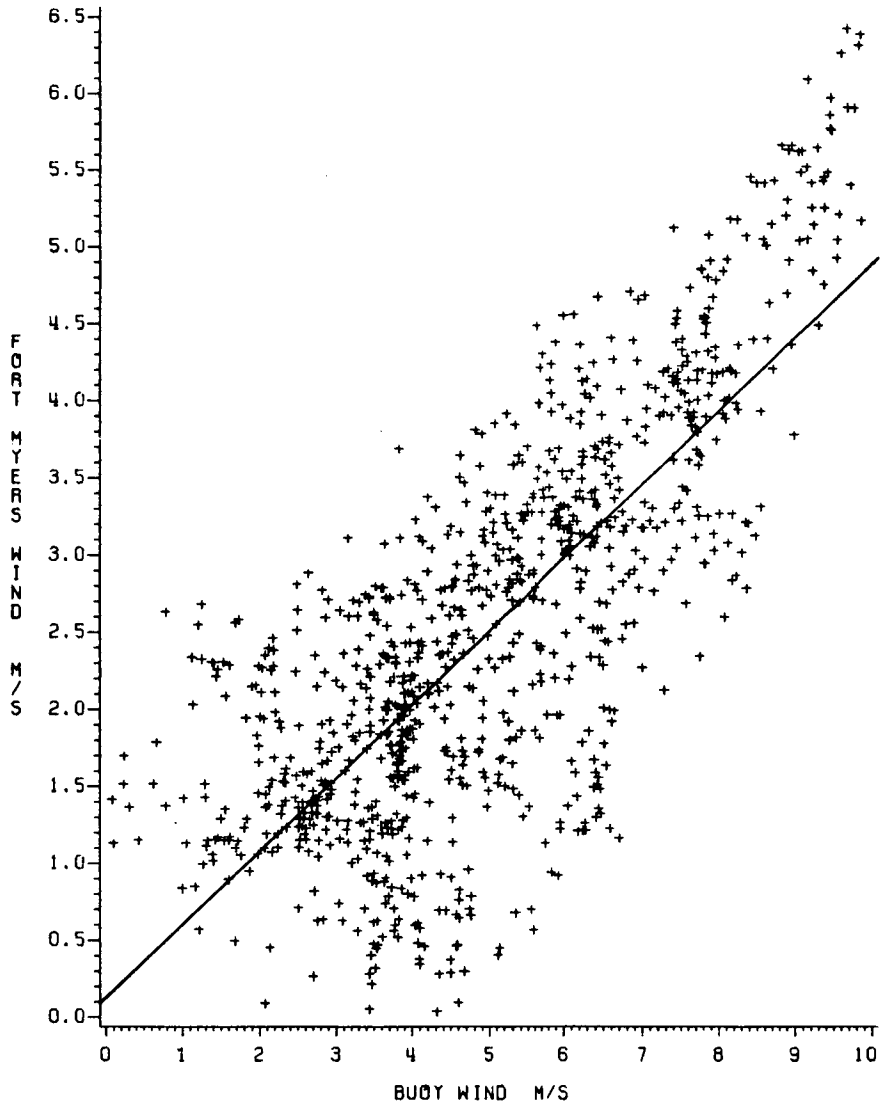

Figure B.1.14: Scatter plot of buoy wind vs lagged Fort Myers wind.

location.

WINTER 1978 CURRENT DATA ANALYSIS

Table B.1.2 shows the first order statistics for the data as calculated by Mitchum and Sturges (1981). The notation in the left-most column is defined as follows: U, V, O, I, 1, 2, τ_x and τ_y denote the cross-shelf component, alongshore component, offshore site, inshore site, upper meter, lower meter, cross-shelf wind shear stress and alongshore wind shear stress, respectively. Positive cross-shelf and alongshore directions are aligned roughly with the model x and y-direction, respectively. The mean wind stress is seen to be predominately alongshore blowing in a southerly direction at about 5 m s^{-1} (the relationship by Wu, 1980 has been used to calculate wind shear stress). The upper offshore and inshore meters show similar mean currents of about 1.5 cm s^{-1} moving in a west-southwest direction. Mean currents at the lower offshore meter are about 3 cm s^{-1} in a northerly direction.

Figures B.1.15-18 show the spectra of the current components for each of the four current meters. The diurnal and semidiurnal tidal components are plainly evident and dominate the cross-shelf components. The alongshore component is an order of magnitude more energetic than the cross-shelf, and is dominated by low frequency energy. Only a small peak in the current spectra can be seen at some of the meters at the seven day period despite the much more obvious peak in the winds at that period.

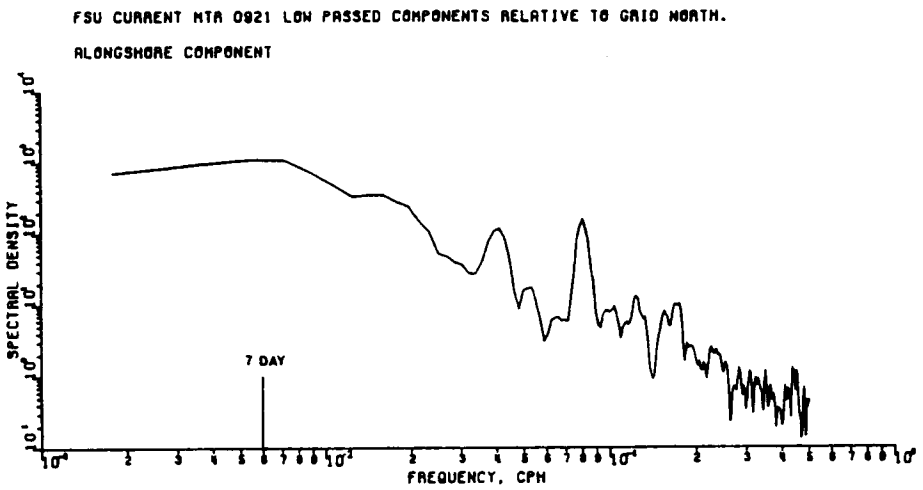

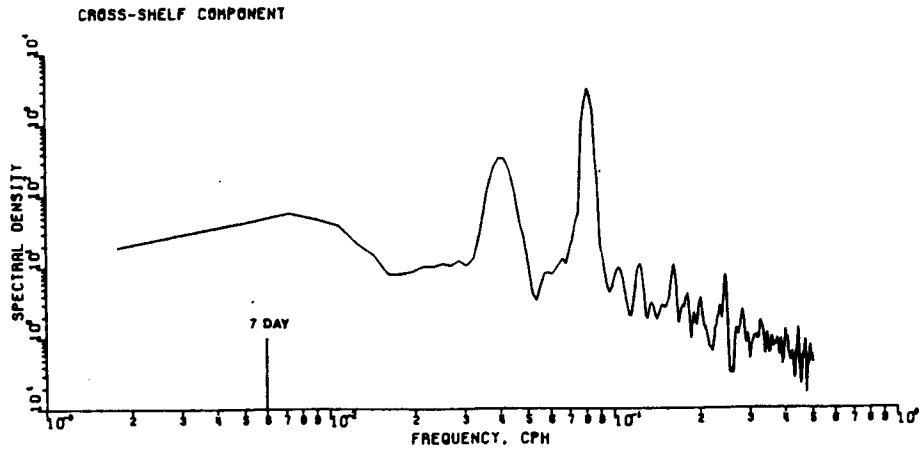

Figure B.1.15: Spectra of inshore upper current meter.

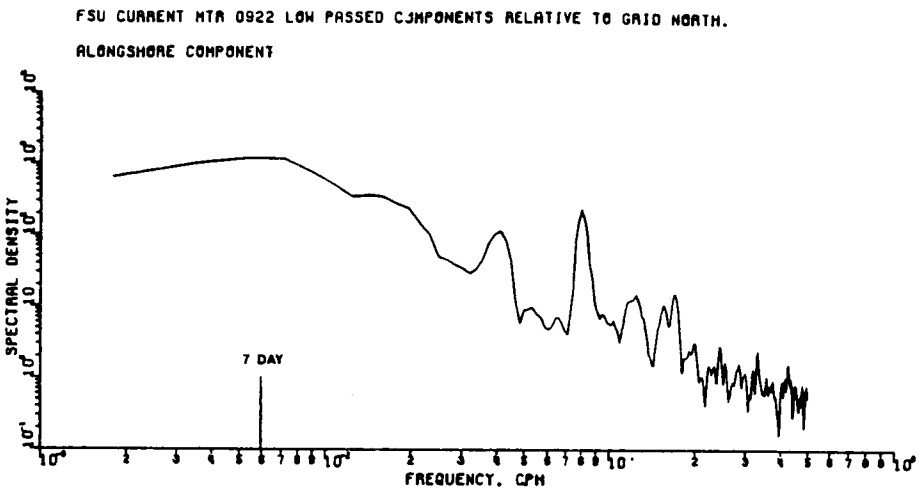

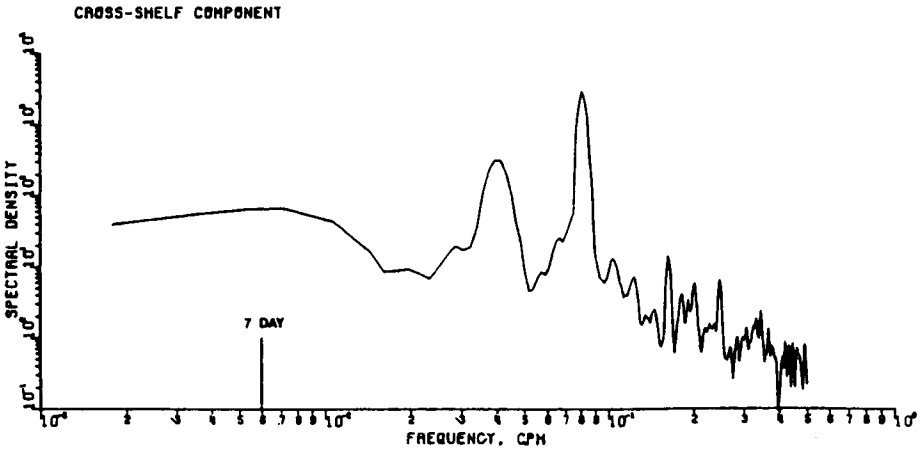

Figure B.1.16: Spectra of inshore lower current meter.

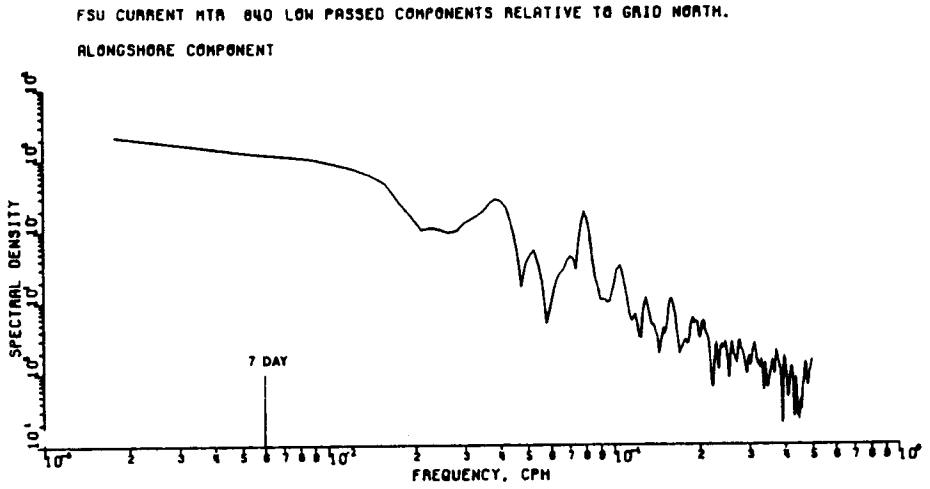

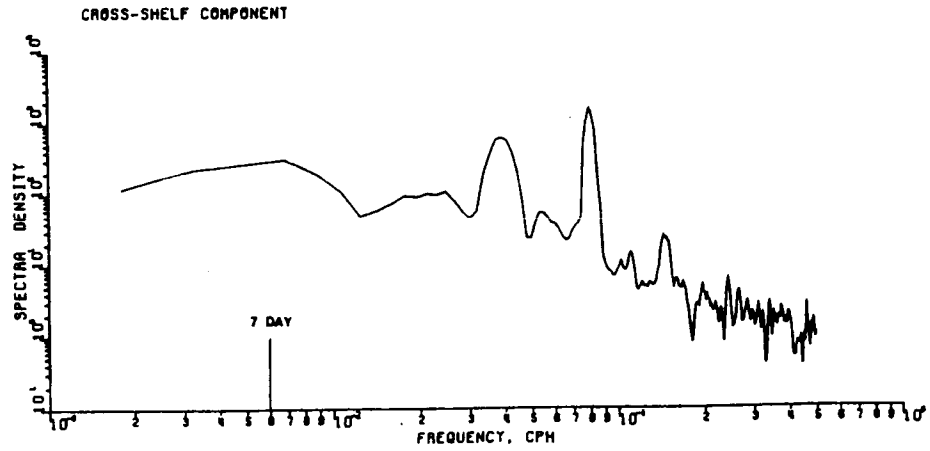

Figure B.1.17: Spectra of offshore upper current meter.

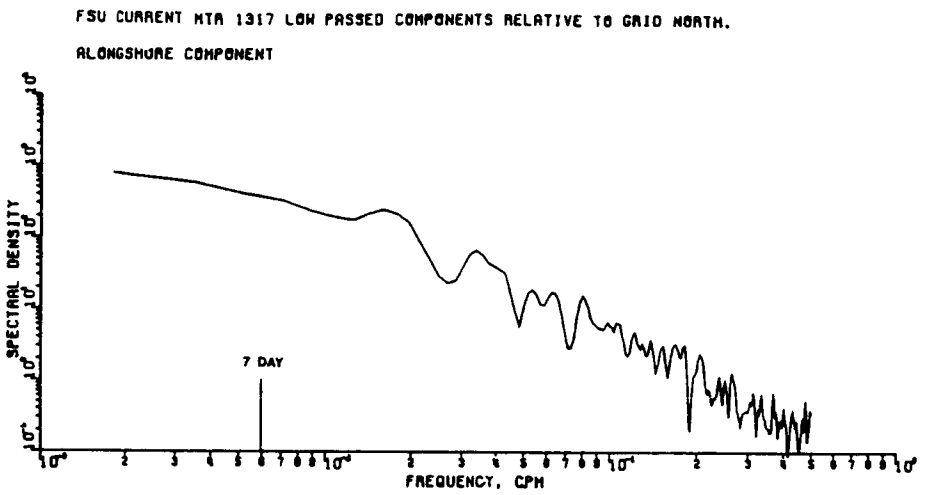

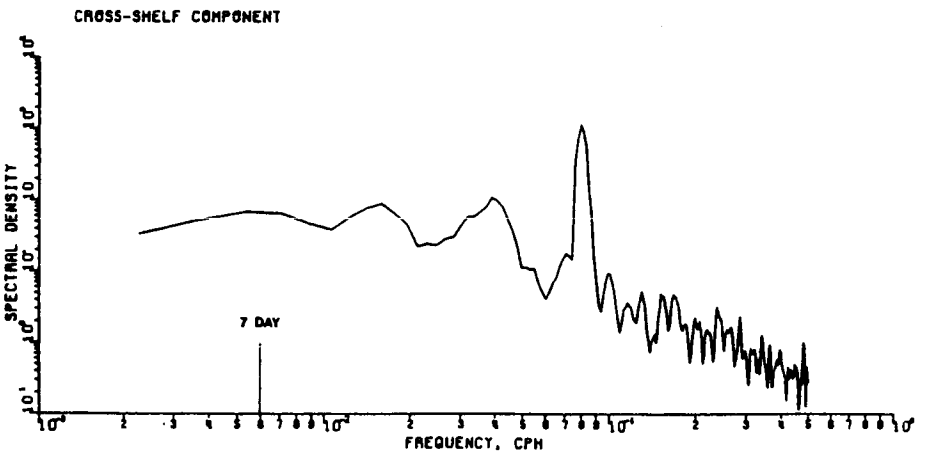

Figure B.1.18: Spectra of offshore lower current meter.

Table B.1.2: First order statistics for FSU Winter 1978 experiment (after Mitchum and Sturges, 1981)

Component	Mean	Trend	Variance
τ_x	-3.0×10^{-2}	-5.4×10^{-4}	5.2×10^{-2}
τ_y	-1.0×10^{-2}	-2.5×10^{-4}	1.0×10^{-2}
V-01	-0.95	-4.6×10^{-2}	211.6
U-01	1.26	-1.4×10^{-2}	276.7
V-02	2.20	-3.0×10^{-2}	75.8
U-02	1.15	-5.2×10^{-3}	119.9
V-I1	-0.66	-3.3×10^{-2}	162.9
U-I1	-1.56	2.2×10^{-3}	283.6
V-I2	-0.66	-3.1×10^{-2}	177.2
U-I2	-1.68	1.1×10^{-3}	267.6

Correlations were also performed between the current data and the local winds. Table B.1.3 summarizes those correlations. Current magnitude was correlated to wind magnitude, and current components were correlated to wind components. A stronger correlation between winds and currents is evident at the inshore site than at the offshore site. Alongshore currents are plainly better correlated to the alongshore wind component than the cross-shelf currents are to the cross-shelf wind component. Currents typically lag winds by about 12 hours.

WINTER 1978 TEMPERATURE DATA ANALYSIS

All the FSU meters were equipped with temperature sensors. Figure B.1.19 shows the temporal change in temperature at the four meters. As might be expected during the winter, the vertical temperature gradient is small. The

BEST CORRELATIONS

BUOY WIND TO FSU CURRENTS (MAGNITUDES)

Current Meter	Buoy Wind	Lag
0840 - Shallow Offshore	0.55	+ 11 hours
1317 - Deep Offshore	0.30	+ 13 hours
0921 - Shallow Inshore	0.66	+ 13 hours
0922 - Deep Inshore	0.71	+ 15 hours

Table B.1.3: Summary of cross correlations between buoy wind and current data, winter 1978 hindcast.

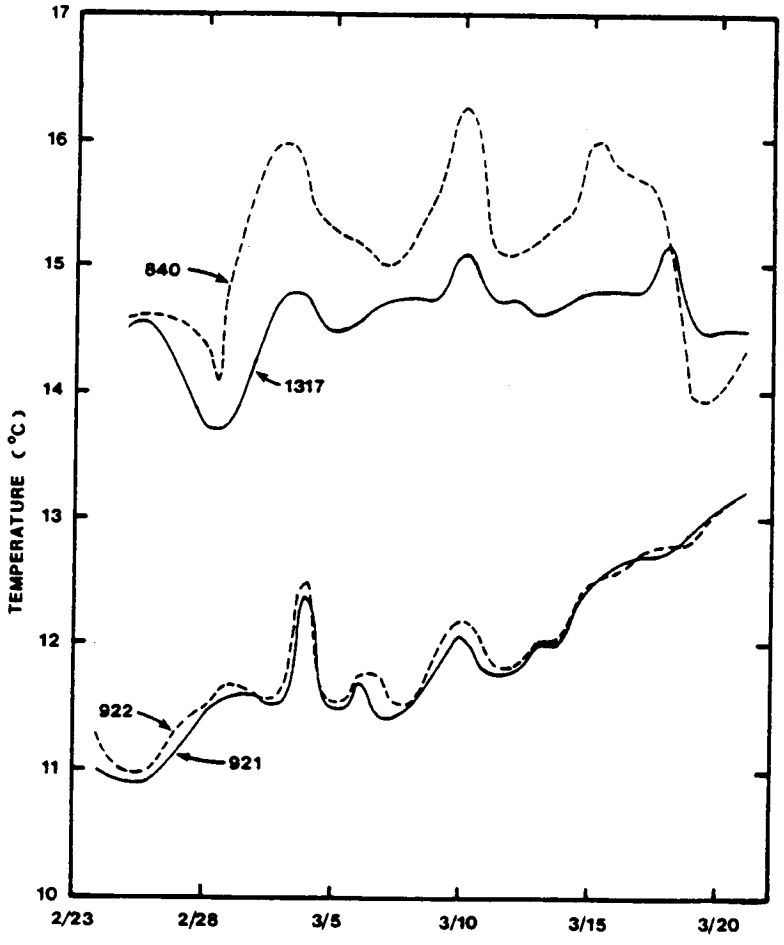

Figure B.1.19: Temperature at four FSU meters. 840=offshore upper, 1317=offshore lower, 921=inshore upper, 922=inshore lower.

horizontal temperature gradient is typically about 2 to 3° C between the inshore and offshore sites. Oscillations in the temperature are well correlated to meteorological events. The slow increase with time of the temperature at the sites is due to the annual heating-cooling cycle.

WINTER 1978 SURFACE ELEVATION DATA ANALYSIS

Spectra and coherence of the unfiltered surface elevation data at Clearwater and Naples for February-March 1978 are shown in Figures B.1.20-21. The semi-diurnal tide is seen to dominate the signal, followed closely by the diurnal tide. Low frequency forcing probably due to the winds is seen to be somewhat more important at Clearwater than Naples. A slight peak at the seven day and a more evident peak at the three day period can be seen at Clearwater. Correlation between the low frequency components at the two stations is good as indicated in Figure B.1.22.

WINTER 1978 LOOP CURRENT POSITION

As indicated in Section 2.2, Loop Current (LC) intrusions have been observed well north of the FSU sites. Satellite observations of the LC during March 1978 show the LC was positioned south of the sites (see Figure B.1.23) at about 27° N latitude.

WINTER 1978 DATA SUMMARY

In summary, the data indicate that during February-March 1978:

1. the strongest atmospheric forcing was associated with large high pressure systems which migrated into the area every 7 to 10 days;

2. winds in the alongshore direction were two to three times stronger than those in the cross-shelf direction;

3. spatial coherence of the wind was good which suggests that the wind

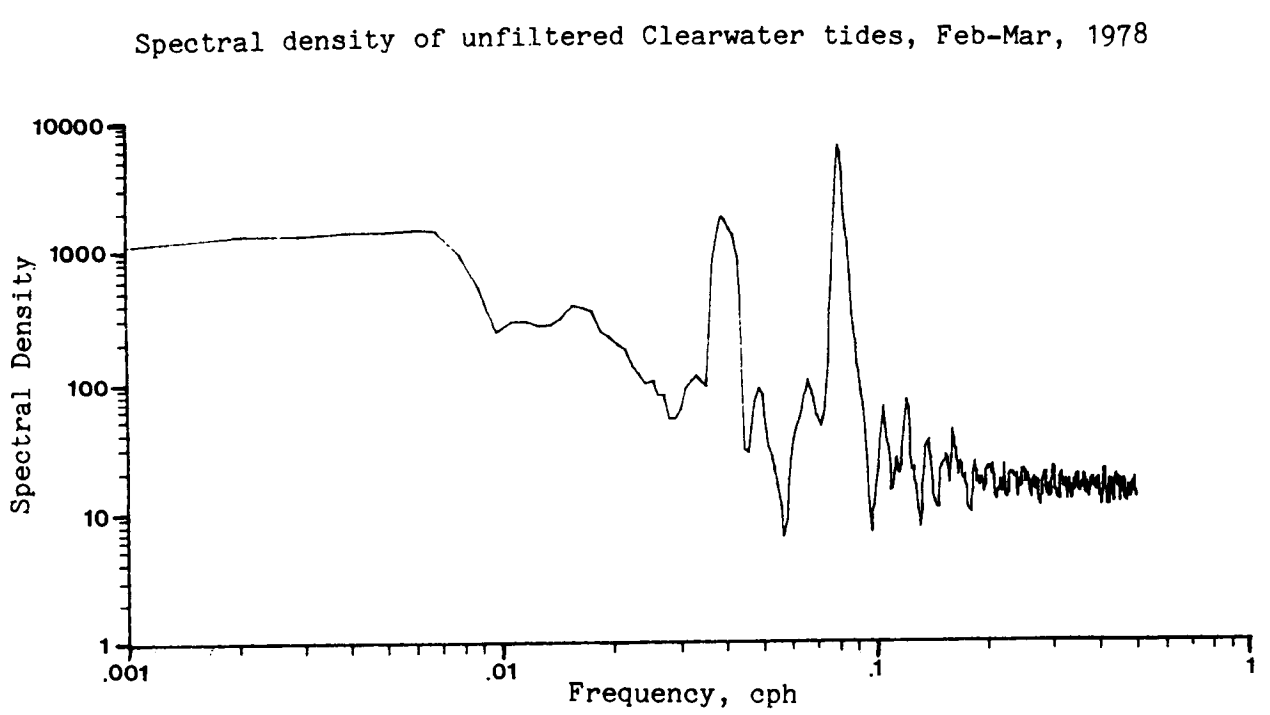

Figure B.1.20: Spectra of surface elevations at Clearwater during 1978 hindcast

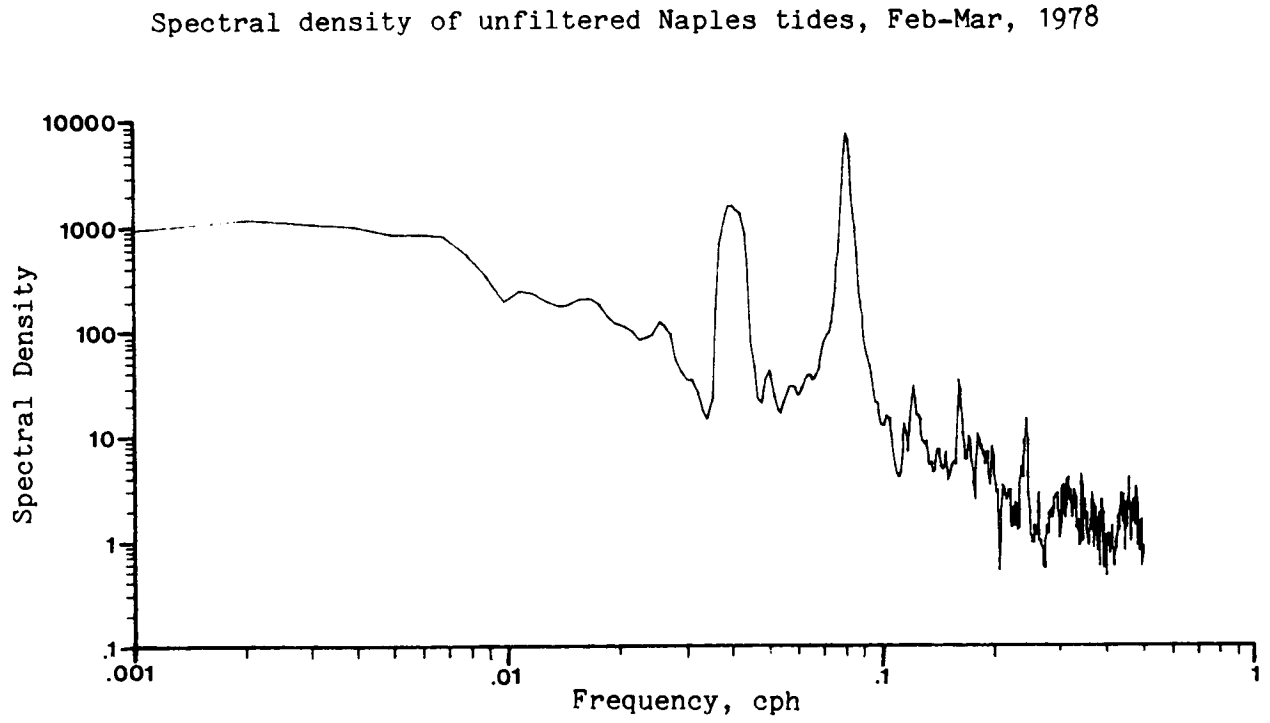

Figure B.1.21: Spectra of surface elevations at Naples during 1978 hindcast.

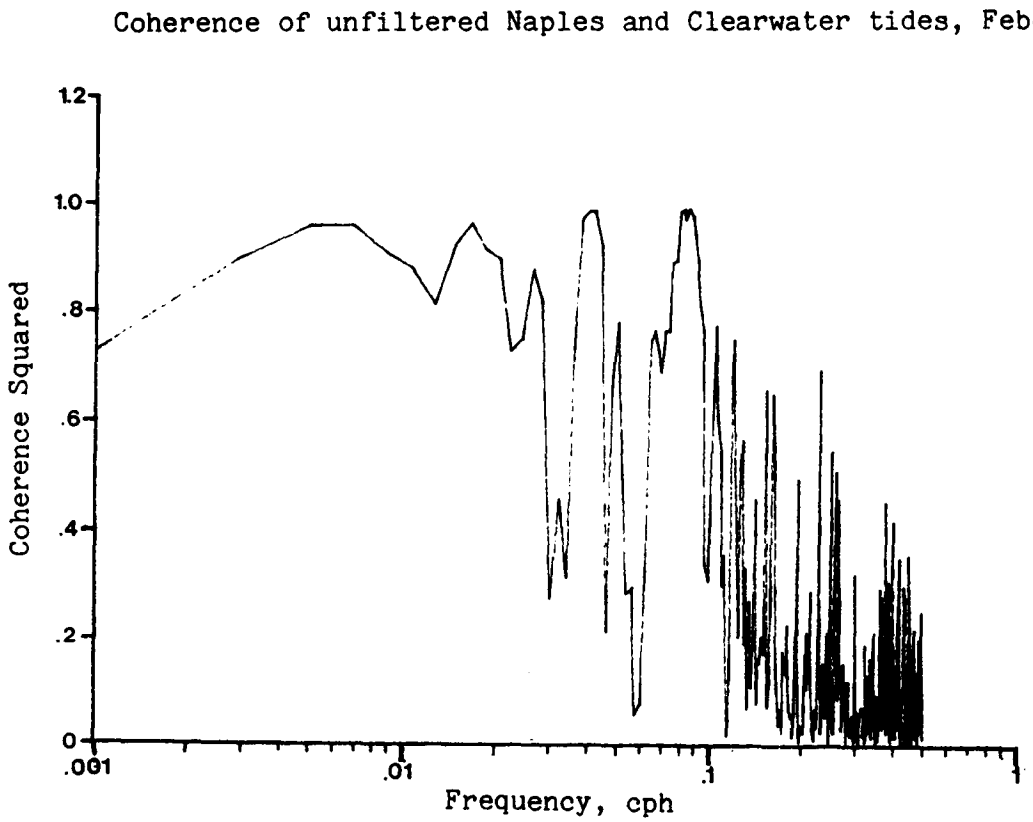

Figure B.1.22: Coherence of unfiltered surface elevations at Naples and Clearwater during 1978 hindcast.

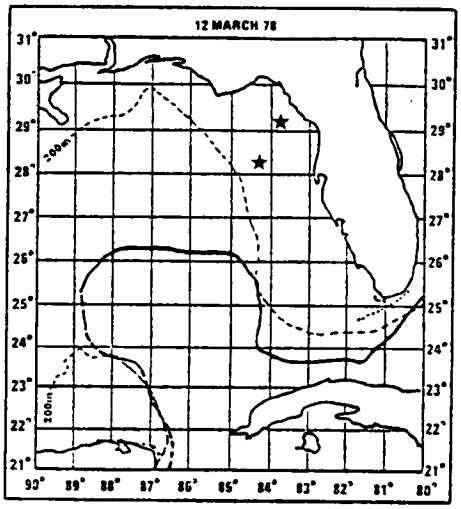
12 MARCH 78
200m

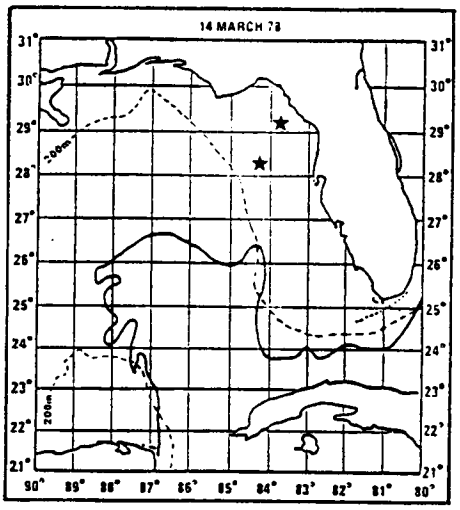
14 MARCH 78
200m

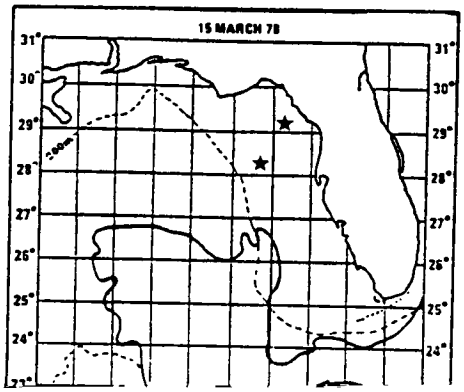
15 MARCH 78
200m

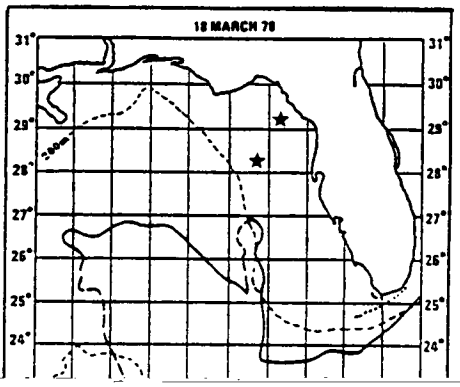
18 MARCH 78
200m

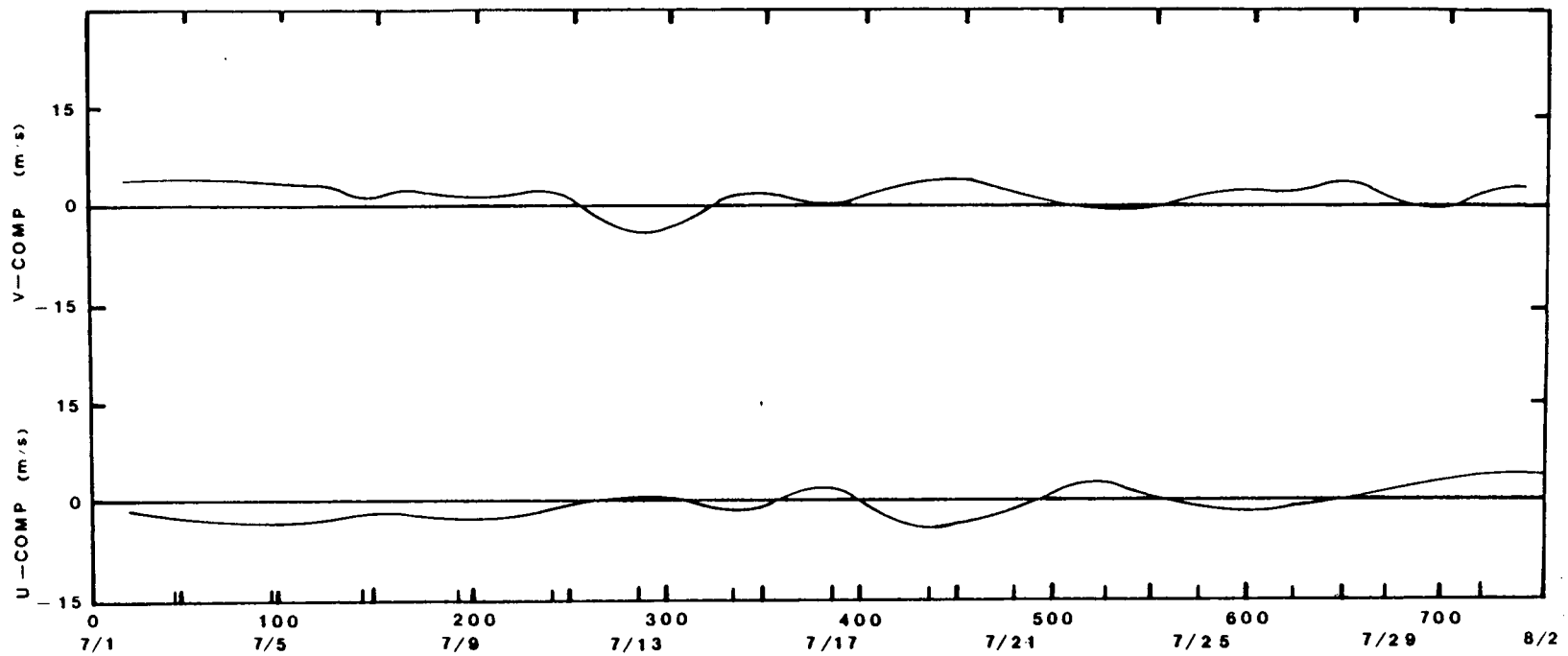

Figure B.2.1: Alongshore and cross-shelf wind components at Key West. Summer 1974 hindcast.

Spectral density of unfiltered Key West winds, Jul-Aug, 1974

Alongshore component

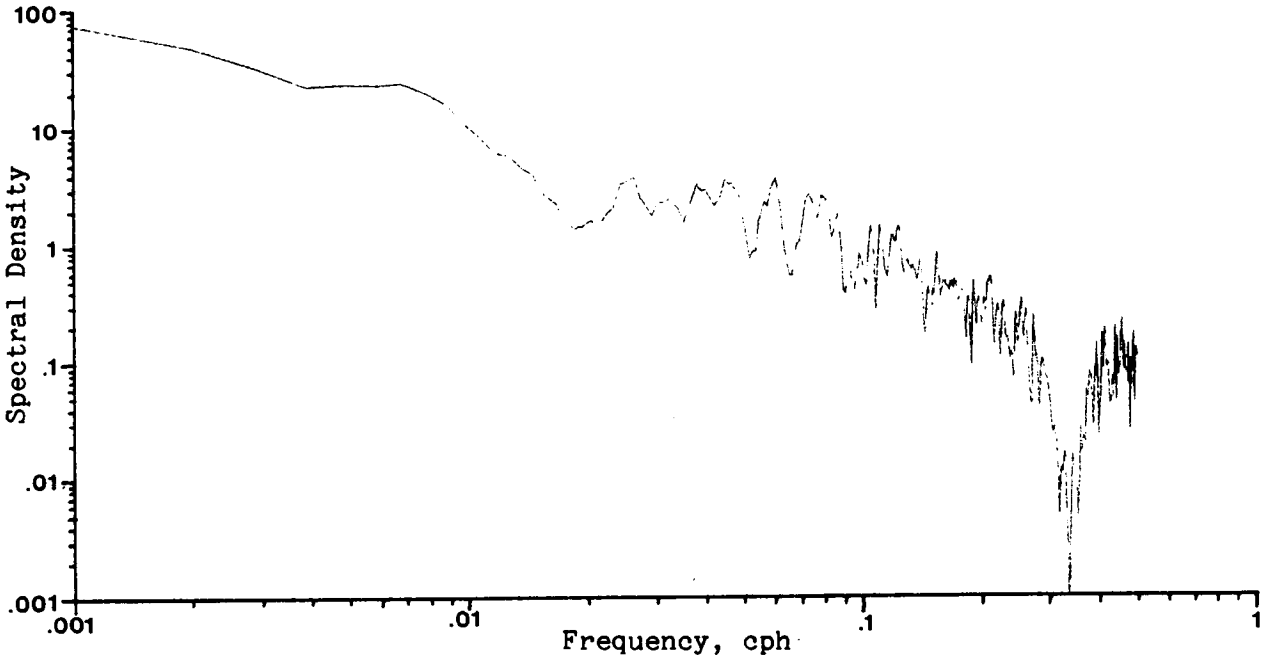

Spectral density of unfiltered Key West winds, Jul-Aug, 1974

Cross-shelf component

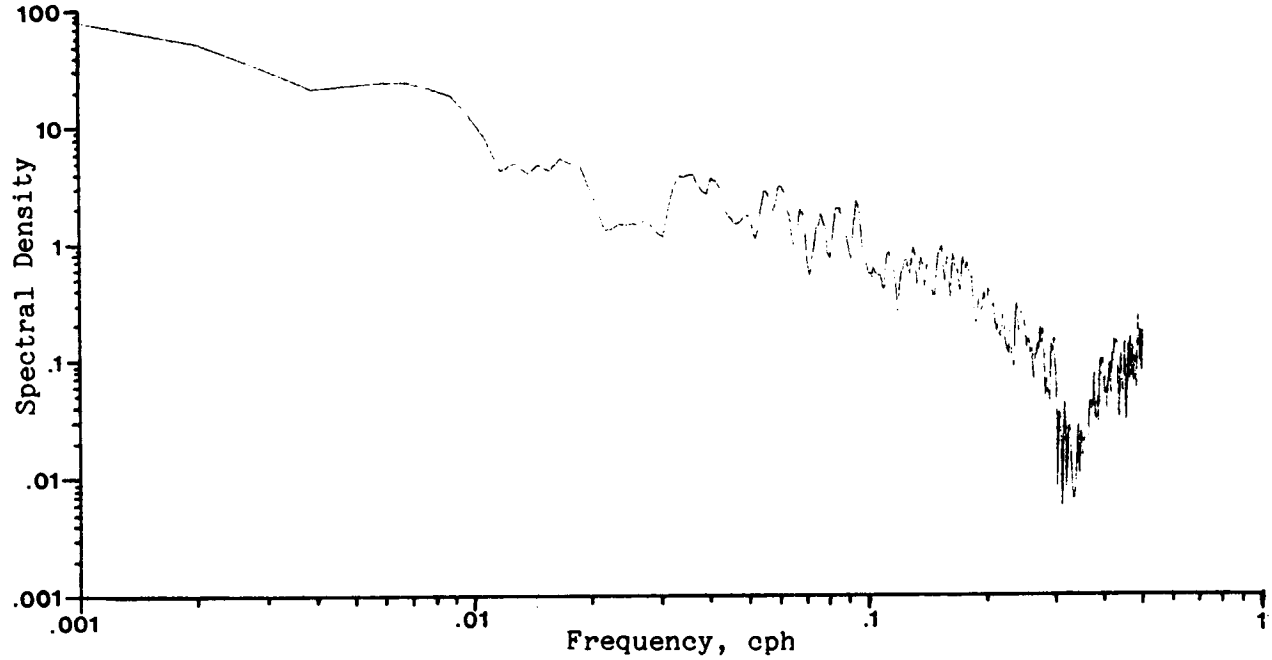

Figure B.2.2: Spectra of unfiltered Key West winds during 1974 hindcast.

Coherence of Key West and Partagas winds, Jul-Aug, 1974

Alongshore component

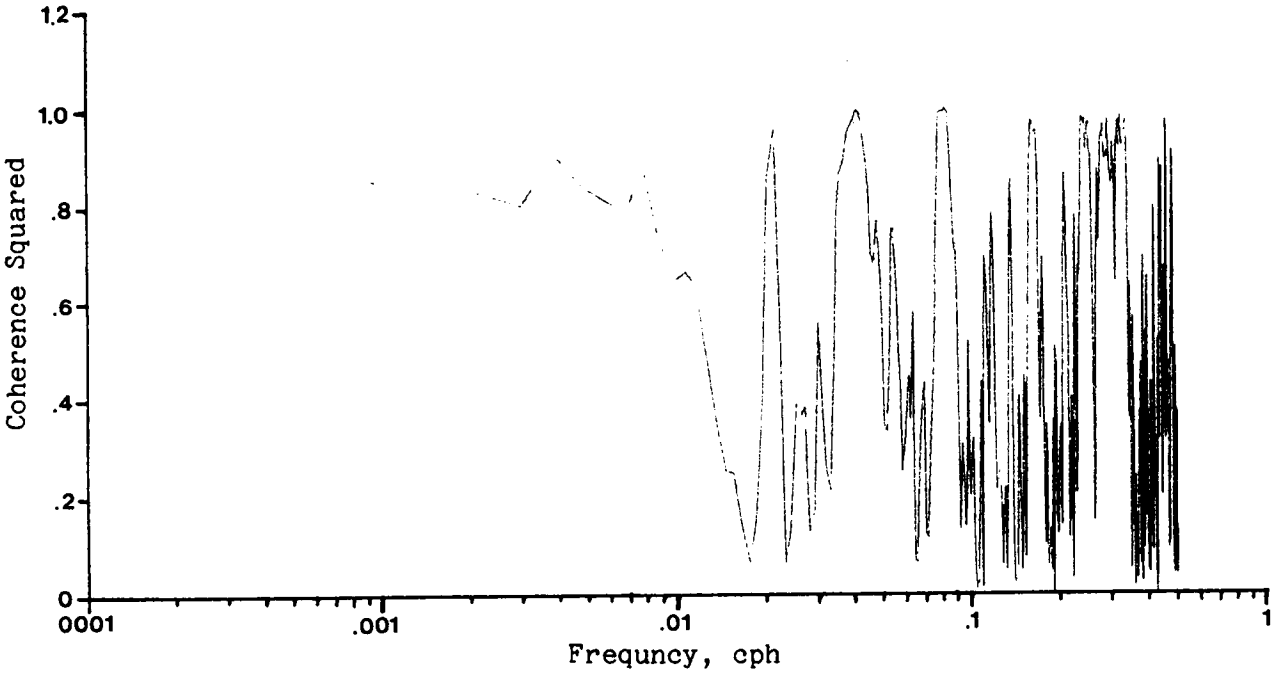

Coherence of Key West and Partagas winds, Jul-Aug, 1974

Cross-shelf component

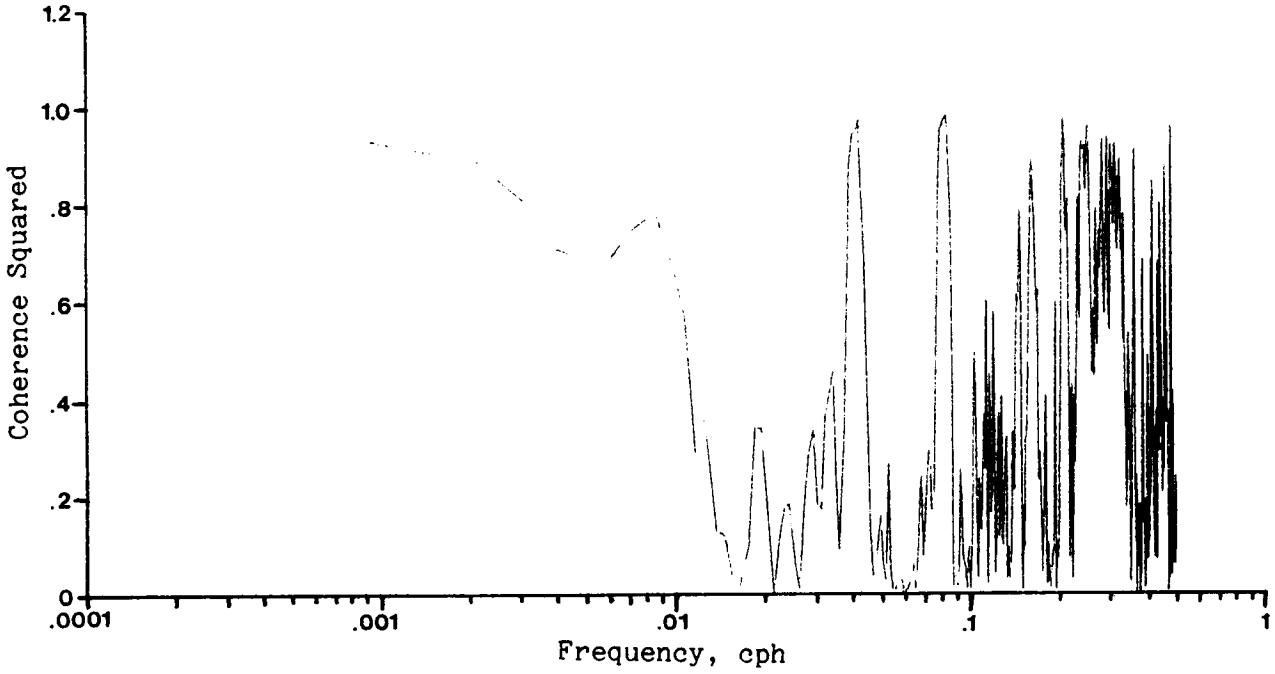

Figure B.2.3: Coherence of filtered Key West winds and Partagas winds. Summer 1974 hindcast.

on Key West in calculating the offshore winds.

The summer wind spectra differ from the winter in a number of ways. Generally there is less low frequency energy in the summer than the winter, and during the summer the cross-shelf and alongshore components are nearly equal at low frequencies.

Unlike the winter, the summer wind spectra do not indicate the predominance of a characteristic meteorologic event such as frontal systems. The coherence between stations also imply less spatial coherence for the summer than for the winter. Figure B.2.4 shows the coherence between Tampa and Key West unfiltered winds. In the low frequency range, the correlation coefficient squared for the alongshore components averages about 0.6. This compares to an average of about 0.9 for the alongshore component at the same stations during the winter of 1978 (see Figure B.1.10).

SUMMER 1974 SURFACE ELEVATION DATA ANALYSIS

Figure B.2.5-6 show the spectra of the unfiltered surface elevations at Clearwater and Naples. The low frequency energy is about an order of magnitude less than during the winter 1978. Coherence of the surface elevations at the two stations is considerably less than observed during the winter 1978 as seen from a comparison of Figures B.1.22 and B.2.7.

SUMMER 1974 DATA SUMMARY

To summarize:

1. the low frequency summer winds are much less energetic than the low frequency winter winds - maximum offshore summer winds are 7 m s^{-1} as compared to the winter when maxima of 15 m s^{-1}. The alongshore and cross-shelf components during summer are roughly equal. No dominant low frequency is evident for the summer winds.

COHERENCE OF UNFILTERED KEY WEST AND TAMPA WINDS, JUL-AUG 1974

ALONGSHORE COMPONENT

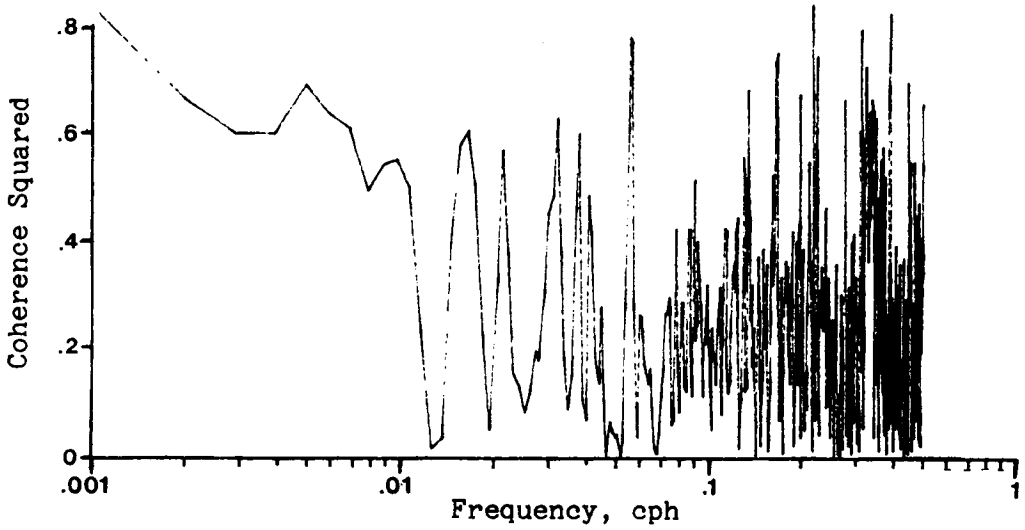

COHERENCE OF UNFILTERED KEY WEST AND TAMPA WINDS, JUL-AUG 1974

CROSS-SHELF COMPONENT

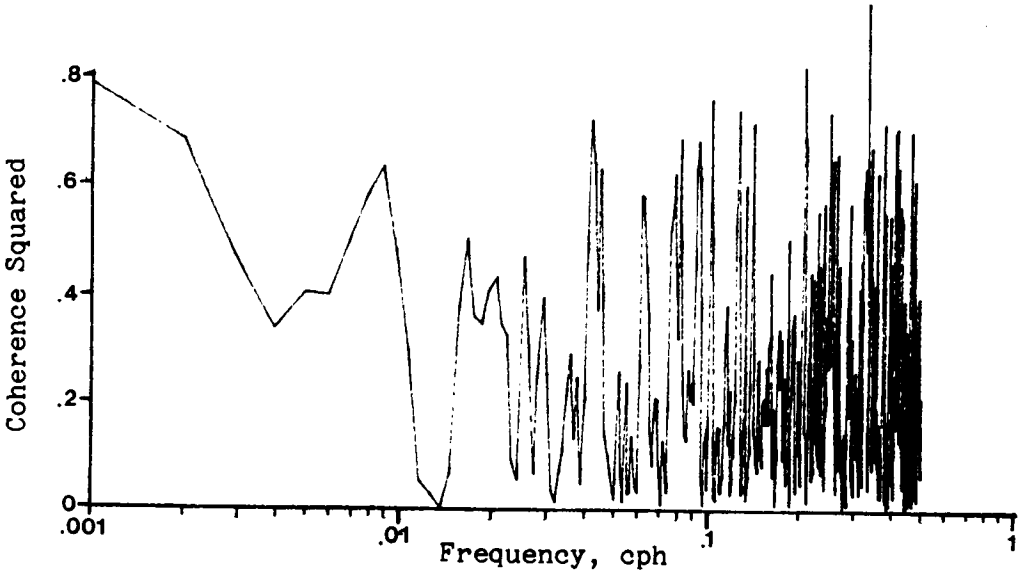

Figure B.2.4: Coherence of unfiltered Key West winds and Tampa winds. Summer 1974 hindcast.

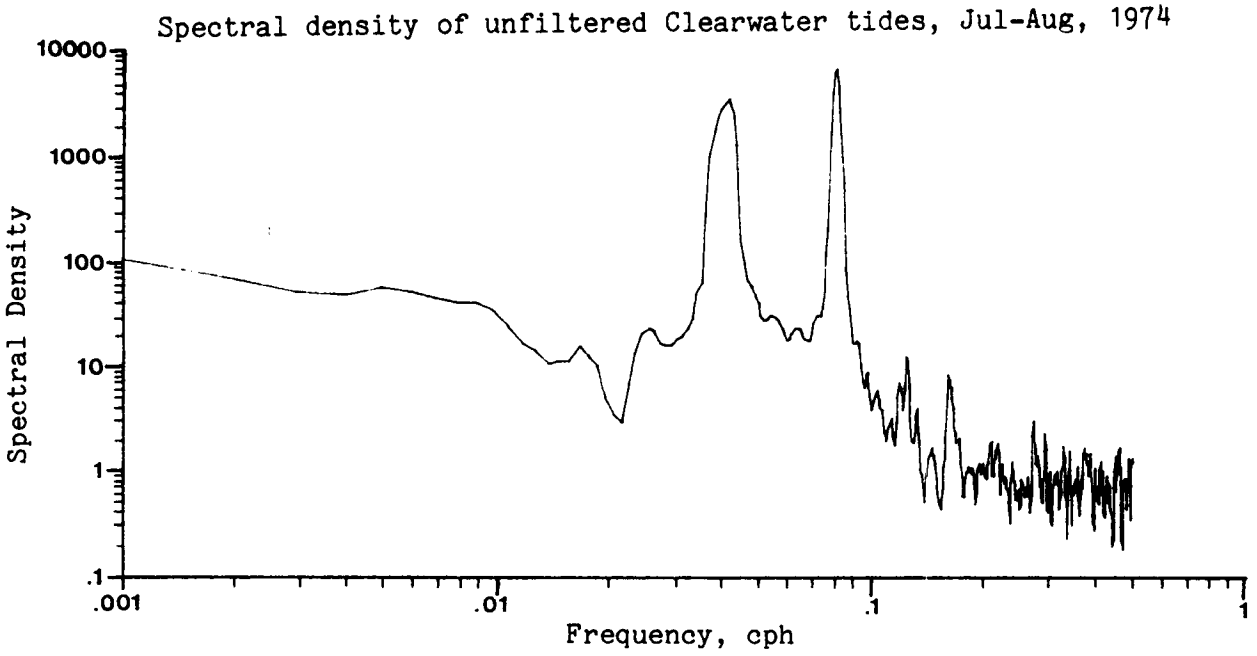

Figure B.2.5: Spectra of unfiltered Clearwater surface elevations during 1974 hindcast

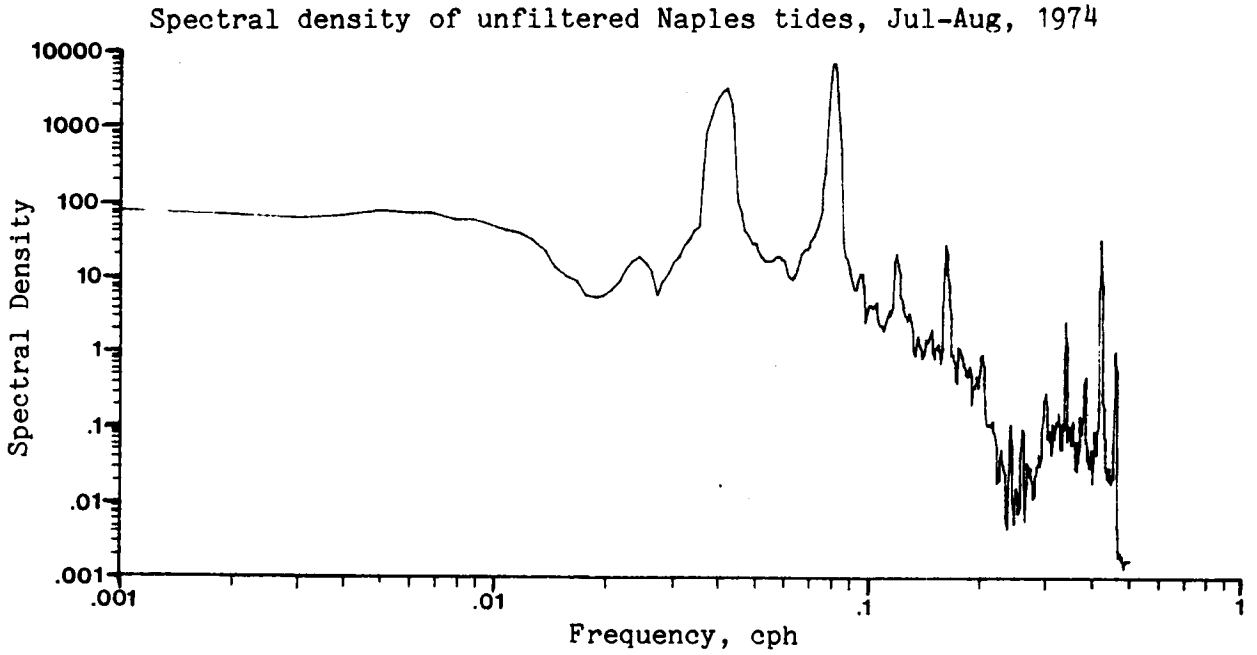

Figure B.2.6: Spectra of unfiltered Naples surface elevations during 1974 hindcast.

Coherence of unfiltered Naples and Clearwater tides, Jul-Aug, 1974

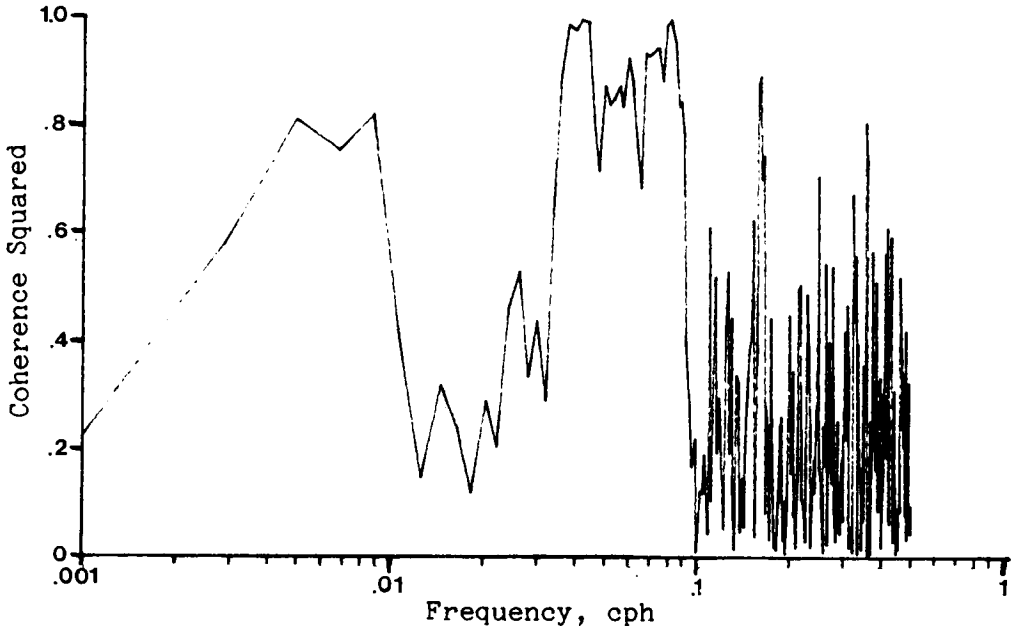

Figure B.2.7: Coherence of unfiltered Naples and Clearwater surface elevations. Summer 1974 hindcast.

Phase of unfiltered Naples and Clearwater tides, Jul-Aug, 1974

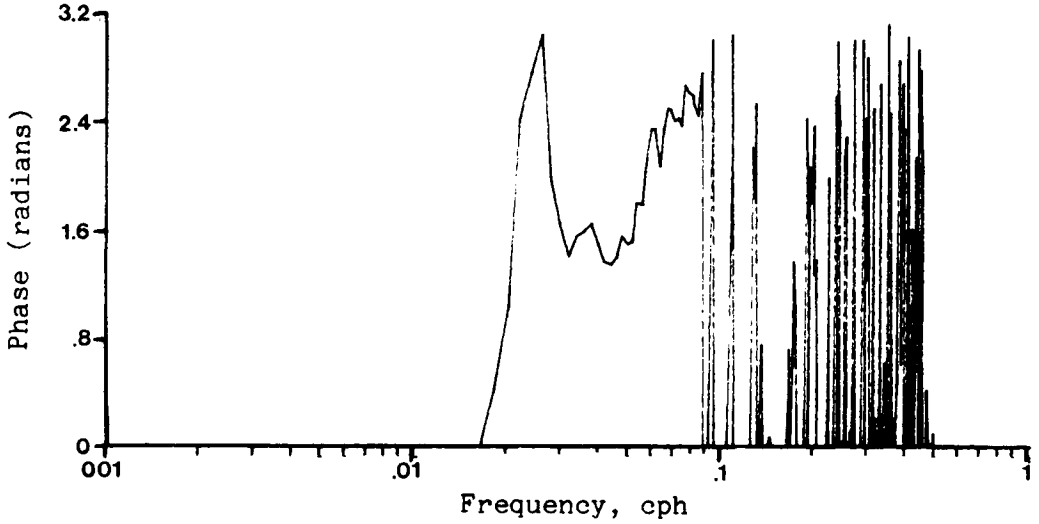

Figure B.2.8: Phase of unfiltered Naples and Clearwater surface elevations. Summer 1974 hindcast.

2. surface elevations are small, experiencing a range of +/- 5 cm (Figure 5.2.1). No dominant period is evident for the filtered surface elevations.

3. the spatial coherence of the low frequency wind is appreciably less than during the winter 1978 with typical correlation coefficients squared values of 0.6 for summer vs 0.9 for winter.

4. coherence between the low frequency wind and surface elevations is generally weak. Of the two components, the cross-shelf is somewhat better correlated than the alongshore component.

B.3 Winter 1973

February-March was chosen for the hindcast because of the existence of both current velocity data and extensive hydrographic data. Figure B.3.1 shows the details of the moorings during the time period and the locations of each station on the model grid. Most of the stations were located near the open ocean boundary of the model and so are potentially useful in specifying the open ocean boundary condition for the model, but the data are not very helpful for comparison with model results. Station F is the single exception. Data are available at F starting on 8 February 1973 and extending to 5 March 1973.

In addition to the velocity and hydrographic data available from the SDE, there are also surface elevation data from government installations at Naples, Cedar Keys and St. Petersburg and wind data from four stations at Key West, Tampa, Fort Myers, and Apalachicola.

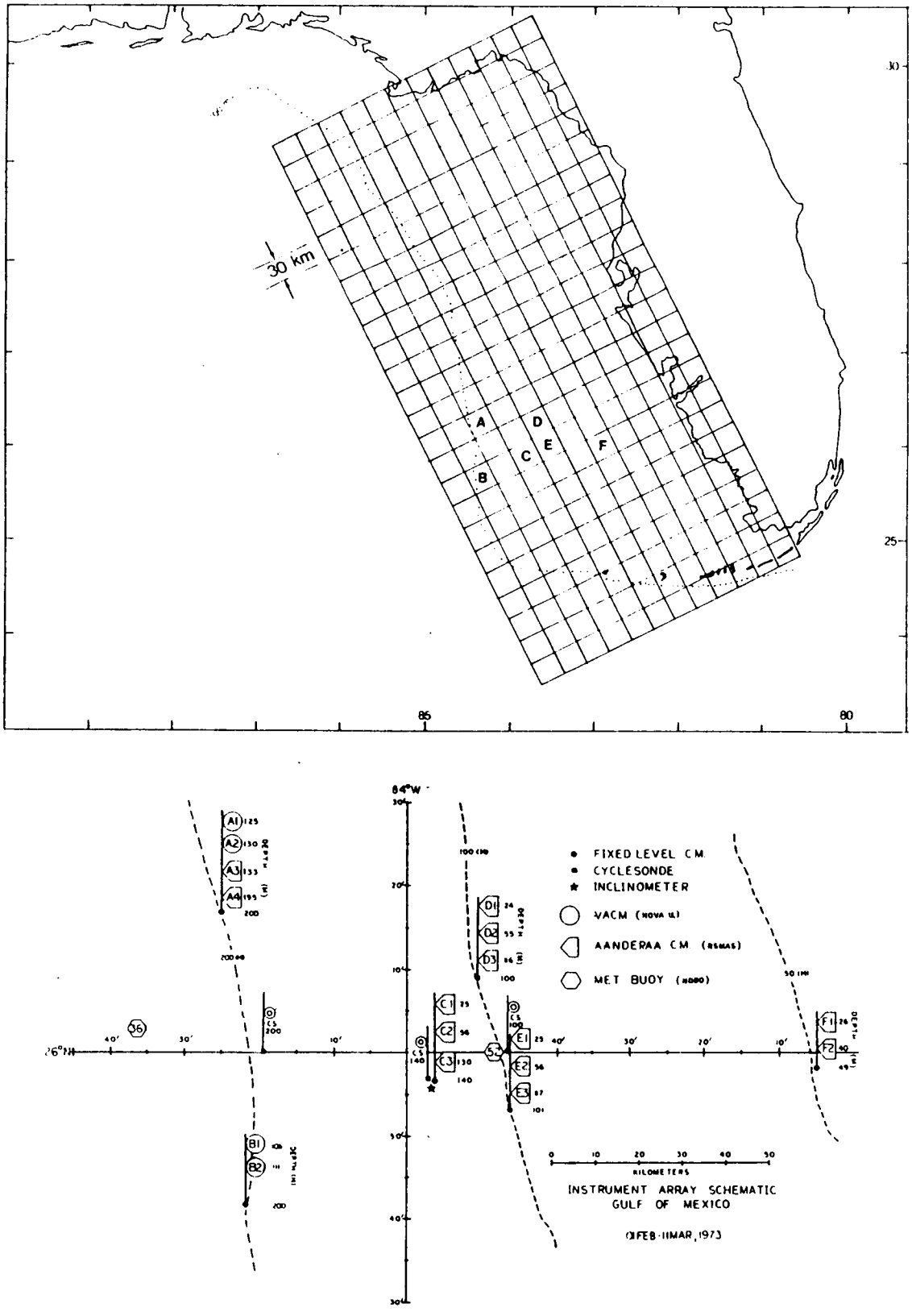

Figure B.3.1: Location of SDE sites during February-March 1973. Winter 1973 hindcast (Price and Mooers, 1974c).

The LC was positioned about midway along the shelf during the time period as indicated in the infrared satellite photos shown in Figure B.3.2. Thus the SDE data from this time period were greatly influenced by LC effects.

WINTER 1973 WIND DATA ANALYSIS

A time series plot of the alongshore and cross-shelf wind components at Key West is shown in Figure B.3.3. Figure B.3.4 shows the spectra of the unfiltered Key West winds. A strong peak is apparent in the alongshore component at about the 7 day period indicating the dominance of the winter frontal system movement described earlier. The winds are generally weaker than the Winter 1978 experiment although one particularly strong frontal system passed the area on February 10 with maximum wind speeds of 14 m s^{-1}.

WINTER 1973 CURRENT DATA ANALYSIS

The current vectors at stations E and F are shown in Figure B.3.5. An inconsistency of about 3 days was found in the starting time for the published data at station F. Subsequent conversations with Jim Price revealed that the starting date specified on the data tape was approximately 3 days late. This correction has been incorporated in all plots shown in this report.

Figure B.3.6 shows progressive vector plots of the low frequency currents for all stations. The complexity of the currents is readily apparent and no doubt explains why only one of the many scientists involved in the SDE study ever published an interpretation of the low frequency SDE results.

Rotary spectra and time series of temperature and velocity are available for all meters and are published in Price and Mooers (1974c). Figure B.3.7 shows a sample of the rotary spectra at Station E. Substantial low frequency energy is evident in the figure. It is apparent from a review of the data and Niiler's (1976) discussion that this energy is associated with eddies originating from the interaction of the LC with WFS waters.

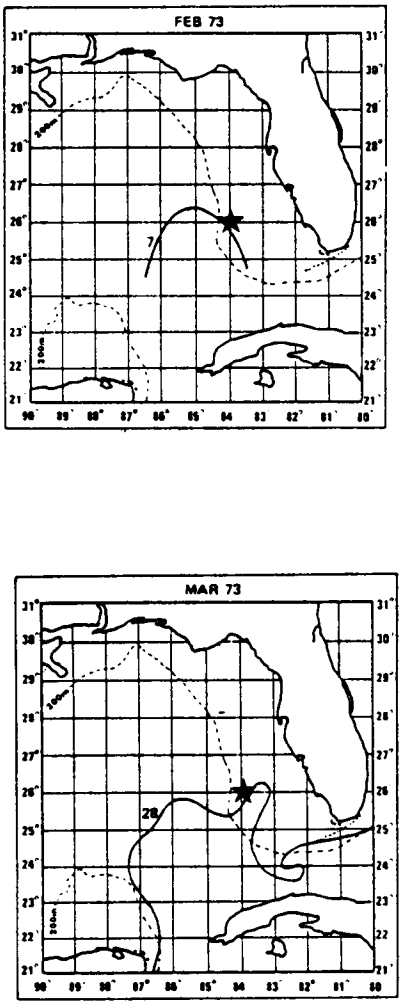

Figure B.3.2: Location of the LC during the study period. Winter 1973 hindcast (Vukovich et al. 1978). Star marks deployment area of SDE current meters.

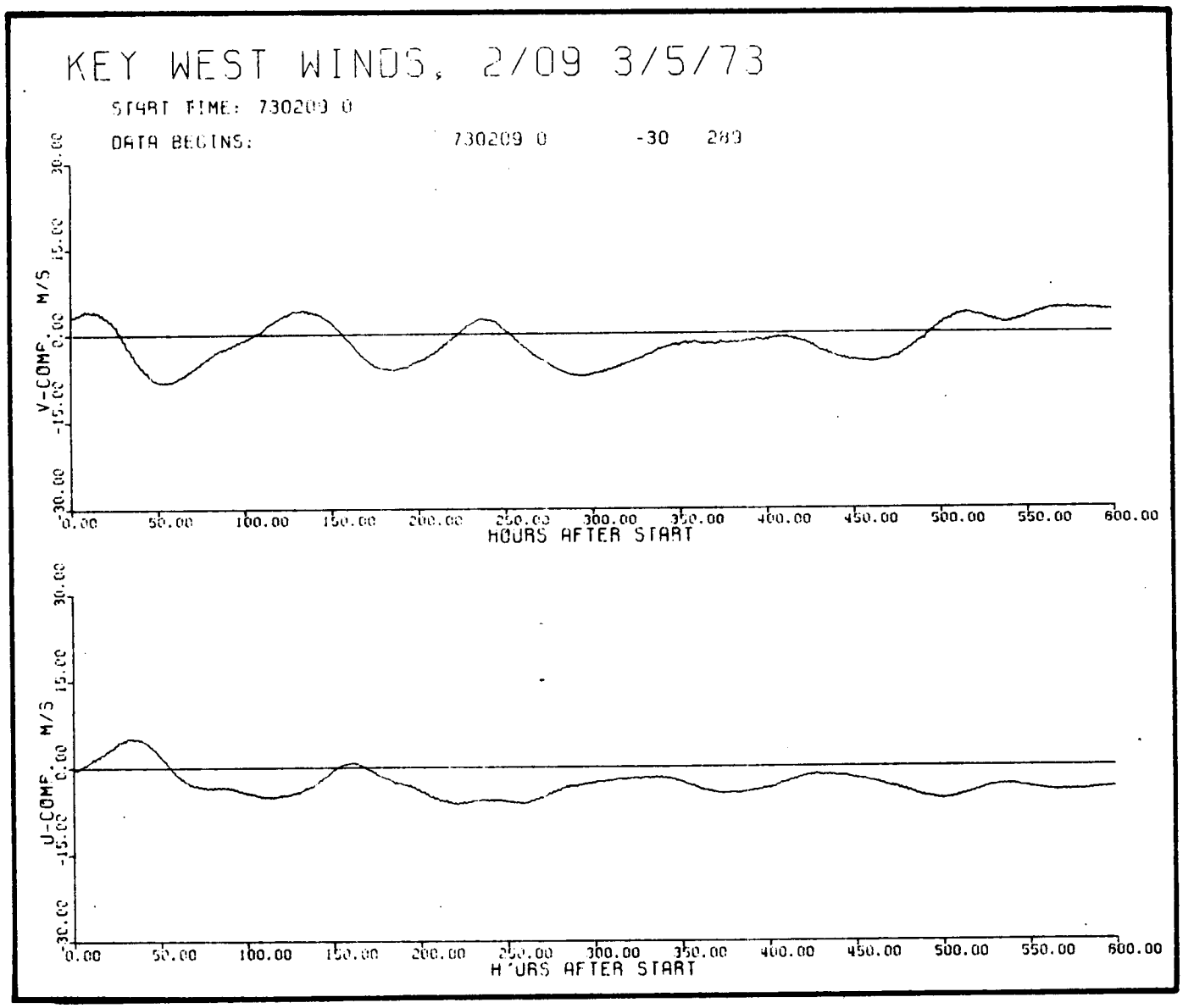

Figure B.3.3: Alongshore and cross-shelf wind components at Key West. Winter 1973 hindcast.

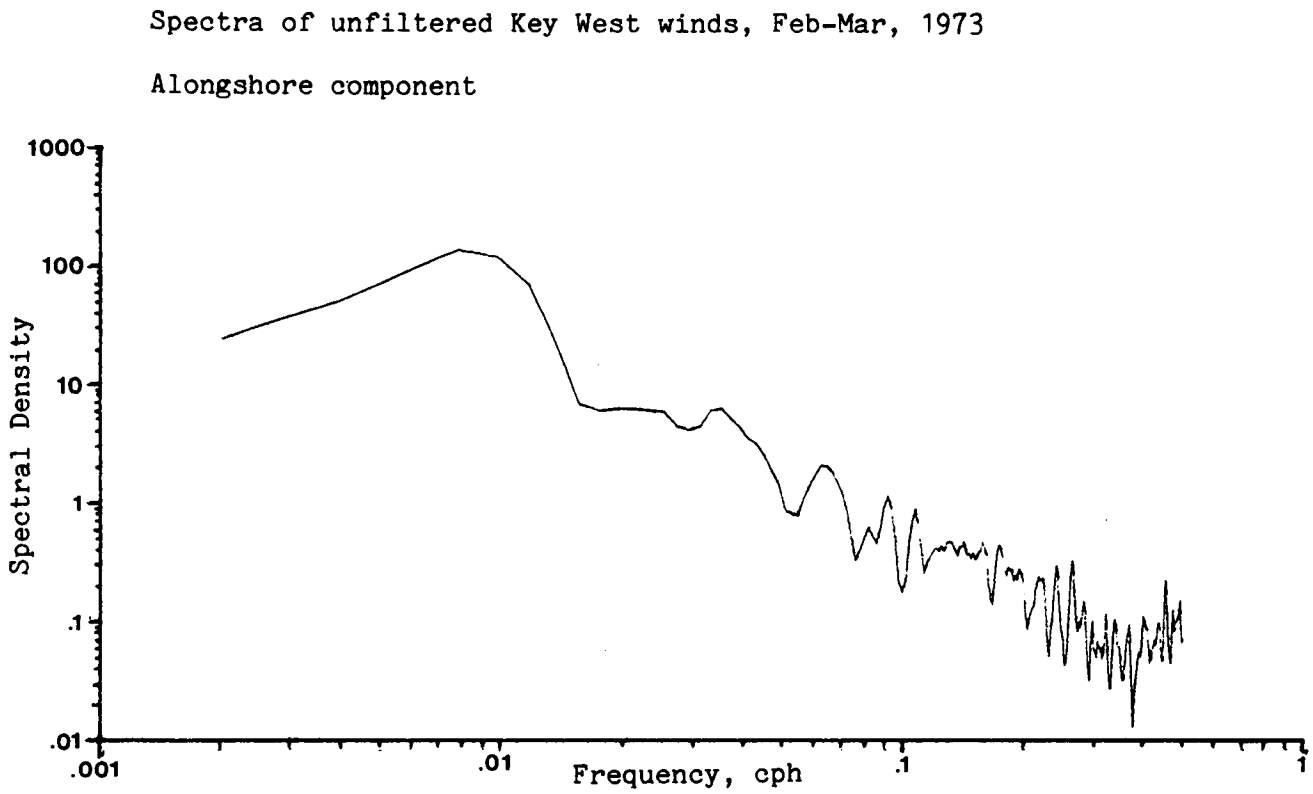

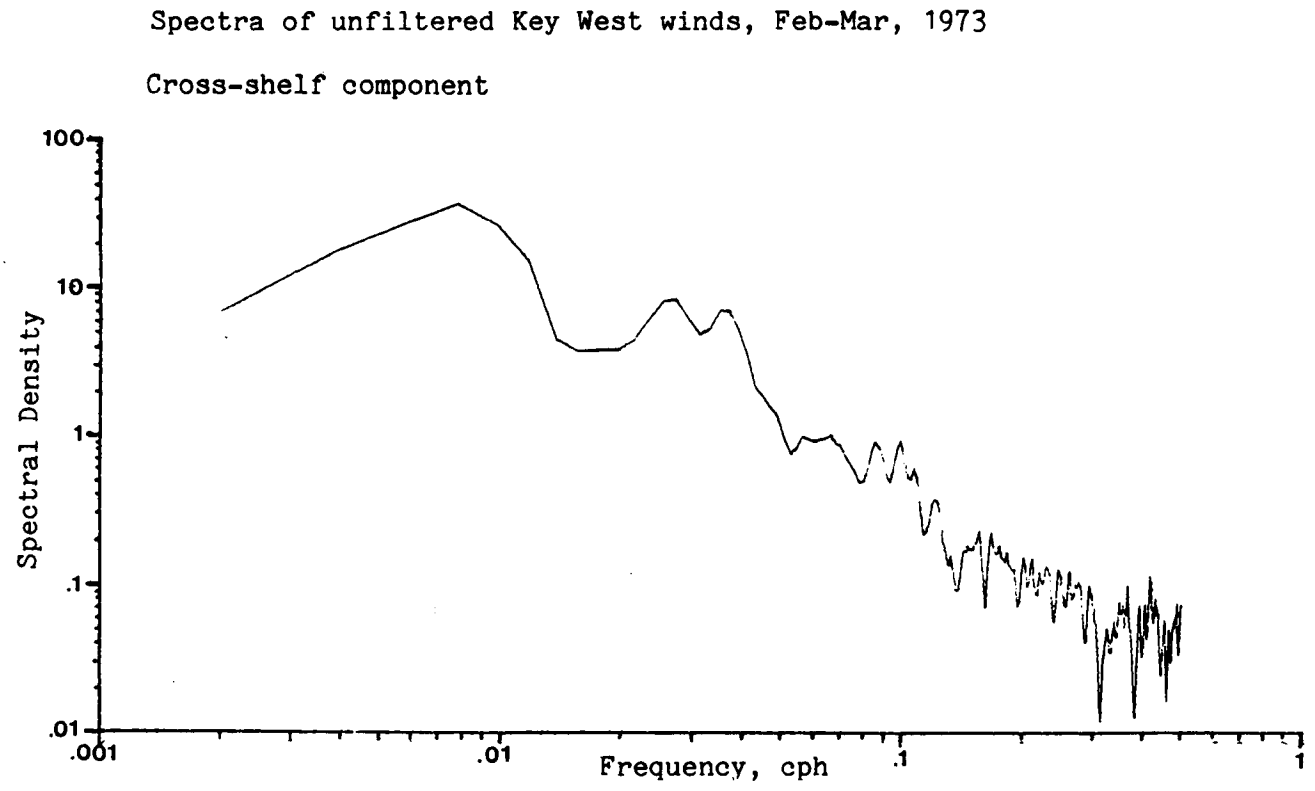

Figure B.3.4: Spectra of unfiltered Key West winds. Winter 1973 hindcast.

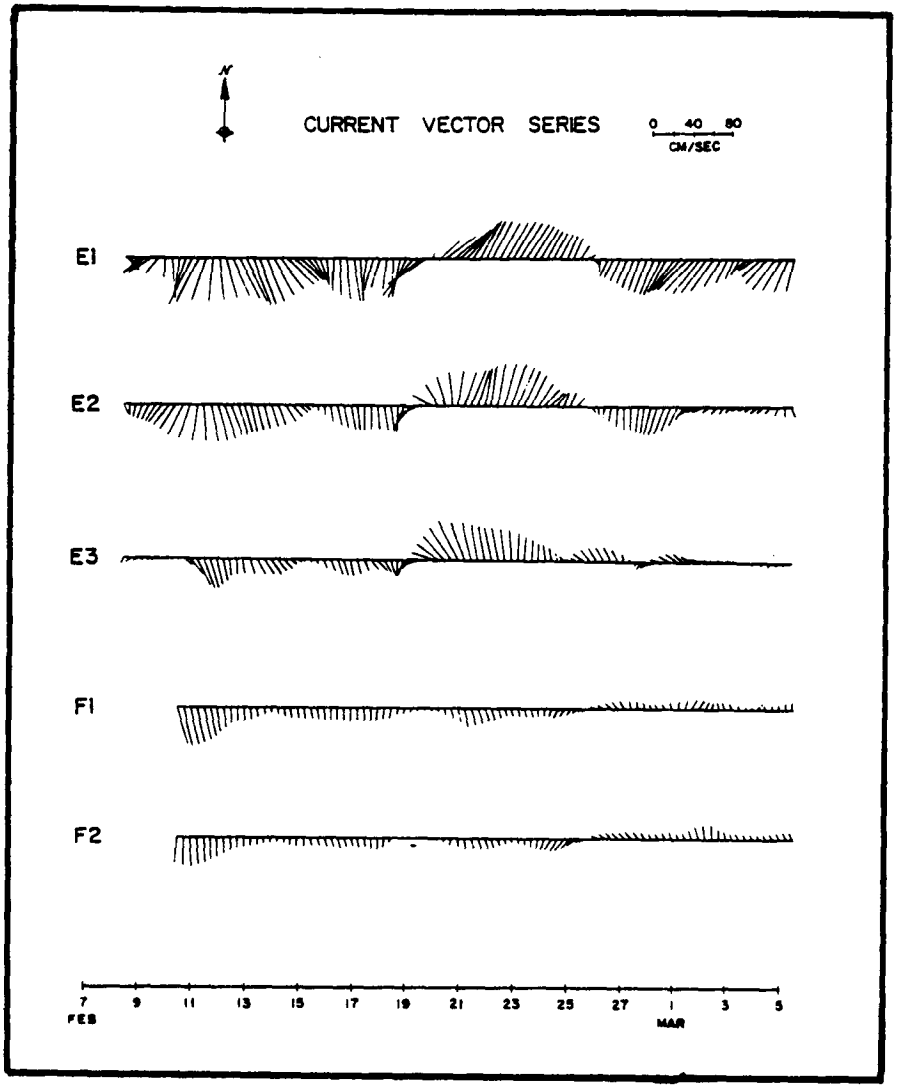

Figure B.3.5: Current vector series at stations E and F. Winter 1973 hindcast (Price and Mooers, 1974c).

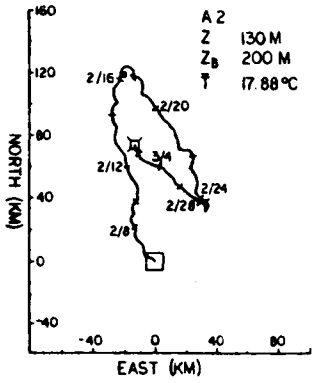

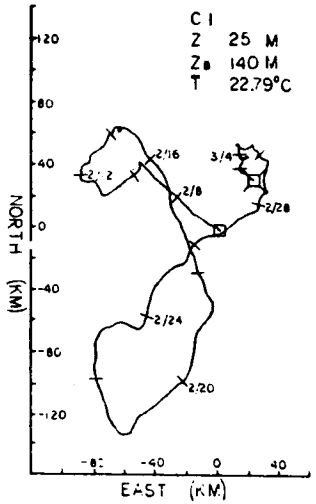

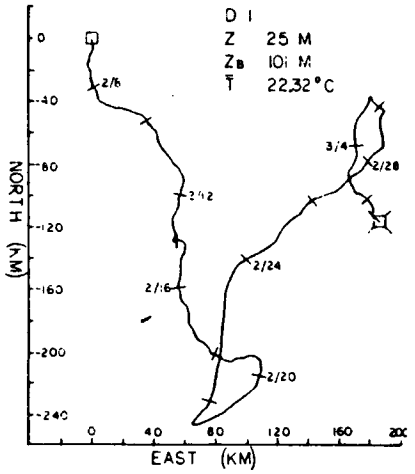

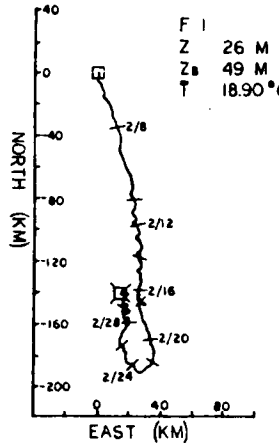

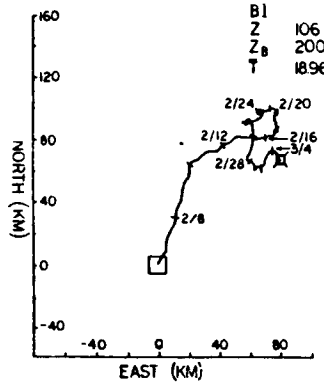

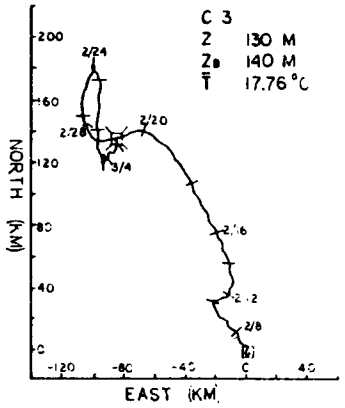

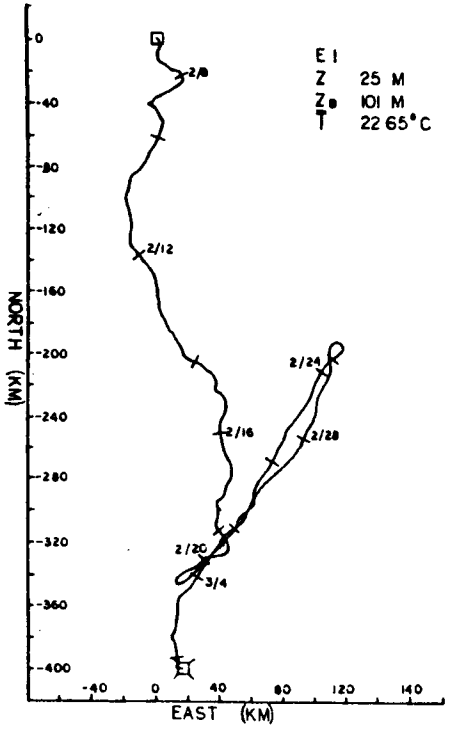

Figure B.3.6: Progressive vector plots at stations A-F. Winter 1973 hindcast (Price and Mooers, 1974c).

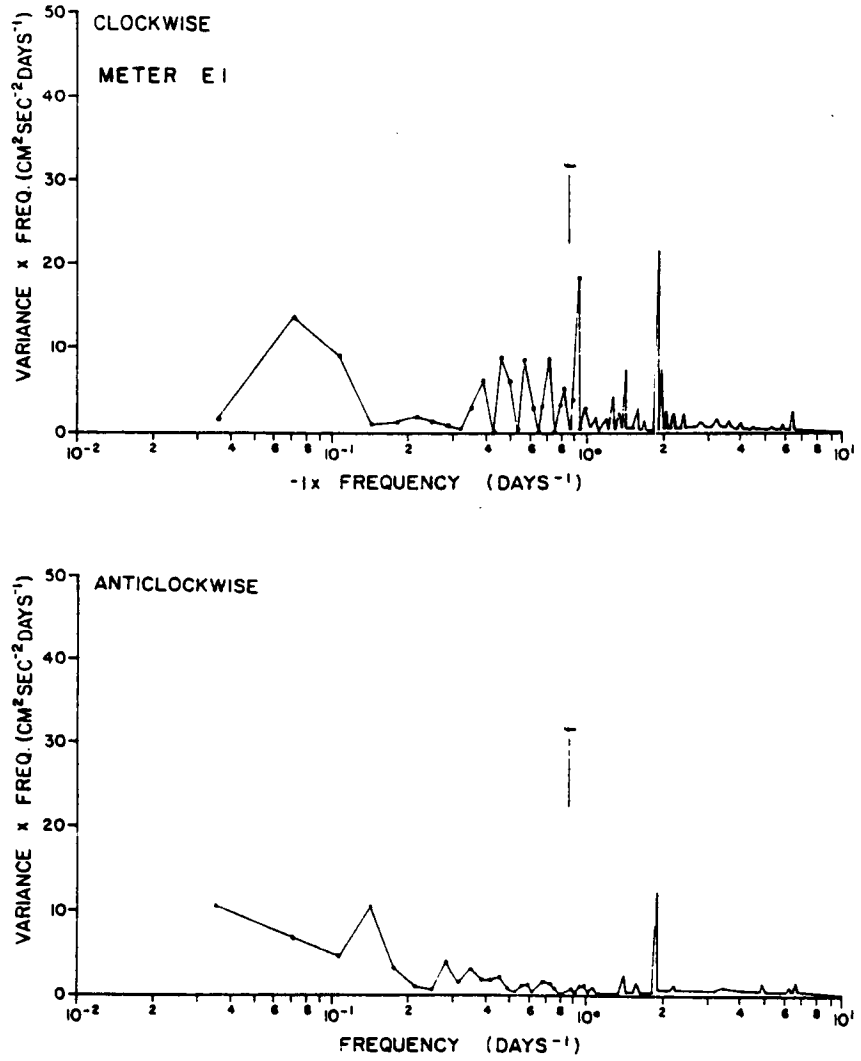

Figure B.3.7: Rotary spectra at station E1.
Winter 1973 hindcast (Price and Mooers, 1974c).

Some other observations on the low frequency data suggested by Niiler and our analyses include:

1. The variance of the alongshore currents is larger than the variance of the cross-shelf currents. Current direction becomes progressively more aligned with the local isobaths at a given station as one moves closer to the bottom.

2. Coherence between low frequency winds and currents reveal a weak correlation (relative to the Winter 1978) even at stations as shallow as F (e.g. Figure B.3.8).

3. Coherence between meters located on the same mooring but at different depths indicate good vertical coherence in shallow water and somewhat weaker correlation as one moves nearer the shelf break. Figure B.3.9 demonstrates the good coherence between meters F1 and F2.

4. Spatial coherence is significant for meters on the same isobath, but weak for other sites. Niiler suggests that the low-frequency events apparent at stations on the break propagate to the north along the 150 m isobath.

5. The eddies observed at sites of 100 m or deeper, show strong horizontal thermal structure. This structure becomes weaker as one moves onto the shelf and virtually disappears at station F. Figure B.3.10 demonstrates this.

CALCULATION OF NET DRIFT IN THE PRESENCE OF LC EFFECTS

Net drift is of essential interest to the WFS study. One common method of estimating this quantity is to connect the start and end points in the progressive vector plots shown in B.3.6. This is the same as computing a

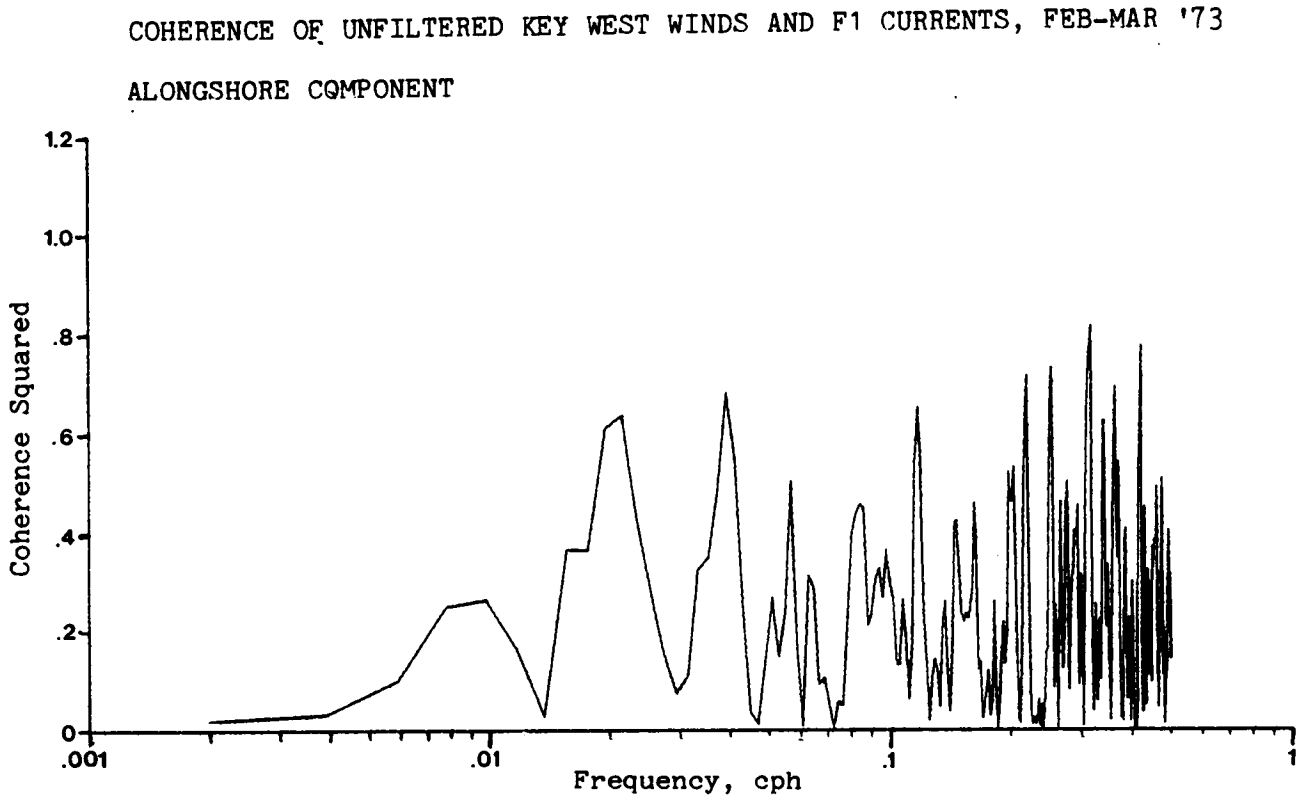

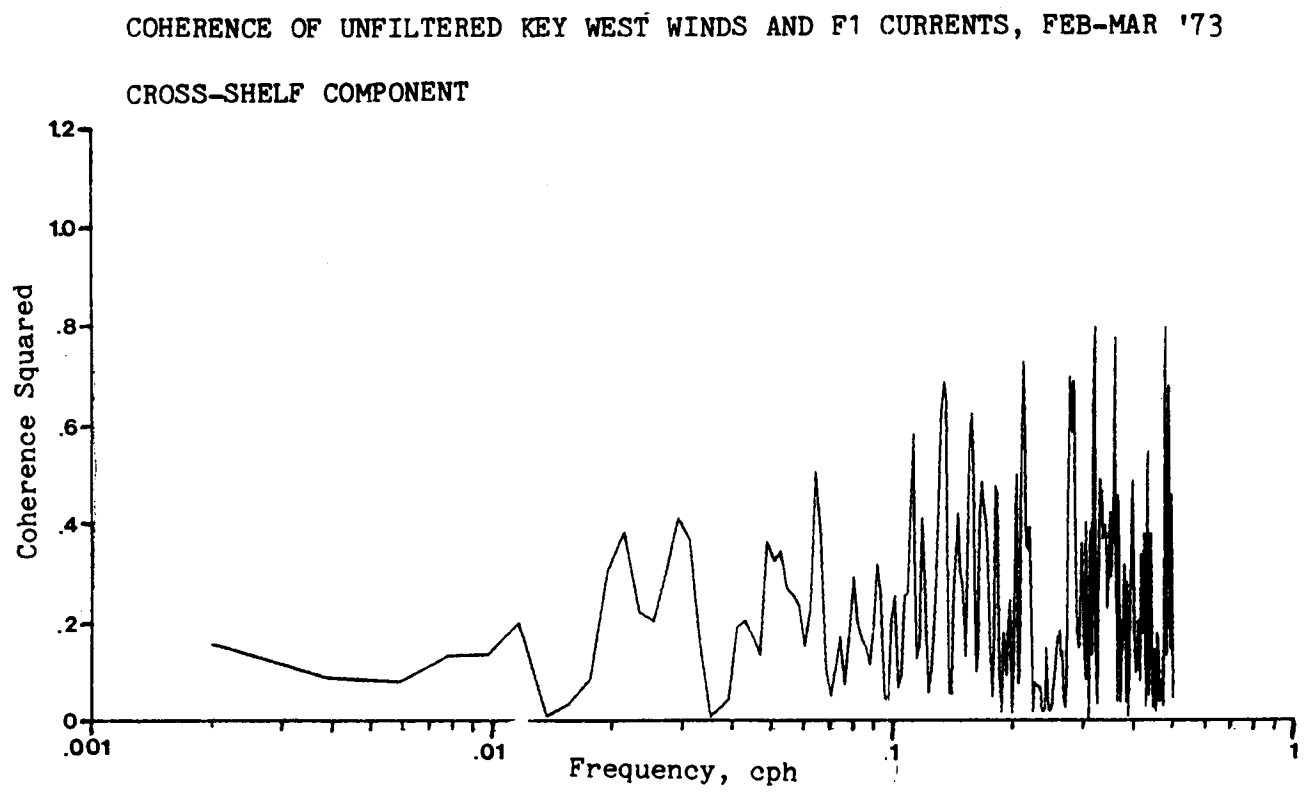

Figure B.3.8: Coherence of unfiltered Key West wind and currents at F1. Winter 1973 hindcast.

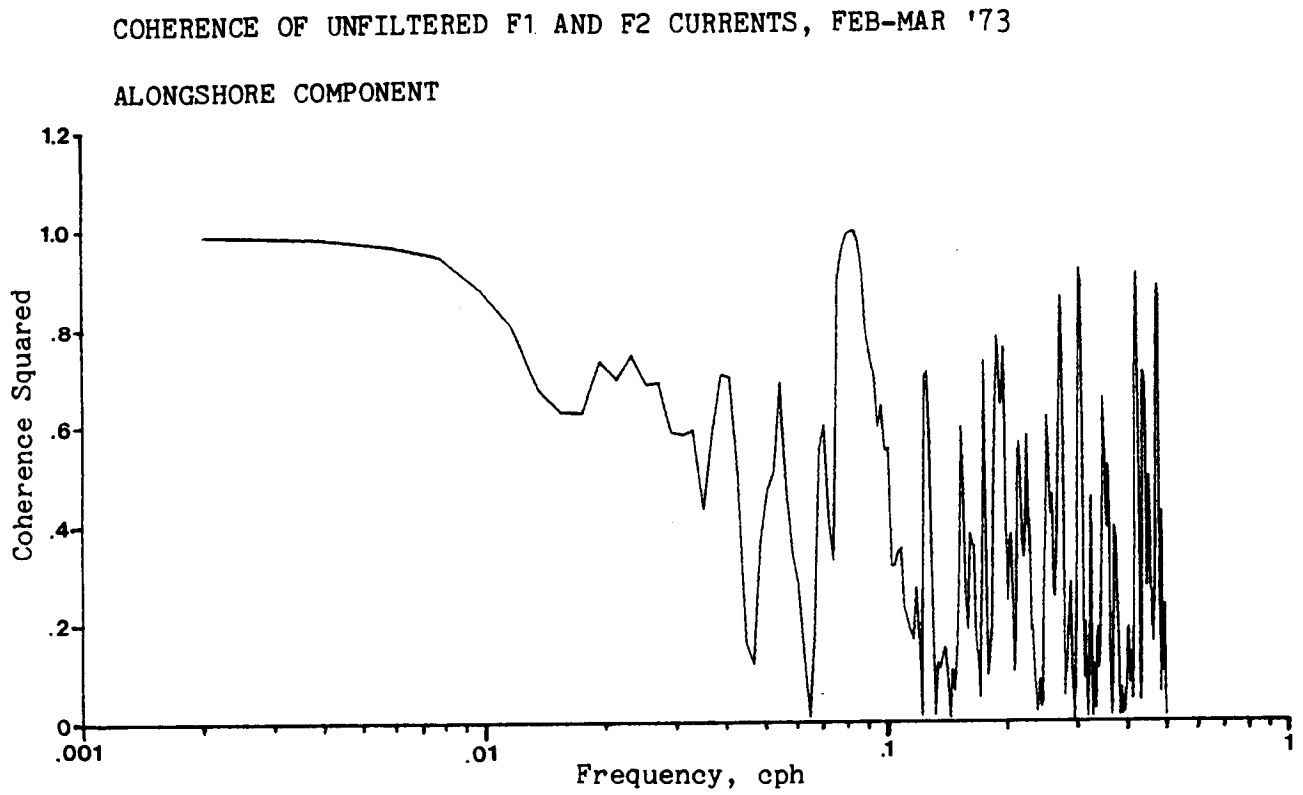

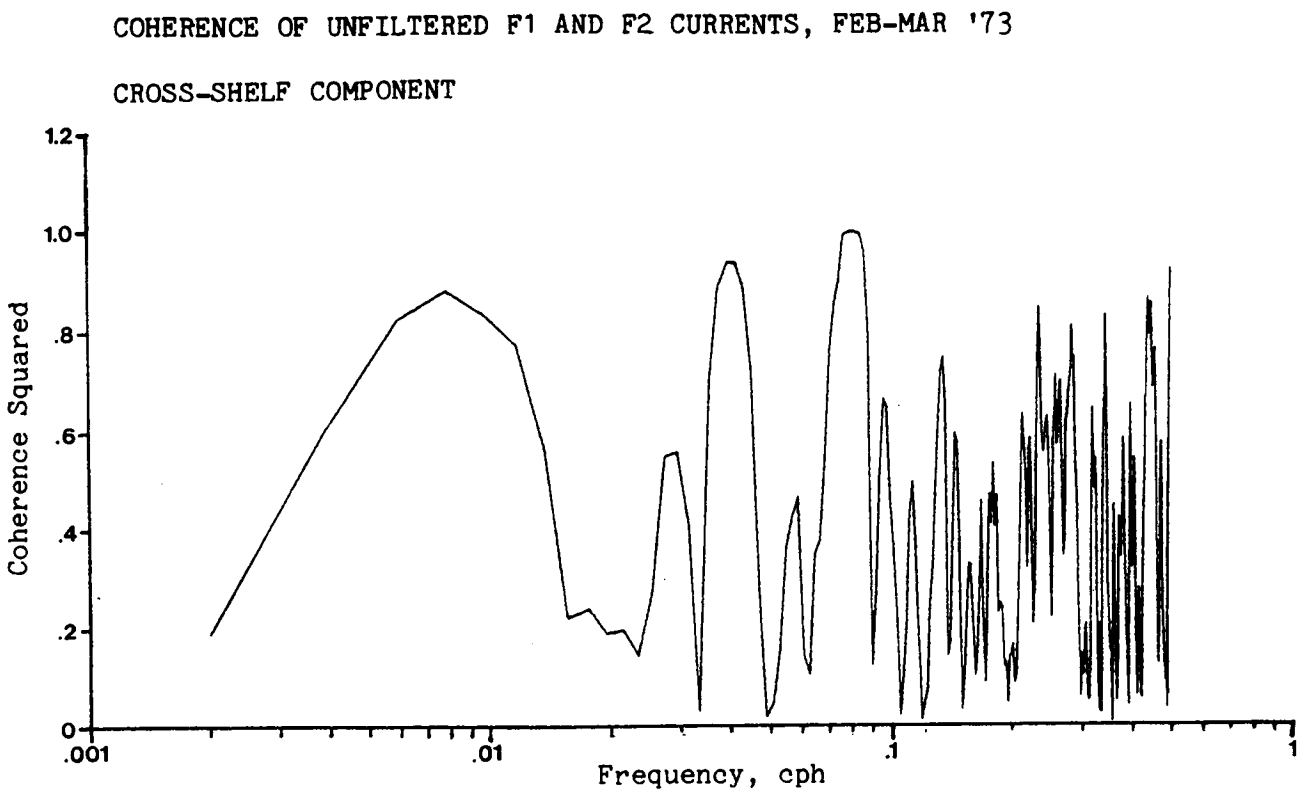

Figure B.3.9: Coherence of unfiltered currents at meters F1 and F2. Winter 1973 hindcast.

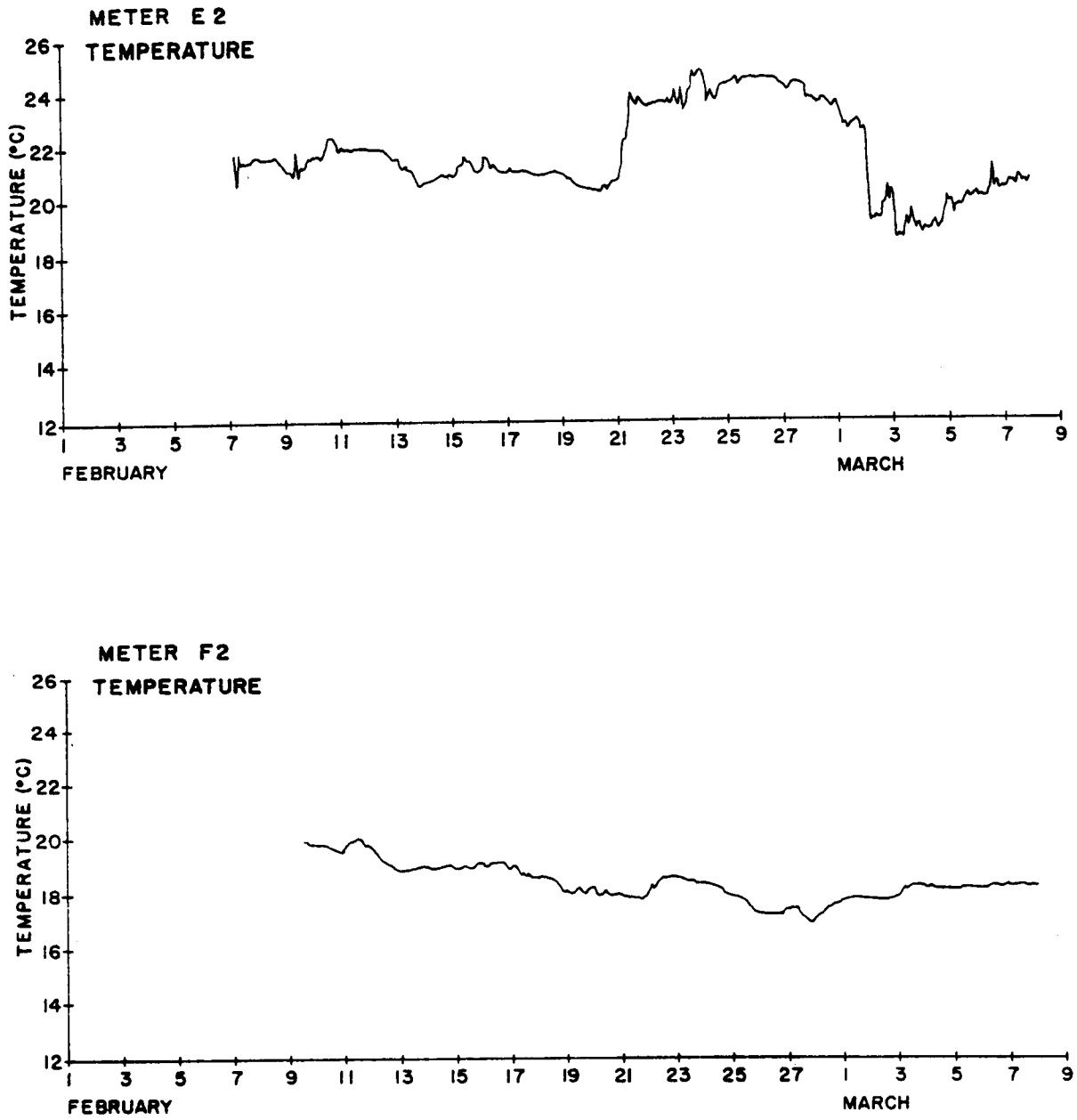

Figure B.3.10: Time series of temperature at stations E2 and F2. winter 1973 hindcast (Price and Mooers, 1974c).

vector average of the time series. A vector average of the SDE data indicate that meters at stations in 150 m or deeper display a net northerly flow while meters at the shallower sites display a net southerly flow.

Unfortunately, these measurements are almost certainly not indicative of long term drift in the area. The duration of the measurement period was only about 30 days which is of the same order as the period of the eddies dominating flow at the sites. Thus the net drift indicated in the calculations above is biased because it includes incomplete eddy cycles. It would take many months of consecutive data at a site before net drift calculations based on time series averages could be meaningful. Even with a duration on the order of several months, it is possible that time series averages may be significantly biased by a few exceptionally strong events. This biasing is probably why Niiler's long term drift currents show such diverse directions. Because of the short duration of the current meter record and the strong influence of the LC, it is impossible to construct a comprehensible picture of the long term drift currents on the WFS using the SDE data.

There still remains some hope of estimating net drift if we first understand the forcing processes involved. Based upon his review of meters near the break, Niiler has suggested that the currents there are dominated by the eddy wave field shown in Figure 2.5.1. In essence, Niiler suggests that the flow regime at the break is dominated by by barotropic eddies consisting of alternating warm (originating from the LC) and cold eddies (originating from the WFS). He further suggests that these eddies propagate onto the shelf, probably not penetrating any further than the 40 m isobath.

In Section 4.2 the propagation of barotropic eddies was investigated using the model. At this point it is useful to review the model results and compare them to the SDE data.

We proceed by first noting the following concerning stations C, D, and E: (1)

the currents are significantly more complex and variable (both in the vertical and horizontal directions) than currents at A, B, and F as demonstrated in the progressive vector plots in Figures B.3.6; and (2) the three stations are located within 30 km of each other and thus are essentially outside the resolution of the model grid of 30 km. These two observations suggest that it is impractical for the present version of the model to simulate currents at stations C, D and E.

For these reasons we will concentrate on sites A, B, and F. Currents at sites A and B can be simplified into three time periods with predominant flow directions: 7-16 February, northerly (7-21 for B); 17-28 February, southerly (22-28 for B); and 1-7 March, northerly. Average currents are 10 cm s^{-1} while maximum speeds reach about 40 cm s^{-1}. Currents at F can be broken into two time periods with predominant flow directions: 8-23 February, southerly; and 24 February to 5 March, northerly. Average currents are 10 cm s^{-1} with maximums of about 30 cm s^{-1}. Model runs with wind forcing indicate that the wind contributes a maximum of about 7 cm s^{-1} at F during the first period and essentially zero velocity during the second period.

Model run 13.21 corresponds to the forcing recommended by Niiler and the results are shown in Figures 4.2.8. The model starts at an arbitrary time so we would naturally expect a phase lag between the model and the data. This phase lag is easily resolved by comparing the periods identified in the data above with the various plan views shown in Figures 4.2.8. Such a comparison suggests that the data starting point of 7 February corresponds to model hour 48 (Figure 4.2.8a). At this time the model shows northerly currents at A (grid 3,11) and B (grid 3,9) of 25 cm s^{-1} and a southerly current at F (grid 7,8) of 10 cm s^{-1} which is consistent with the data for 7 February. Two days later (i.e. model=96, (Figure 4.2.8b) data=2/9), the comparison between modeled currents and data remain good. However, moving forward two more days (i.e. model=144 (Figure 4.2.8c), data=2/11), the model shows a shift to the south at all three stations, while the data remain unchanged from the

previous period.

Thus, the model indicates a reversal in current direction every 4, days while the data indicate a current reversal about every 8 days. In essence the wave front propagates northward in the model at about twice the speed implied in the data. The phase speed used in the model is roughly 50 cm s^{-1} (i.e. wavelength/period = 600 km/ 16 days), the average value recommended by Niiler. However, the model results suggest the phase speed be halved. This can be accomplished by either reducing the wavelength, increasing the period or both. Reducing the wavelength to 300 km and retaining the 16 day period will give a 25 cm s^{-1} phase speed but reversals in direction will still occur every 4 days. Only if we increase the period to 32 days and retain the 600 km length will the modeled current reverse every 8 days.

Figure B.3.11 compares observed currents with modeled currents using a forcing period of 32 days. Station A and F compare reasonably well although the model does not simulate the initiation of the third period at A very well. The model predicts currents at B well during the first period but does poorly during the second period.

LC EFFECTS ON OFFSHORE SURFACE ELEVATIONS

It is also of interest to look at surface elevations. Two offshore pressure gauges were deployed during the SDE study but they were not installed until April 1974. Nevertheless, the results are of interest and the low frequency time series are shown in Figure B.3.12. Note that the gauge located at station L2 malfunctioned, displaying an erroneous long-term drift. Comparing L2 and W1 suggests that the variance in the signal at L2 is reasonable. There are two oscillations of interest at the two gauges - one with a period of 10-100 days and the other of a seasonal nature (only evident at W1 because of long term drift of instrument at L2). The latter period is due to seasonal heating and possibly the seasonal migration of the LC.

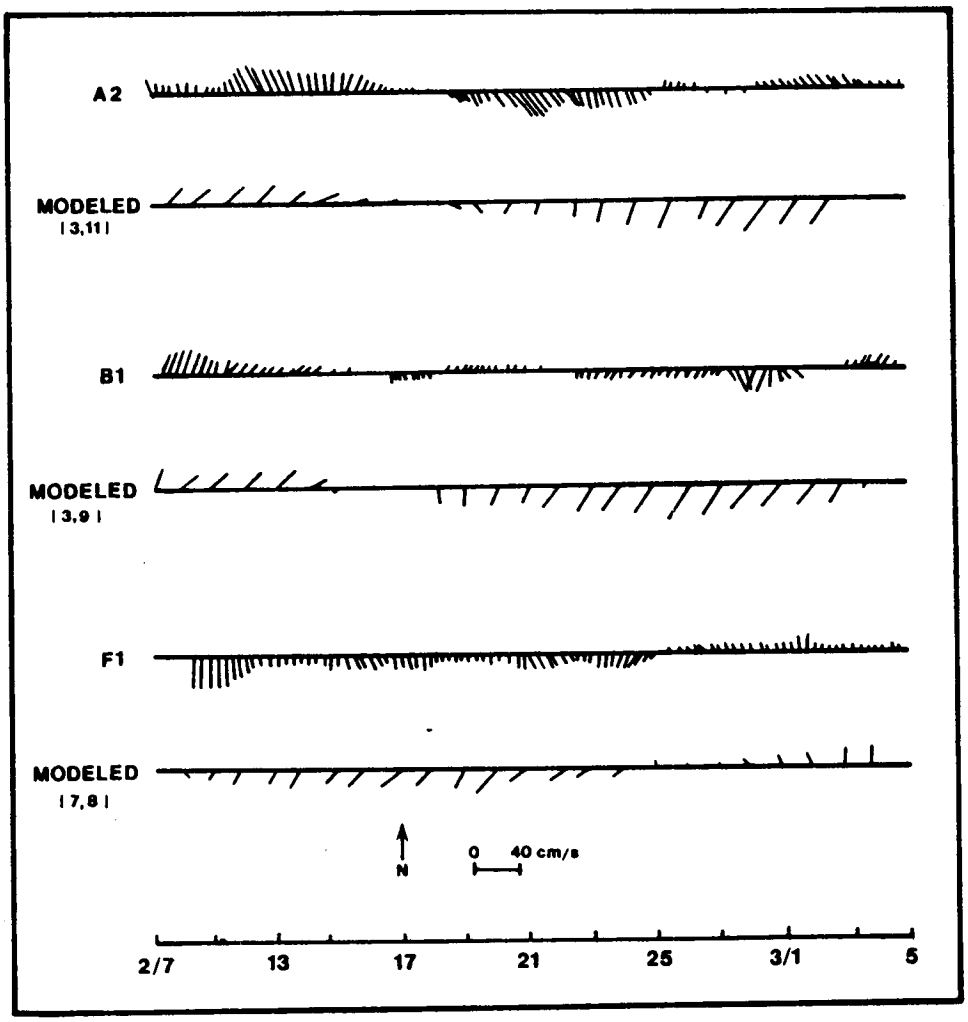

Figure B.3.11: Comparison of modeled and observed currents at sites A, B, and F. Model is forced with sinusoidal variation of wavelength 600 km and period 32 days.

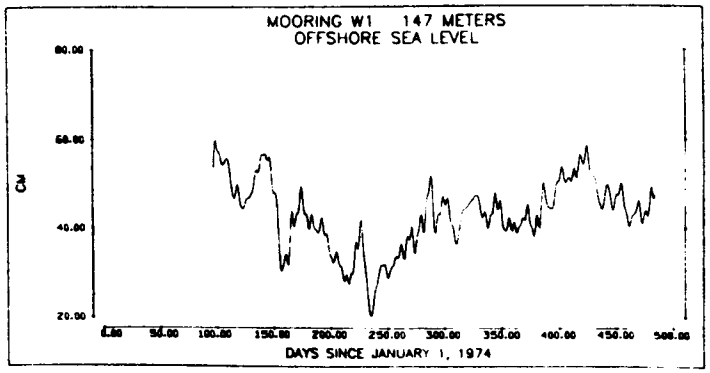

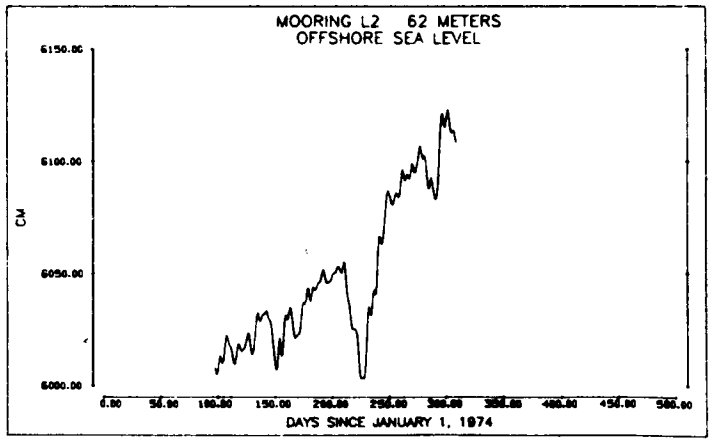

Figure B.3.12: Offshore sea level measured at station W1 and L2 (Koblinsky & Niiler, 1980).

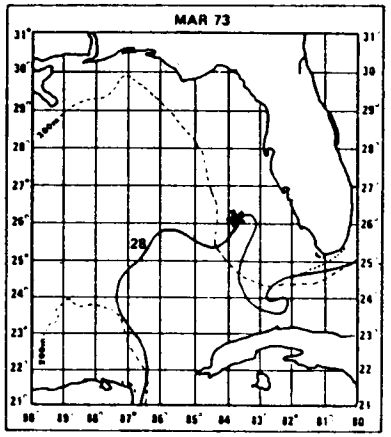

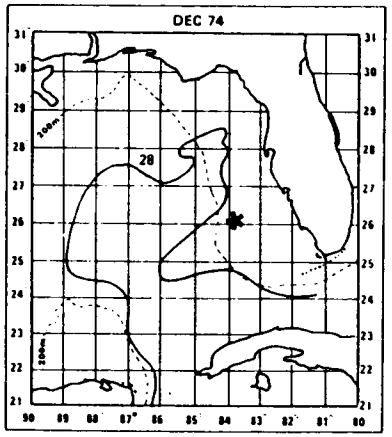

Figure B.3.13: Formation of warm intrusion along the WFS break (Vukovich et al., 1978). Star marks location of SDE array.

The 10-100 day oscillations are due to the migration of eddies. These appear to be of two types: a small amplitude (i.e. 3 cm), high frequency component with about a 10 day period and a higher amplitude (i.e. 10 cm), lower frequency component which appears to be linked to individual events of poorly defined periodicity. These events are clearly seen at both sites at about days 150, 240, and 300. The events have several interesting characteristics:

1. they are conspicuously absent at the St Petersburg and Naples coastal tide gauges;

2. each event lasts about 5-10 days; and

3. events at L2 are characterized by a sudden drop in pressure below the running mean; i.e. the events are warm tongues or eddies. There are apparently no events consisting of sudden cold, intrusions at L2.

The observed surface elevations contrast markedly with the model results. At the offshore stations, the model (using a 32 day period of oscillation) creates a surface amplitude of 10 cm at W1 (4,12) and 15 cm at L2 (7,12). These are about a factor of three larger than the amplitudes of the equivalent oscillations observed at W1 and L2.

At Naples and St. Petersburg, the model yields surface elevations of 25 cm. Though no comprehensive study of LC effects on coastal elevations has yet been completed, several researchers have investigated low frequency coastal surface fluctuations, most notably Marmorino (1981) and Mitchum and Sturges (1981). These studies as well as Sturges (personal communication, 1982) suggest that if the LC does influence coastal elevations it should be by no more than 5-10 cm. This is an order of magnitude less than predicted by the model.

These results are alarming and suggest that the model forcing and/or the cross-shelf energy transfer are overstated. Given previous tuning of N_v and

c_b, the only way to control the latter is to decrease N_h. If this is done to the degree necessary to decrease coastal elevations to a more reasonable 5 cm then modeled velocities at A, B, and F are much too small. One might also try to increase the forcing at the shelf accompanied by a decrease in N_h. There are two difficulties with this. First it would be difficult to justify a larger value for the shelf forcing on physical grounds and secondly, it appears impossible to find a value for N_h which will be low enough to decrease coastal surface elevations to O(5 cm), yet large enough to maintain a velocity of O(10 cm s^{-1}) at station F.

SUMMARY OF MODELING LC EFFECT VIA AN EDDY WAVE FIELD

In summary, forcing the model with the eddy wave field reproduces the SDE currents on the shelf reasonably well, but the model predicts excessively large values for the surface elevations. The situation cannot be rectified by manipulating the tunable parameters in the model. Some potential reasons for this shortcoming are:

1. the baroclinic component of the eddies has been ignored yet the hydrographic data show substantial baroclinicity is often associated with the eddies;

2. a monochromatic wave was implemented in the model to simulate the eddy wave forcing at the western boundary but spectral data indicate the eddies contain a broad band of energy which is far from monochromatic;

3. the currents at the model boundary used to drive the flow have been assumed to vary as 100 cosine($0.7z\ H^{-1}$), where H is the local water depth, z is the distance from the surface and the units of velocity are cm s^{-1}. This simple function contrasts with the complex vertical variations sometimes observed in the current data;

4. the sharp bathymetric gradient near the break may be inadequately

simulated in the model because of discretization error resulting from the rather large model grid size of 30 km. This may ultimately cause errors in the modeled velocities since the data do indicate a strong dependence of velocity on topography at the deeper levels; and

5. eddy advection onto the shelf is approximated in the model via a linear lateral eddy viscosity term. It is probable that the nonlinear advective terms which are neglected in the model are frequently important when attempting to model the eddies and thus neglect of these terms may be a source of error. A similar problem may arise with the linear bottom friction coefficient particularly in the shallow shelf waters.

EVIDENCE FOR LATERAL SHEAR OF SHELF WATER BY THE LC

While it is difficult to investigate the Niiler suggestion further with existing data it is possible to explore an alternative hypothesis. Suppose that Niiler's suggested eddies do not migrate far onto the shelf but move primarily northward along the break which serves as a wave guide. Further suppose that the major effect of the LC at stations on the shelf is via a southerly drift due to a diffusion of momentum from the LC which is occasionally interrupted by the invasion of warm eddies or tongues from the LC. There is certainly some qualitative evidence in the infrared satellite photography to suggest the occurrence of such events (e.g. Figure B.3.13).

Further evidence for this hypothesis appears in the hydrographic data from the Winter 1973 experiment. Figure B.3.14 shows STD profiles from section 6 taken during 7-9 February 1973, within one day of the deployment of the meters at the three sites. The center of a warm eddy or tongue is evident at station 319. Indigenous shelf waters occupy the region from about the 100 m isobath to the coast. For the purposes of this discussion, the 22^{o} C isotherm has been assumed to be indicative of LC water.

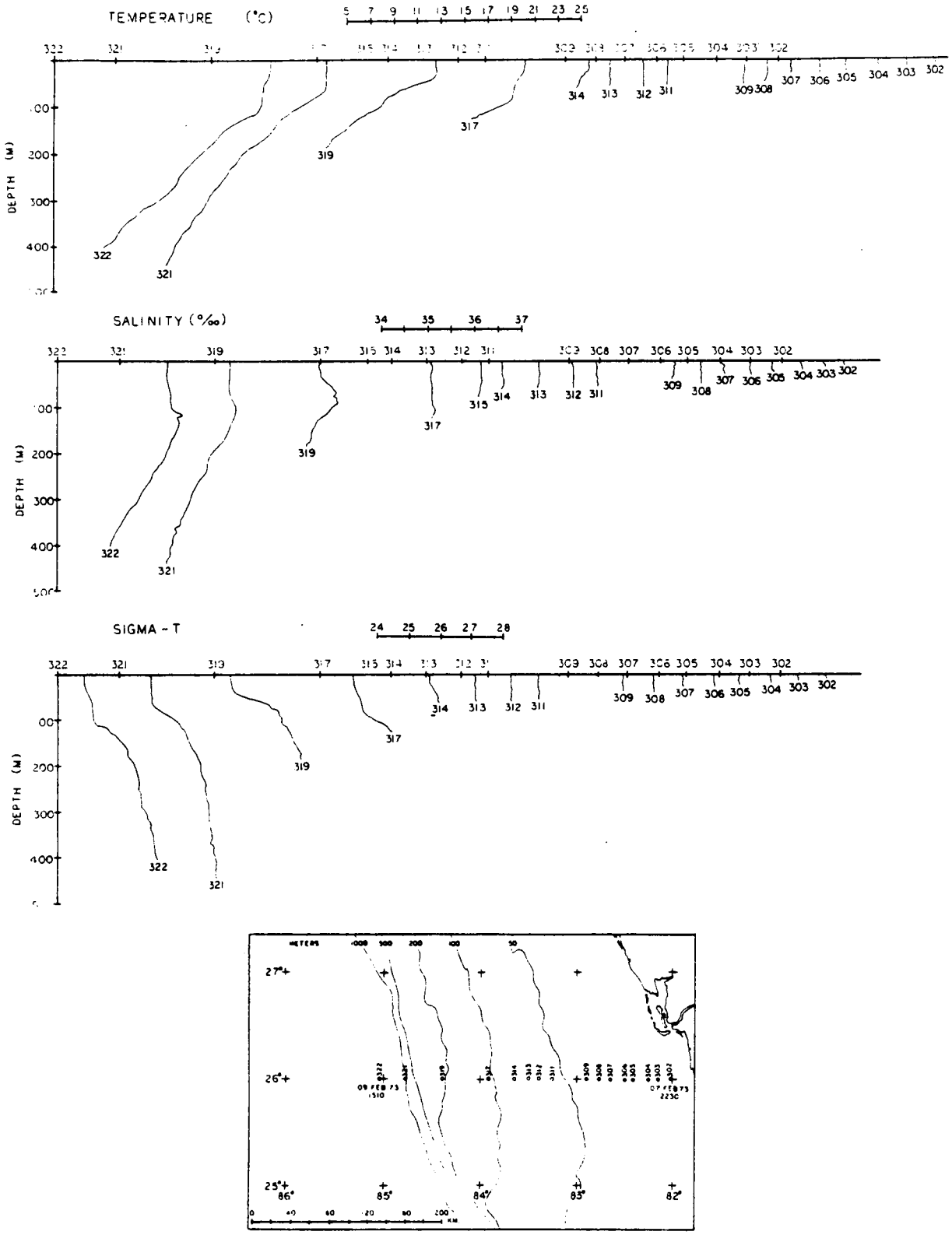

Figure B.3.14: Hydrographic section 6, February 7-9, 1973. (Price and Mooers, 1974d).

Section 6 also shows a simple hydrographic structure on the shelf, with vertical isotherms and isopycnals. A similar picture of relatively quiescent thermal conditions on the shelf is shown in sections 7 and 8 taken over the following four days. It should be noted that the hydrographic reports by Price and Mooers (from which Figure B.3.14 is taken) also include STD contours interpreted from the STD profiles but the contours should be reviewed with caution as there are a number of misleading interpretations.

Figure B.3.15 shows STD profiles and contours from section 10 taken about four days later. The profiles imply little change over the intervening four days - the eastward edge of the LC remains at about the 100 m isobath.

No other sections are available in the area until section 16, taken 11 days later during 24-26 February (Figure B.3.16). The contours have been shown in this figure so that the complex LC intrusion is more readily apparent. It is unclear from the STD data whether the eastern edge of the front has reached the 50 m isobath at this point, but section 20 (Figure B.3.17) strongly implies that the front had reached the area by 1 March. Section 21 (Figure B.3.18) taken 2 days later implies that the eastward extent of the front has not moved appreciably (as indicated by the position of the 22°C isotherm located at about the 50 m isobath).

The exact nature of the front is indeterminate because of the lack of hydrographic data. One possibility is that the contours shown in B.3.16 reflect the presence of a large, cyclonic cold-cored eddy. Another possibility is that the cold section centered at 84° 20' W is a cold water tongue with the main body of the LC adjacent on the left and a warm tongue of LC water on the right. In the following discussion, the intruding LC waters will simply be referred to as a "front".

The passage of a front is also traced in the current measurements at sites D, E, and F. From Figure B.3.6, we see a strong southerly drift at all sites from the time of deployment on 8 February until about 21 February when we

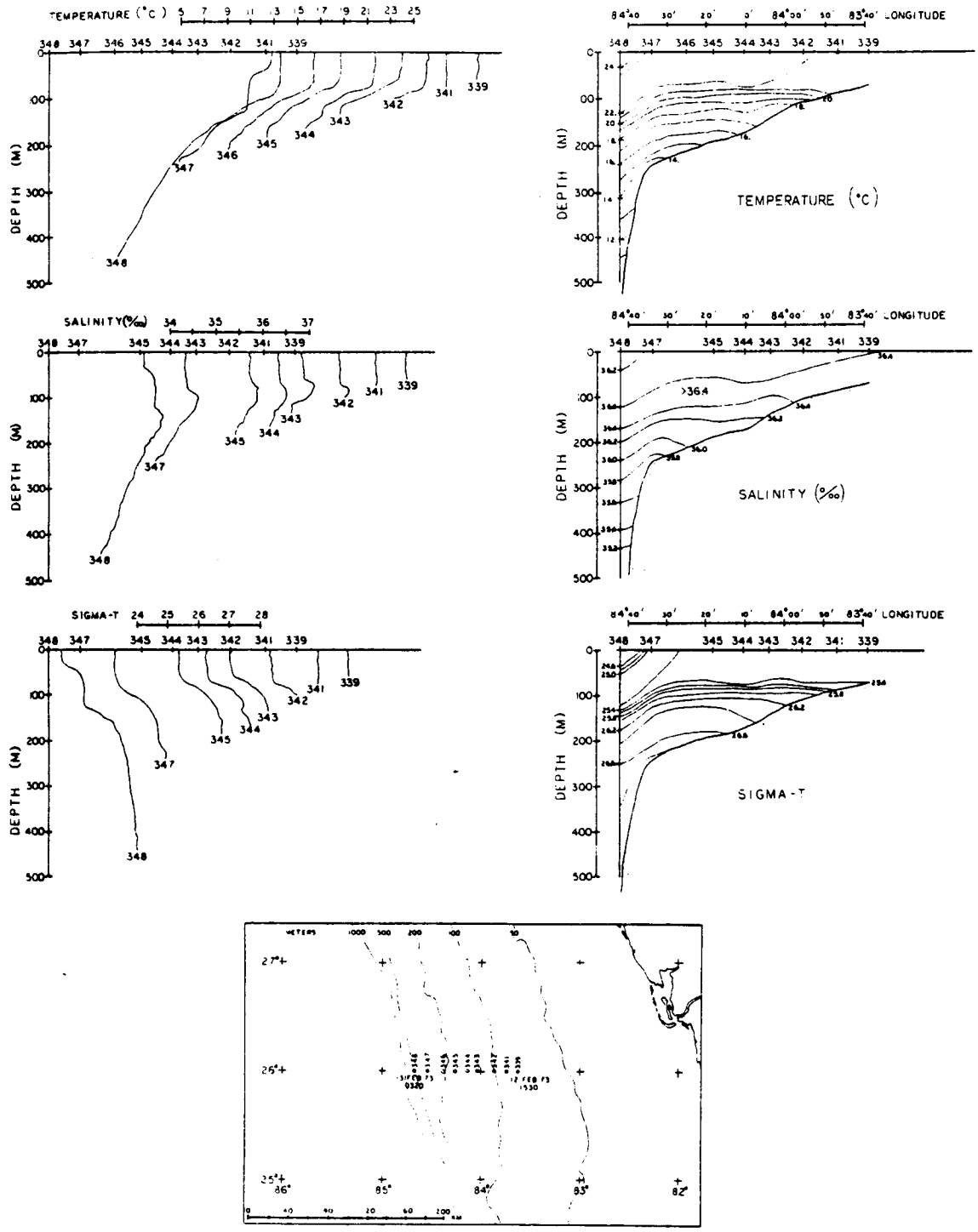

Figure B.3.15: Hydrographic section 10, February 12-13, 1973. (Price and Mooers, 1974d).

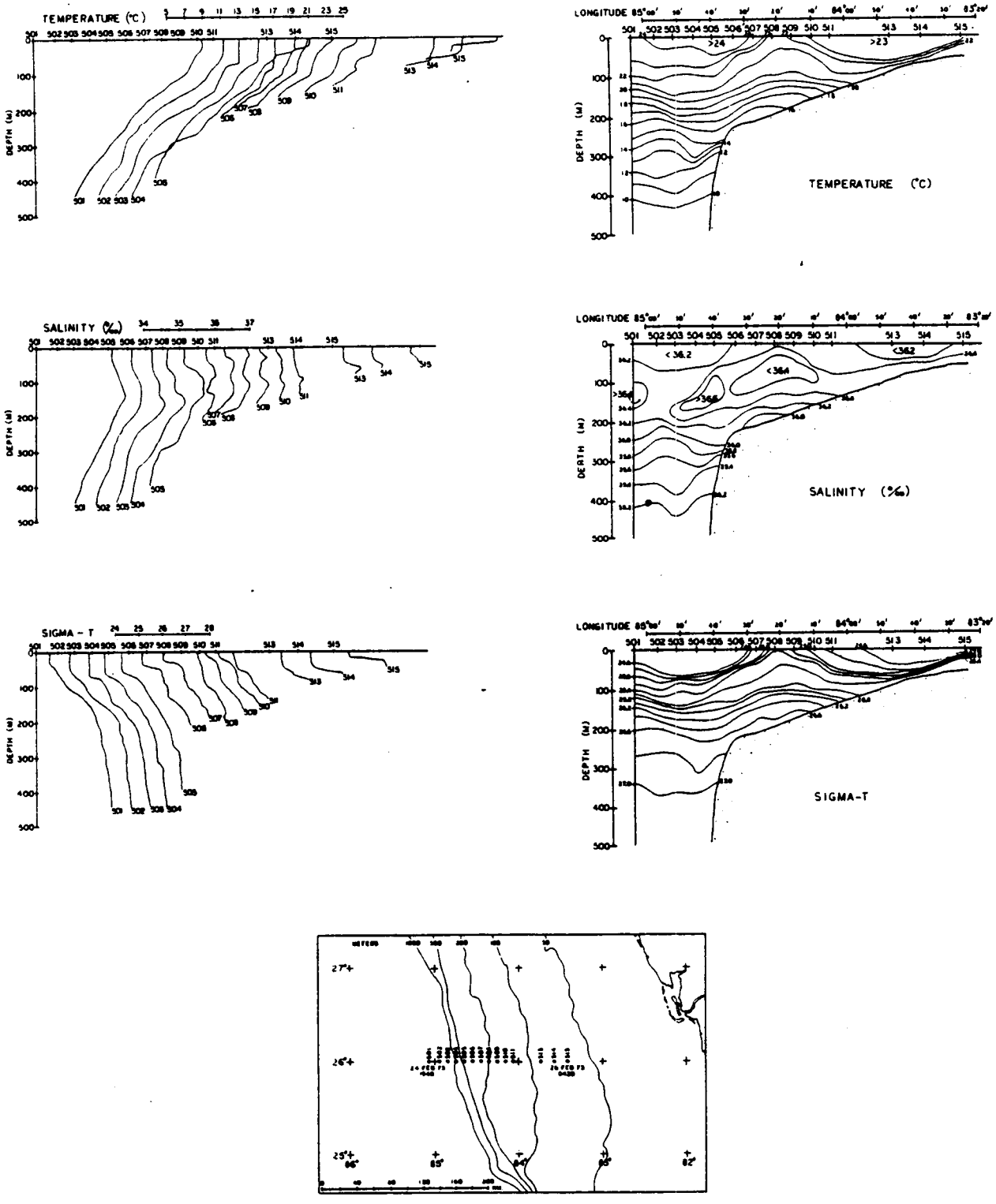

Figure B.3.16: Hydrographic section 16 February 24-26, 1973. (Price and Mooers, 1974d).

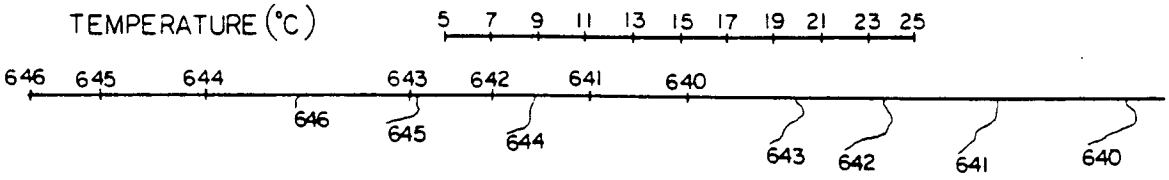

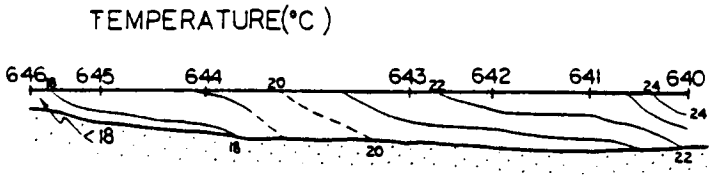

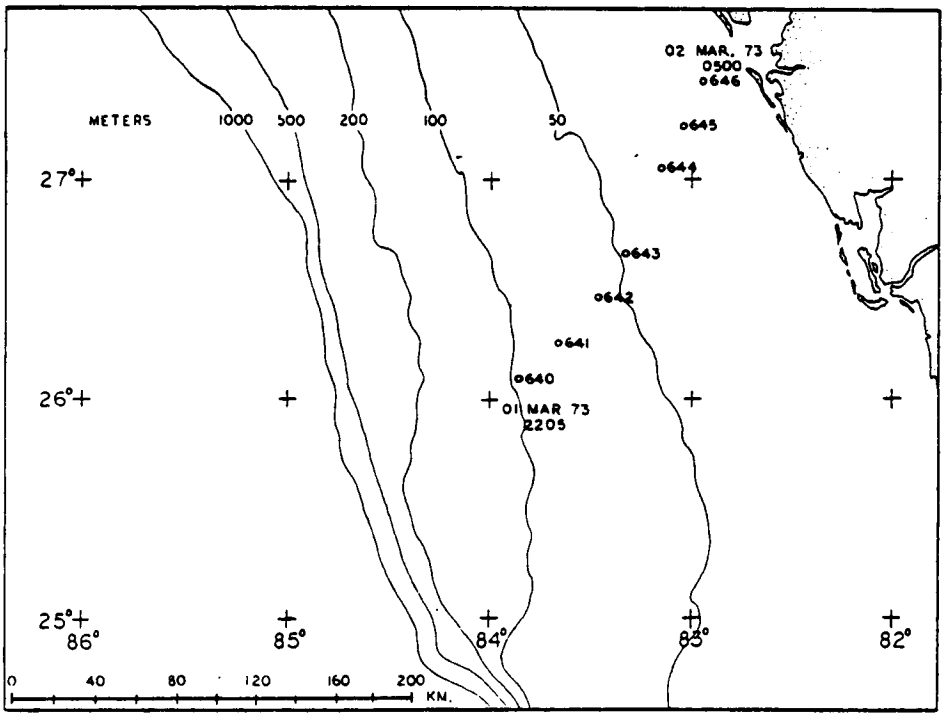

Figure B.3.17: Hydrographic section 20, March 1-2, 1973. (Price and Mooers, 1974d).

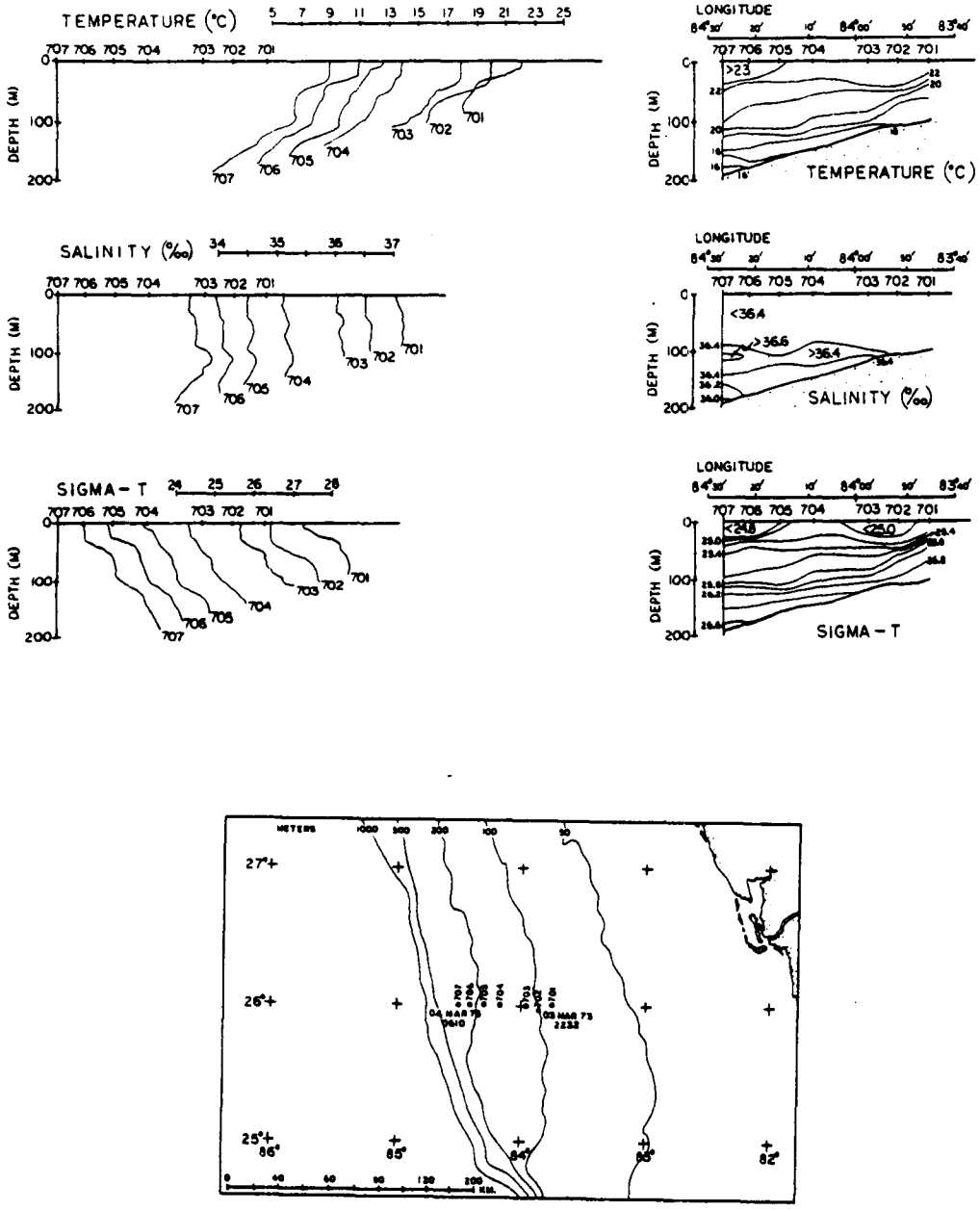

Figure B.3.18: Hydrographic section 21, March 3-5, 1973. (Price and Mooers, 1974d)

observe a sharp jump in the temperature record at D and E (e.g. Figure B.3.10). The temperature shift is accompanied by a reversal in current direction at D and E to the north corresponding to the approach of the eastward edge of the front. The front passes station E on about the 26th of February and station D on the 2nd of March as demonstrated by the rapid reversal in current direction shown in Figure B.3.6 and hydrographic section 16 (Figure B.3.17). Currents and temperature appear to recover their background values on about 3 March but only for a couple of days. Subsequent hydrographic data and the last few hours of the upper meters at E and D imply that another front begins to impinge on the area on about the 5th of March.

Currents at Station F are not affected by the eddy until about 27 February when the currents reverse and become primarily northerly. This direction persist to the end of the record on 8 March.

The ability to clearly observe the rapid spatial variations in density and currents associated with impinging LC waters is enlightening. The dynamics of the front are in clear contrast to the relative quiescence that was apparent on the shelf during 8-20 February. The homogeneous nature of the density and current field during this time period implies that the southward currents were not due to LC intrusions, but rather a net southerly drift on the shelf due to a larger scale lateral shear imposed on the shelf waters by the LC.

It would be desirable to test this hypothesis with other data from the SDE. The offshore pressure gauge at the 60 m isobath supports the hypothesis since it indicates the passage of fronts which occur on a nonperiodic basis. The only other SDE data on the shelf were taken during the Fall experiment, October-December 1973. Regretfully, there was only one meter at the 50 m isobath and it was deployed for just 30 days. Also hydrographic data were limited, consisting largely of time series at one stationary location.

WINTER 1973 DATA SUMMARY

In general, the conclusions which can be drawn from the data regarding LC effects on circulation on the shelf are severely limited by the short duration of the current meter record at the shallow water site. Nevertheless, the following observations are offered:

1. The offshore winds are dominated by the passage of cold fronts every 7 to 10 days.

2. The currents near the shelf break are apparently dominated by eddy fields shed from the LC consisting of alternating cyclonic and anticyclonic eddies. The eddies induce currents with a period on the order of 15 days and maximum amplitude of 50 cm s^{-1}. The temperature fluctuations associated with passage of the eddies are approximately $4^{o}C$.

3. Niiler suggests flow on the shelf is dominated by eddies similar to those observed at the break, the difference being that the shelf filters some of the eddy frequencies. The eddies would result in no net advection over climatological (on the order of months) time periods.

4. An alternative interpretation of the shelf data suggests that a general southerly flow is induced by large scale lateral shearing of shelf waters by the LC. Warm fronts occasionally migrate from the LC onto the shelf and cause significant flow reversals of the order 10 cm s^{-1}.

5. Currents at sites with water depths in excess of 100 m are negligibly correlated with wind. Currents at sites in shallower water are only weakly correlated to the wind.

6. It is difficult to infer net drift from a vector average of the data unless the duration of the measurement period is on the order of many

months. With shorter durations, it is likely that the calculation will be biased by a few extreme events or that a non-integral number of eddy cycles will be measured.

APPENDIX C

Publications by NECE personnel on the WFSCM

Circulation Study of the Western Florida Shelf

Cortis Cooper and Adrian H. Humphreys, III

New England Coastal Engineers, Inc.
Bangor, ME 04401

ABSTRACT

The paper is based on a study being funded by the Bureau of Land Management (BLM). The primary purpose of the study is to develop a numerical circulation model which can provide accurate current velocities for oil spill impact assessment. Besides the relevance to other sites of potential offshore petroleum development, the study which is described is also pertinent to calculation of currents during extreme storm events, a problem of particular interest in design and construction of offshore structures including OTEC plants. The paper describes the West Florida Shelf Study and summarizes the existing oceanographic and meteorologic data which has been identified and archived during the study. Some of the mechanisms which govern flow in the region are identified and discussed. The 3-dimensional model used in the study is briefly described as are the modeling techniques that to be used in upcoming phases of the study.

1. INTRODUCTION

The primary purpose of the West Florida Shelf Study is to provide accurate current velocity predictions to be used as input into the USGS/BLM oil spill trajectory model. Local winds are included in the USGS/BLM model and so the study will focus on modeling of currents driven by climatalogical events with characteristic time scales on the order of weeks and months. Modeling is to provide currents at the surface, mid-depth and bottom of the water column and thus a fully 3-dimensional model is necessary. A secondary purpose of the study is to assess the available data base, identify data gaps, and recommend future data collection efforts needed to improve modeling accuracy. Model sensitivity studies will help provide the latter information.

The study area is shown in Figure 1. BLM is mainly interested in the southeastern region of the shelf extending from the coastline to the 100 meter bathymetric contour. However, due to modeling considerations, the region to be modeled will include the entire shelf from the Florida pan-handle to the Keys, and seaward to at least the 200 meter bathymetric contour for much of the shelf.

The West Florida Shelf Study began in November 1980 and is scheduled for completion in May 1982. Conceptually, the study can be broken into three major work tasks: (1) assembling, reviewing, and analyzing data, (2) modeling of currents including model tuning and verification; and (3) conducting a workshop.

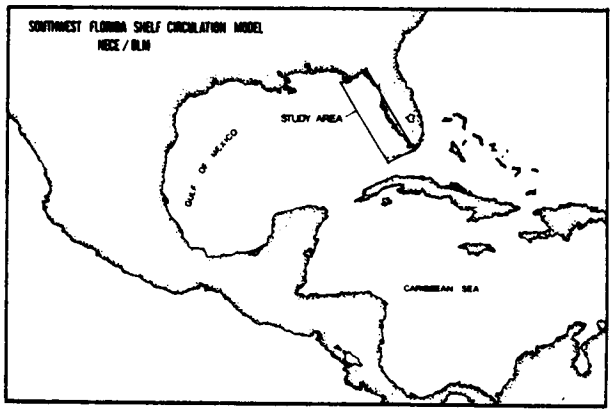

Figure 1: West Florida Shelf Study Area

The workshop, entitled the "Gulf Circulation Studies Workshop", was held in New Orleans on May 14 and 15. Seventeen eminent oceanographers and meteorologists who have specialized in Gulf circulation attended the conference with the purpose of:

- identifying the important circulation processes in the Gulf;
- identifying gaps in the existing data base;
- establishing a set of priorities for future data collection efforts; and
- outlining a three-year data collection program for the Gulf.

Proceedings of the workshop have recently been published and are available upon request.

Circulation on the shelf is driven by many processess including winds, astronomical tides and the so called Gulf Loop Current. The latter process exerts a particularly complex influence on shelf circulation as indicated in Figure 2 which is an infared satallite photo of the region. The Loop Current can be seen as the dark water mass

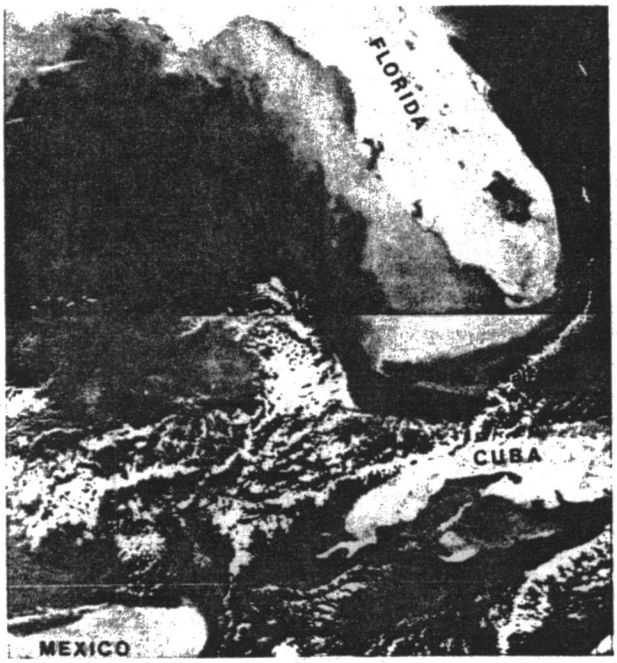

Figure 2: Infared Satellite Photograph of Study Area

entering through the Yucatan Channel, looping northward of Cuba into the Gulf, and exiting through the Florida Straits. A large eddy on the order of 200 km appears to have detached from the Loop Current and is migrating northward. Huh et.al(1) has shown these eddies to migrate within 8 km of the coastline. Also shown in the figure is a zone of lateral shear extending along the shelf break and appearing as wispy, dark strands representing the propogation of warmer Loop Current water onto the shelf.

Not only does the Loop Current exhibit a complex spatial variation, it displays an equally complex temporal variation. Figure 3 shows the extreme positons of the Loop Current during the four year period between 1974 and 1977 as reported by Vukovich et al. (2). Roughly 20 years ago Leipper (3) hypothesized that the Loop Current displayed an annual cycle. Molinari et al. (4) and Maul (5) used satallite data in the mid 70's to support the hypothesis. However, recent modeling by Hurlbert and Thompson (6) has indicated the cycle is probably closer to 300 days. In light of these results, Maul (7) examined new data and re-analyzed older data. He tentatively concluded that the data does indeed support the Hurlbert and Thompson findings. The frequency of the cycle will likely not be resolved in the near future in part because much of the data base originates from infrared satellite photos. Substantial data gaps exist in the satellite data base during periods of cloudiness and during the summer thus making it difficulte to resolve the cyclic frequency. Studies are planned during the upcoming BLM sponsored three-year data collection program which should help resolve this issue.

2. SUMMARY OF EXISTING DATA BASE

Figures 4 and 5 show the spatial and temporal distribution of the major data sources available for the region. Each of these sources is discussed in more detail below.

2.1 Shelf Dynamics Experiment

This study produced the most extensive set of current meter data for the Florida Shelf. Data was collected intermittently over a period of two years, from February 1973 to May 1975. Responsibility for the experiment was shared by Nova University, the University of Miami, Florida State University, and the University of Washington. In addition to velocity data, water temperature and surface level recordings were taken. Extensive analysis has been performed on the data by Price et al. (8), Koblinsky and Niiler(9), Plaisted et al. (10), and Niiler (11). Niiler (11) reports the following with regard to his interpretation of the data:

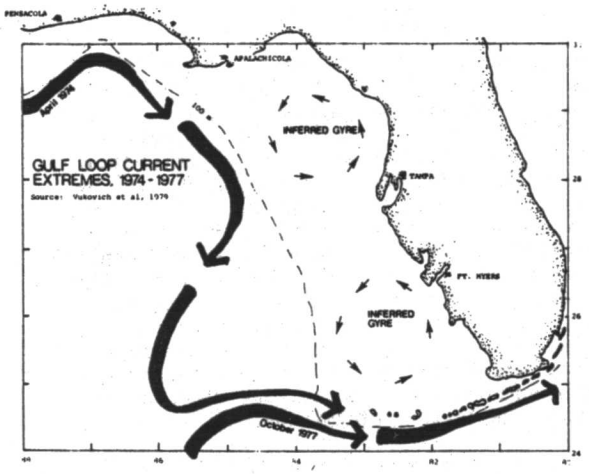

Figure 3: Gulf Loop Current Extremes between 1974-1977

*Numbers in parentheses refer to References listed at end of paper.

- winds : southeast trade winds dominate the region in summer. Cold front passages every 5 to 10 days dominate the winter weather.

- hydrographic conditions : south of latitude 25° N the Loop current adjoins the shelf all year. The Loop Current is marked by high salinity of 36.6% and its intrusions on the shelf can be identified by the occurance of high salinity water masses. In summer the mixed layer depth is about 30 meters, increasing in winter to 100-150 meters with the temperature of the mixed layer decreasing as one moves toward the shore on the shelf.

- currents : winds do affect currents in the winter, but no correlation exists between winds and currents in the summer. In water 100 meters deep, there was generally a southward drift at 40 m over the 8 month period examined. The drift was northward at the 80 m in summer and southward at 80 m in winter. In water 150 meters deep, bottom currents are northward in summer, southward in winter.

2.2 FSU - Cedar Keys Current Meter Data

In February 1978 four current meters were deployed at two stations on the northwest shelf in 44 and 22 meters of water. Prior to the West Florida Shelf Study no analysis had been attempted on the data. Because the data is the only high quality data in the northern portion of the shelf considerable time has been spent during the study in examining the data. Figures 6 and 7 show standard stick plots of the winds and velocity

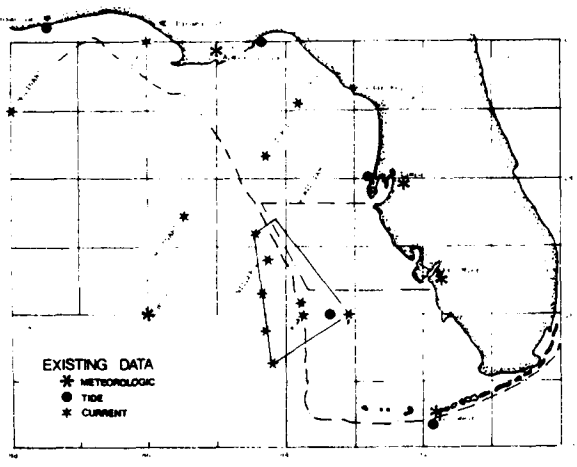

Figure 4: Sites of Major, Existing Oceanographic and/or Meteorolgic Data Sources

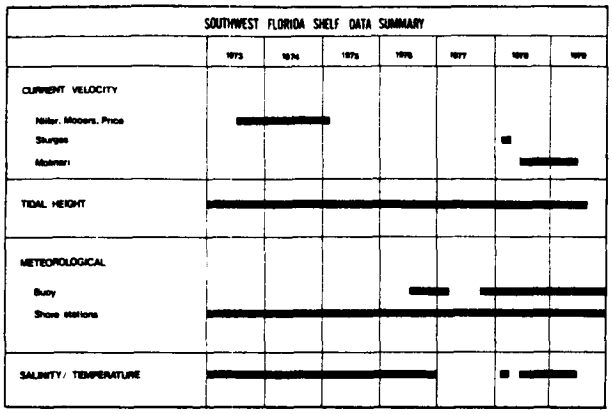

Figure 5: Temporal Distribution of Major Data Services

data taken during the study. Winds were actually recorded at a National Data Buoy Office (NDBO) weather buoy moored off the shelf approximately 200 km from the current meter moorings. Though the weather buoy is somewhat far from the current meter sites it was felt to be more representative of wind at the sites than was wind data collected at surrounding land-based stations.

The data shown in the two figures has been filtered of tidal frequencies using a Doodson filter. A strong correlation is apparent between the wind and the currents at both stations and at both depths, although the correlation is less strong at the deep offshore meter. Further studies including spectral analysis are presently underway to quantify the observed correlations.

2.3 OTEC Current Meter Data

Temperature, velocity and salinity data were collected and reported by Molinari (12) at a potential OTEC site off the northern Florida Shelf. Four meters were installed at nominal depths of 150, 250, 550, and 950 meters in 1000 meters of water from June 1978 through June 1979. Though the site is somewhat removed from the region of primary concern for this study, Molinari does offer some interesting and relevant conclusions such as:

- tidal energy constitutes only a small fraction of the total energy;

- roughly 10% of the average speeds exceeded 22-25 cm/s at all depths. Approximately 50% of the average speeds exceeded 10 cm/s at all depths;

- a maximum speed of 70 cm/s was recorded at 150 m depth coincident with a cold front passage;

- on average the flow was to the northwest at all depths;

- effects of the Loop Current were not generally detectable except for one occurance when the Loop Current reached to within 50 km of the site; and

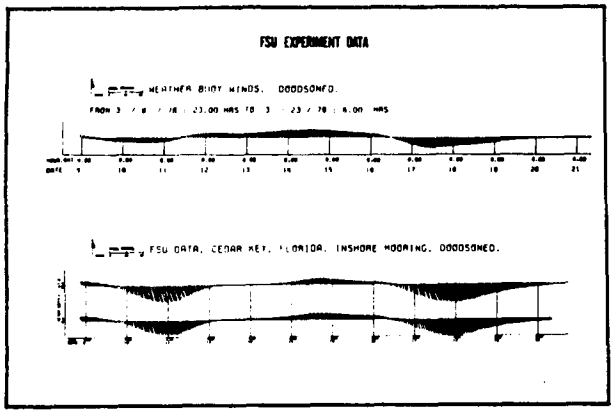

Figure 6: Wind and Current Time Series for Inshore FSU Data (Water Depth = 22m)

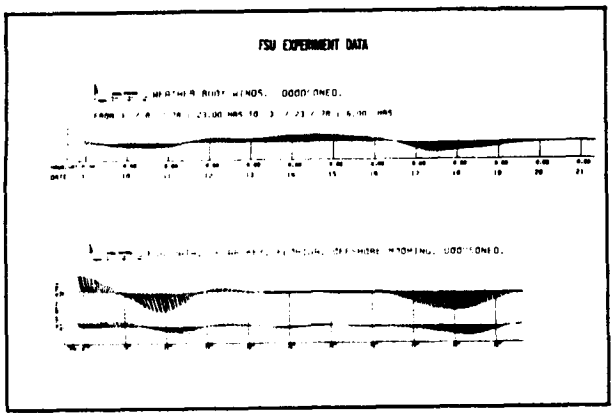

Figure 7: Wind and Current Time Series for Offshore FSU Data (Water Depth = 44m)

- mixed layer depths ranged from 60 m in winter to 5-10 m in summer.

2.4 Drift Bottle Data

Three major drift bottle studies have been conducted along the shelf. Project Hourglass, reported by Williams (13), lasted 28 months from 1965 to 1967. Surface drift bottles were released periodically from 16 sites on the shelf between Ft. Mevers and Tampa. Two interesting phenomena are apparent from the Williams data:

- releases on the inner shelf region were equally likely to drift either north or south during the months April through September, and

- releases on the outer shelf consistently exhibited southward drift, except for the months of August and September in 1965 and again in 1967 when releases exhibited a northward drift.

Drift bottle data was also taken from September 1960 through December 1962 and is reported by Tolbert (14). Releases were made from a platform 20 km off Panama City, Florida. Most of the bottles were blown ashore between Cape San Blas and Pensacola on the north Gulf coast, but 20% of the bottles were carried by wind-induced surface currents to the Loop Current and recovered in the Florida Keys or the east Florida coast.

The third major drift bottle study is reported by Gaul and is graphically summarized by Ichiye, et al. (15). Releases were made off the Pensacola-Panama City area in somewhat deeper water than Tolbert's. The study period extended from April 1963 to October 1964. Releases typically ended up on the east Florida Shelf and Florida Keys. However during certain periods, a significant number of releases ended up on the Texas and Mexican Gulf coasts. A small but significant portion of releases (i.e. 10%) were typically found along the west Florida coast for many of the releases.

2.5 Surface Elevation Data

National Ocean Survey gauges have been located at four land stations along the west Florida coast at Key West, Tampa (Clearwater), Appalachicola (Shell Point), and Pensacola and data is available for much of the last decade. The only surface elevation data on the shelf was taken during the Shelf Dynamics Experiment (see section 2.1 above).

2.6 Meteorolgy Data

Met data is available for most of the past decade from four National Weather Service land stations at Key West, Ft. Meyers, Tampa, and Appalachicola. In addition an NDBO weather buoy has been located approximately 200 km off the shelf and data is consistenly available for the past 4 years.

2.7 Hydrographic Data

Some hydrographic data is available on the shelf. Cruises were made in the region during the early 70's and available at NODC. Salinity and temperature data from current meters are available from the Shelf Dynamics Experiment, FSU study, and OTEC site study.

3. CIRCULATION MODEL

The model, GAL, which is being used in the West Florida Shelf Study takes its name from the Galerkin numerical technique upon which the model is based. Model formulation is founded on the description of the vertical variation of the horizontal velocity by a series expansion (Heaps (16, 17)). A thorough description of the model is included in Pearce and Cooper (18).

3.1 Governing Equations

The model is based on the Navier Stokes Equations which, after some simplifying assumptions, can be written in the form used in the model as:

$$0 = \frac{\partial u}{\partial t} + \frac{\rho s}{\rho} g \frac{\partial \eta}{\partial x} - N_H (\nabla^2 u) \frac{\partial}{\partial z}(N_v \frac{\partial u}{\partial z}) - f v + \frac{1}{\rho} \frac{\partial P_a}{\partial x} + \frac{g}{\rho} \int_z^{\zeta} \frac{\partial \rho}{\partial x} d\zeta \quad (1a)$$

where:

- t - the time variable.
- x,y - the horizontal coordinates in a right-handed Cartesian coordinate system.
- z - the vertical coordinate, measured as positive downward from the still water level.
- u,v - the horizontal velocity components in the x and v directions, respectively
- ρ_s - the density of the fluid, where the s subscript indicates the value at the water surface.
- g - the gravitational constant, 9.8 m/sec.
- η - the water height of the free surface above datum, z=0.
- N_h - a constant simulating the lateral shear stress terms.
- N_v - the vertical eddy viscosity coefficient.
- f - the Coriolis parameter, 2 sin , where is the angular velocity of the earth.
- P_a - the atmospheric pressure.

Note that the vertical velocity, w, is assumed negligible and this simplifies the Navier Stokes Equation in the z direction to an expression of the hydrostatic pressure. The effects of stratification on vertical momentum exchange can be included in the model via vertical variations of N_v.

The other governing equation used in the model formulation is the continuity equation:

$$\frac{\partial U}{\partial x} + \frac{\partial V}{\partial y} = \frac{\partial \eta}{\partial t} \quad (2) \quad .$$

where:

- U - the mass flux per unit length in the x direction or $\int$ udz.
- V - the mass flux per unit length in the y direction or $\int$ vdz.

3.2 Boundary Conditions

The surface boundary conditions are:

$$\tau_{sx} = (-\rho N_v \frac{\partial u}{\partial z})\Big|_{z=0} \qquad \tau_{sy} = (-\rho N_v \frac{\partial v}{\partial z})\Big|_{z=0} \quad (3)$$

where and are the specified shear stresses at the surface in the x and v direction, respectively.

At the bottom, a linearized friction law is used or:

$$\tau_{bx} = (\rho c_b u)\Big|_{z=H} \qquad \tau_{by} = (\rho c_b v)\Big|_{z=H} \quad (4)$$

where τ_{bx} and τ_{by} are the bottom shear stresses, H is the still water depth, andc_b is the drag coefficient.

The remaining boundary conditions vary somewhat according to the water body being modeled. For the West Florida Shelf Study the following lateral boundary conditions appear appropriate at this point in time:

- the mass fluxes perpendicular to a coastline are set to zero;
- the surface gradient perpendicular to the lateral ocean boundary is set to zero (a lateral boundary is defined as the boundary running from the open water boundary to the coastline); and
- a lateral shear is applied along the open ocean boundary to simulate the stress applied by the Loop Current.

3.3 Numerical Solution Technique

It is important to note that the parameters u, v, η, and N_v are all functions of (x, y, z, t), and the parameters N_h, η, c_b, and P_a are functions of horizontal space. Parameters which must be specified are N_h, N_v, f, P_a, c_b, τ_s, ρ, and the unknowns are u, v, and η.

The governing equations and boundary conditions (i.e. Equations 1, 2, 3, and 4) are transformed using the Galerkin technique. This manipulation explicitly eliminates z from the transformed equations and thus greatly simplifies the eventual solution process. The dependency of u and v on z is implicitly retained in the final equations and the u and v velocity profiles can be regained whenever desired.

Application of the Galerkin technique begins by hypothesizing a vertical distribution of the unknown velocities, u and v, in terms of a series expansion known as the trial function. The function used in the model is:

$$\hat{u} = \frac{\tau_{sx} z^2 (z-H)}{\rho_s H^2 N_b} + \frac{\tau_{sx}}{\rho_s \alpha} \ln(\frac{N_b}{N_v}) + \sum_{I=I}^{I=I'} c_I \cos(\frac{a_I z}{H}) \quad (5)$$

where:

- u, v - approximate x and y components of the velocity, respectively.
- N_b - vertical eddy viscosity at the bottom, z=H.
- - slope of N_v in the surface layer.
- I' - number of terms used in the cosine series.
- a_I - constants given by the expression; a_I=tan $a_I z/H$.
- c_I - the undetermined constants.

A similar function exists for v. The relationships for the y-direction are not shown here for the sake of brevity. However, the reader should remember that these equations are included in the model.

Note that all parameters in (5) are specified except the undetermined coefficients, c_I (for the y-direction the undetermined coefficients are d_I).

Note that all parameters in (5) are specified except the undetermined coefficients, c_I (for the y-direction the undetermined coefficients are d_I).

The trial functions are substituted into (1a, b) and, in general, there will be a residual associated with this substitution since the trial functions are not the exact solutions. The residual, R, is multiplied by a weighting factor, W, to facilitate later computation and the product is minimized by integrating over the water depth and setting the result to zero, or for the x-direction:

$$\int_{-h}^{H} RW\,dz = \int_{-h}^{H} \left[\left(\frac{\partial u}{\partial z} + \frac{\rho s}{\rho} g \frac{\partial \eta}{\partial x} - N_H \nabla^2 u - f\hat{v} + \frac{1}{\rho}\frac{\partial P_a}{\partial x} + \frac{g}{\rho}\int_{-h}^{z} \frac{\partial \rho}{\partial x}\,d\zeta\right)\right] \cos\frac{a_I z}{H}\,dz = 0 \quad (6)$$

Again, a similar expression exists for the y-direction.

Before the integration in (6) can be performed, it is necessary to specify a distribution for N_v. This is accomplished by assuming N_v to vary in a multi-linear fashion. Performing the integration in (6) yields a set of I' linear, partial differential equations in which z has been explicitly eliminated or:

$$0 = \frac{\partial c_I}{\partial t} - N_H \nabla^2 C_J - f d_I + B_I \frac{\partial \eta}{\partial x} + A_I - \sum_{J=1}^{J=I'} c_J E_{IJ} \quad (7)$$

where A_I, B_I, and E_I are constants which arise from the integration.

Equation 7 and its equivalent in the y-direciton represent a set of 2I' equations with 2I'+1 unknowns (i.e. c_I, d_I, and). To solve for the unknowns one more equation linking c_I, d_I, and e must be used and this is provided by substituting (5) into the continuity equation, (2).

The existing version of the model uses a finite difference scheme to discretize (7), its equivalent in the y-direction, and the transformed continuity equation. While this descretization scheme has proven satisfactory it is not limiting since other schemes, such as finite elements could also be used.

The key in applying the Galerkin technique is in choosing the initial trial functions, (5). In order for the model scheme to economically and accurately simulate the velocity structure, (5) must be able to converge rapidly to the vertical velocity profile to be modeled. Equation (5) has proven to be quite adequate in this regard. Usually only three cosine terms (i.e., I'=3) have proven necessary for the wide variety of flow fields simulated thus far.

Some of the GAL applications have included wind-induced flow which is often characterized by large velocity gradients near the surface. Such flow fields can not be adequately modeled by many existing models including Heap's model. In large part due to (5), the model has proven computationally economical - costs being about the same as for a vertically averaged model. Readers interested in further details regarding the computation of the model are referred to Pearce and Cooper (18).

4. Focus of Future Effort

The West Florida Shelf Study is at mid-term. Initial efforts have concentrated on acquisition and review of data and on conducting the workshop. Initial model tuning is underway and verification should begin by August 1981. Figure 8 shows the model grid which is being used at this stage of model tuning. Model comparisons are initially being made with the FSU - Cedar Keys Current Meter Data. These are real time simulations.

Further comparisons will be made using averaged water surface elevation data at the shore stations. Unfortunately, no other current meter data is available for comparison purposes. The most extensive current data originates from the Shelf Dynamics experiment which was sited at the shelf break and at the edge of the model grid. The Shelf Dynamics data will be used to construct the appropriate boundary conditions for the model.

As part of the final product of the study, a set of current atlases will be constructed to reflect climatological conditions. Since the Loop Current clearly plays an important role in the shelf circulation it must be included in the current atlases. This presents somewhat of a problem since it is difficult if not impossible to identify a typical Loop Current position with any given season or month. Therefore, the approach envisioned at this point is to create a matrix of current charts as implied by Figure 9. Each square in figure would represent one set of current plots at three levels, surface, mid-depth, and bottom.

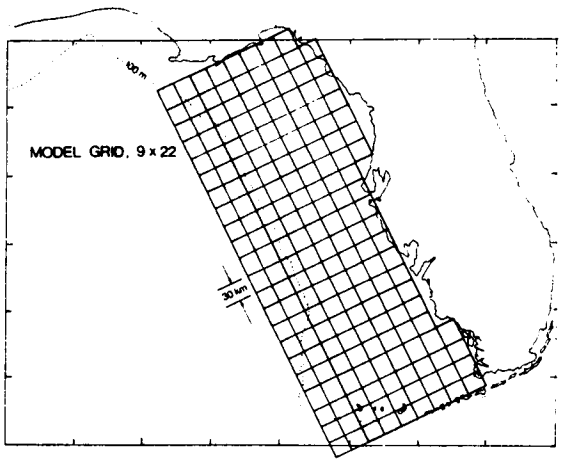

Figure 8: Horizontal Discretization Used in West Florida Shelf Model

NORTHERN LIMIT OF LOOP CURRENT	SEASON			
	SPRING	SUMMER	FALL	WINTER
NORTH OF 28 N	CURRENT ATLAS A	CURRENT ATLAS B	CURRENT ATLAS C	CURRENT ATLAS D
BETWEEN 26 N & 28 N	CURRENT ATLAS E	CURRENT ATLAS F	CURRENT ATLAS G	CURRENT ATLAS H
SOUTH OF 26 N	CURRENT ATLAS I	CURRENT ATLAS J	CURRENT ATLAS K	CURRENT ATLAS L

Figure 9: Matrix of Current Charts to be Created as Part of Final Product for the Study

REFERENCES

1. Huh O.,K., W.J. Wiseman, Jr., and L.J. Rouse, Jr.,"Intrusion of Loop Current Waters Onto the West Florida Continental Shelf," J. Geophysical Res., V 86, No C5, May 20, 1981, 4186-4192.

2. Vukovich F.,M., B.W. Crissman, M. Bushnell, and W.J. King,"Some Aspects of the Oceanography of the Gulf of Mexico Using Satellite and In Situ Data", J. Geophysical Res., V 84, C12, Dec. 20, 1979, 7749-7768.

3. Leipper,D.F.,"A Sequence of Current Patterns in the Gulf of Mexico," J. Geophysical Res., V 75, No. 3, Jan.1970, pp. 537-657

4. Molinari, R.L., S. Baig, D.W. Behringer, G.A. Maul and R. Legeckis,"Winter Intrusions of the Loop Current," Science, V 198, Nov. 1977, pp. 505-507

5. Maul, G.,"An Evaluation of the use of the Earth Resources Technology Satellite for Observing Ocean Current Boundaries in the Gulf Stream System," NOAA T. R. ERL 335-AOML 18, Jan 1975

6. Hurlburt, H.,E., and J.D. Thompson,"A Numerical Study of Loop Current Instrusions and Eddy Shedding",J. Physical Ocean.,V 10, Oct. 1980, 1611-1651.

7. Maul, G., "A Current Data Collection Program for the Gulf Loop Current", Keynote Address appearing in the Proceedings of the Gulf Circulation Studies Workshop, 14-15 May 1981, New Orleans, Bureau of Land Management.

8. Price, J.F. et al.,"Current Meter Data Report from the Fall 1973 Experiment," U. of Miami Scientific Data R., UM-RSMAS-74035, 59p

9. Koblinsky, C.J. and P.P. Niiler,"Direct Measurement of Circulation on West Florida Continental Shelf," January 1973-May 1975, Data Report 76, ref. 79-13, Oregon State U., School of Ocean., March 1980

10. Plaisted, R.O., K.M. Waters and P.P. Niiler,"Current Meter Data Report from the NSF Continental Shelf Dynamics Program, 1973-1973," Scientific Data R., Nova U., Phy. Oceanographic Lab., Jan. 1975

11. Niiler, P.P.,"Observation of Low Frequency Currents on the West Florida Continental Shelf," Mem. Soc. R. Sciences Lieges, V 6, pp. 331-356, 1976.

12. Molinari, R.L. and D. Mayer,"Physical Oceanographic Conditions at a Potential OTEC Site in the Gulf of Mexico; 27.5 N, 85.5 W," NOAA Tech. Mem. ERL AOML-42, May 1980.

13. Williams, J., W.F. Grey, E.B. Murphy and J.J. Crane,"Drift Bottle Analysis of Surface Circulation," Prog. in Oceanography 4 (pt. 3), pp 1-134, Aug. 1977.

14. Tolbert, W.H. and G.G. Salsman,"Surface Circulation of the Eastern Gulf Of Mexico as Determined by Drift Bottle Studies," J. Geophysical Res., V 69 , No 2, pp 223-230, 1964.

15. Ichiye, K. and Carnes,"Assessment of Currents and Hydrography of the Eastern Gulf of Mexico," Cont. No.601, Texas A&M U., Dept. of Ocean.

16. Heaps, N.S.,"On the Numerical Solution of the Three dimensional Hydrodynamic Equations for Tides and Storm Surges," Mem. Soc. R. Scie. Liege, 6,(2),1972,143-180.

17. Heaps, N.S.,"Development of a Three-Dimensional Model of the Irish Sea",Rapp. P.-V. Reun. Cons. Int. Explor. Mer., Dec. 1974,147-162.

18. Pearce, B.R. and C.K. Cooper, "Numerical Circulation Model for Wind Induced Flow", ASCE, HY3, March 1981, 16110, 285-301.

CIRCULATION STUDY OF THE WEST FLORIDA SHELF

ABSTRACT

Paper to be presented and published by 18th Coastal Engineering Conference, Johannesburg, South Africa, November, 1982.

1. INTRODUCTION

The west Florida shelf (WFS) is a broad relatively flat shelf, 600 km long and 200 km wide as indicated in Figure 1. Existing and prospective energy-related development on the WFS pose several potential negative impacts to other uses of the shelf and coastline. Examples include the impact of an oil spill on recreational beaches or indigenous fauna and flora. To identify the probable spatial distribution of these impacts a circulation study of the WFS was begun in 1980. The study consisted of two phases: (1) accumulation and review of existing data and (2) application of a circulation model as a diagnostic and predictive tool.

The vertical structure of currents on the WFS is far from uniform. This fact coupled with the large variety of characteristic densities associated with potential pollutants, required that the circulation model be capable of predicting the vertical as well as horizontal structure of the currents. Modeling focused on calculation of residual currents (i.e. currents with time scales of order weeks and months). Shorter term processes are included in a later phase of modeling not described here.

2. REVIEW OF DATA

As part of the study, a review of the existing data base in the region was performed. The results of the review and some of the more important data analysis are summarized.

Three major processes affect residual currents on the WFS:

- the Gulf Loop Current (LC), a current which originates from the Caribbean, enters through the Yucatan Straits, flows northward toward the Mississippi River, loops east and then south along the WFS, and finally exits as the Gulf Stream through the Florida Straits. Currents within the LC are of O(100 cm s^{-1}) and generate complex, low frequency (i.e. periods of greater than 1 day) currents well onto the WFS of O(10 cm s^{-1}). The most northward extension of the LC varies by approximately 600 km during a period of O(1 year).
- Wind. Winter meteorology is dominated by the passage of extratropical storm systems generating alternating periods of southerly and northerly winds with maximum speeds of O(10 m s^{-1}) extending uniformly over the entire shelf. Summer winds are not so easily categorized and in general are less spatially coherent. Mean winds can be broken into three periods: Fall-Winter, 4 m s^{-1} from the ENE; Spring, 5 m s^{-1} from the SE; and Summer 3 m s^{-1} from the SSE.
- Seasonal Thermal Heating. All catalogued hydrographic data from the WFS was statistically analyzed and indicates the existence of significant horizontal and thermal stratification during the summer due to seasonal heating. Horizontal density gradients are strongest along the coast and of O(10^{-5}kg m^{-3} km^{-1}). There is no statistically significant horizontal gradient in the winter, perhaps because the data base is much less extensive.

3. MODEL DESCRIPTION

The model used was a so-called primitive, diagnostic model based on the momentum and continuity equations as described in Copper and Pearce (1982). A brief description of the model is presented.

A weighted residual technique is used in the model formulation to explicitly eliminate the vertical dependency of the velocity components. Application of the technique transforms the 2nd order momentum equations into a set of 1st order equations which are horizontally discretized using a finite difference approach. These manipulations result in an exceptionally efficient algorithm with computational costs roughly equivalent to a vertically averaged model, but with the advantage of retaining the vertical dependency of the velocity components.

The model includes all forcing mechanisms thought to be important on the WFS such as: the Coriolis force, horizontal density gradients, surface pressure gradients, wind stress, bottom friction, turbulent Reynolds stresses (via vertical and horizontal eddy viscosity coefficients) and lateral shearing stresses emulating from the LC.

4. MODEL VERIFICATION

Tuning and verification of the model requires either velocity or surface elevation data with which to compare model simulations. Three data sets were selected for this purpose.

- data from the winter of 1978 which includes 25 days of velocity data from four current meters moored at two sites to the west of Cedar Key. Wind data is available from a weather buoy and four coastal stations, and surface level elevation is available from three coastal stations.
- data from the winter of 1973 which was taken during the 1973-74 Shelf Dynamics Experiment (SDE) conducted along the WFS break south of Tampa. Data includes 30 days of velocity information from two current meters moored at one site in 50 m, as well as calculated offshore wind, observed wind at four coastal stations, and observed surface elevations at three coastal stations.

- data from the summer of 1974 which consists of two months of calculated offshore winds, observed winds from four coastal stations, and observed surface elevations from two coastal stations.

Detailed comparisons of the data with the model are presented. The results can be summarized as follows:

- the model generally hindcasts the coastal surface elevations quite well being within +-5 cm in a range of 40 cm. The exceptions to this are the summer of 1974 and stations at the northern and southern boundary, where the signal is only about +-5 cm. In this range, modeling and data measurement errors become large compared to the true signal.

- the model hindcasts the winter 1978 velocity data reasonably well, generally being within +-5 cm s^{-1} over a range of 15 cm s^{-1}.

- the model hindcasts of the winter 1973 SDE velocity data indicate that wind forcing plays only a minor role in determining the measured currents. Flow is dominated by eddies propagating from the Loop Current shoreward with characteristic time and length scales on the order of 15 days and 150 km.

6. MODEL RESULTS AND CONCLUSIONS

Residual currents driven by winds and horizontal density gradients are presented for the three seasons. Summer currents include vertical stratification effects.

Winter surface currents are about 1 cm s^{-1} and display a net southerly movement implying drifters will tend to be entrained in the LC and advected to the Florida Keys or to the eastern U.S. coast. Spring surface currents are about 3 cm s^{-1} and display a net northerly drift. Summer surface currents are the smallest of the three season, less than 1 cm s^{-1}, and display a northerly movement. Drifters released during the summer and spring season may reach the LC, depending in large part on the northerly extent of the LC and the configuration of larger scale eddies on the shelf. In the case where the LC is relatively far south, a drifter may reach the Gulf coasts of Mississippi, Louisiana, etc. These model results are supported by historical drift bottle results.

Incorporating LC effects into the modeled residual currents proved difficult. The SDE data indicates the LC effects are seen on the shelf mainly as oscillations with amplitudes of O(30 cm s^{-1}) and time scales of 15 days. Niiler (1976) has suggested that these oscillations originate from barotropic eddies generated at the shelf break. However, model studies imply that such a parameterization is far too simple and that the baroclinicity of the eddies is probably an essential element of any realistic model which hopes to simulate the SDE data.

The problem of parameterizing the LC is especially difficult because of the sparsity of current data on the shelf. Only two, 1-month series are available. Longer term data is available in deeper water at the break and suggests that as a first approximation the LC may not contribute to net onshore advection for monthly time scales. The LC's primary effect may simply be as a stirring mechanism which causes no net onshore advection by itself, but in combination with other forcing (most notably the wind) is probably important in determining whether the final destination of drifters is the Gulf or eastern coast. Additional long term Eulerian and Lagrangian current measurements are essential before further progress in modeling LC effects on the WFS can be made.

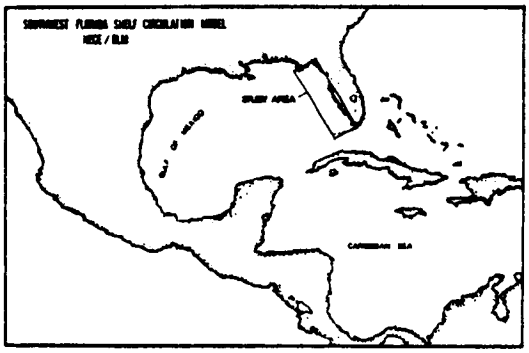

Figure 1: Study Area

ACKNOWLEDGEMENTS

Mr. Adrian Humphreys and Mr. Marcel Moreau of NECE were responsible for much of the data analysis for the study. Prof. R. O. Reid of Texas A&M University served as a consultant on the study and provided many profound and helpful comments and recommendations. Funding for this study was provided by the U.S. Department of Interior, Bureau of Land Management, Dr. Murray Brown, contracting officer.

REFERENCES

Cooper, C.K. and B.R. Pearce (1982). Numerical modeling of hurricane generated currents. J of Physical Oceanography, in press.

Niiler, P.P. (1976), Observations of low frequency currents on the west Florida continental shelf. Memoires Societe Royale des Sciences de Liege X, 331-358.

APPENDIX D

Summary of Important Model Runs During WFS Study

TITLE	Run	$N_v(cm^2/s)$	c_b(cm/s)	$N_H(cm^2/s)$	Grid Config.	West BC	Lat BC	Wind	Beta[1]	Other
Basic wind sens.	5.1	R=12,W_{*_s}=1.0	.100	0	L=10,M=24	se[2]=0	ss[3]=0	2.5 m/s, 0°[4]	No	none
Basic wind sens.	5.2	R=12,W_{*_s}=1.0	.100	0	L=10,M=24	se=0	ss=0	2.5 m/s,90°	No	none
Basic wind sens.	5.3	R=12,W_{*_s}=1.0	.100	0	L=10,M=24	se=0	ss=0	NDBO buoy 1978	No	none
Basic wind sens.	5.4	R=12,W_{*_s}=0.5	.025	10^9	L=12,M=24	se=0	ss=0	10 m/s, 0°	No	none
Basic wind sens.	5.5	R=12,W_{*_s}=0.5	.025	10^9	L=12,M=24	se=0	ss=0	10 m/s,90°	No	none
Basic wind sens.	5.6	R=12,W_{*_s}=0.5	.025	10^9	L=12,M=24	se=0	ss=0	10 m/s,90°	Yes	none
Basic wind sens.	5.7	R=12,W_{*_s}=0.5	.100	10^9	L=12,M=24	se=0	ss=0	10 m/s,90°	Yes	none
Basic wind sens.	5.8	R=12,W_{*_s}=1.0	.025	10^9	L=12,M=24	se=0	ss=0	10 m/s,90°	Yes	none
Basic wind sens.	5.9	R=12,W_{*_s}=0.5	.025	10^7	L=12,M=24	se=0	ss=0	10 m/s,90°	Yes	none
Winter 1978 hind.	6.1	R=12,W_{*_s}=1.0	.050	0	L=10,M=24	se=0	ss=0	NDBO buoy, 2/78	No	none
Winter 1978 hind.	6.1	R=12,W_{*_s}=1.0	.050	0	L=10,M=24	se=0	se=0	NDBO buoy, 2/78	No	none
Winter 1978 hind.	7.1	R=12,W_{*_s}=.25	.050	0	L=10,M=24	se=0	ss=0	NDBO buoy, 2/78	No	none
Winter 1978 hind.	8.1	R=12,W_{*_s}=0.5	.050	0	L=10,M=24	se=0	ss=0	NDBO buoy, 2/78	No	none
Winter 1978 hind.	8.2	R=12,W_{*_s}=0.5	.050	0	L=10,M=24	se=0	ss=0	5 stations,2/78	No	none
Winter 1978 hind.	8.3	R=12,W_{*_s}=0.5	.050	0	L=10,M=24	se=0	sse[5]=0	NDBO buoy, 2/78	No	none
Winter 1978 hind.	10.1	R=12,W_{*_s}=.25	.025	0	L=10,M=24	se=0	ss=0	NDBO buoy, 2/78	No	none
Basic wind sens.	11.1	R=12,W_{*_s}=1.0	.100	0	L=15,M=25	se=0	ss=0	2.5 m/s, 0°	No	none
Basic wind sens.	12.2	R=12,W_{*_s}=1.0	.100	0	L=15,M=24	se=0	se=0	2.5 m/s, 0°	No	none
Basic wind sens.	12.3	R=12,W_{*_s}=1.0	.100	0	L=15,M=24	se=0	se=0	2.5 m/s,90°	No	none
Wind curl sens.	12.4	R=12,W_{*_s}=1.0	.100	0	L=15,M=24	se=0	se=0	W=fcn(x),90°	No	none
Wind curl sens.	12.5	R=12,W_{*_s}=1.0	.100	0	L=15,M=24	se=0	se=0	$W^2_{*_s}$=fcn(x),90°	No	none
Wind curl sens.	12.6	R=12,W_{*_s}=1.0	.100	0	L=15,M=24	se=0	se=0	W=fcn(x),90°	No	none
Lateral shear sens.	13.2	R=12,W_{*_s}=1.0	.100	10^9	L=15,M=24	$d_{1,1,24}$=-1	se=0	0	No	none
Lateral shear sens.	13.3	R=12,W_{*_s}=1.0	.100	10^9	L=10,M=24	$d_{1,1,24}$=-1	se=0	0	No	none
Lateral shear sens.	13.4	R=12,W_{*_s}=1.0	.100	10^8	L=15,M=24	$d_{1,1,24}$=-4	se=0	0	No	none
Lateral shear sens.	13.5	R=12,W_{*_s}=1.0	.100	10^9	L=15,M=24	$d_{1,1,24}$=-4	se=0	0	No	none
Lateral shear sens.	13.6	R=12,W_{*_s}=1.0	.100	10^9	L=15,M=24	$d_{1,1,24}$=ramp	se=0	0	No	none
Lateral shear sens.	13.7	R=12,W_{*_s}=1.0	.100	10^9	L=15,M=24	$d_{1,1,24}$=-4[6]	se=0	0	No	none
Lateral shear sens.	13.8	R=12,W_{*_s}=1.0	.100	10^9	L=15,M=24	$d_{1,1,13}$=ramp	se=0	0	No	none
Lateral shear sens.	13.9	R=12,W_{*_s}=1.0	.100	10^9	L=10,M=24	$d_{1,1,24}$=-.5	se=0	0	No	none

TITLE	Run	N_v(cm^2/s)	c_b(cm/s)	N_H(cm^2/s)	Grid Config.	West BC	Lat BC	Wind	Beta[1]	Other
Lateral shear sens.	13.10	R=12,W_{*_s}=1.0	.100	10^9	L=12,M=24	$d_{1,1,24}$=-.5	se=0	0	No	none
Lateral shear sens.	13.11	R=12,W_{*_s}=1.0	.100	10^9	L=15,M=24	$d_{1,1,24}$=-1.	ss=0	0	No	none
Lateral shear sens.	13.16	R=12,W_{*_s}=1.0	.100	10^9	L=12,M=24	$d_{1,1,24}$=-1.	ss=0	0	No	none
Lateral shear sens.	13.17	R=12,W_{*_s}=0.5	.025	10^9	L=12,M=24	$d_{1,1,24}$=-1.	ss=0	0	Yes	none
Lateral shear sens.	13.18	R=12,W_{*_s}=0.5	.025	10^9	L=12,M=24	$d_{1,1,24}$=ramp	ss=0	0	Yes	none
Lateral shear sens.	13.19	R=12,W_{*_s}=0.5	.025	10^9	L=12,M=24	$d_{1,1,13}$=-1.0	ss=0	0	Yes	none
Lateral shear sens.	13.20	R=12,W_{*_s}=0.5	.025	10^9	L=12,M=24	$d_{1,1,13}$=f(y)	ss=0	0	Yes	none
Lateral shear sens.	13.21	R=12,W_{*_s}=0.5	.025	10^8	L=12,M=24	$d_{1,1,24}$=cos(y)	ss=0	0	Yes	none
Lateral shear sens.	13.22	R=12,W_{*_s}=0.5	.025	10^9	L=12,M=24	$d_{1,1,24}$=cos(y)	ss=0	0	Yes	none
Lateral shear sens.	13.23	R=12,W_{*_s}=0.5	.025	10^9	L=12,M=24	$d_{1,1,24}$=cos(y)	ss=0	0	Yes	none
Lateral shear sens.	13.24	R=12,W_{*_s}=0.5	.025	10^9	L=12,M=24	$d_{1,1,13}$=cos(y)	ss=0	0	Yes	none
Lateral shear sens.	13.25	R=12,W_{*_s}=0.5	.100	10^9	L=12,M=24	$d_{1,1,13}$=cos(y)	ss=0	0	Yes	none
Lateral shear sens.	13.26	R=12,W_{*_s}=0.5	.025	10^9	L=12,M=24	$d_{1,1,13}$=-1.0	ss=0	0	Yes	none
Lateral shear sens.	13.27	R=12,W_{*_s}=1.0	.025	10^9	L=12,M=24	$d_{1,1,13}$=cos(y)	ss=0	0	Yes	none
Lateral shear sens.	13.28	R=12,W_{*_s}=0.5	.025	10^9	L=12,M=24	$d_{1,1,6}$=ramp	ss=0	0	Yes	none
Lateral shear sens.	13.29	R=12,W_{*_s}=0.5	.025	10^9	L=12,M=24	$d_{1,1,6}$=-1.	ss=0	0	Yes	none
Lateral shear sens.	13.30	R=12,W_{*_s}=0.5	.025	10^9	L=12,M=24	$d_{1,1,24}$=-1.	ss=0	0	Yes	none
Lateral shear sens.	13.31	R=12,W_{*_s}=0.5	.025	10^9	L=12,M=24	$d_{1,1,6}$=-1.	ss=0	0	Yes	none
North position of LC	13.32	R=12,W_{*_s}=0.5	.025	10^9	L=12,M=24	$d_{1,1,19}$=-1.	ss=0	0	Yes	none
Mid position of LC	13.33	R=12,W_{*_s}=0.5	.025	10^9	L=12,M=24	$d_{1,1,11}$=-1.	ss=0	0	Yes	none
South position of LC	13.34	R=12,W_{*_s}=0.5	.025	10^9	L=12,M=24	$d_{1,1,3}$=-1.	ss=0	0	Yes	none
North position of LC	13.35	see note 7	.025	10^9	L=12,M=24	$d_{1,1,19}$=-1.	ss=0	0	Yes	none
Mid position of LC	13.36	R=12,W_{*_s}=0.5	.025	10^9	L=12,M=24	$d_{1,1,11}$=-1.	ss=0	0	Yes	none
South position of LC	13.37	R=12,W_{*_s}=0.5	.025	10^9	L=12,M=24	$d_{1,1,3}$=-1.	ss=0	0	Yes	none
Winter 1978 hindcast	15.1	R=12,W_{*_s}=0.5	.050	0	L=15,M=24	se=0	se=0	5 stations,2/78	No	none
Winter 1978 hindcast	15.2	R=12,W_{*_s}=0.5	.050	0	L=12,M=24	se=0	ss=0	5 stations,2/78	No	none
Winter 1978 hindcast	15.3	R=12,W_{*_s}=0.5	.050	0	L=12,M=24	se=0	ss=0	5 stations,2/78	No	mod. bndry bath.
Winter 1978 hindcast	15.4	R=12,W_{*_s}=0.5	.050	0	L=12,M=24	se=0	ss=0	5 stations,2/78	No	mod. bndry bath.
Winter 1978 hindcast	15.5	R=12,W_{*_s}=0.5	.050	0	L=12,M=24	se=0	sse=0	5 stations,2/78	No	mod. bndry bath.
Winter 1978 hindcast	15.6	R=12,W_{*_s}=0.5	.150	0	L=12,M=24	se=0	ss=0	5 stations,2/78	No	mod. bndry bath.
Winter 1978 hindcast	15.7	R=12,W_{*_s}=0.5	.050	0	L=12,M=24	se=0	se=0	5 stations,2/78	No	none
Winter 1978 hindcast	15.8	R=12,W_{*_s}=1.0	.100	0	L=12,M=24	se=0	se=0	5 stations,2/78	No	none
Winter 1978 hindcast	15.9	R=12,W_{*_s}=1.0	.100	0	L=12,M=24	se=0	ss=0	5 stations,2/78	No	none

TITLE	Run	$N_v(cm^2/s)$	c_b(cm/s)	$N_H(cm^2/s)$	Grid Config.	West BC	Lat BC	Wind	Beta[1]	Other
Winter 1978 hindcast	15.10	R=12,W_{*_s}=0.5	.100	0	L=12,M=24	se=0	ss=0	5 stations,2/78	No	none
Winter 1978 hindcast	15.11	R=12,W_{*_s}=0.8	.100	0	L=12,M=24	se=0	ss=0	5 stations,2/78	No	none
Winter 1978 hindcast	15.12	R=12,W_{*_s}=1.0	.100	0_9	L=12,M=24	se=0	ss=0	5 stations,2/78	No	mod. bndry bath.
Winter 1978 hindcast	15.13	R=12,W_{*_s}=1.0	.100	10^9	L=12,M=24	se=0	ss=0	5 stations,2/78	No	none
Winter 1978 hindcast	15.14	R=12,W_{*_s}=1.0	.100	0_9	L=12,M=24	se=0	ss=0	5 stations,2/78	Yes	none
Winter 1978 hindcast	15.15	R=12,W_{*_s}=0.5	.050	10^9	L=12,M=24	se=0	ss=0	5 stations,2/78	Yes	none
Winter 1978 hindcast	15.16	R=12,W_{*_s}=0.5	.050	10^9	L=12,M=24	se=0	ss=0	NDBO buoy, 2/78	Yes	none
Winter 1978 hindcast	15.17	R=12,W_{*_s}=0.5	.025	10^9	L=12,M=24	se=0	ss=0	NDBO buoy, 2/78	Yes	wind started early
Winter 1978 hindcast	15.18	R=12,W_{*_s}=0.5	.025	10^9	L=12,M=24	se=0	ss=0	NDBO buoy, 2/78	Yes	incr. wind factors
Summer 1974 hindcast	16.1	R=12,W_{*_s}=1.0	.100	10^9	L=12,M=24	se=0	ss=0	4 stations,7/74	Yes	none
Summer 1974 hindcast	16.2	R=12,W_{*_s}=0.5	.050	10^9	L=12,M=24	se=0	ss=0	4 stations,7/74	Yes	none
Winter 1973 hindcast	17.1	R=12,W_{*_s}=0.5	.050	10^9	L=12,M=24	se=0	ss=0	4 stations,2/73	Yes	none
Winter 1973 hindcast	17.2	R=12,W_{*_s}=0.5	.010	10^9	L=12,M=24	se=0	ss=0	4 stations,2/73	Yes	mod. south bndry bath.
Winter season wind	18.4	R=12,W_{*_s}=0.5	.025	10^9	L=12,M=24	se=0	ss=0	W=4.5m/s,184	Yes	none
Spring season wind	18.5	R=12,W_{*_s}=0.5	.025	10^9	L=12,M=24	se=0	ss=0	W=5.5m/s,137	Yes	none
Summer season wind	18.5	R=12,W_{*_s}=0.5	.025	10^9	L=12,M=24	se=0	ss=0	W=4.0m/s,120	Yes	none
Stratified sens.	19.1	see note 8	.025	10^9	L=12,M=24	se=0	ss=0	W=10m/s,90°	Yes	none
Stratified sens.	19.2	see note 9	.025	10^9	L=12,M=24	se=0	ss=0	W=10m/s,90°	Yes	none
Stratified sens.	19.3	see note 10	.025	10^9	L=12,M=24	se=0	ss=0	W=10m/s,90°	Yes	none
Stratified sens.	19.4	same as 19.3 but 1/4	.080	10^9	L=12,M=24	se=0	ss=0	W=10m/s,90°	Yes	none
Stratified sens.	19.5	see note 11	.080	10^9	L=12,M=24	se=0	ss=0	W=10m/s,90°	Yes	none
Stratified sens.	19.6	same as 19.5	.080	10^9	L=12,M=24	se=0	ss=0	W=10m/s,90°	Yes	improv. model at row 2
Stratified sens.	19.7	see note 7	.025	10^9	L=12,M=24	se=0	ss=0	W=10m/s,90°	Yes	none
Horiz. Den. sens.	20.1	R=12,W_{*_s}=0.5	.025	10^9	L=12,M=24	se=0	ss=0	0	Yes	horiz grad., no vert.
Horiz. Den. sens.	20.2	R=12,W_{*_s}=0.5	.025	10^9	L=12,M=24	se=0	ss=0	0	Yes	horiz grad & H=50m
Horiz. Den. sens.	20.3	R=12,W_{*_s}=0.5	.025	10^9	L=12,M=24	se=0	ss=0	0	Yes	horiz & vert grad,H=50
Horiz. Den. sens.	20.4	R=12,W_{*_s}=0.5	.025	10^9	L=12,M=24	se=0	ss=0	0	Yes	same grad,mod. bath
Horiz. Den. sens.	20.5	R=12,W_{*_s}=0.5	.025	10^9	L=12,M=24	se=0	ss=0	0	Yes	same grad, H=f(x)
Horiz. Den. sens.	20.6	R=12,W_{*_s}=0.5	.025	10^9	L=12,M=24	se=0	ss=0	0	Yes	same grad,mod.bath

TITLE	Run	$N_v(cm^2/s)$	c_b(cm/s)	$N_H(cm^2/s)$	Grid Config.	West BC	Lat BC	Wind	Beta[1]	Other
Horiz. Den. sens.	20.7	R=12,W_{*_S}=0.5	.025	10^9	L=12,M=24	se=0	ss=0	0	Yes	more realistic grad.
Horiz. Den. sens.	20.8	R=12,W_{*_S}=0.5	.025	10^9	L=12,M=24	se=0	ss=0	0	Yes	summer gradient
Horiz. Den. sens.	20.9	same as 19.7	.025	10^9	L=12,M=24	se=0	ss=0	0	Yes	summer gradient
Horiz. Den. sens.	20.10	R=12,W_{*_S}=0.5	.025	10^9	L=12,M=24	se=0	ss=0	0	Yes	sum horiz but no ver
Composite Fall-wint	21.1	R=12,W_{*_S}=0.5	.025	10^9	L=12,M=24	$d_{1,1,13}$=-1.	ss=0	W=4.5m/s,184o	Yes	none
Composite Spring	21.2	R=12,W_{*_S}=0.5	.025	10^9	L=12,M=24	$d_{1,1,11}$=-1.	ss=0	W=5.5m/s,137o	Yes	none
Composite Summer	21.3	same as 19.7	.025	10^9	L=12,M=24	$d_{1,1,19}$=-1.	ss=0	W=4.0m/s,120o	Yes	none
Composite Spring	21.4	R=12,W_{*_S}=0.5	.025	10^9	L=12,M=24	$d_{j,1,11}$=-1.	ss=0	W=5.5m/s,137o	Yes	none
Composite Summer	21.5	same as 19.7	.025	10^9	L=12,M=24	$d_{j,1,19}$=-1.	ss=0	W=4.0m/s,120o	Yes	none
Composite Fall-wint	21.6	R=12,W_{*_S}=0.5	.025	10^9	L=12,M=24	$d_{j,1,13}$=-1.	ss=0	W=4.5m/s,184o	Yes	none

---

Notes:

1. Column indicating whether spatially variable Coriolis parameter was used in simulation

2. se = abbreviation for "surface elevation"

3. ss = abbreviation for "surface slope" normal to boundary.

4. wind direction is given as positive in a ccw direction with respect to the grid positive x-axis.

5. sse = both surface elevation and surface slope.

6. $d_{j,l,m}$ are the undetermined parameters in the y-direction at grid element (l,m) where l is the x increment and m is the y increment. The value for m indicates that all rows less than or equal to m have been set to the specified value, e.g. d(1,1,13) = -1.0 means all d (j=1) in column 1, rows 1-13, have been set to -1.0 m/s.

7. two layered stratified conditions have been specified. The mixed layer depth has been set to 30% of the local grid element depth, and the lower layer has been set to 70%. N_v in the mixed

layer is set to 3H/200 and in the lower to 0.3 H/200 or in shortened notation; $N_v = 3\ H_m/200$ for 0.LT.z.LT.30%H and $N_v = 0.3\ H_1/200$ for z.GT.30%H

8. two layered stratified conditions have been specified with $N_v = 2\ H_m/200$ for 0.LT.z.LT.20 m and $N_v = 0.2\ H_1/200$ for z.GE.20m.

9. two layered stratified conditions have been specified with $N_v = 2\ H_m/200$ for 0.LT.z.LT.20 m and $N_v = 0.8\ H_1/200$ for z.GE.20 m.

10. two layered stratified conditions have been specified with $N_v = 1$ H/200 for 0.LT.z.LT.20 m and $N_v = .1$ H/200 for z.GE.20 m.

11. two layered stratified conditions have been specified with $N_v = 1$ H/200 for 0.LT.z.LT.30% H and $N_v = .1$ H/200 for z.GE.30% H.

APPENDIX E

Implementation of Model Modifications

E.1 Beta Plane Approximation

Referring to Figure E.1.1 we see that the distance from the origin to the center of an arbitrary element is $d_{\ell,m}$ defined as:

$$d_{\ell,m} = \sqrt{\{(\ell-1)\ \Delta L\}^2 + \{(m-1)\ \Delta L\}^2} = \Delta L\ \sqrt{(m-1)^2 + (\ell-1)^2}$$

Where ℓ and m are integer counters in the x- and y- directions, respectively. The angle between the line $d_{\ell,m}$ and the x-axis is:

$$\psi_{\ell,m} = \tan^{-1} \frac{(m-1)\ \Delta L}{(\ell-1)\ \Delta L}$$

The angle between the meridian and the x-axis is ψ' which can be written in terms of ψ and Θ where Θ is the angle between true north and the x-axis or:

$$\psi'_{\ell,m} = \psi + 90° - \Theta$$

The normal distance between the meridian and the arbitrary element can now be written as:

$$L_{\ell,m} = d_{\ell,m} \sin \psi'$$

The latitude of the element can be written in terms of the latitude of the origin and a relative change, $\Delta\phi$ or:

$$\phi_{\ell,m} = \phi_{1,1} + \Delta\phi_{\ell,m}$$

Where $\Delta\phi$ can be expressed in terms of $L_{\ell,m}$ and the radius of the earth, or:

$$\Delta\phi_{\ell,m} \simeq \sin^{-1} \frac{L_{\ell,m}}{r}$$

Note that the curvature of the earth has been assumed negligible. The latitude of the element becomes:

$$\phi_{\ell,m} = \sin^{-1} \{\frac{L_{\ell,m}}{r}\} + \phi_{1,1}$$

The coriolis paramenter for the element now becomes:

$$f_{\ell,m} = 2\Omega \sin \phi_{\ell,m}$$

Where Ω is the angular speed of the earth's rotation.

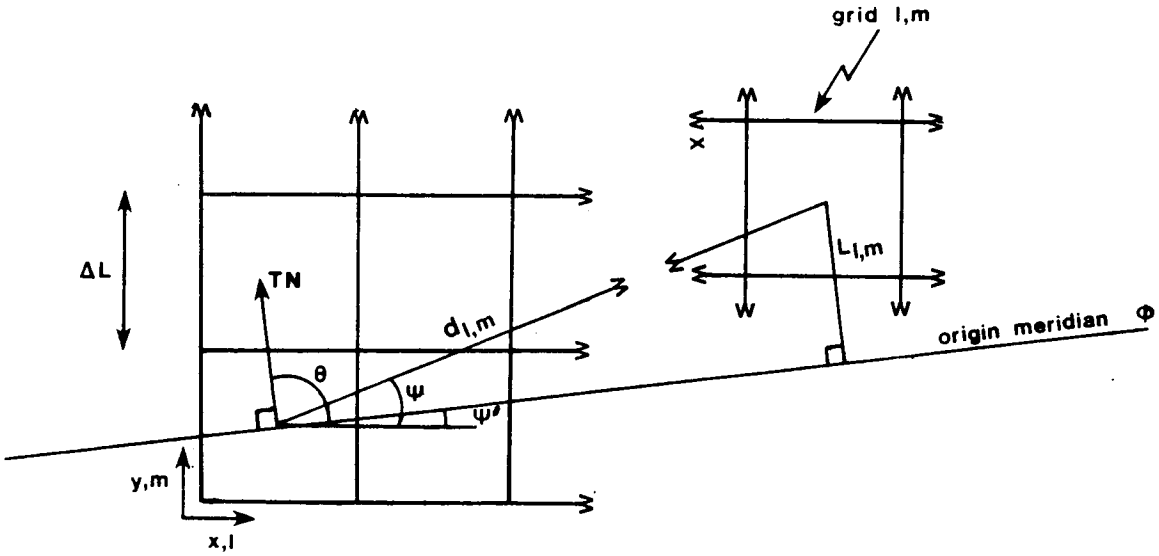

Figure E.1.1: Definition of Variables.

E.2 Second Order Lateral Shear Stress Term

The lateral eddy viscosity term of the x-momentum equation is called term 3 for convenience and is written as:

$$3 = \int_0^H \{- \frac{\partial}{\partial x} (N_H \frac{\partial u}{\partial x}) - \frac{\partial}{\partial y} (N_H \frac{\partial u}{\partial y}) \quad \Omega_J dz \qquad (1)$$

We note that the second derivative of the basis function is:

$$\frac{\partial^2 u}{\partial x^2} = \frac{\partial^2}{\partial x^2} \quad \frac{u_*^2 \, z^2 \, (z-H)}{H \; H_b} + \frac{u_*^2}{\alpha} \text{Ln} \left(\frac{N_b}{N_{V1}}\right) + \sum_{I=1}^{I'} c_I \cos \frac{a_I z}{H}$$

$$\frac{\partial^2 u}{\partial x^2} \simeq \sum_{I=1}^{I'} \frac{\partial^2 c_I}{\partial x^2} \cos \frac{a_I z}{H} \qquad (2)$$

Where it is assumed that u_*^2, H, N_V, and a_I vary slowly or not at all with "x". Substituting (2) into (1) gives:

$$3 \simeq \sum_{I=1}^{J'} \int_0^H - N_H \cos \frac{a_I z}{H} \{\frac{\partial^2 c_I}{\partial x^2} + \frac{\partial^2 c_I}{\partial y^2}\} \Omega_J dz$$

or more simply:

$$\simeq - N_H \sum_{I=1}^{J'} \nabla^2 c_I \int_0^H \cos \frac{a_I z}{H} \cos \frac{a_J z}{H} dz \qquad \text{where:} \quad \nabla^2 = \frac{\partial^2}{\partial x^2} + \frac{\partial^2}{\partial y^2}$$

Integrating yields:

$$\simeq - N_H \nabla^2 c_J \left(\frac{H}{2} + \frac{H}{4a_J} \sin 2a_J\right)$$

or finally:

$$\simeq \frac{-N_H \nabla^2 c_J Hq_J}{2} \qquad (3) \qquad \text{where:} \qquad q_J = \left(1 + \frac{1}{2a_J} \sin 2a_J\right)$$

Applying a central difference approximation for $\nabla^2 c_J$ gives:

$$\frac{\partial^2 c_J}{\partial x^2} = \frac{c(J,\ell+1,m) - 2c(J,\ell,m) + c(J,\ell-1,m)}{\Delta x^2}$$

$$\frac{\partial^2 c_J}{\partial y^2} = \frac{c(J,\ell,m+1) - 2c(J,\ell,m) + c(J,\ell,m-1)}{\Delta x^2}$$

$$\nabla^2 c_J = \{c(J,\ell,m+1) + c(J,\ell+1,m) - 4c(J,\ell,m) + c(J,\ell,m-1) + c(J,\ell-1,m)\ \frac{1}{\Delta x^2}$$

Substituting this expression into (3) gives:

$$3 = \frac{-N_H \nabla^2 c_J Hq_J}{2}$$

E.3 Density Gradient Term

For convenience we call the density gradient of the x-momentum equation 8, which is written as:

$$8 = g \int_0^H \frac{1}{\rho} \left(\int_0^z \frac{\partial \rho}{\partial x} \, d\xi \right) \Omega_J dz \qquad (1)$$

assume a layered density model with constant variation between layers as shown in Figure E.3.1

Note: the layer depths are not functions of x or y. P' will be a function of z.

The integral within the parentheses of (1) evaluated at a point p on a layer boundary using a central differences scheme is:

$$\int_0^z \frac{\partial \rho}{\partial x} \, d\xi = \frac{1}{2\Delta L} \int_0^z \{ \rho_p \, (\ell+1,m) - \rho_p \, (\ell-1,m) \} \, d\xi \qquad (2)$$

Let $\Delta\rho_{xp} = \rho_p \, (\ell+1,m) - \rho_p \, (\ell-1,m)$ and substitute into (2) yields:

$$\int_0^z \frac{\partial \rho}{\partial x} \, d\xi = \frac{1}{2\Delta L} \left\{ \int_0^{H_1} \Delta\rho_{x1} \, d\xi + \int_{H_1}^{H_2} \Delta\rho_{x2} \, d\xi + \ldots\ldots \int_{H_{P-1}}^{z} \Delta\rho_{xP} \, d\xi \right.$$

where: P = the level in which $H_{P-1} \leq z < H_P$

carrying out the integration yields:

$$\int_0^z \frac{\partial \rho}{\partial x}\, d\xi = \frac{1}{2\Delta L} \{H_1 \Delta\rho_{x1} + (H_2 - H_1)\Delta\rho_{x2} + \ldots\ (z-H_{P-1})\Delta\rho_{xP}\}$$

let $\Delta H_p = H_p - H_{p-1}$, $H_o = 0$

substituting this into the above equation yields:

$$\int_0^z \frac{\partial \rho}{\partial x}\, d\xi = \frac{1}{2\Delta L} \{ \sum_{p=1}^{P-1} (\Delta H_p\ \Delta\rho_{xp}) + (z-H_{P-1})\ \Delta\rho_{xP}\} \qquad (3)$$

substituting (3) into (1) yields:

$$8 = g \int_0^H \frac{1}{\rho} \frac{1}{2\Delta L} \{ \sum_{p=1}^{P-1} \Delta H_p\ \Delta\rho_{xp} + (z-H_{P-1})\Delta\rho_{xP}\}\ \Omega_J dz$$

or:

$$8 = \frac{g}{2\Delta L} \int_0^H \frac{1}{\rho} \left(\sum_{p=1}^{P-1} \Delta H_p\ \Delta\rho_{xp}\right)\ \Omega_J dz + \int_0^H \frac{1}{\rho}\ (z-H_{P-1})\ \rho_{xP}\ \Omega_J dz \qquad (4)$$

noting the first integral in (4) as I, it can be written as:

$$I = \int_0^H \frac{1}{\rho} \left(\sum_{p=1}^{P-1} H_p \Delta\rho_{xp} \right) \cos \frac{a_I z}{H} \, dz$$

for convenience let $i = \sum_{p=1}^{p-1} H_p \Delta\rho_{xp}$, then

$$I = \int_0^{H_1} \frac{1}{\rho_1} (i) \cos \frac{a_I z}{H} \, dz + \int_{H_1}^{H_2} \frac{1}{\rho_2} (i) \cos \frac{a_I z}{H} \, dz + \ldots \int_{H_{p'-1}}^{H_{p'}} (i) \cos \frac{a_I z}{H} \, dz$$

substituting in i gives:

$$I = \frac{1}{\rho_2} \int_{H_1}^{H_2} \Delta H_1 \, \Delta\rho_{x1} \cos \frac{a_I z}{H} \, dz + \frac{1}{\rho_3} \int_{H_2}^{H_3} (\Delta H_1 \, \Delta\rho_{x1} + \Delta H_2 \, \Delta\rho_{x2}) \cos \frac{a_I z}{H} \, dz$$

$$+ \ldots\ldots + \frac{1}{\rho_{p'}} \int_{H_{p'-1}}^{H_{p'}} (\Delta H_1 \, \Delta\rho_{x2} + \Delta H_2 \, \Delta\rho_{x2} + \ldots . \Delta H_{p'-1} \, \Delta\rho_{x(p'-1)} \cos \frac{a_I z}{H} \, dz \qquad (5)$$

For convenience we let:

$$\int_{H_{p-1}}^{H_p} \cos \frac{a_I z}{H} \, dz = \frac{H}{a_I} \sin \frac{a_I z}{H} \Big|_{H_{p-1}}^{H_p} = \frac{H}{a_I} \left(\sin \frac{a_I H_p}{H} - \sin \frac{a_I H_{p-1}}{H} \right)$$

let $\zeta_p \equiv \frac{H_p}{H}$ $\qquad$ $s_{pJ} = \frac{H}{a_I} (\sin \zeta_p a_I - \sin \zeta_{p-1} a_I)$

note s_{pJ} will not change unless H, c_b, or N_b changes

substituting these expression into (5) gives

$$I = \frac{1}{\rho_2} \Delta H_1 \ \Delta\rho_{x1} \ s_{2J} + \frac{1}{\rho_3} (\Delta H_1 \ \Delta\rho_{x1} + \Delta H_2 \ \Delta\rho_{x2}) \ s_{3J}$$

$$+ \ldots + \frac{1}{\rho_{p'}} (\Delta H_1 \ \Delta\rho_{x1} + \Delta H_2 \ \Delta\rho_{x2} + \ldots \Delta H_{p'-1} \ \Delta\rho_{x(p'-1)}) \ s_{p'J}$$

Collecting terms gives:

$$I = \sum_{p=1}^{p'-1} \frac{s_{p+1,J}}{\rho_{p+1}} \left(\sum_{k=1}^{k=p} \Delta H_k \ \Delta\rho_{xk} \right) \qquad (6)$$

Now we evaluate the 2nd integral in (4):

$$II = \int_0^H \frac{1}{\rho} (z - H_{P-1}) \ \Delta\rho_{xP} \ \Omega_J dz$$

breaking the integral into segments gives:

$$II = \int_0^{H_1} \frac{\Delta\rho_{x1}}{\rho_1} (z-0) \cos \frac{a_I z}{H} dz + \int_{H_1}^{H_2} \frac{\Delta\rho_{x2}}{\rho_2} (z - H_1) \cos \frac{a_I z}{H} dz$$

$$+ \ldots\ldots \int_{H_{p'-1}}^{H_{p'}} \frac{\Delta\rho_{xp'}}{\rho_{p'}} (z - H_{p'-1}) \cos \frac{a_I z}{H} dz$$

let: $\int_{H_{k-1}}^{H_k} z \cos \frac{a_J z}{H} dz + H^2 \phi_{kJ} = H^2 \{ \frac{\cos \frac{a_J z}{H}}{a_J} + \frac{z}{H a_J} \sin \frac{a_J z}{H} \} \Big|_{H_{k-1}}^{H_k}$

then II becomes:

$$II = H^2 \frac{\Delta\rho_{x1}}{\rho_1} \phi_{1J} + H^2 \frac{\Delta\rho_{x2}}{\rho_2} \phi_{2J} - \frac{\Delta\rho_{x2}}{\rho_2} H_1 \frac{H}{a_I} \sin \frac{a_I z}{H} \Big|_{H_1}^{H_2}$$

$$+ \ldots + H \frac{\Delta\rho_{xp'}}{\rho_{p'}} \phi_{p'J} - \frac{\Delta\rho_{xp'}}{\rho_{p'}} H_{p'-1} \frac{H}{a_I} (\sin \frac{a_I z}{H}) \Big|_{H_{p'-1}}^{H_{p'}}$$

collecting terms gives:

$$II = H^2 \sum_{p=1}^{p'} \frac{\Delta\rho_{xp}}{\rho_p} \phi_{pJ} - \sum_{p=2}^{p'} H_{p-1} s_{pJ} \frac{\Delta\rho_{xp}}{\rho_p}$$

note ϕ_{pJ} will not change unless H, c_b, or N_b change

Now inserting expressions for I and II into (4) gives:

$$8 = \frac{g}{2\Delta L} \sum_{p=1}^{p'-1} \frac{s_{p+1,J}}{\rho_{p+1}} \left(\sum_{k=1}^{k=p} \Delta H_k \Delta\rho_{xk} \right)$$

$$+ H \sum_{p=1}^{p'} \frac{\Delta\rho_{xp}}{\rho_p} \phi_{pJ} - \sum_{p=2}^{p'} H_{p-1} s_{pJ} \frac{\Delta\rho_{xp}}{\rho_p}$$

rearranging a bit gives:

$$8 = \frac{g}{2\Delta L}\left[\frac{H^2\Delta\rho_{x1}}{\rho_1}\,\phi_{1J} + \sum_{p=2}^{p'}\frac{1}{\rho_p}\left[s_{pJ}\left\{\sum_{k=1}^{p-1}(\Delta H_k\,\Delta\rho_{xp}) - H_{p-1}\,\Delta\rho_{xp}\right\} + \Delta\rho_{xp}\,\phi_{pJ}\,H^2\right]\right]$$

terms 2 and 7 in momentum equation are also affected by a gradient in ρ. Term 2 is the surface gradient term or:

$$2 = \int_0^H \frac{\rho_s}{\rho}\, g\, \frac{\partial\eta}{\partial x}\, \Omega_J dz$$

Evaluating ρ for each density layer gives

$$2 = \rho_s g\, \frac{\partial\eta}{\partial x} \int_0^H \frac{\Omega_J}{\rho}\, dz = \rho_s g\, \frac{\partial\eta}{\partial x} \sum_{p=1}^{p'} \frac{1}{\rho_p} \int_{H_{p-1}}^{H_p} \cos\left(\frac{a_J z}{H}\right) dz$$

or in more simple notation:

$$2 = \rho_s g\, \frac{\partial\eta}{\partial x}\, H\, EE_J$$

where $EE_J = \sum_{p=1}^{p'} \frac{1}{\rho_p a_J}\left\{\sin\left(\frac{a_J H_p}{H}\right) - \sin\left(\frac{a_J H_{p-1}}{H}\right)\right\}$

The atmospheric pressure gradient term 7 becomes

$$7 = \int_0^H \frac{\partial p_a}{\partial x} \frac{1}{\rho} \Omega_J dz = \frac{\partial p_a}{\partial x} \sum_{p=1}^{p'} \frac{1}{\rho_p} \int_{H_{p-1}}^{H_p} \cos\left(\frac{a_J z}{H}\right) dz$$

$$7 = \frac{\partial p_a}{\partial x} EE_J$$

Note that we have only shown the terms for the x-momentum equations. Similar expressions exist in the y-direction and are included in the model coding.

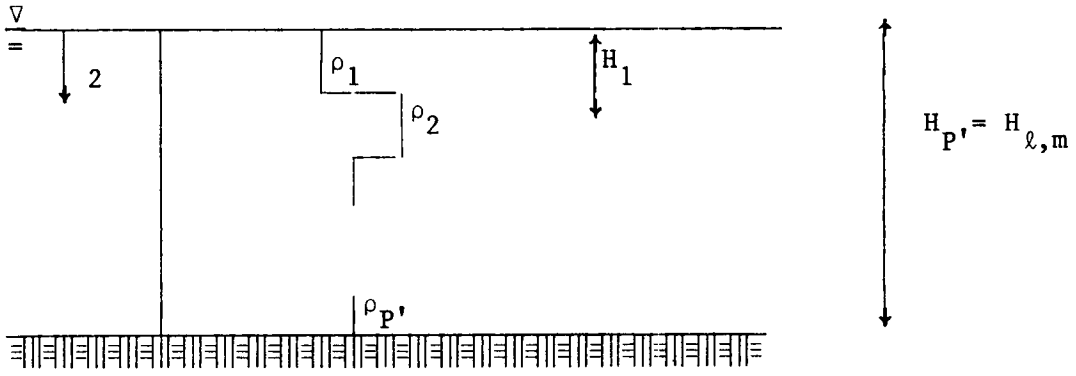

Figure E.3.1

APPENDIX F

Analytic Solutions

F.1: Analytic Solution for Shear Induced Flow Along an Infinite Coast

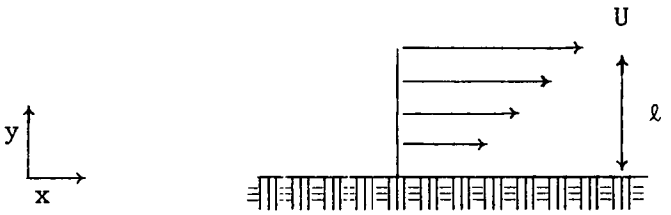

The situation is shown in the figure. We assume no coriolis and $U = f(z)$ only. We wish to find $u(z,y)$ at steady state. The governing equation is:

$$N_v \frac{\partial^2 u}{\partial z^2} + N_H \frac{\partial^2 u}{\partial y^2} = 0$$

or:

$$\frac{\partial^2 u}{\partial z^2} = - \frac{1}{c^2} \frac{\partial^2 u}{\partial y^2} \quad (1) \quad \text{where} \quad c^2 = + \frac{N_v}{N_H}$$

The auxillary conditions are

$$u = U \quad @ \quad y = \ell \quad \text{where} \quad U = d_1 \cos \frac{\pi z}{2H}$$

$$u = 0 \quad @ \quad y = 0$$

$$\frac{\partial u}{\partial z} = 0 \quad @ \quad z = 0$$

$$u = u_b = 0 \quad @ \quad z = h$$

We begin by separating variables let $u = YZ$

$$(1) \Rightarrow YZ'' = -\frac{1}{c^2} ZY''$$

$$\frac{Z''}{Z} = -\frac{1}{c^2}\frac{Y''}{Y} = \lambda$$

3 possibilities exist:

1) $\lambda = 0 \Rightarrow u = (Ez + F)(Gy + H)$

2) $\lambda = \beta^2 \Rightarrow u = (A \cosh \beta z + B \sinh \beta z)(C \sin c \beta y + D \cos c \beta y)$

3) $\lambda = -\sigma^2 \Rightarrow u = (A' \cos \sigma z + B' \sin \sigma z)(C' \sinh \sigma cy + D' \cosh \sigma cy)$

The first possibility:

$u(z,0) = 0 \Rightarrow H=0 \Rightarrow u = (E'z + F')y$

$u_z(o,y) = 0 \Rightarrow (E')(y) = 0 \Rightarrow E' = 0 \Rightarrow u = F'y$

$u(h,y) = 0 \Rightarrow F'y = 0 \Rightarrow F' = 0$

$\therefore$ no solution from this possible λ

The second possibility:

$u(g,y) = 0 \Rightarrow B=0$

$u(h,y) = 0 \Rightarrow A=0$

$\therefore$ no solution for $\lambda=\beta$

The third possibility:

$u(z,0) = 0 \Rightarrow D'= 0 \Rightarrow u = (A' \cos \sigma z + B' \sin \sigma z) \sinh \sigma cy$

$u(0,y) = 0 \Rightarrow B'= 0$

$$u = A' \cos \sigma z \sinh \sigma cy$$

$u(h,y) = 0 \Rightarrow A' \cos \sigma h \sinh \sigma cy$

$$\sigma h = \frac{n\pi}{2} \Rightarrow \sigma = \frac{n\pi}{2h} \qquad n = 1, 3, 5.....$$

So the solution becomes:

$$u = \sum_{\substack{n=1 \\ n \text{ odd}}}^{\infty} A'_n \cos \frac{n\pi}{2H} z \sinh \frac{n\pi}{2H} cy$$

other b.c. => $u(z,\ell) = U = d_1 \cos \frac{\pi z}{2H}$

$$d_1 \cos \frac{\pi z}{2H} = \sum_{\substack{n=1 \\ n \text{ odd}}}^{\infty} + A'_n \cos \frac{n\pi}{2H} z \sin h \frac{n\pi c \ell}{2H}$$

multiply by $\cos \frac{m\pi z}{2H}$ and integrate from 0 to 2H

$$d_1 \int_0^{2H} \frac{\cos m\pi z}{2H} \cos \frac{\pi z}{2H} dz =$$

$$\sum_{\substack{n=1 \\ n \text{ odd}}}^{\infty} A'_n \sinh \frac{n\pi c \ell}{2H} \int_0^{2H} \cos \frac{n\pi}{2H} z \cos \frac{m\pi}{2H} z dz \qquad (2)$$

only non-zero solution is m=1=n in which case note that:

$$\int_0^{2H} \frac{\cos^2 \pi z}{2H} dz = H$$

using this fact changes (2) to:

$$d_1 H = H A'_1 \sinh \frac{n\pi c \ell}{2H} \Rightarrow A'_1 = \frac{d_1}{\sinh \frac{n\pi c \ell}{2H}}$$

The final solution becomes:

$$u = \frac{d_1}{\sinh \frac{\pi c \ell}{2H}} \cos \frac{\pi z}{2H} \sinh \frac{\pi c}{2H} y$$

F.2: Analytic Solution for Two Layer Density Driven Flow in an Infinitely Long Channel

The situation is shown in the figure. We assume:

1. N_v = constant
2. $\frac{\partial \rho}{\partial x}$ = constant
3. $H_1 \neq H_2 \neq$ fcn (x,t)

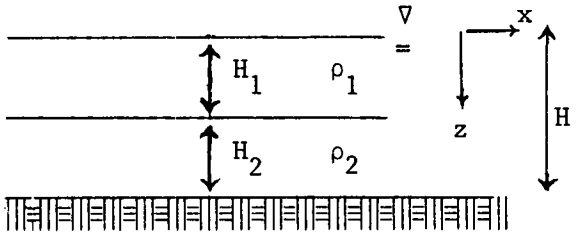

The governing equation is:

$$\frac{g}{\rho} \int_0^z \frac{\partial \rho}{\partial x} \, d\xi = N_v \frac{\partial^2 u}{\partial z^2} \, s \qquad (1)$$

It is most convenient to split the problem into two layers:

Layer 1

Integrating (1) yields:

$$\frac{g}{\rho_1} \frac{\partial \rho_1}{\partial x} \frac{z^2}{2} = N_v \frac{\partial u}{\partial z} + c \qquad (2)$$

@ surface $\quad -N_v \frac{\partial u}{\partial z} = u_{*s}^2 \Rightarrow \quad c = u_{*s}^2$

Integrating (2) yields:

$$c + \frac{g}{N_v \rho_1} \frac{\partial \rho_1}{\partial x} \frac{z^3}{6} = u + \frac{u_{*s}^2 \, z}{N_v}$$

At the interface, $z = H_1$, $u = u_I$

$$u = \frac{g}{6\rho_1 N_v} \frac{\partial \rho_1}{\partial x} (z^3 - H_1^3) + \frac{u_{*s}^2}{N_v} (H_1 - z) + u_I \qquad (3)$$

Layer 2

$$\frac{g}{\rho} \int_0^z \frac{\partial \rho}{\partial x} d\xi = N_v \frac{\partial^2 u}{\partial z^2}$$

$$\frac{1}{\rho_2} \int_0^{H_1} \frac{\partial \rho_1}{\partial x} d\xi + \frac{1}{\rho_2} \int_{H_1}^z \frac{\partial \rho_2}{\partial x} d\xi = \frac{N_v}{g} \frac{\partial^2 u}{\partial z^2}$$

$$\frac{1}{\rho_2} \frac{\partial \rho_1}{\partial x} H_1 + \frac{1}{\rho_2} \frac{\partial \rho_2}{\partial x} (z - H_1) = \frac{\rho_2 N_v}{g} \frac{\partial^2 u}{\partial z^2}$$

$$\frac{H_1}{\rho_2} \{\frac{\partial \rho_1}{\partial x} - \frac{\partial \rho_2}{\partial x}\} + \frac{1}{\rho_2} \frac{\partial \rho_2}{\partial x} z = \frac{N_v}{g} \frac{\partial^2 u}{\partial z^2} \qquad \text{let} \quad \Gamma_1 = \frac{H}{\rho_2} \{\frac{\partial \rho_1}{\partial x} - \frac{\partial \rho_2}{\partial x}\}$$

Integrating yields:

$$\Gamma_1 z + \frac{1}{\rho_2} \frac{\partial \rho_2}{\partial x} \frac{z^2}{2} = \frac{N_v}{g} \frac{\partial u}{\partial z} + c \qquad (4)$$

at bottom $\quad - N_v \frac{\partial u}{\partial z} = u_{*b}^2$

$$c = \Gamma_1 H + \frac{\partial \rho_2}{\partial x} \frac{H^2}{\rho_2^2} + \frac{u_{*b}^2}{g}$$

(4) becomes:

$$\Gamma_1 (z-H) + \frac{1}{2\rho_2} \frac{\partial \rho_2}{\partial x} (z^2 - H^2) - \frac{u_{*b}^2}{g} = \frac{N_v}{g} \frac{\partial u}{\partial z}$$

Integrating yields:

$$g\Gamma_1 \left(\frac{z^2}{2} - Hz\right) + \frac{g}{2\rho_2} \frac{\partial \rho_2}{\partial x} \left(\frac{z^3}{3} - H^2 z\right) - \frac{u_{*b}^2}{g} z = N_v u + c \qquad (5)$$

At the interface, $z=H_1$, $u=u_I$

$$c = g\Gamma_1 \left(\frac{H_1^2}{2} - H H_1\right) + \frac{g}{2\rho_2} \frac{\partial \rho_2}{\partial x} \left(\frac{H_1^3}{3} - H^2 H_1\right) - u_{*b}^2 H_1 - u_I N_v$$

(5) becomes:

$$u = g \frac{\Gamma_1}{N_v} \left(\frac{z^2}{2} - Hz - \frac{H_1^2}{2} + H H_1\right) + \frac{g}{2\rho_2 N_v} \frac{\partial \rho_2}{\partial x} \left(\frac{z^3}{3} - H^2 z - \frac{H_1^3}{3} + H^2 H_1\right)$$

$$+ \frac{u_{*b}^2}{N_v} (H_1 - z) + u_I \qquad (6)$$

Need expression for u_{*b}^2

At the interface $\frac{\tau_I^{①}}{\rho_1} = \frac{\tau_I^{②}}{\rho_2}$ @ $z=H_1$

$$\tau_I = \rho_1 N_v \frac{\partial u_1}{\partial z}\Big|_{z=H_1} = \rho_2 N_v \frac{\partial u_2}{\partial z}\Big|_{z=H_1} \qquad (7)$$

Equation (2) can be used to evaluate $\frac{\partial u_1}{\partial z}$ or

$$\frac{\partial u}{\partial z} = \frac{g}{N_v \rho_1} \frac{\partial \rho_1}{\partial x} \frac{z^2}{2} - \frac{u_{*s}^2}{N_v} \qquad @ \quad z=H_1$$

$$\rho_1 \frac{\partial u}{\partial z} = \frac{g}{N_v} \frac{\partial \rho_1}{\partial x} \frac{H_1^2}{2} - \frac{u_{*s}^2 \rho_1}{N_v} \qquad (8)$$

Similarly for the second layer, (4) implies:

$$\frac{\partial u_2}{\partial z} = \Gamma_1 (z-H) + \frac{1}{2\rho_2} \frac{\partial \rho_2}{\partial x} (z^2 - H^2) - \frac{u_{*b}^2}{g} = \frac{N_v}{g} \frac{\partial u}{\partial z}$$

$$\rho_2 \frac{\partial u}{\partial z} = \frac{g\rho_2}{N_v} \Gamma_1 (z-H) + \frac{g}{2N_v} \frac{\partial \rho_2}{\partial x} (z^2 - H^2) - \frac{u_{*b}^2}{N_v} \rho_2 \qquad (9)$$

Equating (8) & (9) as implied by (7) yields:

$$\frac{g\rho_2}{N_v} \Gamma_1 (H_1 - H) + \frac{g}{2N_v} \frac{\partial \rho_2}{\partial x} (H_1^2 - H^2) - \frac{u_{*b}^2 \rho_2}{N_v} = \frac{g}{N_v} \frac{\partial \rho_1}{\partial x} \frac{H_1^2}{2} - \frac{u_{*s}^2 \rho_1}{N_v}$$

$$u_{*b}^2 = \{- g \frac{\partial \rho_1}{\partial x} \frac{H_1^2}{2} + u_{*s}^2 \rho_1 + g\rho_2 \Gamma_1 (H_1 - H) + \frac{g}{2} \frac{\partial \rho_2}{\partial x} (H_1^2 - H^2)\} \frac{1}{\rho_2} \qquad (10)$$

To evaluate u_I, note that

$$u\Big|_{z=H} = u_b = \frac{u_{*b}^2}{c_b}$$

substituting this expression into (6) and setting z=H

$$u_b = \frac{u_{*b}^2}{c_b} = \frac{g\ \Gamma_1}{N_v}\left(\frac{H^2}{2} - H^2 - \frac{H_1^2}{2} + H\ H_1\right) + \frac{g}{2\rho_2\ N_v}\frac{\partial \rho_2}{\partial x}\left(\frac{H^3}{3} - H^3 - \frac{H_1^3}{3} + H^2\ H_1\right)$$

$$+ \frac{u_{*b}^2}{N_v}\left(H_1 - H\right) + u_I$$

$$u_I = \frac{g\ \Gamma_1}{N_v}\left(\frac{H_1^2}{2} - H\ H_1 + \frac{H^2}{2}\right) + \frac{g}{2\rho_2\ N_v}\frac{\partial \rho_2}{\partial x}\left(\frac{2}{3}\ H^3 + \frac{H_1^3}{3} - H^2\ H_1\right)$$

$$+ \frac{u_{*b}^2}{N_v}\left(H - H_1\right) \qquad (11)$$

The final solution is thus found using (11) and substituting into (6). Note that summation of body forces yields $u_{*b} = -u_{*s}$.

APPENDIX G

Data Reduction

Appendix G

Data Reduction

G.1 Wind Processing

Raw wind data were read from a tape obtained from the National Climatic Center. The following steps were followed in processing the wind data for this study:

1. Most meteorological data is recorded at three hour intervals. The application of a Doodson filter requires hourly data. This problem was resolved by creating identical data points one hour before and one hour after each existing data point. The resulting wind record resembled a step function with wind velocities held constant for three hour intervals. Interpolation to hourly data by linearly averaging adjacent data points was tested, but the final Doodson filtered record produced by interpolation did not differ significantly from the results obtained by filtering the step function record.

2. In order to facilitate the interpretation of model results, the model grid is oriented approximately parallel to bathymetric contours rather than the standard compass directions. As a result, standard wind components which are oriented N-S and E-W must be rotated to coincide with the X-Y axes of the model grid. In the present case, the model Y axis is rotated 27 degrees counterclockwise from true north. Rotation

of the wind data was accomplished by calculating the resultant direction and magnitude of a data point from the standard north and east components, determining the orientation of this resultant vector relative to the model grid, and then resolving this vector into components parallel to the model X and Y axes.

3. The rotated wind record was then Doodson filtered to remove diurnal and semi-diurnal processes such as land-sea breezes.

4. The resulting Doodson filtered u and v components of the wind were plotted to allow visual comparison of wind, tide and current records.

Exceptions:

1. The Feb-Mar 1973 wind record was input manually from paper copy, converted to NODC format, and processed according to the steps above.

2. The data for July-August 1974 originated from a tape furnished by Dr. Koblinsky of Scripps. The data consisted of bi-hourly wind stress values calculated from wind velocities interpreted from regional weather maps by Partagas (1974a,b). These stress values were re-converted to wind speeds using the inverse of the formula used by Koblinsky to convert the wind velocities to wind stress. The resulting wind velocities were processed according to steps 2 through 5 above.

G.2 Tide Processing

Tide data originated from a number of sources:

1. NOS data tape: 1974 Clearwater, Key West and Pensacola.

2. NOS paper copy: 1973 Naples, St. Petersburg, Cedar Key.

3. Shelf Dynamics Experiment tape furnished by Koblinsky: 1974 Naples.

4. Paper copy of NOS data tape furnished by Professor G. Marmorino of Florida State University: 1978 Naples, Clearwater.

5. Paper copy from Dr. Gary Mitchum of Florida State University: 1978 Cedar Keys.

In all cases, data were converted to standard NODC format before processing.

Processing consisted of adjusting the raw tidal record for barometric pressure effects. This was accomplished by obtaining a barometric pressure time series from the nearest available meteorological station for the same time period as the tidal record to be processed. The barometric pressure record was first averaged to determine the mean atmospheric pressure for the time period, and the difference between this mean and an hourly barometric pressure reading was multiplied by a conversion factor (1 mb=.98533cm of seawater) and the result applied to the corresponding hourly sea level data. A Doodson filter was then applied to the tidal record to remove the astronomical tide and isolate sea level changes due to other forcing mechanisms.

The resulting Doodson filtered tidal record was plotted to allow visual comparison of wind and tide records and for comparison to surface elevation data output by the model.

G.3 Current Processing

Current velocity data originated from tapes provided by Dr. Wilton Sturges of

Florida State University (1978 FSU data) and Dr. Chester Koblinski currently at Scripps (1973 SDE data).

Current velocity values were read from tape and translated to NODC format. The U and V components of velocity were then rotated to conform to the orientation of the model grid axes. Rotation of the current data was accomplished by calculating the resultant direction and magnitude of a data point from the standard north and east components, determining the orientation of this resultant vector relative to the model grid, and then resolving this vector into components parallel to the model X and Y axes.

The rotated current record was then Doodson filtered to remove the astronomical components of the current and to allow a direct comparison to wind records.

The Doodson filtered U and V components of the currents were plotted to allow visual comparison of wind and current records and for comparison to current velocity data output by the model.

The Department of the Interior Mission

As the Nation's principal conservation agency, the Department of the Interior has responsibility for most of our nationally owned public lands and natural resources. This includes fostering sound use of our land and water resources; protecting our fish, wildlife, and biological diversity; preserving the environmental and cultural values of our national parks and historical places; and providing for the enjoyment of life through outdoor recreation. The Department assesses our energy and mineral resources and works to ensure that their development is in the best interests of all our people by encouraging stewardship and citizen participation in their care. The Department also has a major responsibility for American Indian reservation communities and for people who live in island territories under U.S. administration.

The Minerals Management Service Mission

As a bureau of the Department of the Interior, the Minerals Management Service's (MMS) primary responsibilities are to manage the mineral resources located on the Nation's Outer Continental Shelf (OCS), collect revenue from the Federal OCS and onshore Federal and Indian lands, and distribute those revenues.

Moreover, in working to meet its responsibilities, the **Offshore Minerals Management Program** administers the OCS competitive leasing program and oversees the safe and environmentally sound exploration and production of our Nation's offshore natural gas, oil and other mineral resources. The MMS **Minerals Revenue Management** meets its responsibilities by ensuring the efficient, timely and accurate collection and disbursement of revenue from mineral leasing and production due to Indian tribes and allottees, States and the U.S. Treasury.

The MMS strives to fulfill its responsibilities through the general guiding principles of: (1) being responsive to the public's concerns and interests by maintaining a dialogue with all potentially affected parties and (2) carrying out its programs with an emphasis on working to enhance the quality of life for all Americans by lending MMS assistance and expertise to economic development and environmental protection.